Enhanced London Dispersion Effects in Copper(I) Thiolate Complexes

and Cyclotristannane/Distannene Thermal Interconversion

By

WENXING ZOU

DISSERTATION

Submitted in partial satisfaction of the requirements for the degree of DOCTOR OF PHILOSOPHY

in

Chemistry

in the

OFFICE OF GRADUATE STUDIES

of the

UNIVERSITY OF CALIFORNIA

DAVIS

Approved:

_____

Philip P. Power, Chair

_____

Alan Balch

_____

Louise A. Berben

_____

Jesús M. Velázquez

Committee in Charge

2023

Table of Contents

List of Symbols, Nomenclature, or Abbreviations

Å	Angstrom (10^{-10} m)
Ar^{iPr4}	C_6H_3-2,6-(C_6H_3-2,6-*i*Pr_2)$_2$
Ar^{iPr6}	C_6H_3-2,6-(C_6H_2-2,4,6-*i*Pr_3)$_2$
Ar^{Me6}	C_6H_3-2,6-(C_6H_2-2,4,6-Me_3)$_2$
ca.	approximately
DFT	Density Functional Theory
Dipp	C_6H_3-2,6-*i*Pr_2
Ether	Diethyl Ether
IR	Infrared
*i*Pr	isopropyl
Mes	C_6H_2-2,4,6-Me_3
NMR	Nuclear Magnetic Resonance
PhMe	Toluene
Trip	C6H2-2,4,6-*i*Pr_3
THF	Tetrahydrofuran
*t*Bu	t-Butyl
UV-vis	Ultraviolet –visible
VT	Variable Temperature
ΔG	Gibbs Free-Energy Change
ΔH	Enthalpy Change
ΔS	Entropy Change
δ	chemical shift
ε	molar absorption coefficient
ν	frequency

Acknowledgements

My most profound appreciation goes to Prof. Philip P. Power, my Ph.D. advisors, for his time, effort, patience and understanding in helping me succeed in my studies. His vast wisdom and wealth of experience have inspired me throughout my studies. All guidance, encouragement and influence throughout the projects from him have been invaluable. He has inspired me to become an independent researcher and helped me realize the power of critical reasoning. He also demonstrated what a brilliant and hard-working scientist can accomplish.

I am also grateful to everyone with whom I have collaborated externally; they are Prof. Stefan Grimme, Dr. Markus Bursch and Dr. Petra S. Vasko. I thank their input in computational studies described in Chapters 3 to 4 and the outstanding feedback from them during manuscript preparation. The completion of all publications I have achieved would not have been possible without their support and guidance. In addition, I would like to express my gratitude to Dr. James C. Fettinger and Dr. Ping Yu for their technical assistance in X-ray crystallography and NMR experiments throughout my research.

I would like also to thank the following people who create a friendly and welcomed culture in our group, without whom I would not have been able to survive my coursework and research, and without whom I would not have made it through my PhD program. Thanks to their generosity and encouragement, my time spent studying and living in the UC Davis has been truly rewarding. The lab members include: Dr. Clifton Wagner, Dr. Cary R. Stennett, Dr. Kristian L. Mears, Dr. Ting Yi (Charlie) Lai, Dr. Joshua D. Queen, Dr. Qihao Zhu, Alice C. Phung, Connor P. Mc Loughlin, Phuong Anh (Sam) Cao and Yanran Li, and all the other former visiting students that I know. It has been an amazing experience working with you!

I would also like to thank Prof. Louise A. Berben, Prof. Alan Balch and Prof. Jesús M. Velázquez for their service to be on my thesis committee. They generously gave their time and offered me valuable comments toward improving my work.

I cannot forget friends who went through hard times together, cheered me on, and celebrated each accomplishment: Yuting Fan, Yi Wu, Nhu Tran, Yang Xiao, Yuxia Li, Zheng Ju and Wen Fu.

To conclude, I deeply thank my parents for their unconditional trust, timely encouragement, and endless patience. It was their love that raised me up again when I got weary. They are not only family, but also my best friends and great companion, loved, supported, encouraged, entertained, and helped me get through this agonizing period in the most positive way, always motivating me for pursuing my goals. It would have been impossible to finish my studies without their unwavering support over the past few years.

Abstract

This dissertation describes the synthesis and characterization of a series of copper(I) thiolates and Tin-containing derivatives featuring as attractive London dispersion effects and rare structures with unusual chemical behavior.

Chapter 2 describes the synthesis of the first two-coordinate, dimeric copper thiolato complexes $\{CuSAr^*\}_2$ and comparison of copper thiolates with their lithium congeners. Reactions of the large terphenyl thiols $HSAr^*$ (Ar^* = very bulky terphenyl ligands) with stoichiometric amounts of mesitylcopper(I) afforded the corresponding two-coordinate, dimeric copper thiolato species $\{CuSAr^*\}_2$. These complexes feature centrosymmetric dimeric structures with planar Cu_2S_2 core in which the two Cu atoms are bridged by sulfurs from two terphenyl thiolato ligands, which bear a resemblance to the Cu_A site in nitrous oxide reductase in which two cysteines also bridge two copper atoms. Single X-ray crystallography shows that the Cu derivatives feature much longer Cu--Cu distances than the Li--Li distances in their dimeric Li congeners. Given the very similar effective ionic radii of the Li^+ (0.59 Å) and Cu^+ (0.60 Å) ions, this unusual phenomenon is probably a consequence of stronger dispersion interactions which are caused by a higher degree of instantaneous induced dipoles between copper atoms.

Chapter 3 is an extension of the studies in Chapter 2. Further investigation of the reactions described in Chapter 2 revealed that the adjustment of the amount of mesitylcopper(I) afforded a new type of heteroleptic aryl Cu(I) thiolato compounds with formula $\{Cu_2(SAr^*)Mes\}_2$ (Ar^* = very bulky terphenyl ligands). The molecular structures of those compounds show they all display tetrametallic Cu_4 cores in which two thiolato or two mesityl ligands bridge the metals. It is noteworthy that the use of relatively less bulky thiolato ligands yielded products that feature the

expected conventional alternating thiolato and mesityl bridging patterns. Nevertheless, switching to bulkier ligands afforded a previously unknown structural arrangement in which the two thiolato ligands are adjacent to each other. The new complex with cis arrangement of the ligands is sterically counterintuitive which is likely due to London dispersion (LD) energy effects. Dispersion corrected DFT calculations have been carried out to show that **3** has the highest LD effect stabilization arising from the increased numbers of C-H···H-C interactions of the isopropyl ligand substituents.

Chapter 4 depicts the London dispersion effects in an equilibrium of distannene and a tristannane with identical substituents. $\{Sn(C_6H_2\text{-}2,4,6\text{-}Cyp_3)_2\}_3$, a new cyclotrisyannane, was produced by reacting lithium salt $\{LiC_6H_2\text{-}2,4,6\text{-}Cyp_3{\cdot}Et_2O\}_2$ with $SnCl_2$ in Et_2O at -78°C. Variable temperature (VT) ^{119}Sn NMR spectroscopy shows $\{Sn(C_6H_2\text{-}2,4,6\text{-}Cyp_3)_2\}_3$ can be converted to the distannene $\{Sn(C_6H_2\text{-}2,4,6\text{-}Cyp_3)_2\}_2$ upon heating in hydrocarbon solution. However, the presence of the corresponding monomer $:Sn(C_6H_2\text{-}2,4,6\text{-}Cyp_3)_2$ at elevated temperature was not detected neither by VT ^{119}Sn NMR spectroscopy nor by ^{1}H-DOSY NMR spectroscopy. The suppression of the formation of the monomeric stannylene is a reflection of enhanced London dispersion energy between the two $Sn(C_6H_2\text{-}2,4,6\text{-}Cy_3)_2$ units in the $\{Sn(C_6H_2\text{-}2,4,6\text{-}Cyp_3)_2\}_3$ and $\{Sn(C_6H_2\text{-}2,4,6\text{-}Cyp_3)_2\}_2$, as evidenced by multiple computational studies. Van't Hoff analysis revealed a cyctristannane $\{Sn(C_6H_2\text{-}2,4,6\text{-}Cyp_3)_2\}_3$ to distannene $\{Sn(C_6H_2\text{-}2,4,6\text{-}Cyp_3)_2\}_2$ conversion $\Delta H_{conv.}$ energy value of 33.36 kcal mol^{-1} and a $\Delta S_{conv.}$ value of 0.102 kcal mol^{-1} K^{-1}, which gives $\Delta G_{conv.}^{300\ K} = 2.86$ kcal mol^{-1}.

Chapter 5 described novel reactivities of stannylene $:Sn(C_6H_3\text{-}2,6\text{-}(C_6H_3\text{-}2,6\text{-}i\text{Pr}_2)_2)_2$ with phenylacetyene and diphenylacetylene. Stannylenes have shown high reactivities towards

unsaturated small molecules (CO, alkene, alkyne, azide, etc…) due to their relatively modest HOMO-LUMO gap. However, only a few reactions of stannylene ($:SnR_2$) with alkynes have been investigated so far. This chapter depicts the reactions of diaryl stannylene $Sn(C_6H_3\text{-}2,6\text{-}(C_6H_3\text{-}2,6\text{-}i\text{Pr}_2)_2)_2$ with terminal or non-terminal alkynes in benzene at elevated temperature, from which aryl alkyl stannylene products were isolated and characterized by X-ray crystallography and spectroscopy.

Chapter 1. General Introduction: London Dispersion Effects in Molecular Structures and Chemical Behavior

London dispersion (LD) interactions, also known as dispersion forces or instantaneous dipole-dipole induced forces or even non-covalent interactions, is a type of temporary intermolecular force when the electrons in two adjacent atoms occupy positions that make the atoms form temporary dipoles.[1-4] LD forces are ubiquitously present and cumulative, despite their causes may be difficult to grasp, they are of great importance to the stability of various types of molecules.

For instance, the structure stabilization of macromolecules, such as DNA, is mainly determined by non-covalent interactions, among which hydrogen bonding and the stacking interaction are prominent. Despite LD forces are temporary and weak (individual C-H···H-C interactions are relatively small (<1 kcal mol^{-1})),[5] the cumulative effect of numerous C-H-H-C interactions contributes to a significant net decrease in the free energy of DNA molecules.[6] Molecular dynamics simulations have shown that the London dispersion can provide the native structure of a biomolecular complex with the largest additional stabilization.[7]

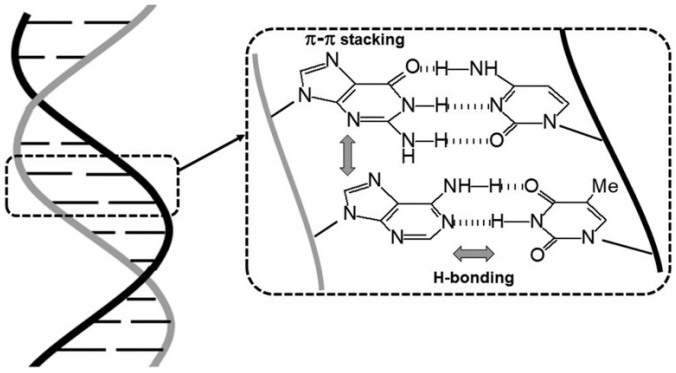

Figure 1.1 Schematic representation of interstrand H-bonding and intrastrand π-π stacking interactions.[8]

Recently there has been an increasing awareness of the significance of attractive London dispersion forces in the stability of inorganic/organometallic molecules with sterically bulky substituents.[9-12] In this report, recent research progress in this field was described based on different categories of dispersion energy donor (DED) ligands.

Bulky amido ligands

Bulky amido ligand -$N(SiMe_3)_2$ has been used as ligand to stabilize main group/transition metal complexes for several decades.[13] This ligand has enabled the isolation of numerous inorganic/organometallic species that were hitherto unknown. Seminal work includes the preparation of tetrameric $\{MN(SiMe_3)_2\}_4$ (M = Ni, Cu),[14] divalent $[M\{N(SiMe_3)_2\}_2]_2$ (M = Mn, Fe, Co)[15-17] and trivalent $M\{N(SiMe_3)_2\}_3$ (M = Sc,[18] Ti,[19] V,[20] Cr,[21] Mn,[22] Fe,[23] Co[22]), as well as tetrylenes $E\{N(SiMe_3)_2\}_2$ (E = Ge, Sn, Pb) reported by Lappert in the 1970s.[24] However, the LD stabilization effects of this type of ligand was only recognized in recent years.[25]

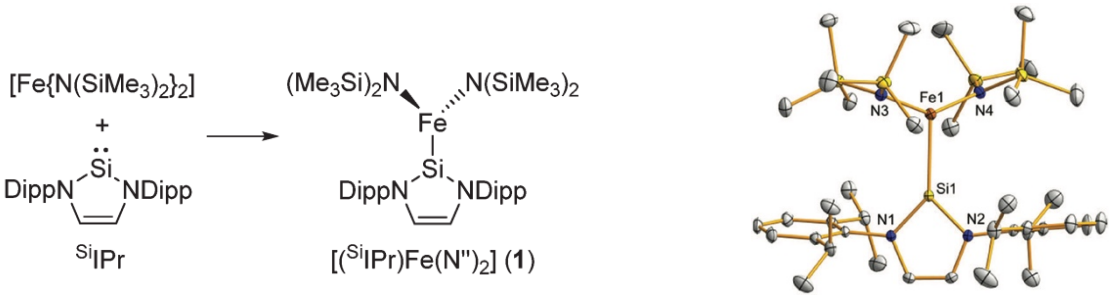

Figure 1.2 The synthesis (left) and molecular structure (right) of the three-coordinate iron-silylene complex.[26]

The amido ligand -$N(SiMe_3)_2$ has been used to synthesize a three-coordinate iron-silylene complex (Figure 1.2).[26] Computational studies revealed that this compound is stabilized by ligand-ligand

dispersion forces, dispersion interactions between the amido $SiMe_3$ substituents and the isopropyl substituents on the NHSi ligand considerably enhance the stability of the compound.[26]

Power and co-workers described a dispersion forces-driven disproportionation reaction, by which the first linear coordinated Cu(II) complex $Cu\{N(SiMe_3)Dipp\}_2$ (Dipp = C_6H_3-2,6-iPr$_2$) was prepared (Figure 1.3).[27] Single X-ray crystallography shows this complex features an inversion center with a rigorously linear geometry at the Cu atom. The eclipsed conformation of the two -$N(SiMe_3)Dipp$ ligands can maximize LD interaction across the C_{ipso}-Si1-N1-Cu1-N1A-Si1A-C_{ipso} core array and therefore facilitate the disproportionation. The LD stabilization energy that generated by the -$N(SiMe_3)Dipp$ ligands amounts to 20.8 kcal mol^{-1} in this species.[27]

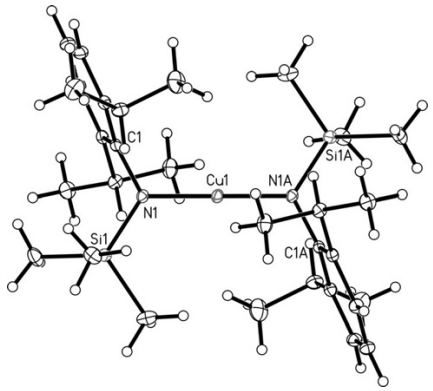

Figure 1.3 Molecular structure of the first linear coordinated Cu(II) complex $Cu\{N(SiMe_3)Dipp\}_2$ (Dipp = C_6H_3-2,6-iPr$_2$).[27]

Several other related transition metal derivatives with identical ligand $M\{N(SiMe_3)Dipp\}_2$ (Dipp = C_6H_3-2,6-iPr$_2$, M= Fe, Co, Ni) have also been synthesized by the same research group (Figure 1.4),[28,29] with calculated dispersion stabilization energy amounting to 22-29 kcal mol^{-1}.[28]

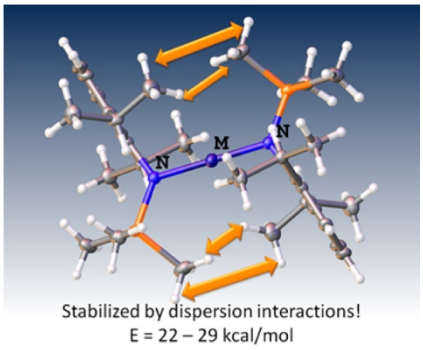

Figure 1.4 High spin, two-coordinate first row transition metal-amido complexes, $M\{N(SiMe_3)Dipp\}_2$ (M = Fe, Co, Ni)[28]

β-diketiminate ligands

Theoretical examination of the molecular structures of {(BDI^{Mes})CuM(BDI^{Dip})} (M = Al, Ga, BDI^{Mes} = *N*,*N*′-bis(2,4,6-trimethylphenyl)pentane-2,4-diiminate, BDI^{Dip} = *N*,*N*′-bis(2,6-diisopropylphenyl) pentane-2,4-diiminate) (Figure 1.5), which were reported by Power and coworkers,[30] shows that approximately 50% of the interaction enthalpies can be attributed to LD interactions between the BDI^{Mes} and BDI^{Dip} groups (109 and 106 kJ mol^{-1} for Al and Ga derivatives, respectively).

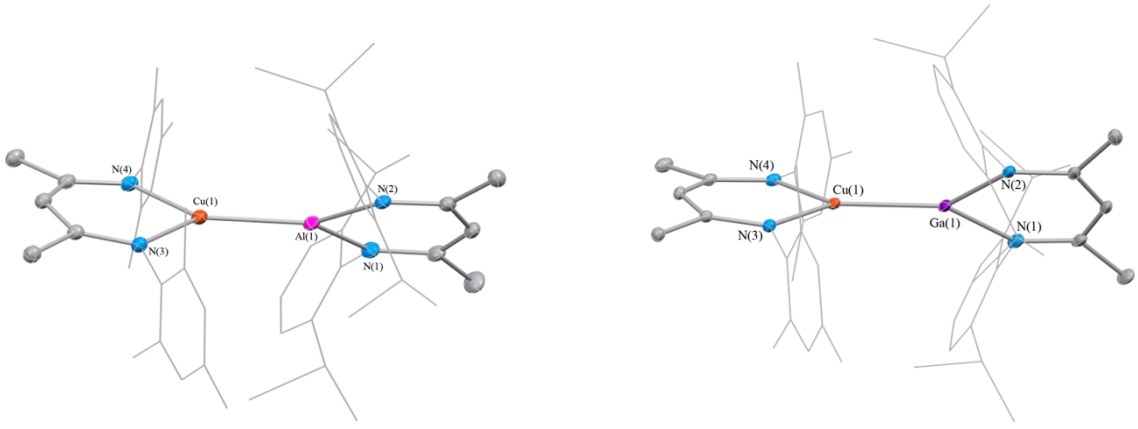

Figure 1.5 Molecular structures of {(BDI^{Mes})CuAl(BDI^{Dip})} (BDI^{Mes} = *N*,*N*′-bis(2,4,6-trimethylphenyl)pentane-2,4-diiminate, BDI^{Dip} = *N*,*N*′-bis(2,6-diisopropylphenyl)pentane-2,4-diiminate) (left) and {(BDI^{Mes})CuGa(BDI^{Dip})} (right).[30]

Moreover, several new first-row transition metal (M = Cr, Mn, Fe, Co, Cu) aluminylene complexes were prepared by Crimmin group and bonding patterns of those species were studied.[31] Energy decomposition analysis (EDA) and DFT calculations show that dispersion plays a crucial role in stabilizing these compounds. The dispersion contribution ranges between 44%-80% of the total interaction energy. Both short-range and long-range dispersion interactions have been confirmed.[31]

Adamantyl and norbornyl ligands

Adamantyl and norbornyl substituents can generate LD interactions due to their abundant C-H moieties and thus can provide stabilization energy. Schoenebeck and coworkers have reported a selective ortho-functionalization of adamantyl substituted arenes.[32] This approach made use of tri-*t*Bu substituted Pd(I) dimer as a catalyst to synthesize diversely substituted therapeutically important adamantylarenes. Theoretical studies show that the attractive Pd*t*Bu$_3$···adamantyl dispersion forces overcome steric repulsion and stabilize the transition state for oxidative addition, which is unusual with current understanding in metal catalyzed cross-coupling chemistry.

Shuji Akai group have reported a London dispersion-controlled noncatalytic [2+2] cyclodimerization (Figure 1.6), which selectively afforded proximal biphenylenes in high yields and regioselectivities. Adamantyl substituent at the 3-position on benzene served as a dispersion-

directing group, controlled the reaction and produced the proximal adduct exclusively in excellent yield.[33]

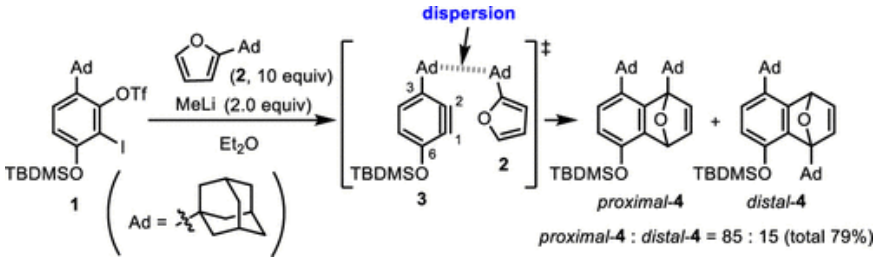

Figure 1.6 London dispersion-controlled noncatalytic [2+2] cyclodimerization.[33]

Power group has described the preparation of a sodium 1-adamantoxide (OAd^1) complex of formula $[Na(OAd^1)(HOAd^1)_2]$, which was produced by reduction of 1-adamantanol with excess of the sodium metal.[34] X-ray diffraction of the product molecule shows that it displays a monomeric structure, with the reduced alkoxide (OAd^1) and two unreduced $HOAd^1$ donors coordinate to the sodium center (Figure 1.7). The reduction of the 1-adamantanol is inhibited from completion despite excess of sodium metal were used. The computational analysis clearly suggested the point that this compound would not be isolated without LD stabilization.

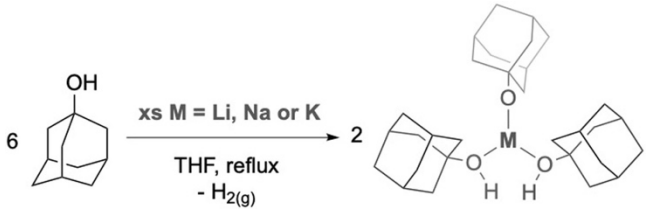

Figure 1.7 Synthetic route to alkali metal complexes $[M(OAd^1)(HOAd^1)_2]$[34]

The stability of transition metal complex examples can also be rationalized on the basis of norbornyl ligands. Examples include $M(nor)_4$ (M = Hf, Zr, Ti, V, Cr, Mn, Fe, Co, Ni, Mo; nor = 1-bicyclo[2,2,1]hept-1-yl), a series of tetranorbornyl compounds first reported by Bower and

Tennent in 1972[35] and then Theopold in the 1986.[36] Re-examination of these complexes by density functional theory (DFT) confirmed that dispersion force attraction between norbornyl substituents is fundamental to the stability of these species. Dispersion correction resulted in shortened M-C bond lengths for the stable complexes (Table 1.1), along with dispersion stabilization energy amounting to 45.9 kcal mol^{-1} ($Fe(nor)_4$) and 38.3 kcal mol^{-1} ($Co(nor)_4$).[37]

Table 1.1 Selected calculated structural parameters for $M(nor)_4$ (M=Fe,Co, Ni).[37]

M	Fe			Co			Ni	
	B3PW91	-D3	Exp.[10]	B3PW91	-D3	Exp.[9]	B3PW91	-D3
M-C [Å]	1.939 (av.)	1.910 (av.)	1.993 (av.)	1.976 (av.)	1.942 (av.)	1.920 (av.)	2.009 (av.)	2.016 (av.)
C-M-C [°]	109.5 (av.) 109.3, 108.4, 111.0, 110.7, 108.9, 108.6	109.5 (av.) 109.5, 108.3, 110.8, 110.5, 109.0, 108.7	109.5 (av.) 109.4, 109.0, 109.7, 109.4, 109.8, 109.7	109.6 (av.) 111.8, 114.1, 97.8, 97.2, 119.2, 117.6	109.7 (av.) 119.3, 116.6, 97.0, 97.0, 114.6, 113.6	109.5 (av.) 113.4, 106.9, 106.9, 109.0, 109.0, 111.7	109.4 (av.) 95.7, 117.2, 108.4, 108.0, 116.8, 110.4	109.4 (av.) 94.9, 115.5, 109.8, 109.7, 115.6, 110.7

Terphenyl ligands

Classical terphenyl ligands (Figure 1.8)[38-40] provide further evidence of the importance of LD effects, especially in main group complexes with multiple bonds. The close contacts between the ring substituents of the terphenyl ligands are responsible for the enhanced stability of these molecules and may have a distinctive influence on their bond lengths or dissociation behaviors.

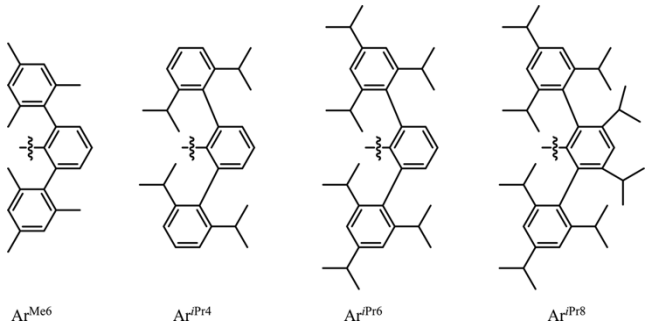

Figure 1.8 Schematic drawings of the terphenyl ligands.[41]

A series of tetralene compounds E{C_6H_3-2,6-(C_6H_2-2,4,6-*i*Pr_3)$_2$}$_2$ (E = Ge, Sn, Pb) were prepared by reacting ECl_2 and 2 equiv. of terphenyl lithium salt Et_2O·C_6H_3-2,6-(C_6H_2-2,4,6-*i*Pr_3)$_2$ (Figure 1.9).[41] X-ray crystallography shows that the C_{ipso}-E-C_{ipso} interligand angles of these compounds fall within the range of 107.61–112.55°. These interligand bond angles are somewhat narrower in comparison to those observed in analogous species with less bulky terphenyl substituents, despite the increased size of the terphenyl substituent Ar^{iPr6} (cf. Ge(Ar^{iPr4})$_2$: 112.77(4)°;[42] Ge(Ar^{Me6})$_2$: 114.4(2)°;[43] Ge(*p*-SiMe$_3$-Ar^{Me6})$_2$: 115.85(14)°;[44] Sn(Ar^{iPr4})$_2$: 117.56(8)°;[43] Sn(C_6H-2,6-(2,4,6-$Me_3C_6H_2$)$_2$-3,5-*i*Pr_2)$_2$: 123.44(14)°;[44] Pb(Ar^{iPr4})$_2$: 121.5(3)°;[45] Pb(C_6H-2,6-(2,4,6-$Me_3C_6H_2$)$_2$-3,5-*i*Pr_2)$_2$: 123.89(12)°).[46] Computational analysis shows the relatively narrow interligand angles arises from the London dispersion interactions between the Ar^{iPr6} (Ar^{iPr6} = -C_6H_3-2,6-(C_6H_2-2,4,6-*i*Pr_3)$_2$) groups caused by increased number of isopropyl substituents.[41]

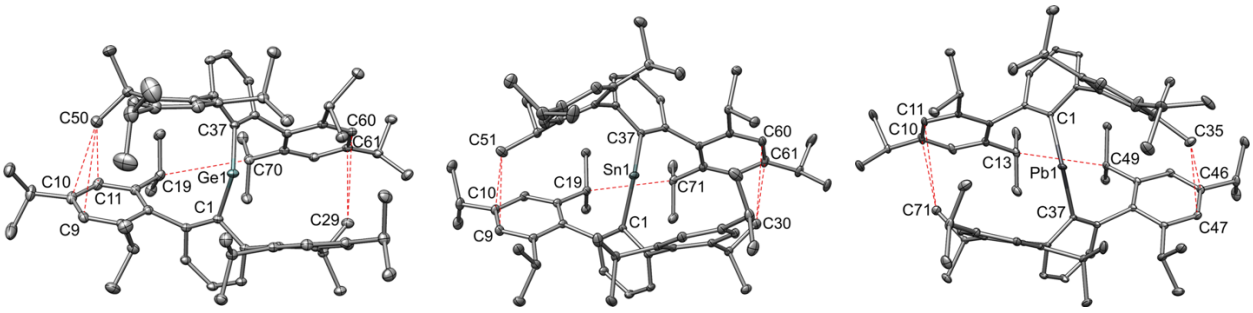

Figure 1.9 Molecular structure of E{C_6H_3-2,6-(C_6H_2-2,4,6-*i*Pr_3)$_2$}$_2$ (E = Ge (left), Sn (middle), Pb (right)). Close H-H contacts are shown as red dotted line.[41]

The Power group has described counterintuitive steric effects caused by LD forces in heavier group 14 (Si–Pb) dichalcogenolate.[47] Several molecules with formula of M(ChAr)$_2$ (M = Si, Ge, Sn, Pb; Ch = O, S, or Se; Ar = bulky m-terphenyl ligand, including two new acyclic silylenes) were synthesized, inspection of the structures of these species revealed a reverse relationship between

the S-M-S bond angles and the size of the ligands used (Figure 1.10). Unlike normal steric expectations, the interligand angles of those complexes were observed to become narrower as the bulk of the ligand is increased. DFT calculations with dispersion corrections led to the conclusion that dispersion forces are a key factor in stabilizing their acute interligand angles since LD dispersion energies increase as the angles become narrower.

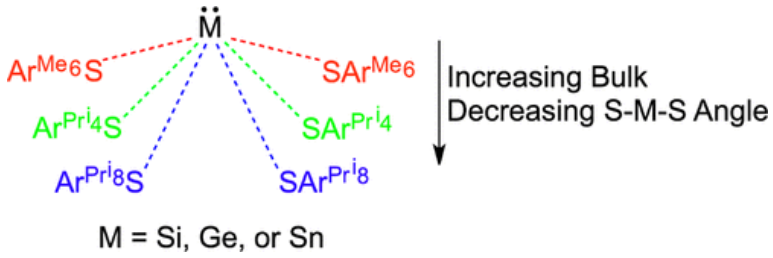

Figure 1.10 Reverse relationship between the S-M-S bond angles of heavier group 14 (Si–Pb) dichalcogenolates and the size of the ligands.[47]

Another example is a novel monomeric aluminum imide (iminoalane) recently reported by the same group (Figure 1.11).[48] The product complex features a short Al-N bond of 1.625(4) Å, which is shorter than those of other related species (1.796-1.842 Å). Energy decomposition analysis (EDA) indicated dispersion stabilization energy accounts for –89 kJ mol^{-1}, which is a crucial contribution along with steric effects from the terphenyl ligands, to provide sufficient stabilization for this compound at ambient temperature.

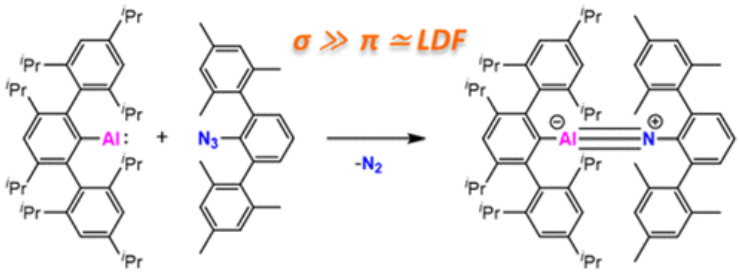

Figure 1.11 Synthesis of the monomeric aluminum imide.[48]

Based on the early work mentioned above, we became interested in the effects of the size of terphenyl substituents on the structures to see if the unusual steric effects observed for Cu(I) thiolato complexes. The synthesis, characterization and computational analysis of a series of neutral Cu(I) thiolato complexes were described in Chapter 2 and 3.

N-heterocyclic carbene (NHC) ligands

One of the most remarkable examples of NHC-stabilized complex is the disilicon structure from Robinson's lab.[49] The kinetic stabilization to this highly reactive molecule is a result of steric hinderance given the similar ratios of organic shell ligands around inorganic cores.[39,49] Re-evaluation of this complex by DFT calculation shows intramolecular dispersion stabilization provided by the organic substituents on the carbenes are as large as ca. 30 kcal mol^{-1},[50] which leads to additional intrinsic thermodynamic stabilization to the molecule.

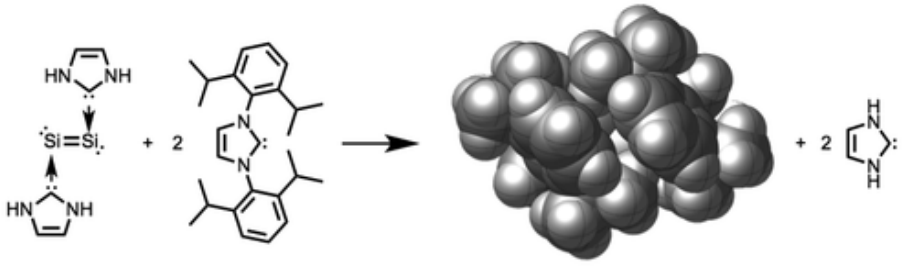

Figure 1.12 NHC-stabilized disilicon compound.[50]

NHC ligands have also been widely used in the preparation of heavier dipnictenes, including diphosphenes,[51-55] diarsene[56-57] and dibismuthene (Figure 1.13).[58-59] Recent inspection of these species with quantum chemical calculations provided further insight into the LD contribution to the structural stability of those dipnictene compounds. Theoretical studies clearly demonstrated

the essential contribution of London dispersion energy to the overall stability of those species and also highlight the importance of bulky NHC ligands for the successful isolation of highly reactive main group molecules.[60,61]

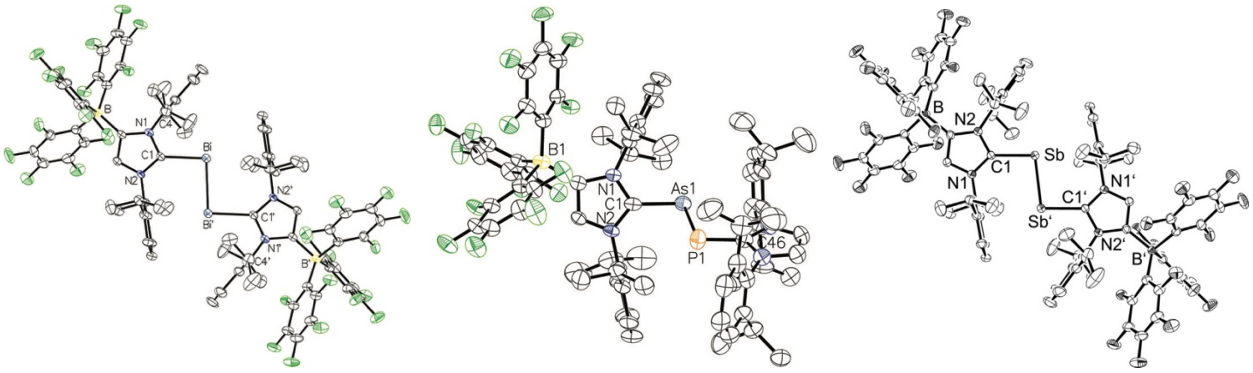

Figure 1.13 NHC supported dibismuthene (left), arsaphosphene (middle) and distibene (left).[60,61]

Tri-cyclohexyl/pentyl substituted phenyl ligands

More recently, the Power group described a new dispersion effect donor (DED) ligand which can stabilize a dimeric R_2SnSnR_2 complex both in solid state and solution.[62] The vast majority of distannene molecules (R_2SnSnR_2) have only weak Sn-Sn interactions and typically dissociate into monomeric stannylene (SnR_2) fragments in hydrocarbon solutions. However, the reaction of $SnCl_2$ with 2 equiv. of LiC_6H_2-2,4,6-Cy_3·OEt_2 (Cy = cyclohexyl) afforded a distannene $\{Sn(C_6H_2$-2,4,6-$Cy_3)_2\}_2$ (Figure 1.14), which remains a dimer in solution even upon heating to 100°C. Whereas the use of a less sterically demanding, hydrogen-poor ligand LiC_6H_2-2,4,6-Ph_3 (Ph = phenyl) afforded only the corresponding monomeric stannylene $:SnC_6H_2$-2,4,6-Ph_3 (Figure 1.14). Computational analysis revealed that stability of $\{Sn(C_6H_2$-2,4,6-$Cy_3)_2\}_2$ is a consequence of the London dispersion attraction between multiple close contacts of ligand C-H moieties across the Sn=Sn bond. The monomer $:SnC_6H_2$-2,4,6-Ph_3, however, does not associate to a dimer due to the lack of sufficient close H-H contacts.

Figure 1.14 Molecular structure of distannene $\{Sn(C_6H_2\text{-}2,4,6\text{-}Cy_3)_2\}_2$ (left) and stannylene $:SnC_6H_2\text{-}2,4,6\text{-}Ph_3$ (right). Close H-H contacts are shown as red dotted lines.

Given that the aryl ligand scaffold may be easily modified with various substituents, we became interested in examining how systematically modifying the bulk of the substituents on the aryl ring (that is, the number of C-H moieties) would affect the attraction between $:SnR_2$ units. We thus decided to investigate the tris(cyclopentyl)phenyl ligand, $\text{-}C_6H_2\text{-}2,4,6\text{-}Cyp_3$ (Cyp=cyclopentyl), which has one fewer CH2 unit per alkyl substituent compared to the $\text{-}C_6H_2\text{-}2,4,6\text{-}Cy_3$ ligand, anticipating that the isolated distannene, i.e., $\{Sn(C_6H_2\text{-}2,4,6\text{-}Cyp_3)_2\}_2$, may have significant structural or chemical differences in comparison to $\{Sn(C_6H_2\text{-}2,4,6\text{-}Cy_3)_2\}_2$. Details of this study (synthesis, characterization, computational evaluation and other analysis) are provided in Chapter 4.

References:

[1] R. Eisenschitz and F. London, Über das Verhältnis der van der Waalsschen Kräfte zu den homöopolaren Bindungskräften, *Z. Phys*. **1930**, *60*, 491-527.

[2] F. London, The General Theory of Molecular Forces, *Trans. Faraday Soc.* **1937**, *33*, 8-26.

[3] W. Callister. Fundamentals of Materials Science and Engineering: An Interactive. Text. John Wiley & Sons, Inc. **2000**, p. 25.

[4] R. G. Parr, Quantum Chemistry: Classic Scientific Papers, *Phys. Today*, **2001**, *54*, 63-64.

[5] P. P. Power, An Update on Multiple Bonding between Heavier Main Group Elements: The Importance of Pauli Repulsion, Charge-Shift Character, and London Dispersion Force Effects, *Organometallics*, **2020**, *39*, 4127-4138.

[6] J. Hwang, B. E. Dial, P. Li, M. E. Kozik, M. D. Smith and K. D. Shimizu, How Important Are Dispersion Interactions to the Strength of Aromatic Stacking Interactions in Solution? *Chem. Sci.* **2015**, *6*, 4358-4364.

[7] L. Andrezálová, Z. Országhová, Covalent and Noncovalent Interactions of Coordination Compounds with DNA: An Overview, *J. Inorg. Biochem.* **2021**, *225*, 111624-111640.

[8] M. Kolář, T. Kubař and P. Hobza, On the Role of London Dispersion Forces in Biomolecular Structure Determination. *J. Phys. Chem. B*, **2011**, *115*, 8038-8046.

[9] J. P. Wagner, P. R. Schreiner, London Dispersion in Molecular Chemistry-Reconsidering Steric Effects, *Angew. Chem. Int. Ed.* **2015**, *54*, 12274-12296.

[10] D. J. Liptrot, P. P. Power, London Dispersion Forces in Sterically Crowded Inorganic and Organometallic Molecules, *Nat. Rev. Chem.* **2017**, *1*, 1-12.

[11] M. A. Strauss and H. A. Wegner, Molecular Systems for the Quantification of London Dispersion Interactions, *Eur. J. Org. Chem.* **2019**, *2019*, 295-302.

[12] M. Bursch, E. Caldeweyher, A. Hansen, H. Neugebauer, S. Ehlert and S. Grimme, Understanding and Quantifying London Dispersion Effects in Organometallic Complexes, *Acc. Chem. Res.* **2019**, *52*, 258-266.

[13] D. L. Kays, Extremely Bulky Amide Ligands in Main Group Chemistry, *Chem. Soc. Rev.* **2016**, *45*, 1004-1018.

[14] H. Bürger, U. Wannagat, Silylamido-Verbindungen von Chrom, Mangan, Nickel Und Kupfer. *Monatsh. Chem.* **1964**, *95*, 1099-1102.

[15] B. Horvath, R. Möseler and E. G. Horvath, Manganese(II) Silylamides. *Zeitschrift für Anorg. und Allg. Chemie*, **1979**, *450*, 165-177.

[16] M. M. Olmstead, P. P. Power and S. C. Shoner, Three-Coordinate Iron Complexes: X-Ray Structural Characterization of the Iron Amide-Bridged Dimers $[Fe(NR_2)_2]_2$ (R = $SiMe_3$, C_6H_5) and the Adduct $Fe[N(SiMe_3)_2]_2(THF)$ and Determination of the Association Energy of the Monomer $Fe\{N(SiMe_3)_2\}_2$ in Solution. *Inorg. Chem.* **1991**, *30*, 2547-2551.

[17] B. D. Murray and P. P. Power, Three-Coordinate Metal Amides of Manganese(II) and Cobalt(II): Synthesis and X-Ray Structure of the First Tris(Silylamide) of Manganese and the X-Ray Crystal Structures of $[M_2(N(SiMe_3)_2)_4]$ (M = Mn, Co). *Inorg. Chem.* **1984**, *23*, 4584-4588.

[18] D. H. Woen, G. P. Chen, J. W. Ziller, T. J. Boyle, F. Furche and W. J. Evans, Solution Synthesis, Structure, and CO_2 Reduction Reactivity of a Scandium(II) Complex, $\{Sc[N(SiMe_3)_2]_3\}^-$. *Angew. Chem. Int. Ed.* **2017**, *56*, 2050-2053.

[19] M. A. Putzer, J. Magull, H. Goesmann, B. Neumüller and K. Dehnicke, Synthese, Eigenschaften Und Kristallstrukturen Der Titan(III)-Amido-Komplexe $Ti[N(SiMe_3)_2]_3$, $[TiCl_2\{N(SiMe_3)_2\}(THF)_2]$ Und $[Na(12\text{-Krone-}4)_2][TiCl_2\{N(SiMe_3)_2\}_2]$. *Chem. Ber.* **1996,** *129*, 1401-1405.

[20] C. L. Wagner, N. A. Phan, J. C. Fettinger, L. A. Berben and P. P. Power, New Characterization of $V\{N(SiMe_3)_2\}_3$: Reductions of Tris[Bis(Trimethylsilyl)Amido]Vanadium(III) and

Chromium(III) to Afford the Reduced Metal(II) Anions $[M\{N(SiMe_3)_2\}_3]^-$ (M = V and Cr). *Inorg. Chem.* **2019**, *58*, 6095-6101.

[21] R. D. Köhn, G. Kociok-Köhn and M. Haufe, The Chemistry of 1,3,5-Triazacyclohexane Complexes, 3. High Yield Synthesis of $[Cr\{N(SiMe_3)_2\}_3]$ and Accurate Structure Determination by Cocrystallization with Me_6Si_2. *Chem. Ber.* **1996**, *129*, 25-27.

[22] J. J. Ellison, P. P. Power and S. C. Shoner, First Examples of Three-Coordinate Manganese(III) and Cobalt(III): Synthesis and Characterization of the Complexes $M[N(SiMe_3)_2]_3$ (M = Mn or Co). *J. Am. Chem. Soc.* **1989**, *111*, 8044-8046.

[23] M. B. Hursthouse and P. F. Rodesiler, Crystal and Molecular Structure of Tris(Hexamethyldisilylamido)Iron(III). *J. Chem. Soc. Dalton Trans.* **1972**, *19*, 2100-2102.

[24] D. H. Harris and M. F. Lappert, Monomeric, Volatile Bivalent Amides of Group IVB Elements, $M(NR^1_2)_2$ and $M(NR^1R^2)_2$ (M=Ge, Sn, or Pb; $R^1 = Me_3Si$, $R^2 = Me_3C$), *J. C. S. Chem. Commun.* **1974**, *21*, 895-896.

[25] D. J. Liptrot, J.-D. Guo, S. Nagase and P. P. Power, Dispersion Forces, Disproportionation, and Stable High-Valent Late Transition Metal Alkyls. *Angew. Chem. Int. Ed.* **2016**, *55*, 14766-14769.

[26] M. M. Hänninen, K. Pal, B. M. Day, T. Pugha and R. A. Layfield, A Three-Coordinate Iron–Silylene Complex Stabilized by Ligand–Ligand Dispersion Forces. *Dalton Trans.* **2016**, *45*, 11301-11305.

[27] C. L. Wagner, L. Tao, E. J. Thompson, T. A. Stich, J. Guo, J. C. Fettinger, L. A. Berben, R. D. Britt, S. Nagase and P. P. Power, Dispersion-Force-Assisted Disproportionation: A Stable Two-Coordinate Copper(II) Complex, *Angew. Chem. Int. Ed.* **2016**, *55*, 10444-10447.

[28] C.-Y. Lin, J. Guo, J. C. Fettinger, S. Nagase, F. Grandjean, G. J. Long, N. F. Chilton and P. P. Power, Dispersion Force Stabilized Two-Coordinate Transition Metal–Amido Complexes of the –N(SiMe$_3$)Dipp (Dipp = C$_6$H$_3$-2,6-Pri_2) Ligand: Structural, Spectroscopic, Magnetic, and Computational Studies, *Inorg. Chem.* **2013**, *52*, 13584-13593.

[29] C. L. Wagner, L. Tao, J. C. Fettinger, R. David Britt and P. P. Power, Two-Coordinate, Late First-Row Transition Metal Amido Derivatives of the Bulky Ligand -N(SiPri_3)Dipp (Dipp = 2,6 diisopropylphenyl): Effects of the Ligand on the Stability of Two-Coordinate Copper(II) Complexes, *Inorg. Chem.* **2019**, *58*, 8793-8799.

[30] K. L. Mears, C. R. Stennett, E. K. Taskinen, C. E. Knapp, C. J. Carmalt, H. M. Tuononen, and P. P. Power, Molecular Complexes Featuring Unsupported Dispersion-Enhanced Aluminum–Copper and Gallium–Copper Bonds, *J. Am. Chem. Soc.* **2020**, *142*, 19874-19878.

[31] R. Y. Kong and M. R. Crimmin, 1st Row Transition Metal Aluminylene Complexes: Preparation, Properties and Bonding Analysis, *Dalton Trans.* **2021**, *50*, 7810-7817.

[32] I. Kalvet, K. Deckers, I. Funes-Ardoiz, G. Magnin, T. Sperger, M. Kremer and F. Schoenebeck, Selective ortho-Functionalization of Adamantylarenes Enabled by Dispersion and an Air-Stable Palladium(I) Dimer, *Angew. Chem. Int. Ed.* **2020**, *59*, 7721-7725.

[33] T. Ikawa, Y. Yamamoto, A. Heguri, Y. Fukumoto, T. Murakami, A. Takagi, Y. Masuda, K. Yahata, H. Aoyama, Y. Shigeta, H. Tokiwa and S. Akai, Could London Dispersion Force Control Regioselective (2 + 2) Cyclodimerizations of Benzynes? YES: Application to the Synthesis of Helical Biphenylenes, *J. Am. Chem. Soc.* **2021**, *143*, 10853-10859.

[34] K. L. Mears, C. R. Stennett, J. C. Fettinger, P. Vasko and P. P. Power, Inhibition of Alkali Metal Reduction of 1-Adamantanol by London Dispersion Effects, *Angew. Chem. Int. Ed.* **2022**, *61*, e202201318.

[35] B. K. Bower and H. G. Tennent, Transition Metal Bicyclo[2.2.1]hept-1-yls, *J. Am. Chem. Soc.* **1972**, *94*, 2512-2514.

[36] E. K. Byrne, D. S. Richeson and K. H. Theopold, Tetrakis(1-norbornyl)cobalt, A Low Spin Tetrahedral Complex of A First Row Transition Metal, *J. Chem. Soc. Chem. Commun.* **1986**, *19*, 1491-1492.

[37] D. J. Liptrot, J.-D. Guo, S. Nagase and P. P. Power, Dispersion Forces, Disproportionation, and Stable High-Valent Late Transition Metal Alkyls, *Angew. Chem. Int. Ed.* **2016**, **55**, 14766-14769.

[38] B. Twamley, S. T. Haubrich and P. P. Philip, Element Derivatives of Sterically Encumbering Terphenyl Ligands, *Adv. Organomet. Chem.* **1999**, *44*, 1-65.

[39] E. Rivard and P. P. Power, Multiple Bonding in Heavier Element Compounds Stabilized by Bulky Terphenyl Ligands, *Inorg. Chem.* **2007**, *46*, 10047-10064.

[40] D. L. Kays, the Stabilization of Organometallic Complexes Using m-Terphenyl Ligands, *Organomet. Chem.* **2010**, *36*, 56-76.

[41] M. L. McCrea-Hendrick, M. Bursch, K. L. Gullett, L. R. Maurer, J. C. Fettinger, S. Grimme and P. P. Power, Counterintuitive Interligand Angles in the Diaryls E{C_6H_3-2,6-(C_6H_2-2,4,6-*i*Pr_3)$_2$}$_2$ (E = Ge, Sn, or Pb) and Related Species: The Role of London Dispersion Forces, *Organometallics* **2018**, *37*, 2075-2085.

[42] D. J. Liptrot and P. P. Power, London Dispersion Forces in Sterically Crowded Inorganic and Organometallic Molecules, *Nat. Rev. Chem.* **2017**, *1*, 0004pp.

[43] R. S. Simons, L. Pu, M. M. Olmstead, P. P. Power, Synthesis and Characterization of the Monomeric Diaryls M{C_6H_3-2,6-Mes_2}$_2$ (M = Ge, Sn, or Pb; Mes = -2,4,6-$Me_3C_6H_2$) and Dimeric

Aryl-Metal Chlorides [M(Cl){C6H$_3$-2,6-Mes$_2$}]$_2$ (M = Ge or Sn), *Organometallics*, **1997**, *16*, 1920-1925.

[44] P. Wilfling, K. Schittelkopf, M. Flock, R. H. Herber, P. P. Power and R. C. Fischer, Influence of Ligand Modifications on Structural and Spectroscopic Properties in Terphenyl Based Heavier Group 14 Carbene Homologues, *Organometallics*, **2015**, *34*, 2222-2232.

[45] G. H. Spikes, Y. Peng, J. C. Fettinger and P. P. Power, Synthesis and Characterization of the Monomeric Sterically Encumbered Diaryls E{C$_6$H$_3$-2,6-(C$_6$H$_3$-2,6-Pr*i*$_2$)$_2$}$_2$ (E = Ge, Sn, or Pb), *Z. Anorg. Allg. Chem.* **2006**, *632*, 1005-1010.

[46] G. L. Wegner, R. J. F. Berger, A. Schier and H. Schmidbaur, Ligand-Protected Strain-Free Diarylgermylenes, *Organometallics*, **2001**, *20*, 418-423.

[47] B. D. Rekken, T. M. Brown, J. C. Fettinger, F. Lips, H. M. Tuononen, R. H. Herber and P. P. Power, Dispersion Forces and Counterintuitive Steric Effects in Main Group Molecules: Heavier Group 14 (Si–Pb) Dichalcogenolate Carbene Analogues with Sub-90° Interligand Bond Angles, *J. Am. Chem. Soc.* **2013**, *135*, 10134-10148.

[48] J. D. Queen, S. Irvankoski, J. C. Fettinger, H. M. Tuononen and P. P. Power, A Monomeric Aluminum Imide (Iminoalane) with Al–N Triple Bonding: Bonding Analysis and Dispersion Energy Stabilization, *J. Am. Chem. Soc.* **2021**, *143*, 6351-6356.

[49] Y. Wang, Y. Xie, P. Wei, R. B. King, H. F. Schaefer III, P. von R. Schleyer and G. H. Robinson, *Science*, **2008**, *321*, 1069-1071.

[50] J. P. Wagner and P. R. Schreiner, London Dispersion Decisively Contributes to the Thermodynamic Stability of Bulky NHC-Coordinated Main Group Compounds, *J. Chem. Theory Comput.* **2016**, *12*, 231-237.

[51] Y. Wang, Y. Xie, P. Wei, R. B. King, H. F. Schaefer III, P. v. R. Schleyer and G. H. Robinson, Carbene-Stabilized Diphosphorus, *J. Am. Chem. Soc.* **2008**, *130*, 14970-14971.

[52] O. Back, B. Donnadieu, P. Parameswaran, G. Frenking and G. Bertrand, Isolation of Crystalline Carbene-Stabilized P_2-Radical Cations and P_2-Dications, *Nat. Chem.* **2010**, *2*, 369-373.

[53] D. Dhara, P. Kalita, S. Mondal, R. S. Narayanan, K. R. Mote, V. Huch, M. Zimmer, C. B. Yildiz, D. Scheschkewitz, V. Chandrasekhar and A. Jana, Reactivity Enhancement of a Diphosphene by Reversible N-heterocyclic Carbene Coordination, *Chem. Sci.* **2018**, *9*, 4235-4243.

[54] A. Beil, R. J. Gilliard Jr. and H. Grützmacher, From the Parent Phosphinidene–Carbene Adduct NHC=PH to Cationic P_4-rings and P_2-cycloaddition Products, *Dalton Trans.* **2016**, *45*, 2044-2052.

[55] O. Back, G. Kuchenbeiser, B. Donnadieu and G. Bertrand, Nonmetal-Mediated Fragmentation of P_4: Isolation of P_1 and P_2 Bis(carbene) Adducts, *Angew. Chem.* **2009**, *121*, 5638-5641.

[56] M. Y. Abraham, Y. Wang, Y. Xie, P. Wei, H. F. Schaefer III, P. von R. Schleyer and G. H. Robinson, Carbene Stabilization of Diarsenic: From Hypervalency to Allotropy, *Chem. Eur. J.* **2010**, *16*, 432-435.

[57] M. Y. Abraham, Y. Wang, Y. Xie, R. J. Gilliard, Jr., P. Wei, B. J. Vaccaro, M. K. Johnson, H. F. Schaefer III, P. v. R. Schleyer and G. H. Robinson, Oxidation of Carbene-Stabilized Diarsenic: Diarsene Dications and Diarsenic Radical Cations, *J. Am. Chem. Soc.* **2013**, *135*, 2486–2488.

[58] L. P. Ho and M. Tamm, Stabilization of a Bismuth-Bismuth Double Bond by Anionic N-Heterocyclic Carbenes, *Dalton Trans.* **2021**, *50*, 1202-1205.

[59] R. Deka and A. Orthaber, Carbene Chemistry of Arsenic, Antimony, and Bismuth: Origin, Evolution and Future Prospects, *Dalton Trans*. **2022**, *51*, 8540-8556.

[60] L. P. Ho, A. Nasr, P. G. Jones, A. Altun, F. Neese, G. Bistoni and M. Tamm, London Dispersion Interactions in Pnictogen Cations $[ECl_2]^+$ and $[E{=}E]_2^+$ (E=P, As, Sb) Supported by Anionic N-Heterocyclic Carbenes, *Chem. Eur. J.* **2018**, *24*, 18922-18932.

[61] L. P. Ho, M.-K. Zaretzke, T. Bannenberg and M. Tamm, Heteroleptic Diphosphenes and Arsaphosphenes Bearing Neutral and Anionic N-heterocyclic Carbenes, *Chem. Commun*. **2019**, *55*, 10709-10712.

[62] C. R. Stennett, M. Bursch, J. C. Fettinger, S. Grimme and P. P. Power, Designing a Solution-Stable Distannene: the Decisive Role of London Dispersion Effects in the Structure and Properties of $\{Sn(C_6H_2\text{-}2,4,6\text{-}Cy_3)_2\}_2$ (Cy = Cyclohexyl), *J. Am. Chem. Soc*. **2021**, *143*, 21478-21483.

Chapter 2. Dimeric Copper and Lithium Thiolates: Comparison of Copper Thiolates with Their Lithium Congeners

Wenxing Zou, Qihao Zhu, James C. Fettinger and Philip P. Power*

Department of Chemistry, University of California, One Shields Avenue, Davis, California 95616, United States

Reprinted with permission from *Inorg. Chem.* **2021**, *60*, 17641-17648.

ABSTRACT: The direct reactions of the large terphenyl thiols $HSAr^{iPr4}$ (Ar^{iPr4}= -C_6H_3-2,6-(C_6H_3-2,6-iPr_2)$_2$) and $HSAr^{iPr6}$ (Ar^{iPr6}= -C_6H_3-2,6-(C_6H_2-2,4,6-iPr_3)$_2$) with stoichiometric amounts of mesitylcopper(I) in THF at ca. 80°C afforded the first well-characterized dimeric copper thiolato species {$CuSAr^{iPr4}$}$_2$ (**1**) and {$CuSAr^{iPr6}$}$_2$ (**2**) with elimination of mesitylene. The complexes **1** and **2** were characterized by NMR and electronic spectroscopy as well as by X-ray crystallography. They have dimeric Cu_2S_2 core structures in which the two copper atoms are bridged by the sulfurs from the thiolato ligands and feature short Cu--Cu distances near 2.4 Å as well as an apparent weak copper-flanking aryl ring interaction from a terphenyl substituent. The structures of the planar Cu_2S_2 cores bear a resemblance to the Cu_A site in nitrous oxide reductase in which two cysteines also bridge two copper atoms. The related dimeric Li_2S_2 structural motif was also observed in the lithium congeners {$LiSAr^{iPr4}$}$_2$ (**3**) and {$LiSAr^{iPr6}$}$_2$ (**4**) which were synthesized directly from the thiols and *n*-BuLi in hexanes. However, despite the very similar effective ionic radii of the Li^+ (0.59 Å) and Cu^+ (0.60 Å) ions, the Li--Li structures display very much longer

(more than ca. 0.5 Å) separations than the corresponding Cu--Cu distances in **1** and **2**, probably as a result of weaker dispersion interactions.

INTRODUCTION

As a class of coordination compounds, metal thiolates have received much attention due to their widespread relevance for many scientific fields, such as bioinorganic chemistry,[1-4] medicine,[5-7] organic synthesis[8-11] and materials science.[12,13] Several metals such as Zn or Cu prefer to coordinate to soft donor atoms such as sulfur,[14] and metal-sulfur bonds are widely present in sulfur-containing proteins which play an important role in maintaining physiological functions. For example, the Cu_A site, a copper containing active site features two copper ions bridged by thiolato ligands (cysteine residues) is found in various enzymes, such as cytochrome c oxidase (CcO),[15,16] and nitrous oxide reductase (N_2OR),[17,18] functions as electron transfer (ET) center in both prokaryotic and eukaryotic cells.[19]

There has been a keen interest in the structures and properties of copper thiolates for many decades. Early work involved the preparation of isolable, stable polynuclear complexes[20-24] or cage compounds[25,26] as well as studies of their magnetic properties. Nevertheless, neutral copper thiolates, which can have aggregation numbers from 3-12,[27] remain relatively rare, and relatively a few structures have been reported. These include those of the trimeric species $\{CuSAr^{Me6}\}_3$ (Ar^{Me6}=-C_6H_3-2,6-(C_6H_2-2,4,6-Me_3)$_2$),[28] the tetrameric $\{CuSC_6H_3\text{-}2,6\text{-}(SiMe_3)_2\}_4$,[29] the hexameric $\{Cu(SC_5H_4N)\}_6$,[30] the octameric $\{CuSC_6H_2\text{-}2,4,6\text{-}iPr_3\}_8$[21] and higher aggregated dodecameric $\{CuSC_6H_4\text{-}2\text{-}SiMe_3\}_{12}$.[24] Bulky alkyl ligands also have been used to synthesize copper(I) thiolato complexes with lower aggregation.[31,32] The higher level of aggregation stems from the excellent bridging characteristics of the thiolato ligands which dictates that they exist as

oligomers or polymers,[33,34] rendering them more difficult to characterize. The standard way to lower aggregation is to use bulky substituents to provide sufficient steric hindrance to prevent association.[35,36] For example, the use of terphenyl substituents at sulfur has proved effective in stabilizing several well-defined molecular metal thiolate species (Figure 2.1). For copper(I) thiolates, the tetrameric copper(I) salt $\{CuSC_6H_3\text{-}2,6\text{-}(SiMe_3)_2\}_4$[29] was isolated by the treatment of $[Cu(CH_3CN)_4]PF_6$ with the corresponding thiol $HSC_6H_3\text{-}2,6\text{-}(SiMe_3)_2$, and the trimeric complex $\{CuSAr^{Me6}\}_3$ (Ar^{Me6}=-C_6H_3-2,6-(C_6H_2-2,4,6-Me_3)$_2$)[28] was prepared by simple salt metathesis reactions of a copper halide with potassium thiolates.

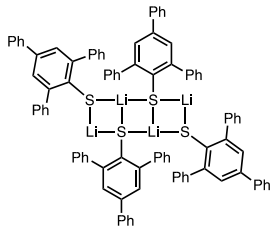

a), Ref: 40

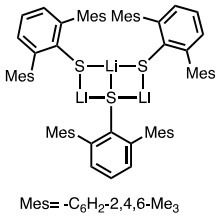

b), Ref: 40

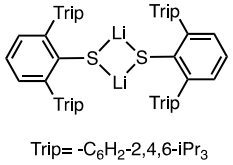

c), Ref: 40

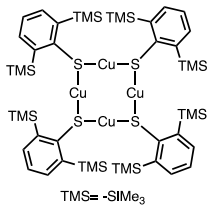

d), Ref: 29

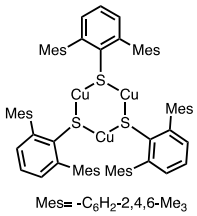

e), Ref. 28

Figure 2.1 Drawings of some of the structure of the known neutral lithium and copper(I) thiolato derivatives of various sterically encumbering aromatic substituents a)-e).[28,29,40]

In essence, these ligands[35-39] have enabled the formation and characterization of several new, characterizable metal thiolato derivatives of the alkali metals[40] and of the first row transition

metals.[35,37] The synthesis and characterization of the THF complexed monomeric lithium salt, $Li(THF)_3SC_6H_2$-2,4,6-Ph_3[41] and an alkyl lithium thiolate complex $[Li_2(thf)_4\{SCH(SiMe_3)_2\}_2]$[42] were reported by Power and coworkers. Later, the structures of Lewis base-free heavier alkali metal (Na, K, Rb and Cs) thiolate salts with different aggregation numbers were described,[40] which showed that aggregation states could be tuned by changing the steric properties of the ligands. It is noteworthy that lithium and copper(I) cations have similar ionic radii (0.59 Å, Li^+ and 0.60 Å, Cu^+)[43] for four-coordinate ions, such that the lithium and copper(I) thiolates might be expected to have similar structural parameters. However, some major differences are observed in the structures of the Li and Cu thiolates even when they have the same aggregation numbers. For instance, in the tetrameric lithium thiolate $\{LiSC_6H_2$-2,4,6-$Ph_3\}_4$ (Figure 1. a)), which has a ladder structure, two of the Li^+ ions are three-coordinate whereas the other two Li^+ ions are two-coordinate. In contrast, in the tetrameric copper(I) thiolate $\{CuSC_6H_3$-2,6-$(SiMe_3)_2\}_4$ (Figure 1. d)) is an essentially square Cu_4 core in which all of the Cu atoms are two-coordinate. A related discrepancy is seen in the structures of the Li thiolate $\{LiSAr^{Me6}\}_3$ (Figure 1. b)) which features one three-coordinate lithium ion and two lithium ions that are two-coordinate, as well as its trimeric copper congener $\{CuSAr^{Me6}\}_3$ (Figure 1. e)) which has a cyclic Cu_3S_3 array in which three copper ions alternate with three thiolato sulfurs. Dimeric copper(I) thiolate complexes remain unknown to date, so that a comparison of the structures of lithium and copper thiolato complexes is not possible. Herein we describe the reactions of two large terphenyl thiols with a stoichiometric amount of mesitylcopper(I) to afford the dimeric complexes (**1**) and (**2**) (Figure 3), or with *n*-BuLi to yield the corresponding dimeric lithium species $\{LiSAr^{iPr4}\}_2$ (**3**) (Figure 3). The three complexes have similar structural parameters with the exception of their metal-metal separations.

EXPERIMENTAL SECTION

General considerations. All manipulations were carried out under anaerobic and anhydrous conditions by using Schlenk techniques or in a Vacuum Atmospheres OMNI-Lab drybox under an atmosphere of dry argon or nitrogen. Solvents were dried by the method of Grubbs[44] and co-workers, stored over potassium or sodium, and then degassed by the freeze-pump-thaw method. All physical measurements were made under strictly anaerobic and anhydrous conditions. The NMR spectra were recorded on a Varian Inova 600 MHz spectrometer, and the ^{1}H NMR spectra were referenced to the residual solvent signals in deuterated benzene, while the ^{13}C NMR spectra were referenced to the residual solvent signals in deuterated THF. IR spectra were recorded as Nujol mulls between CsI plates on a PerkinElmer 1430 spectrometer. UV−vis spectra were recorded as dilute hexane solutions in 3.5 mL quartz cuvettes using an Olis 17 modernized Cary 14 UV−vis−near-IR spectrophotometer or an HP 8452 diode-array spectrophotometer. The terphenyl thiols HSAr^{iPr4}, HSAr^{iPr6} [45] and mesitylcopper(I)[46] were prepared via literature methods. Unless otherwise stated, all materials were obtained from commercial sources and used as received.

{CuSAr^{iPr4}}$_2$ (1): The solid terphenyl thiol HSAr^{iPr4} [45] (0.43 g, 1 mmol) was mixed with solid mesitylcopper(I) (0.182 g, 1 mmol), and ca. 60 mL of THF was added. The solution was heated at 80^{o}C for 2 days, resulting in a pale yellow color. After removal of the solvent under reduced pressure, the pale yellow residue was extracted with ca. 50 mL of hexane. The solution was filtered through celite and concentrated to ca. 15 mL under reduced pressure until the formation of small colorless crystals was observed. The solution was stored in a ca. -18 ^{o}C freezer for 4 days to yield 0.113 g (23%) of **1** as colorless crystals which were suitable for X-ray crystallography. Mp: 252-254^{o}C. ^{1}H NMR (600 MHz, benzene-d_6): δ= 7.06 (d, J = 7.5 Hz, 4H), 6.95 (t, J = 7.5 Hz, 2H),

6.90 (d, *J* = 7.9 Hz, 2H), 6.86 (dd, *J* = 8.5, 6.2 Hz, 1H), 2.83 – 2.75 (m, 4H), 1.32 (d, *J* = 6.9 Hz, 12H), 1.00 (d, *J* = 6.9 Hz, 12H). ^{13}C NMR (150 MHz, THF-d_8): δ= 146.6, 143.2, 141.7, 141.5, 128.6, 122.9, 122.0, 121.8, 30.7, 23.9, 23.6. UV/vis: λ/nm (ε/M^{-1} cm^{-1}): 292 (1700). IR (Nujol; $\tilde{\nu}$/cm^{-1}): 1920w, 1570w, 1453s, 1418w, 1373s, 1350m, 1320w, 1245w, 1170w, 1100m, 1076w, 1053m, 1036m, 995w, 960w, 929w, 916w, 892w, 810m, 795m, 781s, 751s, 738s, 694m, 797w, 622w, 597w, 571w, 540w, 499w, 461m, 398w, 270w.

{CuSAr^{iPr6}}$_2$ (2): The synthesis of **2** was accomplished in a similar manner to the preparation of **1** with the use of the terphenyl thiol HSAr^{iPr6} [45] (0.514 g, 1 mmol) and mesitylcopper(I) (0.182 g, 1 mmol) in ca. 60 mL of THF, which yielded 0.155 g (27%) colorless crystals which were suitable for X-ray crystallography. Mp: 233-237°C. ^{1}H NMR (600 MHz, benzene-d_6): δ= 7.16 (s, 5H), 6.89 (d, *J* = 7.3 Hz, 2H), 6.83 (d, *J* = 7.3 Hz, 1H), 2.87 (dt, *J* = 13.9, 7.0 Hz, 6H), 1.42 (d, *J* = 6.8 Hz, 12H), 1.29 (d, *J* = 6.9 Hz, 12H), 1.12 (d, *J* = 6.7 Hz, 12H). ^{13}C NMR (150 MHz, THF-d_8): δ= 148.5, 147.5, 144.7, 139.7, 131.3, 123.7, 122.6, 36.0, 32.4, 25.6, 25.4. UV/vis: λ/nm (ε/M^{-1} cm^{-1}): 291 (1700). IR (Nujol; $\tilde{\nu}$/cm^{-1}): 1600s, 1376s, 1359m, 1314w, 1172w, 1106w, 1052w, 946w, 877m, 801m, 772w, 748w, 741w, 733w, 651w.

{LiSAr^{iPr4}}$_2$ (3): *n*-BuLi (0.31 mL of a 2.5 M solution in *n*-hexane) was added dropwise to a stirred solution HSAr^{iPr4} [45] (0.30 g, 0.7 mmol) in ca. 30 mL of toluene at 0°C. The reaction was allowed to warm slowly to room temperature after the addition and stirred for another 12 h whereupon the solvent was removed under reduced pressure. The white residue was redissolved in *ca*. 15 mL of toluene and filtered. Storage in a -30 °C freezer for 5 days afforded 0.11 g (33%) of colorless crystals that were suitable for X-ray crystallographic studies. Mp: 196-198°C. ^{1}H NMR (600 MHz, benzene-d_6): δ= 7.16 (s, 5H), 7.12 (s, 1H), 7.03 (d, *J* = 7.4 Hz, 2H), 6.95 (dd, *J* = 8.1, 6.8 Hz, 1H), 2.81–2.73 (m, 4H), 1.20 (d, *J* = 6.9 Hz, 12H), 1.05 (d, *J* = 6.9 Hz, 12H). ^{13}C

NMR (150 MHz, THF-d_8): δ= 156.5, 148.4, 146.5, 145.0, 129.2, 127.1, 123.3, 118.6, 32.1, 26.0, 25.6. UV/vis: λ/nm (ε/M^{-1} cm^{-1}): 294 (1500). IR (Nujol; $\tilde{\nu}$/cm^{-1}): 1569m, 1465s, 1383s, 1359m, 1330w, 1265w, 1255w, 1180w, 1111w, 1088w, 1064w, 1050m, 942w, 929w, 815m, 790m, 772m, 761s, 749s, 709m, 692w, 586w, 555w, 481, 387w, 330w.

X-ray Crystallographic Studies. X-ray-quality crystals of complexes **1** and **2** were obtained from concentrated hexane solution at -18ºC after 4 to 5 days, **3** was recrystallized from concentrated toluene, as described in the Experimental Section. Single crystals were removed from Schlenk tubes and immediately covered with a layer of hydrocarbon oil. Suitable crystals were selected, mounted on a nylon cryo loop, and then placed in the cold nitrogen stream of the diffractometer. Data for **1-3** were collected at 90(2) K with Cu $K\alpha_1$ radiation (λ = 1.5418 Å) using a Bruker DUO diffractometer in conjunction with a CCD detector. The collected reflections were corrected for Lorentz and polarization effects and for absorption by using Blessing's method as incorporated into the program SADABS.[47,48] The structures were solved by direct methods and refined with the SHELXTL (2012, version 6.1) or SHELXTL (2013) software packages.[49] Refinement was by full-matrix least-squares procedures, with all carbon-bound hydrogen atoms included in calculated positions and treated as riding atoms. The thermal ellipsoid plots were drawn using OLEX2 software.[50] A summary of the crystallographic and data collection parameters is given in the Supporting Information (SI).

RESULTS AND DISCUSSION

Synthesis

A number of homoleptic metal (alkali metal[40] and the first-row transition metal[35]) thiolate complexes with various aggregation numbers have been reported and their structures and

properties have been intensively studied. Treatment of thiols with *n*-BuLi has been shown to be an efficient method to obtain the lithium thiolates,[40] while sodium and potassium thiolates can be prepared by direct treatment of thiols with elemental sodium[40] or potassium.[40] The first row transition metal complexes were generally synthesized by treating metal halides with the relevant lithium thiolates or sodium thiolates.[35] For the synthesis of Cu(I) thiolates, various routes have used reagents that have proved to be useful copper sources, for instance, $[Cu(CH_3CN)_4]PF_6$ has been used to synthesize copper(I) thiolato and selenolato complexes,[28] Cu(I) halides[51] and $CuBr(SMe_2)$[52] have proved to be useful copper reagents in producing three-coordinate copper thiolato polymers and trinuclear copper thiolato species, and mesitylcopper(I) has been used to produce copper oxides[53] and copper amides.[54]

Initially, we investigated the treatment of a Cu(I) alkyl $\{CuCH_2SiMe_3\}_4$[55] with the terphenyl thiol $HSAr^{iPr4}$ with the elimination of volatile $SiMe_4$ to synthesize dimeric Cu(I) thiolates (Figure 2.2), however, this reaction resulted in considerable decomposition of the copper alkyl to produce copper metal.

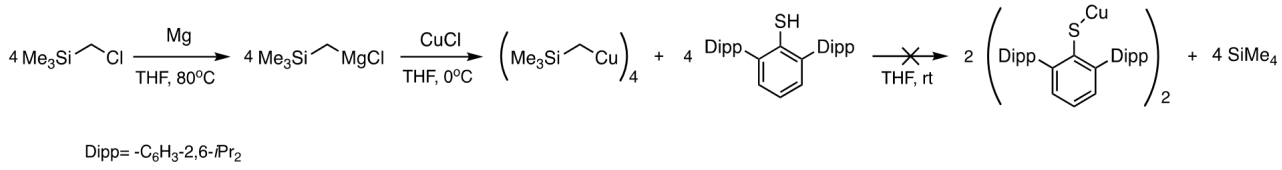

Figure 2.2 Attempted use of $\{CuCH_2SiMe_3\}_4$ for the synthesis of dimeric $\{CuSAr^{iPr4}\}_2$.

We then turned to the use of the more robust mesitylcopper(I) which had been earlier used to obtain the chalcogenide terphenyloxocopper(I) $\{CuOC_6H_3\text{-}2,6\text{-}Ph_2\}_4$[53] or the copper(I) amide $\{CuN\textit{n}Bu_2\}_4$[54] at ambient temperature, the reactions of the terphenyl thiols and a stoichiometric amount of mesitylcopper(I) at 80°C yielded the desired complexes **1** and **2** as shown in Figure 3.

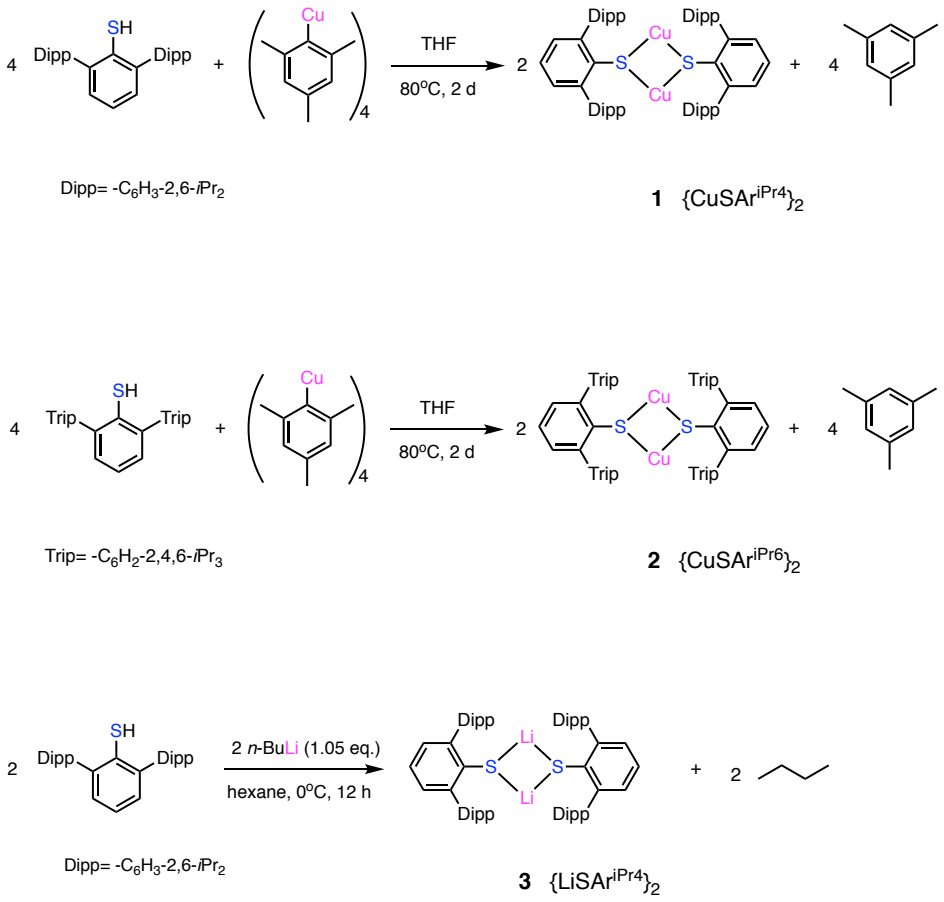

Figure 2.3 Synthesis of complexes **1**-**3**.

The synthesis of complexes **1** and **2** is summarized in Figure 2.3. They were obtained with 23-27% yield by metathesis of the appropriate terphenyl thiols and mesitylcopper(I). The straightforward addition of the terphenyl thiols to mesitylcopper(I) in THF gave pale yellow solutions. The conversions were incomplete at room temperature, but heating at ca. 80°C for 2 days afforded the products **1** and **2**, the mesitylene that was eliminated as the byproduct was observed in the crude ^{1}H NMR spectrum of the reaction mixture. Hexane was chosen as the solvent to grow single crystals of **1** and **2** that were large enough for single crystal X-ray diffraction.

The lithium complex **3** was synthesized (Figure 2.3) in a manner similar to that previously reported for $\{LiSAr^{iPr6}\}_2$.[35] The reaction involved the dropwise addition of a stoichiometric amount 2.5 M *n*-BuLi to a chilled hexane solution of $HSAr^{iPr4}$ at ca. 0°C, the reaction was then allowed to warm to room temperature and stirred overnight. Filtration and concentration under reduced pressure to afford the product in improved yield. Slow addition rates and low temperature are essential since too rapid an addition of *n*-BuLi to $HSAr^{iPr4}$ results in uncontrolled heating. The solution was stored in a ca. -30°C freezer for 5 days to yield crystals of **3** in 33% yield that were suitable for X-ray crystallography.

Structures

The molecular structures of compounds **1** and **2** are shown in Figure 2.4, and important bond distances and angles are given in Table 1. In the solid state, both **1** and **2** have centrosymmetric dimeric structures with planar Cu_2S_2 (a sum of interior angles of 360.0(17)°) core in which the two Cu atoms are bridged by sulfurs from two terphenyl thiolato ligands. In each case, the Cu atoms are coordinated to two thiolato sulfurs so as to produce a V-shaped metal coordination geometry with S-Cu-S angles in the range 115.32(17)-116.87(19)° and Cu-S-Cu angles in the range 63.14(19)-64.68(17)°. The bridging 3-coordinate thiolato sulfur atoms have pyramidal coordination ($\sum\angle°S = 283.97(5)°$ for complex **1** and $\sum\angle°S = 281.79(5)°$ for complex **2**). Complex **1** has different C-S-Cu angles with a wider C1-S1-Cu1 angle (120.21(5)°) than the C1-S1-Cu1′ angle (99.08(5)°), differ by 21.13(5)°. In addition to the unequal C-S-Cu angles, there is a long Cu−η^6 arene interaction between the Cu atom and the centroid of the flanking aryl ring (Cu-centroid distance is 2.39 (6) Å), which is also seen in complex **2** (a Cu-centroid distance of 2.44(7) Å). Inspection of the Cu1−S−Cu1′ angles in **1** and **2** shows that the change of thiolato ligand from SAr^{iPr4} to the_bulkier SAr^{iPr6} group causes a small narrowing of the Cu1−S−Cu1′ angle from

64.68(17)º to 63.14(19)º and a wider S1-Cu-S1′ angle from 115.32(17)º to 116.87(19)º, but the C-S bond lengths (1.78(14) Å for **1** and **2**) in both complexes are essentially the same. The Cu-S bond lengths in **1** and **2** range from 2.28(6) Å to 2.32(7) Å, which are in the normal range for Cu thiolates,[56] but marginally longer than that reported by Walensky and co-workers for the related trimer $\{CuSAr^{Me6}\}_3$.[28] The longer Cu-S bond lengths in **1** and **2** are consistent with the increased bulkiness of the ligands.[29] The Cu--Cu distances in complex **1** and **2** are 2.452(2) Å and 2.410(7) Å, respectively, which are greater than the sum of the covalent radii (2.24 Å) of the two Cu atoms,[57] which does not establish metal-metal bonding, but are within the sum of the van der Waals radii (2.8 Å),[58] suggesting the presence of a correlation-dispersion interaction.[59-61] Additionally, the Cu--Cu distances in both complexes are comparable to those in some previously reported copper(I) complexes,[59,62] and these Cu--Cu distances, in conjunction with computational studies,[59,62] concluded that the Cu--Cu separations in **1** and **2** do not indicate the presence of Cu-Cu bonds. Moreover, it is noteworthy that the Cu--Cu distance of **2** is slightly longer than that of **1**, which produces higher dispersion energy due to the increased numbers of isopropyl groups. The Cu--Cu distances in complex **1** and **2** are considerably shorter than the Cu--Cu distances in Walensky's terphenyl thiolato complex $\{CuSAr^{Me6}\}_3$ (2.85-2.92 Å)[28] and are ca. 0.1 Å shorter than the Cu--Cu distance of the Cu_A site in nitrous oxide reductase (2.51 Å).[63]

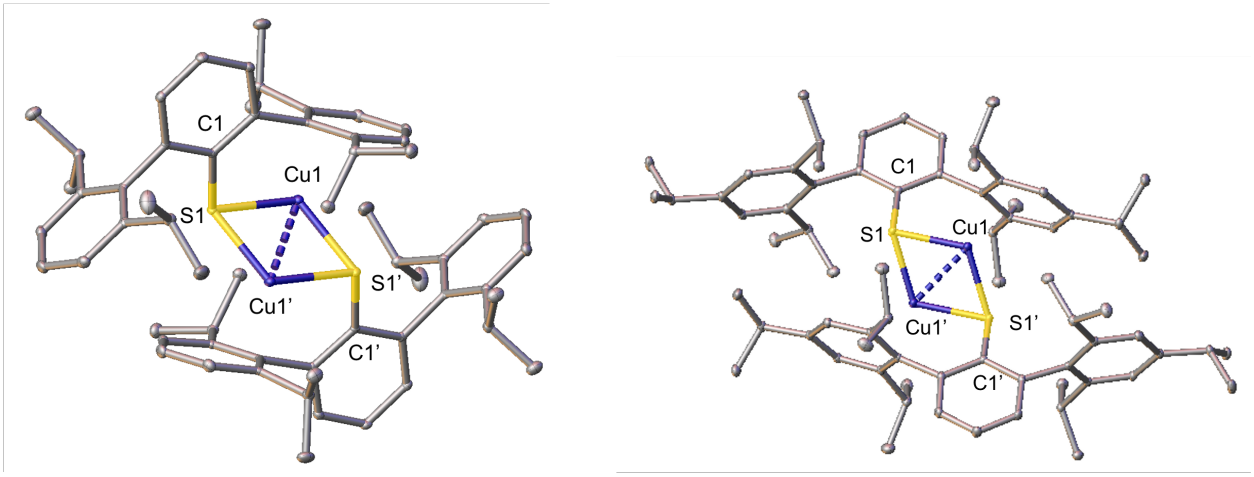

1 **2**

Figure 2.4 Molecular structures of complex **1** (top) and **2** (bottom) with thermal ellipsoids shown at 30% probability. Hydrogen atoms are not shown. Selected bond lengths (Å) and angles (deg) for **1**: S1-Cu1 2.29(6), S1-Cu1′ 2.29(4), S1-C1 1.78(14), Cu1--Cu1′ 2.45(6), C1-S1-Cu1 121.21(5), C1-S1-Cu1′ 99.08(5), Cu1-S1-Cu1′ 64.68(17), S1-Cu1-S1′ 115.32(17). Selected bond lengths (Å) and angles (deg) for **2**: S1-Cu1 2.32(4), S1-Cu1′ 2.28(6), S1-C1 1.78(14), Cu1--Cu1′ 2.41(7), C1-S1-Cu1 121.90(5), C1-S1-Cu1′ 96.75(5), Cu1-S1-Cu1′ 63.14(19), S1-Cu1-S1′ 116.87(19).

The lithium thiolate $\{LiSAr^{iPr4}\}_2$ (**3**) was recrystallized from toluene as a centrosymmetric dimer, the crystals are isomorphous with those of the copper congeners and its molecular structure is depicted in Figure 2.5. It has planar Li_2S_2 core (a sum of interior angles of 360.00(13)°) featuring two bridging thiolato groups which is also very similar to that seen in the lithium thiolate $\{LiSAr^{iPr6}\}_2$ (**4**).[46] The lithium ions also interact with an ortho Trip ring to afford a short Li-centroid distance of 2.13(4) Å, which is relatively shorter than those of the distances in **1** (2.39(6) Å) and **2** (2.44(7) Å). Compared to $\{LiSAr^{iPr6}\}_2$ (**4**) where the Li environment is more hindered, complex **3** displays a Li_2S_2 core with a slightly wider Li-S-Li angle of 77.03(3)° and a slightly greater Li--Li

distance of 2.977(14)°. The Li-S distances in $\{LiSAr^{iPr4}\}_2$ (**3**) (2.38(4) Å) and $\{LiSAr^{iPr6}\}_2$ (**4**) (2.39(5) Å) are similar, indicating essentially equal strengths of metal ligand interactions in these two species.

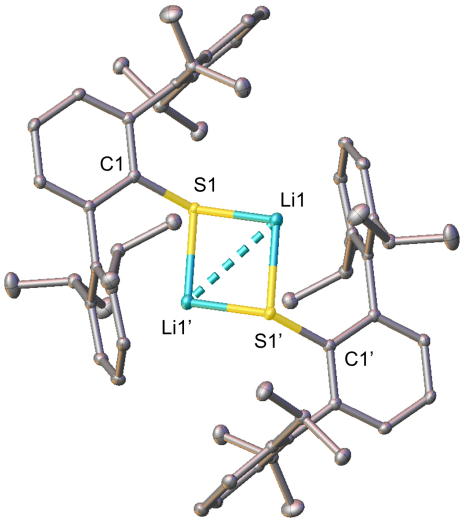

Figure 2.5 Molecular structure of complex **3** with thermal ellipsoids shown at 30% probability. Hydrogen atoms are not shown for clarity. Selected bond lengths (Å) and angles (deg): S1-Li1 2.36(4), S1-Li1′ 2.41(3), S1-C1 1.76(19), Li1--Li1′ 2.97(7), C1-S1-Li1 125.99(10), C1-S1-Li1′ 105.25(10), Li1-S1-Li1′ 77.03(13), S1-Li1-S1′ 102.97(13).

Some important structural parameters of the lithium and copper(I) thiolates are summarized in Table 2.1, it can be seen that the Cu--Cu distances are ca. 0.5 Å shorter than the corresponding Li--Li parameters even though the Li(I) ion has similar ionic radius (0.59 Å) to that of the Cu(I) ion (0.60 Å).[43] This difference can be ascribed to stronger van der Waals attractive dispersion forces between Cu atoms.[59,64] Since Cu has a much greater principal quantum number than Li, the greater number of electrons leads to a higher degree of instantaneous induced dipoles and hence an increased level of attraction which is reflected in a shorter bond distance.[59] It is, also noteworthy

that the Li-centroid interactions are ca. 0.26-0.31 Å shorter than those in **1** and **2**, indicating a greater ionic attraction of the lithium species.

Table 2.1 Selected bond distances (Å) and angles (deg) for compounds **1**-**4**.

compound	$\{CuSAr^{iPr4}\}_2$ (**1**)	$\{CuSAr^{iPr6}\}_2$ (**2**)	$\{LiSAr^{iPr4}\}_2$ (**3**)	$\{LiSAr^{iPr6}\}_2$ (**4**)[46]
M-S-M angles (deg) (avg.)	64.68(17)	62.13(19)	77.03(13)	73.9(2)
S-M-S angles (deg) (avg.)	115.32(17)	116.87(19)	102.97(13)	103.55(2)
M-S distances (Å) (avg.)	2.29(6)	2.30(7)	2.38(4)	2.39(5)
M--M distances (Å)	2.45(6)	2.411(7)	2.972(7)	2.88(7)
M--centroid of flanking ring	2.39(6)	2.44(7)	2.13(4)	2.19 (6)

Spectroscopy

The ^{1}H NMR spectra of **1**-**3** were recorded in C_6D_6 at 25 °C. The ^{1}H NMR spectrum of complex **1** shows two sets of doublets (δ 1.32 ppm and 1.0 ppm) attributable to the ortho substituents of the terphenyl ligands. The complicated pattern of these alkyl hydrogen signals indicates that the slightly different chemical environments of these hydrogen atoms caused by restricted rotation of the isopropyl groups. The spectrum also reveals two overlapping multiplets resonances which are centered at δ 2.79 ppm that correspond to the methine hydrogens of the isopropyl groups. The ^{1}H NMR spectrum of complex **2** displays three sets of doublets (centered at 1.42 ppm, 1.29 ppm and 1.12 ppm) that correspond to the ortho and para substituents of the terphenyl ligands, each integrating to 12 hydrogen atoms. The methine hydrogen peak is shifted downfield to 2.79 ppm

compared to the methine signal (δ 2.87 ppm) of complex **1**. In the ^{1}H NMR spectrum of complex **3**, all of the isopropyl methyl hydrogens are well resolved. As expected, it features a very common splitting pattern to that of complex **1** due to the similar terphenyl groups in their structures. The UV−Vis spectra of complexes **1**-**3** exhibit broad absorption bands in the range of 291 to 294 nm with the molar extinction coefficient in the range of 1500 M^{-1} cm^{-1} to 1700 M^{-1} cm^{-1}, that are consistent with a charge transfer process[41] (HOMO-LOMO gap was calculated as 307 nm for complex **2**) as depicted in the DFT calculations (Figure 2.6).

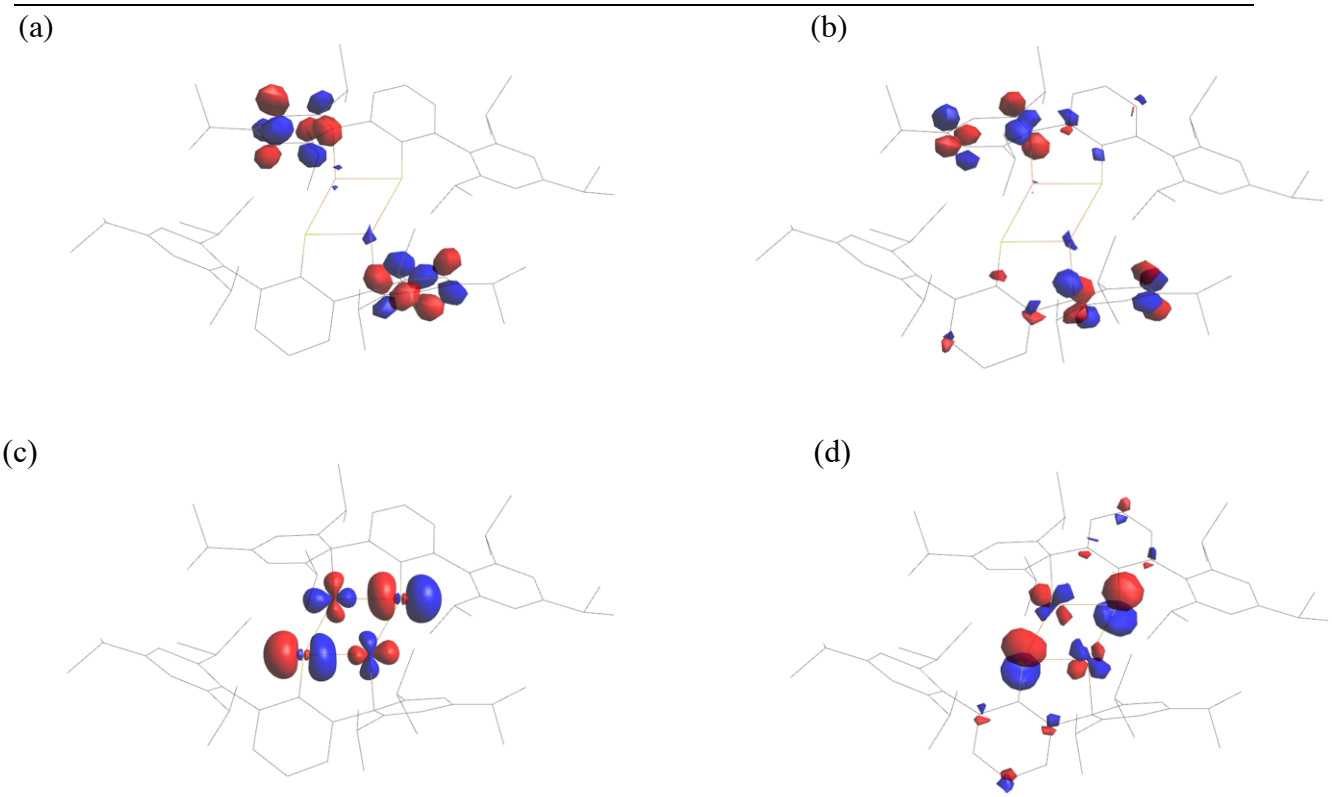

Figure 2.6 Depiction of calculated LUMO+1 (-0.572 eV) (a), LUMO (-0.693 eV) (b), HOMO (-4.736 eV) (c), and HOMO-1 (-5.005 eV) (d) of **2**. HOMO-LUMO gap is calculated to be 390 kJ/mol, hydrogens are not shown for clarity and the isovalue is set at 0.05 with ligand carbons being depicted in wire-frame.

CONCLUSION

In summary, we have isolated two dimeric Cu(I) thiolate complexes **1** and **2** by cupration reactions of bulky terphenyl thiolato ligands with mesitylcopper(I), as well as a new lithium thiolate complex **3** by lithiation of the terphenyl thiol with *n*-butyllithium. The synthesis and structures of **1** and **2** indicate the effectiveness of bulky terphenyl ligands at stabilizing low-aggregate metal thiolates by providing sufficient steric hindrance. A comparison between the structure of thiolates of the lithium and copper salts revealed much shorter M--M distances in the copper species probably as a result of stronger dispersion force between the metals.

Author Contributions

P. P. Power proposed and supervised the overall project. W. Zou carried out all experimental section, including synthesis, spectroscopy and data analysis. Q. Zhu performed theoretical studies. J. C. Fettinger finalized X-ray data. W. Zou and P. P. Power wrote and edited the paper.

ASSOCIATED CONTENT

Supporting Information.

The following files are available free of charge.

^{1}H and ^{13}C {^{1}H} spectra, crystallographic data, and details of computational studies (PDF)

Accession Codes

CCDC 2092550-2092552 contain the supplementary crystallographic data for this paper. These data can be obtained free of charge via www.ccdc.cam.ac.uk/data_request/cif, or by emailing data_request@ccdc.cam.ac.uk, or by contacting The Cambridge Crystallographic Data Centre, 12 Union Road, Cambridge CB2 1EZ, UK; fax: +44 1223 336033.

AUTHOR INFORMATION

Corresponding Author

Philip P. Power − Department of Chemistry, University of California, Davis, Davis, California 95616, United States; orcid.org/0000-0002-6262-3209; Email: pppower@ucdavis.edu

Authors

Wenxing Zou − Department of Chemistry, University of California, Davis, Davis, California 95616, United States; orcid.org/0000-0002-5462-8982

Qihao Zhu − Department of Chemistry, University of California, Davis, Davis, California 95616, United States; orcid.org/0000-0002-5566-4491

James C. Fettinger − Department of Chemistry, University of California, Davis, Davis, California 95616, United States; orcid.org/0000-0002-6428-4909

Notes

The authors declare no competing financial interest.

ACKNOWLEDGMENTS

We thank the U.S. National Science Foundation and for the purchase of a dual source X-ray diffractometer (Grant No. CHE-0840444). We also thank Jade Pratt for her initial work on the preparation of complex **1**.

References

[1] Zhang, S. and Warren, T. H. Three Coordinate Models for the Binuclear Cu_A Electrontransfer Site, *Chem. Sci*. **2013**, *4*, 1786-1792.

[2] Rosenzweig, A. C. Nitrous Oxide Reductase from Cu_A to Cu_Z, *Nat. Struct. Bio*. **2000**, *7*, 169-171.

[3] Zhang, L.; Bill, E.; Kroneck, P. M. H. and Einsle, O. Histidine-Gated Proton-Coupled Electron Transfer to the Cu_A Site of Nitrous Oxide Reductase, *J. Am. Chem. Soc.*, **2021**, *143*, 830−838.

[4] Henkel, G. and Krebs, B. Metallothioneins: Zinc, Cadmium, Mercury, and Copper Thiolates and Selenolates Mimicking Protein Active Site Features - Structural Aspects and Biological Implications, *Chem. Rev*., **2004**, *104*, 801−824.

[5] Howard-Lock, H. E. Structures of Gold(I) and Silver(I) Thiolate Complexes of Medicinal Interest: A Review and Recent Results, *Metal-Based Drugs*, **1999**, *6*, 201-209.

[6] Romero-Canelón, I. and Sadler, P. J. Systems Approach to Metal-Based Pharmacology, *Proc. Natl. Acad. Sci. U. S. A.,* **2015**, *112*, 4187-4188.

[7] Green, A. R.; Presta, A.; Gasyna, Z. and Stillman, M. J. Luminescent Probe of Copper-Thiolate Cluster Formation within Mammalian Metallothionein, *Inorg. Chem.,* **1994**, *33*, 4159-4168.

[8] Chen, C.; Weng, Z. and Hartwig, J. F. Synthesis of Copper(I) Thiolate Complexes in the Thioetherification of Aryl Halides, *Organometallics*, **2012**, *31*, 8031−8037.

[9] Seebach, D.; Jaeschke, G.; Pichota, A. and Audergon, L. Enantioselective 1,4-Addition of Aliphatic Grignard Reagents to Enones Catalyzed by Readily Available Copper(I) Thiolates Derived from TADDOL, *Helv. Chim. Acta* **1997**, *80*, 2515−2519.

[10] Delp, S. A.; Munro-Leighton, C.; Goj, L. A.; Ramírez, M. A.; Gunnoe, T. B.; Petersen J. L. and Boyle, P. D. Addition of S-H Bonds Across Electron-Deficient Olefins Catalyzed by Well-Defined Copper(I) Thiolate Complexes, *Inorg. Chem*., **2007**, *46*, 2365−2367.

[11] Williams, D. L. H. the Chemistry of S-Nitrosothiols, *Acc. Chem. Res*., **1999**, *32*, 869-876.

[12] Keller, H.; Simak, P. and Schrepp, W. Surface Chemistry of Thiols on Copper: An Efficient Way of Producing Multilayers, *Thin Solid Films* **1994**, *244*, 799-805.

[13] Sandhyarani, N. and Pradeep, T. An Investigation of the Structure and Properties of Layered Copper Thiolates, *J. Mater. Chem.,* **2001**, *11*, 1294-1299.

[14] Festa, R. A. and Thiele, D. J. Copper: An Essential Metal in Biology, *Curr. Biol.,* **2011**, *21*, R877– R883.

[15] Wikstrom, M. Cytochrome c Oxidase: 25 Years of the Elusive Proton Pump, *Biochim. Biophys. Acta,* **2004**, *1655,* 241–247.

[16] Iwata, S.; Ostermeier, C.; Ludwig, B. and Michel, H. Structure at 2.8 Å Resolution of Cytochrome c Oxidase from *Paracoccus denitrificans, Nature*, **1995**, *376*, 660–669.

[17] Suharti; Strampraad, M. J. F.; Schröder, I. and de Vries, S. A Novel Copper A Containing Menaquinol NO Reductase from *Bacillus azotoformans, Biochemistry*, **2001**, *40*, 2632-2639.

[18] Brown, K.; Tegoni, M.; Prudencio, M.; Pereira, A. S.; Besson, S.; Moura, J. J.; Moura I. and Cambillau, C. A Novel Type of Catalytic Copper Cluster in Nitrous Oxide Reductase. *Nat. Struct. Biol.,* **2000**, *7*, 191–195.

[19] Babcock, G. T. and Wikström, M. Oxygen Activation and the Conservation of Energy in Cell Respiration, *Nature,* **1992**, *356*, 301-309.

[20] Tang, K.; Aslam, M.; Block, E.; Nicholson, T. and Zubieta, J. Steric Control of Aggregation in Neutral Silver(I) Thiolates, $[AgSR]_n$. Crystal and Molecular Structures of $[AgSCH(SiMe_3)_2]_8$,

A Discrete Molecular Biscycle of Weakly Interacting $[AgSCH(SiMe_3)_2]_4$ Units, and of $[AgSC(SiPhMe_2)_3]_3$ and $[AgSC(SiMe_3)_3]_4$, Discrete Molecular Monocycles Containing Linearly Coordinated Silver(I) and Doubly Bridging Mercapto Sulfur Donors from Novel Sterically Hindered Thiolate Ligands. A Comparison with the Nonmolecular Structure of $[Ag_4\{SCH_2(SiMe_3)\}_3]_n$, *Inorg. Chem.,* **1987**, *26*, 1488-1497.

[21] Yang, Q.; Tang, K.; Liao, H.; Han, Y.; Chen, Z. and Tang, Y. Synthesis and X-Ray Crystal Structure of $[Cu(SC_6H_2\text{-iso-}Pr_3)]_8$, *J. Chem. Soc. Chem. Commun*., **1987**, *14*, 1076-1077.

[22] Liu, C. W.; Stubbs, T.; Staples, R. J. and Fackler Jr., J. P. Syntheses and Structural Characterizations of Two New Cu-S Clusters of Dialkyl Dithiophosphates: A Sulfide-Centered Cu^I_8 Cube, $\{Cu_8[S_2P(O^iPr)_2]_6(\mu_8\text{-}S)\}$, and a Distorted Octahedral $\{Cu_6[S_2P(OEt)_2]_6\cdot 2H_2O\}$ Cluster, *J. Am. Chem. Soc*., **1995**, *117*, 9778-9779.

[23] Dance, I. G. A Model for the Non-Molecular Structures of the Thiolates, MSR, of Copper and Silver, *Polyhedron*, **1988**, *7*, 2205-2207.

[24] Block, E.; Gernon, M.; Kang, H.; Liu, S. and Zubieta, J. Synthesis and Structural Characterization of $[Cu(SC_6H_4\text{-}o\text{-}SiMe_3)]_{12}$, An Unusual Example of A 'Paddle-Wheel' Dodecametallic Thiolate Cluster, *J. Chem. Soc. Chem. Commun*., **1988**, *15*, 1031-1033.

[25] Gonzalez-Duarte, P.; Sola, J.; Vives, J. and Solans, X. $[Ag_5[\mu_2\text{-}S(CH_2)_3NHMe_2]_3[\mu_2\text{-}S(CH_2)_3NMe_2]_3]^{2+}$, the First Thiolate Complex of a Metal with Trigonal Bipyramido-M_5-Trigonal Prismo-S_6 Polyhedral Stereochemistry, *J. Chem. Soc. Chem. Commun*., **1987**, *21*, 1641-1642.

[26] Nicholson, J. R.; Abrahams, I. L.; Clegg, W. and Garner, C. D. Preparation, Crystal Structure, and Spectroscopic Characterization of the Tetranuclear Copper-Thiolate Cluster $[Cu_4(o\text{-}(SCH_2)_2C_6H_4)_3]^{2-}$ as Its Tetraphenylphosphonium(1+) Salt, *Inorg. Chem*., **1985**, *24*, 1092-1096.

[27] Janssen, M. D.; Grove, D. M.; Van Koten, G. Copper(I), Lithium, and Magnesium Thiolate Complexes: An Overview with Due Mention of Selenolate and Tellurolate Analogs and Related Silver(I) and Gold(I) Species, *Prog. Inorg. Chem.,* **1997**, *46,* 97–149.

[28] Rungthanaphatsophon, P.; Barnes, C. L. and Walensky, J. R. Copper(I) Clusters with Bulky Dithiocarboxylate, Thiolate, and Selenolate Ligands, *Dalton Trans*., **2016**, *45*, 14265–14276.

[29] Block, E.; Kang, H.; Ofori-Okai, G. and Zubieta*,* J. the Crystal and Molecular Structure of a Tetranuclear Copper Thiolate Cluster, $[Cu\{SC_6H_3\text{-}2,6\text{-}(SiMe_3)_2\}]_4$, *Inorg. Chim. Acta.,* **1990**, *167*, 147-148.

[30] Castro, R.; Duran, M. L.; Garcia-Vazquez, J. A.; Romero, J.; Sousa, A.; Castellano, E. E.; Zukerman-Schpector, J. Copper(I) Complexes with 4,6-Dimethylpyrimidine-2-thione (Hdmpymt); the Crystal and Molecular Structure of $[Cu_6(dmpymt)_6]$, *J. Chen. Soc. Dalton. Trans*., 1992, 17, 2559-2563.

[31] Melzer, M. M.; Mossin, S.; Cardenas, A. J. P.; Williams, K. D.; Zhang, S.; Meyer, K.; Warren, T. H. A Copper(II) Thiolate from Reductive Cleavage of an S-Nitrosothiol, *Inorg. Chem*., **2012**, *51*, 8658-8660.

[32] Yan, H.; Hohman, J. N.; Li, F. H.; Jia, C.; Solis-Ibarra, D.; Wu, B.; Dahl, J. E. P.; Carlson, R. M. K.; Tkachenko, B. A.; Fokin, A. A. Hybrid Metal-organic Chalcogenide Nanowires with Electrically Conductive Inorganic Core Through Diamondoid-Directed Assembly, *Nat. Mat*., **2017**, *16*, 349-355.

[33] Parish, R. V.; Salehi, Z.; Pritchard, R. G. Five-Coordinate Sulfur in A Polymeric Copper(I) Thiolate Complex, *Angew. Chem. Int. Ed. Engl.,* **1997**, *36*, 251-253.

[34] Lawton, S. L.; Rohrbaugh, W. J. and Kokotailo, G. T. Crystal and Molecular Structure of the Tetranuclear Metal Cluster Complex Copper(I) O,O'-Diisopropylphosphorodithioate,Cu_4[(iso-PrO)$_2$$PS_2$]$_4$, *Inorg. Chem.,* **1972**, *11*, 612-618.

[35] Pratt, J.; Bryan, A. M.; Faust, M.; Boynton, J. N.; Vasko, P.; Rekken, B. D.; Mansikkamaki, A.; Fettinger, J. C.; Tuononen, H. M. and Power, P. P. Effects of Remote Ligand Substituents on the Structures, Spectroscopic, and Magnetic Properties of Two-Coordinate Transition-Metal Thiolate Complexes, *Inorg. Chem*., **2018**, *57*, 6491−6502.

[36] Dilworth, J. R. and Hu, J. Complexes of Sterically Hindered Thiolate Ligands, *Adv. Inorg. Chem.,* **1994**, *40,* 411-459.

[37] Nguyen, T.; Panda, A.; Olmstead, M. M.; Richards, A. F.; Stender, M.; Brynda, M. and Power, P. P. Synthesis and Characterization of Quasi-Two-Coordinate Transition Metal Dithiolates M(SAr)$_2$ (M = Cr, Mn, Fe, Co, Ni, Zn; Ar = C_6H_3-2,6(C_6H_2-2,4,6-Pri$_3$)$_2$), *J. Am. Chem. Soc.,* **2005**, *127*, 8545-8552.

[38] Power, P. P. and Shoner, S. C. the Neutral Transition Metal Thiolates [M(SAr)$_2$]$_2$ (M=Mn, Fe or Co, Ar=2,4,6-*t*-Bu$_3$$C_6H_2$), *Angew. Chem. Int. Ed. Engl.,* **1991**, *30*, 330-332.

[39] Ellison, J. J.; Ruhlandt-Senge, K. and Power, P. P. Synthesis and Characterization of Thiolato Complexes with Two-Coordinate Iron(II), *Angew. Chem. Int. Ed. Engl.,* **1994**, *33*, 1178-1180.

[40] Niemeyer, M. and Power, P. P. Donor-Free Alkali Metal Thiolates: Synthesis and Structure of Dimeric, Trimeric, and Tetrameric Complexes with Sterically Encumbered Terphenyl Substituents, *Inorg. Chem.,* **1996**, *35*, 7264-7272.

[41] Ruhlandt-Senge, K. and Power, P. P. the Synthesis and Characterization of Metal Derivatives of the New, Conveniently Prepared, Bulky Thiolato Ligand 2,4,6-Triphenylbenzenethiol, *Bull. Soc. Chim. France*, **1993**, *129*, 594-598.

[42] Aslam, M.; Bartlett, R. A.; Block, E.; Olmstead, M. M.; Power, P. P. and Sigel, Gary E. the First X-Ray Crystal Structural Characterizations of Alkali Metal Alkyl Thiolates: X-Ray Crystal Structures of $[Li_2(thf)_4\{SCH(SiMe_3)_2\}_2]$ and $[Li_2(thf)_{3.5}\{SC(SiMe_3)_3\}_2$ (thf = tetrahydrofuran). *J. Chem. Soc. Chem. Commun*., **1985**, *23*, 1674-1675.

[43] Shannon, R. D. Revised Effective Ionic Radii and Systematic Studies of Interatomic Distances in Halides and Chaleogenides, *Acta Cryst*., **1976**, *A32*, 751-767.

[44] Pangborn, A. B.; Giardello, M. A.; Grubbs, R. H.; Rosen, R. K.; Timmers, F. J. Safe and Convenient Procedure for Solvent Purification, *Organometallics*, **1996**, *15*, 1518-1520.

[45] Barnett, B. R.; Mokhtarzadeh, C. C.; Lummis, P.; Wang, S.; Queen, J. D.; Gavenonis, J.; Schüwer, N.; Tilley, T. D.; Boynton, J. N.; Power, P. P.; Ditri, T. B.; Weidemann, N.; Agnew, D. W.; Figueroa, J. S.; Smith, P. W.; Carpenter, A. E.; Pratt, J. K.; Mendelson, N. D.; Figueroa, J. S. Terphenyl Ligands and Complexes, *Inorganic Synthesis*, **2018**, *37*, 85-122.

[46] Tsuda, T.; Yazawa, T.; Watanabe, K.; Fujii, T. and Saegusa, T. Preparation of Thermally Stable and Soluble Mesitylcopper(I) and Its Application in Organic Synthesis, *J. Org. Chem*., **1981**, *46*, 192-194.

[47] Sheldrick, G. M. SADABS, Siemens Area Detector Absorption Correction; Göttingen Universitaẗ: Göttingen, Germany, **2008**, p33.

[48] Blessing, R. H. An Empirical Correction for Absorption Anisotropy. *Acta Cryst. Sect. A: Found. Cryst.,* **1995**, *51*, 33−38.

[49] Sheldrick, G. M. SHELXTL, version 6.1; Bruker AXS: Madison, WI, **2002**.

[50] Dolomanov, O. V.; Bourhis, L. J.; Gildea, R. J.; Howard, J. A. K.; Puschmann, H. OLEX2: A Complete Structure Solution, Refinement and Analysis Program. *J. Appl. Cryst.,* **2009**, *42*, 339–341.

[51] Troyano, J.; Perles, J.; Amo-Ochoa, P.; Martínez, J. I.; Gimeno, M. C.; Fernández-Moreira, V.; Zamora, F. and Delgado, S. Luminescent Thermochromism of 2D Coordination Polymers Based on Copper(I) Halides with 4-Hydroxythiophenol, *Chem. - Eur. J.*, **2016**, *22*, 18027-18035.

[52] Groysman, S. and Holm, R. H. A Series of Mononuclear Quasi-Two-Coordinate Copper(I) Complexes Employing a Sterically Demanding Thiolate Ligand, *Inorg. Chem*., **2009**, *48*, 621-627.

[53] Lopes, C.; Håkansson, M. and Jagner, S. Carbonylation of A Tetrameric Aryloxocopper(I) Cluster, *Inorg. Chem*., **1997**, *36*, 3232-3236.

[54] Tsuda, T.; Watanabe, K.; Miyata, K.; Yamamoto, H. and Saegusa, T. Preparation and Characterization of Copper(I) Amides, *Inorg. Chem.,* **1981**, *20*, 2728-2730.

[55] Kleijn, H. and Vermeer, P. [(Trimethylsilyl)methyl]copper(I) Species: Versatile Reagents to Prepare Functionally Substituted Allylic Silanes, *J. Org. Chem*., **1985**, *50*, 5143-5148.

[56] Dance, I. G.; Bowmaker, G. A.; Clark, G. R. and Seadon, J. K. the Formation and Crystal and Molecular Structures of Hexa(μ-organothiolato) Tetracuprate(I) Cage Dianions: Bis(tetramethylammonium) Hexa(μ-methanethiolato)-Tetracuprate(I) and Two Polymorphs of Bis(tetramethylammonium) hexa(μ-benzenethiolato)-Tetracuprate(I), *Polyhedron,* **1983**, *2*, 1031-1043.

[57] Pyykkö, P. and Atsumi, M. Molecular Single-Bond Covalent Radii for Elements 1-118, *Chem. Eur. J.,* **2009**, *15*, 186-197.

[58] Tatewaki, H.; Hatano, Y.; Naka, T.; Noro, T. and Yamamoto. S. Atomic Radii for Depicting Atoms in a Molecule II: The Effective Atomic Radius and van der Waals Radius from ^{1}H to ^{54}Xe, *Bull. Chem. Soc. Jpn.*, **2010**, *83,* 1203-1210.

[59] Pyykkö, P. Strong Closed-Shell Interactions in Inorganic Chemistry, *Chem. Rev*., **1997**, *97*, 597-636.

[60] Harisomayajula, N. V. S.; Makovetskyi, S.; Tsai, Y. C. Cuprophilic Interactions in and between Molecular Entities. *Chem. - Eur. J.,* **2019**, *25*, 8936−8954.

[61] Liu, Y.; Taylor, L. J.; Argent, S. P.; McMaster, J. and Kays, D. L. Group 11 *m*-Terphenyl Complexes Featuring Metallophilic Interactions, *Inorg. Chem.,* **2021**, *60*, 10114-10123.

[62] Mehrotra, P. K. and Hoffmann, R. Cu(I)-Cu(I) Interactions. Bonding Relationships in d^{10}-d^{10} Systems, *Inorg. Chem*., **1978**, *17*, 2187-2189.

[63] Mishra, S.; Bhandari, A.; Singh, D.; Gupta, R.; Olmstead, M. M. and Patra, A. K. Bis(μ-thiolato)-dicopper Containing Fully Spin Delocalized Mixed Valence Copper−Sulfur Clusters and Their Electronic Structural Properties with Relevance to the Cu_A Site, *Inorg. Chem*., **2021**, *60*, 5779−5790.

[64] Sculfort, S. and Braunstein, P. Intramolecular d^{10}-d^{10} Interactions in Heterometallic Clusters of the Transition Metals, *Chem. Soc. Rev.,* **2011**, *40*, 2741–276.

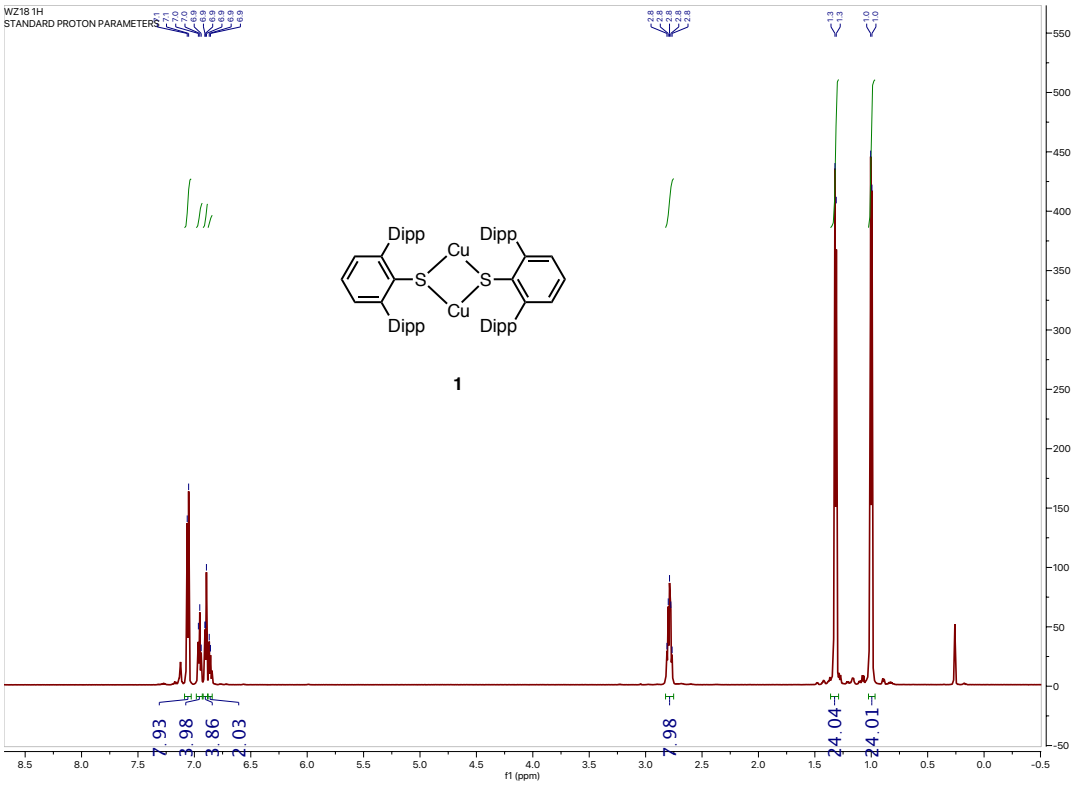

Figure S2.1 ^{1}H NMR spectrum of $\{CuSAr^{iPr4}\}_2$ (**1**) (600 MHz, C_6D_6, 298 K)

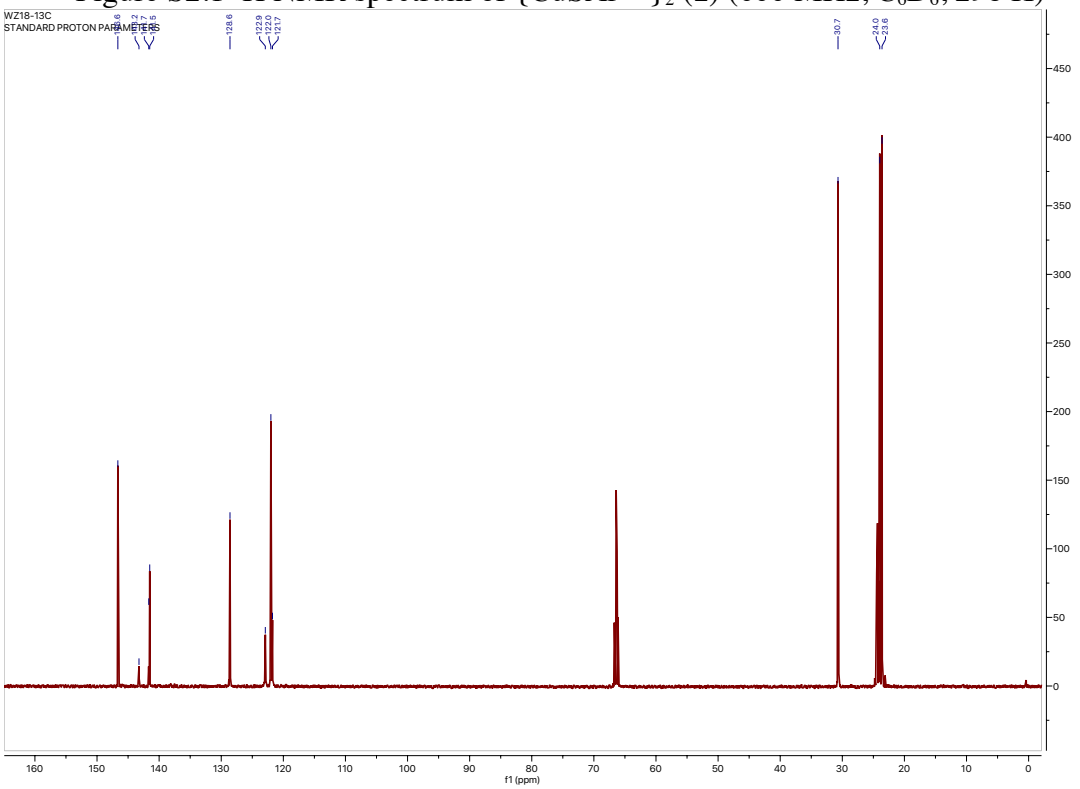

Figure S2.2 $^{13}C\{^{1}H\}$ spectrum of $\{CuSAr^{iPr4}\}_2$ (**1**) (150 MHz, C_6D_6, 298 K)

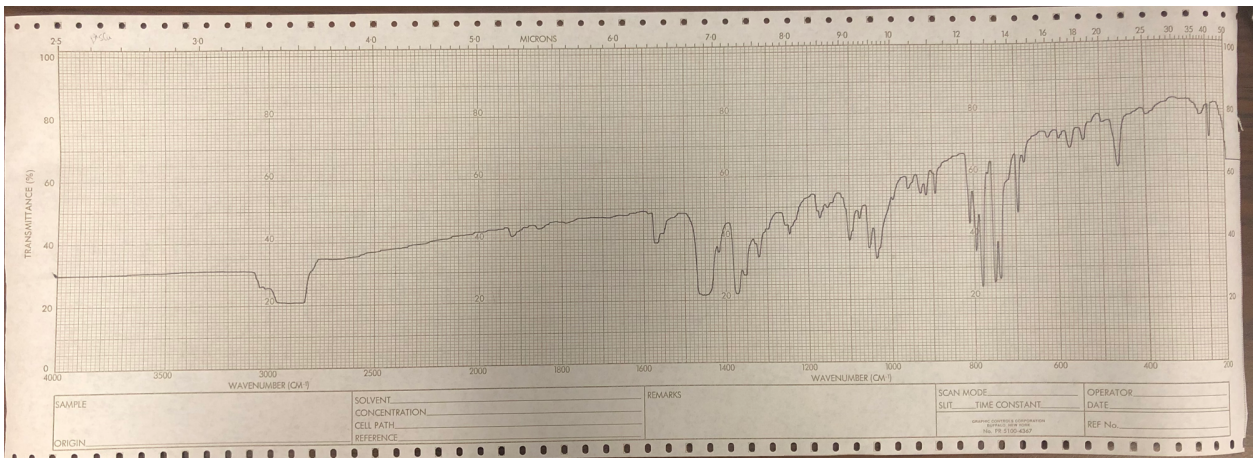

Figure S2.3 Infrared spectrum as a Nujol mull of $\{CuSAr^{iPr4}\}_2$ (**1**) at 25°C

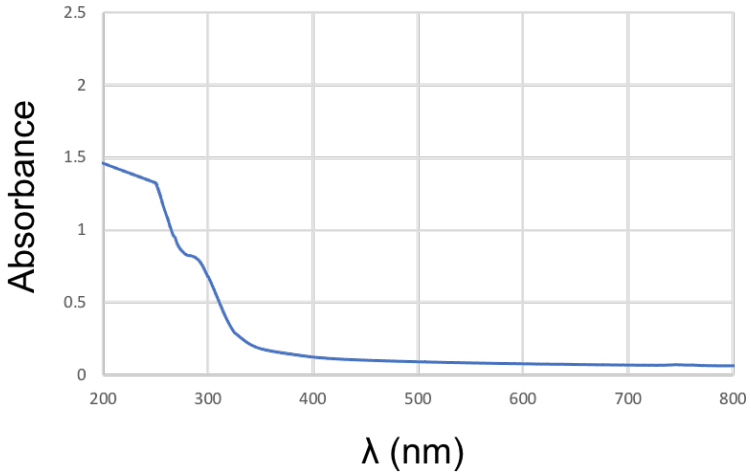

Figure S2.4 UV-Vis spectrum of $\{CuSAr^{iPr4}\}_2$ (**1**) at 25 °C (470 μM in hexanes)

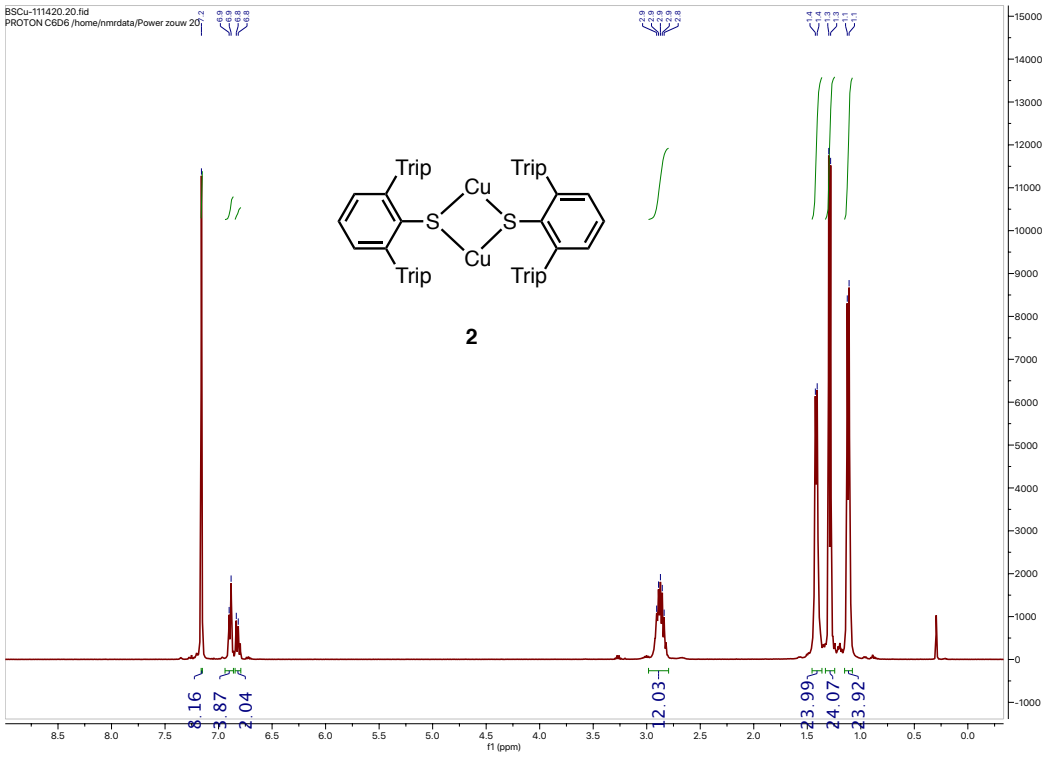

Figure S2.5 ^{1}H NMR spectrum of $\{CuSAr^{iPr6}\}_2$ (**2**) (600 MHz, C_6D_6, 298 K)

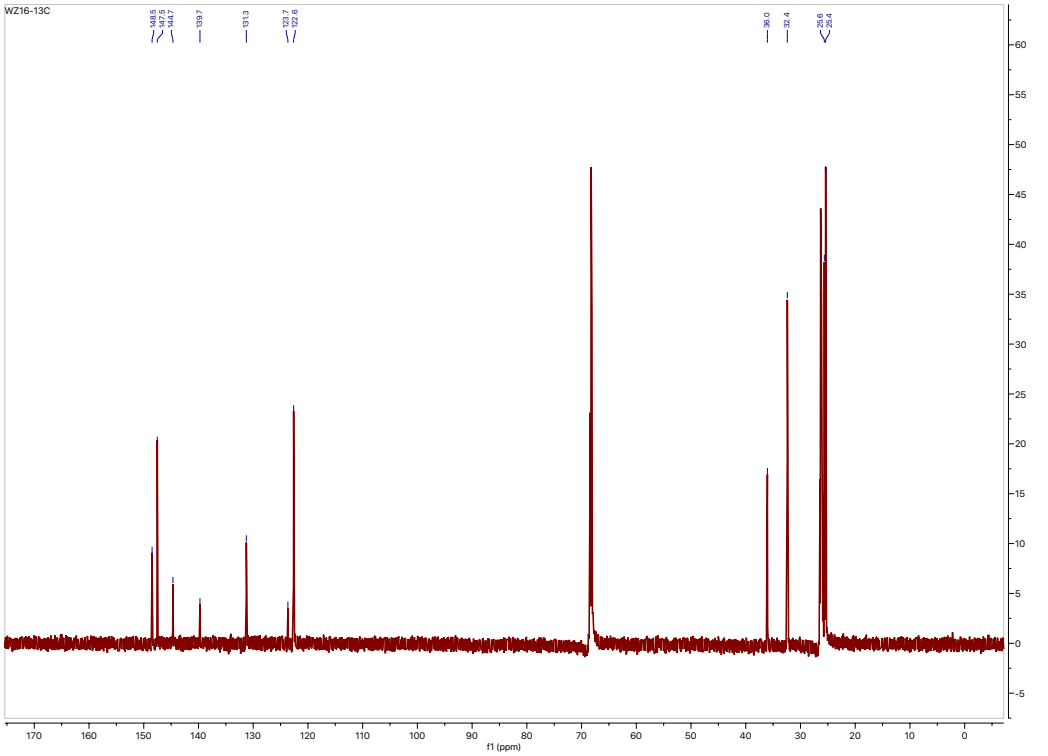

Figure S2.6 $^{13}C\{^{1}H\}$ NMR spectrum of $\{CuSAr^{iPr6}\}_2$ (**2**) (150 MHz, C_6D_6, 298 K)

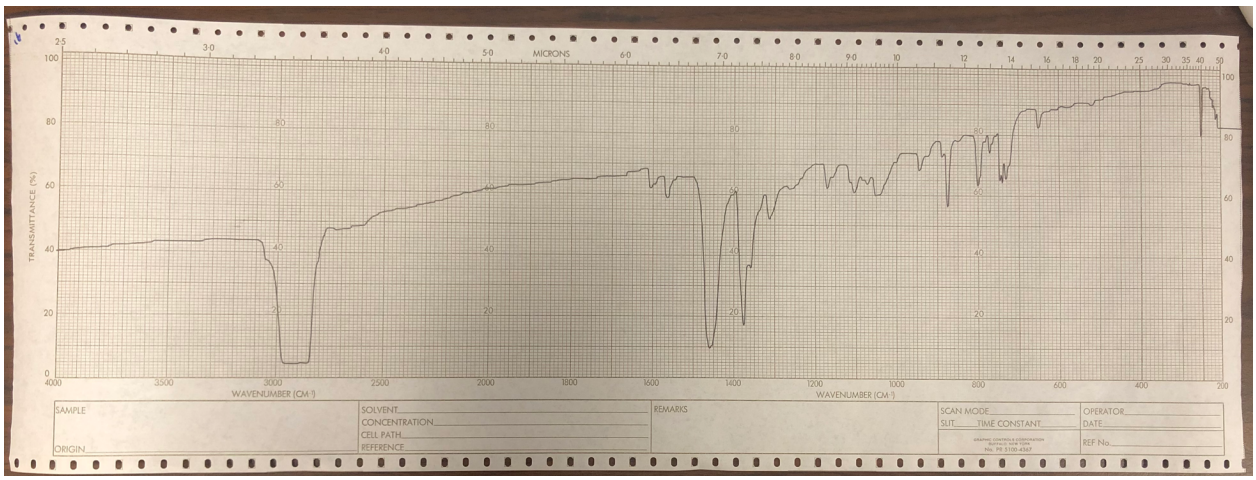

Figure S2.7 Infrared spectrum as a Nujol mull of $\{CuSAr^{iPr6}\}_2$ (**2**) at 25°C

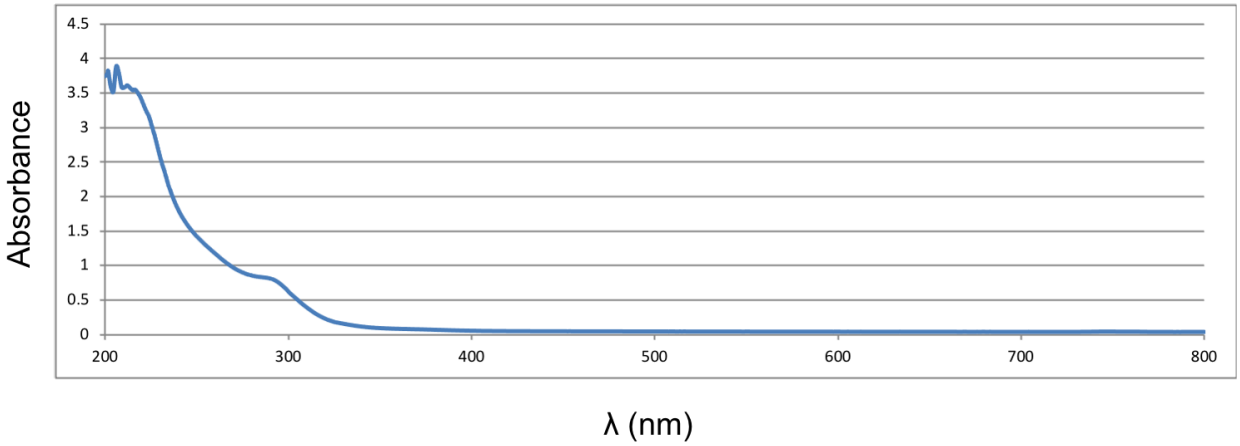

Figure S2.8 UV-Vis spectrum of $\{CuSAr^{iPr6}\}_2$ (**2**) at 25 °C (465 μM in hexanes)

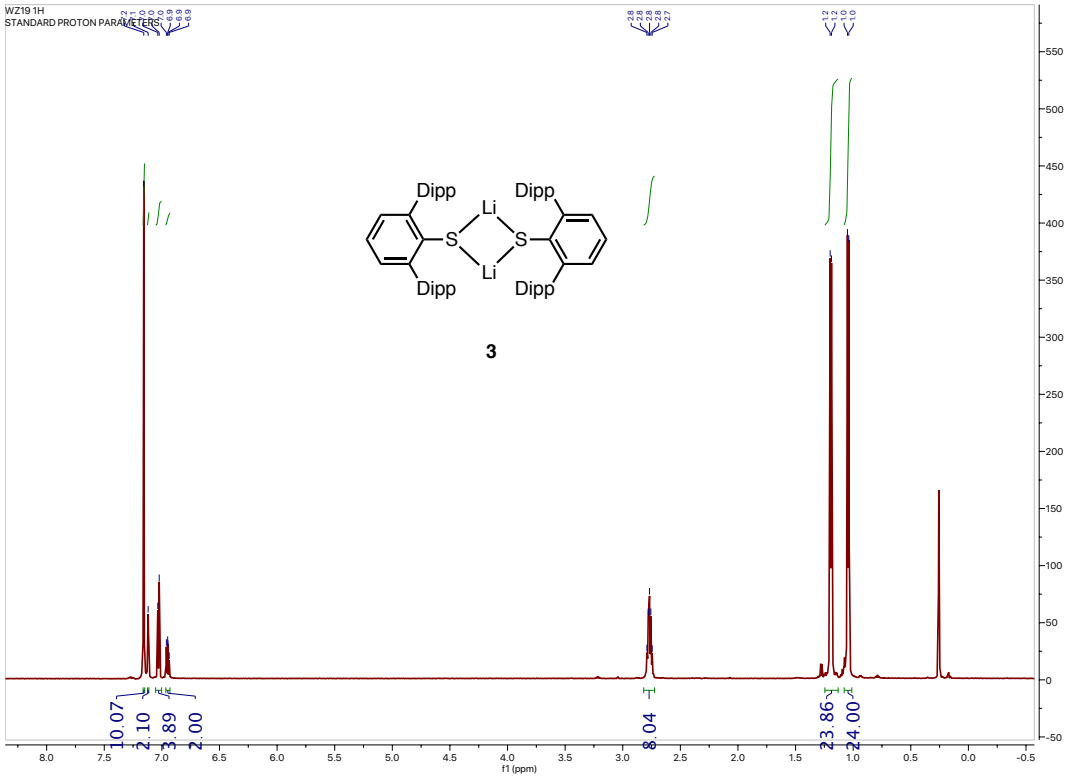

Figure S2.9 ^{1}H NMR spectrum of {LiSAr^{iPr4}}$_2$ (**3**) (600 MHz, C_6D_6, 298 K)

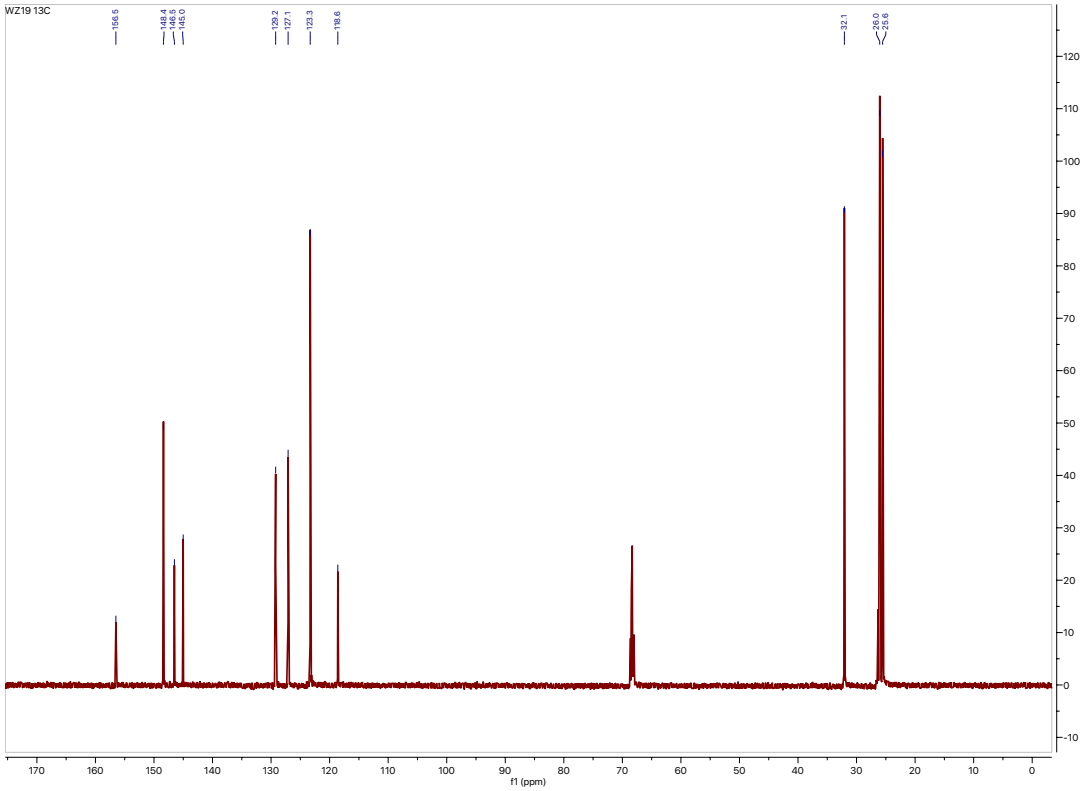

Figure S2.10 ^{13}C{^{1}H} spectrum of {LiSAr^{iPr4}}$_2$ (**3**) (150 MHz, C_6D_6, 298 K)

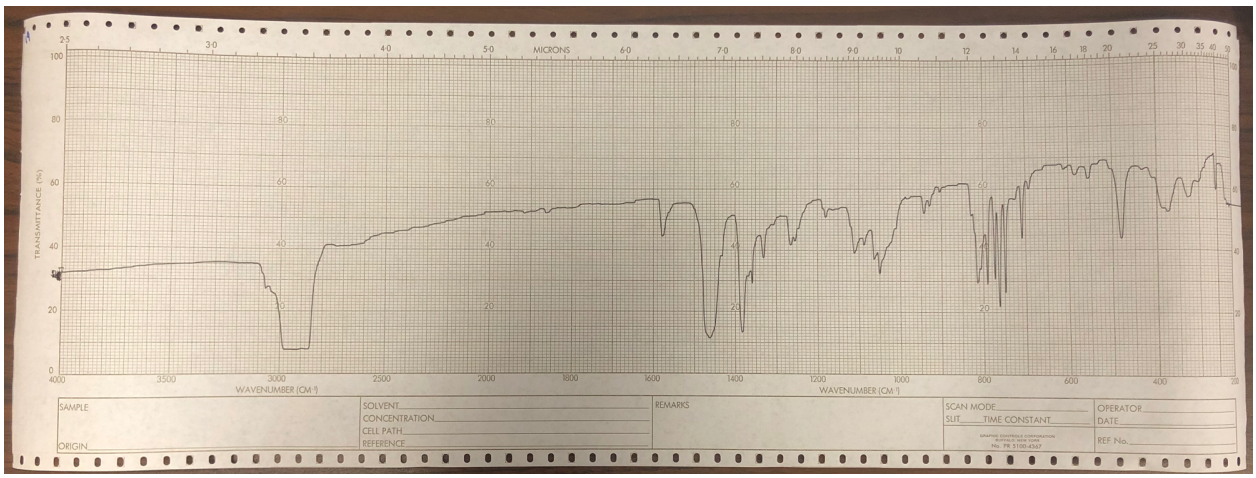

Figure S2.11 Infrared spectrum as a Nujol mull of {LiSAr^{iPr4}}$_2$ (**3**) at 25^{o}C

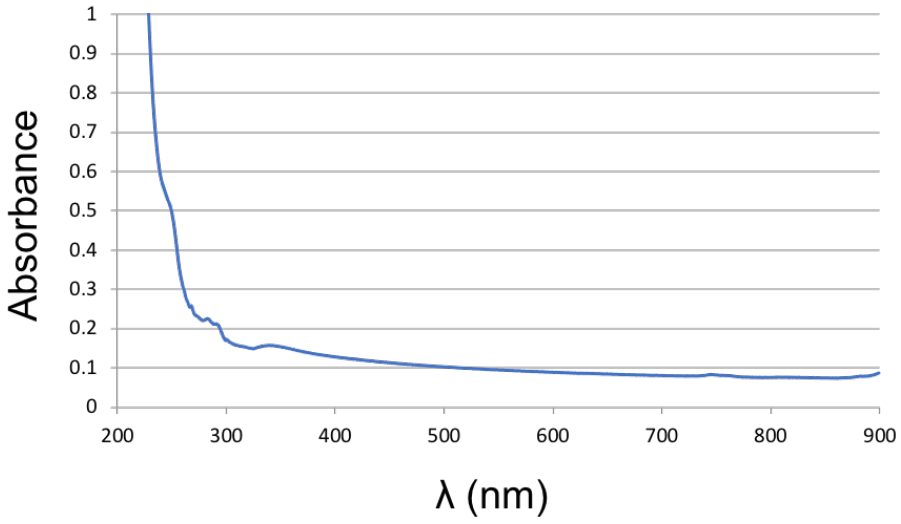

Figure S2.12 UV-Vis spectrum of {LiSAr^{iPr4}}$_2$ (**3**) at 25 °C (140 μM in hexanes)

Table S2.1 Crystallographic data for compounds **1-3**

	1	**2**	**3**
formula	$C_{60}H_{74}Cu_2S_2$	$C_{72}H_{98}Cu_2S_2$	$C_{60}H_{74}Li_2S_2$
fw	984.4	1152.6	872.6
color	colorless	colorless	colorless
cyst syst	monoclinic	monoclinic	monoclinic
space group	P 2_1/n	P 2_1/c	P 2_1/n
a, Å	10.9768(7)	16.4259(15)	10.8353(12)
b, Å	20.7437(11)	16.7574(16)	20.4108(17)
c, Å	11.4158(6)	23.022(2)	11.7325(7)
α, deg	90	90	90
β, deg	90.662(5)	98.527(2)	91.791(12)
γ, deg	90	90	90
V, Å^3	2599(3)	6266.9(10)	2593.5(4)
Z	2	4	2
Density (calculated)	1.260 Mg/m^3	1.224 Mg/m^3	1.118 Mg/m^3
Absorption coefficient	2.025 mm^{-1}	0.786 mm^{-1}	1.187 mm^{-1}
F(000)	1048	2480	944
Crystal size	0.281 x 0.200 x 0.193 mm^3	0.524 x 0.199 x 0.156 mm^3	0.336 x 0.251 x 0.234mm^3
Crystal color and habit	Colorless Block	Colorless Plate	Colorless Plate
Theta range for data collection	4.262 to 69.395°	2.027 to 27.523°	4.332 to 68.585°
Index ranges	-13<=h<=13, -24<=k<=24, -13<=l<=13	-21<=h<=21, -21<=k<=21, -29<=l<=29	-12<=h<=13, -24<=k<=24, -14<=l<=14
Reflections collected	14153	55697	14958
Independent reflections	4776 [R(int) = 0.0159]	14423 [R(int) = 0.0308]	4603 [R(int) = 0.0289]

Data / restraints / parameters	4776 / 0 / 437	14423 / 101 / 786	4603 / 0 / 438
Goodness-of-fit on F^2	1.048	1.030	1.045
Final R indices [I>2sigma(I)]	R1 = 0.0261, wR2 = 0.0704	R1 = 0.0355, wR2 = 0.0963	R1 = 0.0442, wR2 = 0.1172
R indices (all data)	R1 = 0.0268, wR2 = 0.0709	R1 = 0.0450, wR2 = 0.1030	R1 = 0.0508, wR2 = 0.1207
Largest diff. peak and hole	0.317 and -0.374 e.Å^{-3}	0.579 and -0.456 e.Å^{-3}	0.310 and -0.303 e.Å^{-3}

Computational details

The structure was subjected to geometry optimization at the DFT level of theory, with the B3LYP hybrid exchange functional[S1-S4] using Ahlrichs polarized basis set def2-TZVP[S5] basis set together with the RIJCOSX approximation.[S6] In addition, dispersion correction with Becke-Johnson damping (D3BJ)[S7-S8] was used. The resolution of identity approximation was employed with auxiliary basis set def2-TZVP/C[S9-S10] in order to speed up the calculations. The UV-vis absorption spectra of optimized geometry were calculated with time dependent (TD) DFT method. All calculations were carried out using the ORCA 4.2.1 quantum chemistry package.[S11]

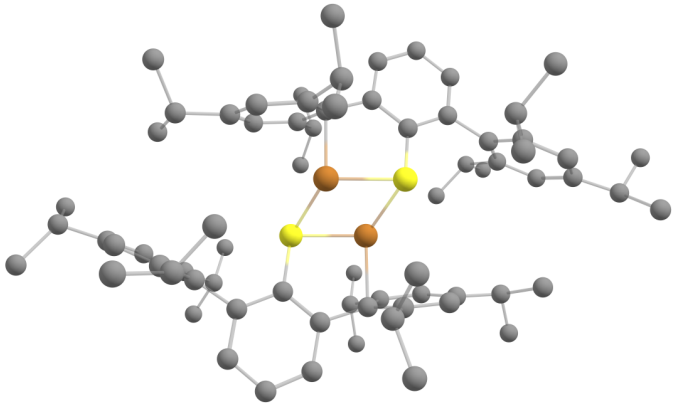

Table S2.2 Calculated dispersion energy of complex **2**.

B3LYP+def2-TZVP	B3LYP-D3BJ	B3LYP	Experimental
Cu···Cu (Å)	2.417	2.415	2.4145
Cu(1)-S(2) (Å)	2.282	2.418	2.2844
Cu(1)-S(1) (Å)	2.323	2.350	2.3227
Cu(2)-S(1) (Å)	2.280	2.417	2.2844
Cu(2)-S(2) (Å)	2.322	2.351	2.3227
Cu(2)-S(2)-C(37) (°)	96.9	98.6	97.1
Cu(1)-S(1)-C(1) (°)	96.9	98.7	97.1
S(2)-Cu(2)-S(1) (°)	116.7	119.1	116.8
S(2)-Cu(1)-S(1) (°)	116.6	119.1	116.8
$(Ar^{iPr6}SCu)_2$ (0,1) → 2 $Ar^{iPr6}SCu$ (0,1) BDE = 2E($Ar^{iPr6}SCu$) – E{$(Ar^{iPr6}SCu)_2$}			
BDE/E_{disp} (kcal/mol)	50.4	23.7 / 26.7	

References:

S1. Becke, A. D. A new Xixing of Hartree–Fock and local density-Functional Theories. *J. Chem. Phys.*, **1993,** *98*, 1372-1377.

S2. Lee, C.; Yang, W.; Parr, R. G. Development of the Colle-Salvetti Correlation-Energy Formula into a Functional of the Clectron Density. *Phys. Rev. B,* **1988,** *37*, 785-789.

S3. Vosko, S. H.; Wilk, L.; Nusair, M., Accurate Spin-Dependent Electron Liquid Correlation Energies for Local Spin Density Calculations: A Critical Analysis. *Can. J. Phys.* **1980,** *58*, 1200-1211.

S4. Stephens, P. J.; Devlin, F. J.; Chabalowski, C. F.; Frisch, M. J. Ab Initio Calculation of Vibrational Absorption and Circular Dichroism Spectra Using Density Functional Force Fields. *J. Phys. Chem.,* **1994,** *98*, 11623-11627.

S5. Weigend, F.; Ahlrichs, R. Balanced Basis Sets of Split Valence, Triple Zeta Valence and Quadruple Zeta Valence Quality for H to Rn: Design and Assessment of Accuracy. *PCCP* **2005,** *7*, 3297-3305.

S6. Neese, F.; Wennmohs, F.; Hansen, A.; Becker, U. Efficient, Approximate and Parallel Hartree–Fock and Hybrid DFT Calculations. A 'Chain-of-Spheres' Algorithm for the Hartree–Fock Exchange. *Chem. Phys.*, **2009**, *356*, 98–109.

S7. Grimme, S.; Antony, J.; Ehrlich, S.; Krieg, H. A Consistent and Accurate Ab Initio Parametrization of Density Functional Dispersion Correction (DFT-D) for the 94 Elements H-Pu. *J. Chem. Phys.,* **2010,** *132*, 154104/1-154104/19.

S8. Grimme, S.; Ehrlich, S.; Goerigk, L. Effect of the Damping Function in Dispersion Corrected Density Functional Theory. *J. Comput. Chem.* **2011,** *32*, 1456-1465.

S9. Weigend, F., Accurate Coulomb-Fitting Basis Sets for H to Rn. *PCCP* **2006,** *8*, 1057-1065.

S10. Hellweg, A.; Hättig, C.; Höfener, S.; Klopper, W. Optimized Accurate Auxiliary Basis Sets for RI-MP2 and RI-CC2 Calculations for the Atoms Rb to Rn. *Theor. Chem. Acc.* **2007,** *117*, 587-597.

S11. Neese, F.; the ORCA Program System. *WIREs Computational Molecular Science*, **2012**, *2*, 73-78.

Chaper 3. The Unusual Structural Behavior of Heteroleptic Aryl Copper(I) Thiolato Molecules. Cis vs. Trans Structures and London Dispersion Effects

Wenxing Zou,[a] James C. Fettinger,[a] Petra Vasko,[b,*] Philip P. Power [a,*]

[a] Department of Chemistry, University of California, One Shields Avenue, Davis, California 95616, United States
[b] Department of Chemistry, University of Helsinki, P.O. Box 55, FI-00014, Finland

Reprinted with permission from *Organometallics*, **2022**, *41*, 794-801.

ABSTRACT

A series of heteroleptic aryl copper(I) thiolato complexes of formula $\{Cu_2(SAr)Mes\}_2$ (Ar= C_6H_3-2,6-(C_6H_2-2,4,6-Me_3)$_2$ (Ar^{Me6}), **1**; C_6H_3-2,6-(C_6H_3-2,6-iPr_2)$_2$ (Ar^{iPr4}), **2**; C_6H_3-2,6-(C_6H_2-2,4,6-iPr_3)$_2$ (Ar^{iPr6}), **3**) and $\{Cu_4(SAr)Mes_3\}$ (Ar= C_6H-2,6-(C_6H_2-2,4,6-iPr_3)$_2$-3,5-iPr_2 (Ar^{iPr8}), **4** were synthesized by the reactions of the corresponding bulky terphenyl thiols with mesitylcopper(I) with elimination of mesitylene. All complexes were characterized by single crystal X-ray diffraction analysis and spectroscopy (NMR, infra-red and UV-vis). The data for **1**-**3** revealed tetrametallic Cu_4 core structures in which two thiolato or two mesityl ligands bridge the metals. Although **1** and **2** feature the expected conventional alternating thiolato and mesityl bridging patterns, **3** has a previously unknown structural arrangement in which the two thiolato ligands are adjacent to each other. Since complex **3** has a more crowding aryl group on the thiolato ligands, the cis arrangement of the ligands in **3** is sterically counterintuitive and is likely due to London dispersion (LD) energy effects. Complex **4**, also has an unusual structural pattern in which only a single thiolato ligand is incorporated in the structure probably for steric reasons. It has a planar trapezoidal Cu_4 core in which three Cu--Cu edges are bridged by the mesityl groups while the

remaining Cu--Cu edge is thiolato ligand bridged. Dispersion connected DFT calculations show that **3** has the highest LD effect stabilization arising from the increased numbers of C-H···H-C interactions of the isopropyl ligand substituents.

INTRODUCTION

Sterically crowding ligands are widely used in inorganic/organometallic chemistry to stabilize compounds with unusual coordination numbers, bonding and/or oxidation states.[1-5] Their use is predicated on the notion that such ligands repel each other due to their overlapping electron clouds. In effect, there is intrusion of electronic wave functions on each other's space contrary to the Pauli exclusion principle, i.e., Pauli repulsion. However, in addition to this repulsion, there is growing evidence that attractive London dispersion (LD) interactions between the C-H moieties of the hydrocarbyl substituents of the ligands[5-7] can generate unexpected effects and enable the formation of species with unusual structures. Such effects are manifested for example, in the stable hexaphenylethane derivative $\{C(C_6H_3\text{-}3,5\text{-}^tBu_2)_3\}_2$ of Grimme and Schreiner,[8] the divalent group 14 chalcogenetates,[9] high oxidation state mid to late transition metal alkyls,[10,11] or in the low coordinate copper (II) amides.[12] In pursuit of further examples of low coordinate copper (II) species, we investigated the use of large terphenyl substituted thiolato ligands where dispersion effects had been noted earlier by Ziegler.[5] The use of the terphenyl thiolato ligands has recently afforded the first dimeric copper(I) thiolato derivatives[13] $\{CuSAr^{iPr4}\}_2$ and $\{CuSAr^{iPr6}\}_2$ from the reaction of the thiol with a mesitylcopper(I)[14] precursor. Upon further investigation we found that adjustment of the ratio of the thiolate ligand to copper yielded unknown types of heteroleptic organo/thiolato copper molecules $\{Cu_2(SAr)Mes\}_2$ (Mes = $\text{-}C_6H_2\text{-}2,4,6\text{-}Me_3$; Ar = $\text{-}C_6H_3\text{-}2,6\text{-}(C_6H_2\text{-}2,4,6\text{-}Me_3)_2$ (Ar^{Me6}), **1**; $\text{-}C_6H_3\text{-}2,6\text{-}(C_6H_3\text{-}2,6\text{-}iPr_2)_2$ (Ar^{iPr4}), **2**; $\text{-}C_6H_3\text{-}2,6\text{-}(C_6H_2\text{-}2,4,6\text{-}iPr_3)_2$ (Ar^{iPr6}), **3**) and

{$Cu_4(SAr)Mes_3$} (Ar= C_6H-2,6-(C_6H_2-2,4,6-Me_3)$_2$-3,5-iPr_2 (Ar^{iPr8}), **4**. Whereas **1** and **2** feature the expected alternating thiolato and mesityl ligands in which the pairs of mesityl and thiolato groups appear trans to each other, the more crowded Ar^{iPr6} substituted **3** has a structure in which the mesityl and thiolato groups have mutually cis positions apparently as a result of enhanced ligand dispersion effects. This cis structural arrangement of ligands was unknown in organocopper chemistry featuring Cu_4 core arrays. X-ray crystallographic studies revealed that complexes **1**-**4** display Cu_4 cores but their thiolato ligands were found to have different arrangements relative to the Cu_4 core, Thus, whereas **1** and **2** have symmetrical structures and alternating aryl and thiolate ligands (Figure 3.1), **3** has a unique cis disposition of these ligands. The very large size of the aryl substituents in **4** prevents the incorporation of further thiolato groups.

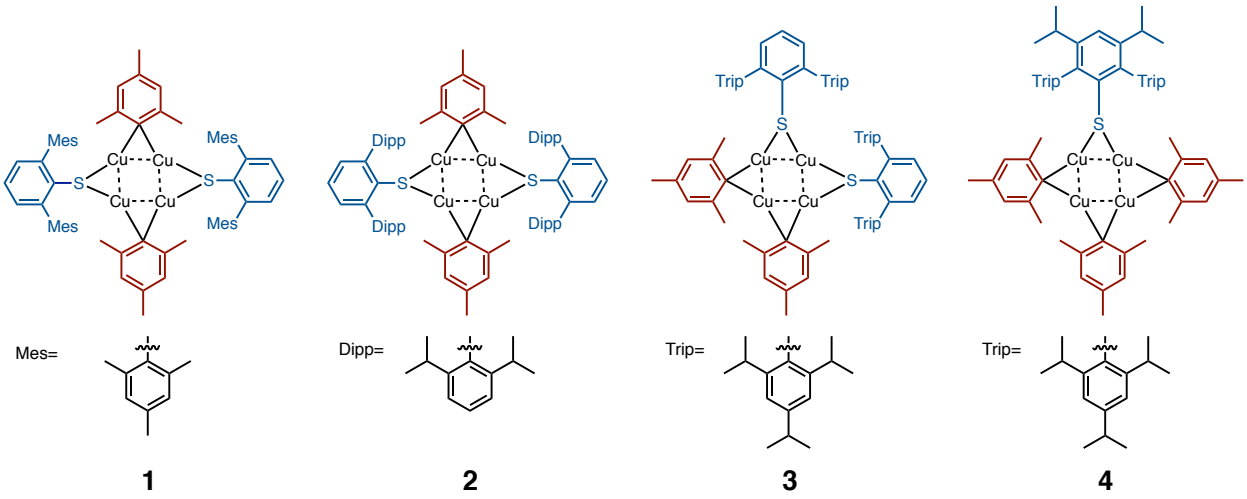

Figure 3.1 complexes **1**-**4** with different ligand arrangements.

RESULTS AND DISCUSSION

Structures

The reactions of the terphenyl thiols ($HSAr^{Me6}$ for **1**, $HSAr^{iPr4}$ for **2**, $HSAr^{iPr6}$ for **3** and $HSAr^{iPr8}$ for **4**) and half equiv of {CuMes}$_4$ in THF at 80^{o}C for two days (in toluene at 110^{o}C, four days for **4**)

afforded the aryl copper terphenyl thiolates **1**-**4**. The structures of the heteroleptic aryl/thiolato copper derivatives **1** and **2** have little precedent but they are related to previously reported heteroleptic tetracopper species $\{Cu_2RindBr\}_2$ (Rind= rigid fused-ring s-hydrindacenyl skeleton)[15] and $\{LAl(R)OCu{\cdot}MesCu\}_2$ (L= $HC[C(Me)N(Dipp)]_2$, R=Me or Et).[16] The compound **1** (Figure 3.2, left) displays a Cu_4 core array arranged in a non-planar parallelogram in which the metals are bridged by the C_{ipso} atoms of the mesityls or thiolato ligand sulfur atoms in an alternating manner. The two sulfur atoms are located on the same side of the Cu_4 core. The S atoms have pyramidalized coordination in which the sum of the angles at S =302.22(14)°. The Cu--Cu distances bridged by the thiolato groups are 2.82(7) and 2.86(7) Å whereas those bridged by the mesityl ligands are ca. 0.4 Å shorter at 2.43(5) and 2.43(5) Å. The latter pair of distances are greater than the sum of the covalent radii (2.24 Å)[17] of two Cu atoms but lie within the sum of the van der Waals radii (2.8 Å),[18] suggesting either no covalent Cu--Cu bonding or weak van der Waals interactions. The lengths of Cu-S bonds range from 2.16(11) to 2.18(9) Å, which are similar to those in other copper thiolates.[19] Likewise, the structure of complex **2** (Figure 3.2, right) is similar to that of **1**, but it has a center of symmetry in which the planar, rectangular Cu_4 core is also coplanar with C_{ipso} atoms C31 and C31′ of the mesityl groups. The two pyramidally coordinated S atoms of the thiolato ligands are located on the opposite side of the Cu_4 plane with a distance between of 0.76(8) Å the S atom and extended Cu_4 core that generates an interplanar angle of 24.91(18)º between these planes. As before, the separation of the Cu atoms bridged by the thiolates (2.92(6) Å) is much greater than the separation between copper atoms bridged by the mesityl groups (2.45(5) Å).

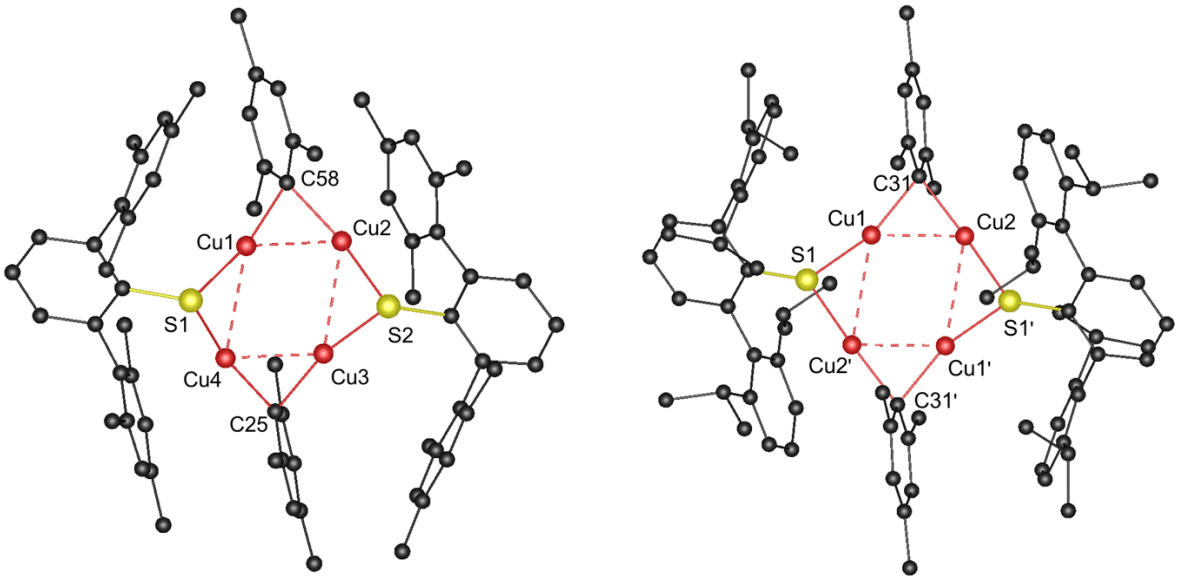

1 **2**

Figure 3.2 Molecular structures of **1** and **2** with thermal ellipsoids shown at 30% probability. Hydrogen atoms are not shown. Selected lengths (Å) and angles (deg) of **1**: Cu1--Cu2 2.43(5), Cu2--Cu3 2.86(7), Cu3--Cu4 2.43(5), Cu4--Cu1 2.82(7), S1-Cu1 2.16(8), S1-Cu4 2.18(8), C58-Cu1 2.00(2), C58-Cu2 1.99(2), Cu1-Cu2-Cu3 77.97(17), Cu2-Cu3-Cu4 101.86(2), Cu1-C58-Cu2 75.20(8), Cu2-S2-Cu3 80.96(3), and for **2**: Cu1--Cu2 2.45(5), Cu1--Cu2′ 2.92(6), S1-Cu1 2.17(6), S1-Cu2′ 2.16(6), C31-Cu1 2.00(2), C31-Cu2 1.97(18), Cu1-Cu2-Cu1′ 80.58(17), Cu2-Cu1′-Cu2′ 99.42(17), Cu1-C31-Cu2 75.86(7), Cu1-S1-Cu2′ 84.73(2).

The combination of the thiol $HSAr^{iPr6}$ and $\{CuMes\}_4$ in THF with stirring at 80°C for two days gave a pale yellow solution which, upon removal of the solvent under reduced pressure and recrystallization from toluene, yielded complex **3** in 16% yield. Complex **3** incorporates two bulkier thiolato ligands, but its structure displays a cis arrangement of the ligands in which the S atoms of thiolato groups bridge the two adjacent Cu--Cu edges. In the solid state, **3** was observed to have a previously unknown and sterically counterintuitive cis arrangement of the ligands (shown

in Figure 3.3, left). The Cu1--Cu2 and the adjacent Cu1--Cu3 edges are bridged by the S atoms of thiolato groups while the Cu2--Cu4 and the adjacent Cu3--Cu4 edges are bridged by the C_{ipso} atoms of mesityl groups. The Cu--Cu distances spanned by the thiolato ligands are more than ca. 0.3 Å longer than the Cu--Cu distances bridged by the mesityl groups (2.42(5) Å), which is consistent with the distances in **1** and **2** above. Complex **3** also has several close interligand H-H contacts across the Cu_4 core within the sum of their van der Waals radii (ca. 2.4 Å) arising from the isopropyl groups of the thiolato and mesityl substituents (indicated with dashed blue lines in Figure 3.3, right), suggesting the LD interaction between thiolato and mesityl CH_3 groups. In contrast, no close interligand H-H contacts were observed in the molecular structures of either **1** or **2**, suggesting the sterically counterintuitive structure of **3** is a consequence of enhanced LD effects caused by increased number of isopropyl substituents.

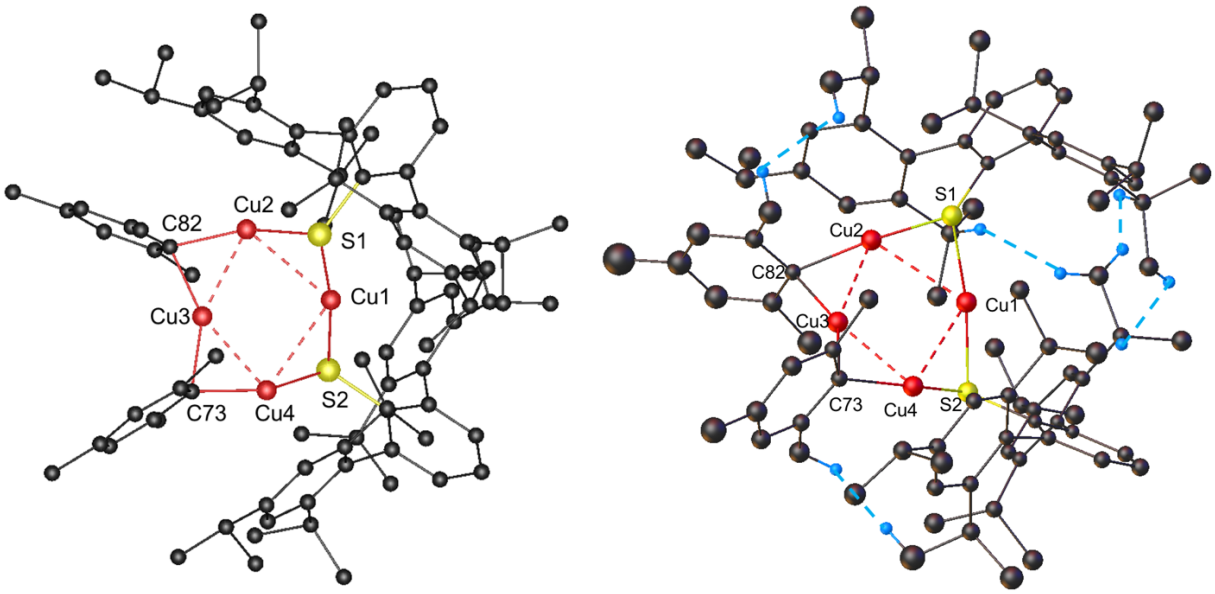

Figure 3.3 Molecular structure of **3** with thermal ellipsoids shown at 30% probability (left). Selected interatomic distances (Å) and angles (deg): Cu1--Cu2 2.73(5), Cu1--Cu4 2.76(5), Cu2--Cu3 2.42(5), Cu3--Cu4 2.42(5), S2-Cu1 2.17(6), S2-Cu4 2.20(6), C82-Cu2 2.01(2) C82-Cu3 2.00(2), Cu1-Cu2-Cu3 77.21(16), Cu2-Cu3-Cu4 111.87(19), Cu3-Cu4-Cu1 76.74(15), Cu4-Cu1-

Cu2 94.10(16), Cu1-S2-Cu4 78.02(2), Cu3-C73-Cu4 74.60(8). Some interligand H-H contacts across the Cu_4 core within the sum of their van der Waals radii (ca. 2.4 Å) are indicated with dashed blue lines (right). All other hydrogens are not shown.

We also investigated the reaction of the extremely bulky Ar^{iPr8} substituted thiol $HSAr^{iPr8}$ and $\{CuMes\}_4$ under similar conditions to those used for **3**, expecting to isolate a further example of a cis-substituted aryl thiolato copper isomer, i.e. $\{Cu_2(SAr^{iPr8})Mes\}_2$, with a structure analogous to that of **3**. The reaction of $HSAr^{iPr8}$ and $\{CuMes\}_4$ in toluene at 110°C for four days gave a yellow solution, from which some colorless crystals were isolated after 4-5 days' storage in a ca. 5 °C refrigerator. However, crystallographic and spectroscopic results showed that the complex incorporated only a single thiolato ligand, which resulted in an unusual, trapezoidal Cu_4 core array in which three Cu--Cu edges are bridged by the mesityls while one Cu--Cu edge is bridged by the thiolato ligand (Figure 3.4).

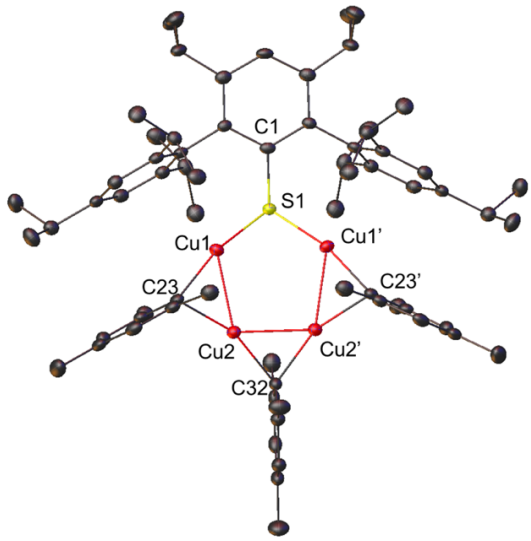

top view

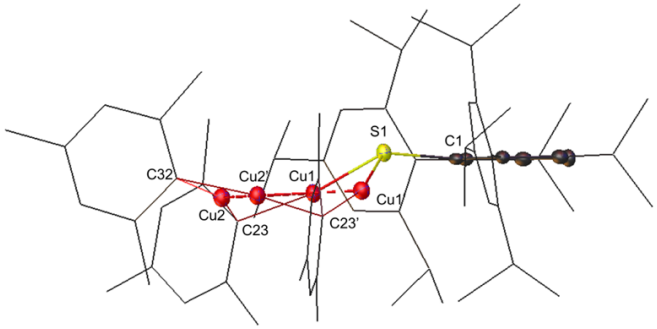

side view (ligands are shown as wire frames)

Figure 3.4 Top view and side view of the molecular structures of **4** with thermal ellipsoids shown at 30% probability (top view). Hydrogen atoms are not shown. Selected distances (Å) and angles (deg): Cu1--Cu2 2.45(5), Cu2--Cu2′ 2.37(8), Cu1--Cu1′ 3.21(8) S1-Cu1 2.17(6), C1-S1 1.78(3), Cu1-C23 1.98(2), Cu2-C32 1.99(2), Cu1-Cu2-Cu2′ 99.91(13), Cu1-S1-Cu1′ 95.43(4), Cu1-C23-Cu2 76.31(7), Cu2-C32-Cu2′ 73.14(10).

As depicted in Figure 3.4, complex **4** has an unusual trapezoid-shaped Cu_4 core with bridging by three mesityl groups and a single thiolato ligand. The essentially planar Cu_4 core lies parallel to the central ring of the thiolato ligand with a vertical distance of 2.11(17) Å (see side view in Figure 3.4), the mesityl group that bridges Cu2 and Cu2′ is essentially perpendicular to the Cu_4 core plane. The sulfur atom S1 is located on the opposite side of the central ring of the thiolato ligand relative to the Cu_4 core (a distance of 0.058(12) Å between the sulfur and the extended central ring). C32 atom is located on the same side of the Cu_4 plane relative to the sulfur atom with a distance between S1 and extended Cu_4 plane of 0.97(9) Å, C23 and C23′ atoms lie on the other side (a distance between C23 and extended Cu_4 plane of 0.74(3) Å). The molecule is symmetric with respect to a mirror plane that is perpendicular to the Cu_4 plane and contains the C1-S1 single bond. The Cu1--Cu2 and Cu2--Cu2′ distances are slightly different (by ca. 0.08(5) Å). The Cu1--Cu2 distance is 2.45(5) Å, which is in the normal range for aryl copper species.[14,20] However, the Cu2--Cu2′ distance was determined to be 2.37(8) Å, which is at the shortest end of the range for Cu(I) thiolates,[13,21] aryl copper complexes[14,20] or even copper amides.[22-24] The Cu1--Cu1′ distance is 3.21(8) Å, which is considerably greater than the sum of the van der Waals radii (2.8 Å),[17] suggesting no significant interaction between these two copper centers.

Spectroscopy

The ^{1}H NMR spectrum of complex **1** is relatively simple and well resolved, showing two singlet signals at 1.98 (12H) and 1.85 (24H) ppm in C_6D_6 attributable to the protons of the methyl groups of the thiolato ligands. There are also two singlet signals centered at 2.28 (12H) and 2.21 (6H) ppm which can be assigned to the methyl hydrogens of the copper mesityl substituents. The ^{1}H NMR spectrum of complex **2** displays two singlets at 1.20 and 1.00 ppm in the aliphatic region for the methyl groups of the isopropyls of the thiolato ligands, each integrating to 24 hydrogens, and the hydrogens of the mesityl groups are observed as 2.33 and 2.29 ppm. In contrast, complex **3** displays a rather complicated ^{1}H NMR spectrum, which is expected due to the magnetic inequivalence caused by the lower symmetry of this molecule. Each isopropyl group has a unique chemical environment, which yields unique chemical shift values making it close to impossible to distinguish them by 1D ^{1}H NMR alone. The ^{1}H NMR spectrum of **4** has two sets of singlets centered at 2.63/2.51 and 1.99/1.76 ppm, respectively, corresponding to para and ortho methyls of the mesityl groups. The spectrum also shows three broadened signals (2.97, 2.54 and 2.41 ppm) expected for the methine hydrogens of isopropyls of the terphenyl thiol. The signals for methyl groups of the isopropyls resonate at 1.77, 1.23 and 1.08 ppm, which are comparable to those of complexes **2** and **3**. The UV−Vis spectra of complexes **1**-**4** show broad absorption bands in the range of 273 to 303 nm with the molar extinction coefficient in the range of 1700 M^{-1} cm^{-1} to 3000 M^{-1} cm^{-1}, featuring a charge transfer process which is also seen in some related species.[13,25]

Computational Studies

To investigate the bonding in the copper species, the structures of compounds **2** and **3** were optimized using density functional theory (DFT) at the PBE1PBE/Def2-TZVP level of theory with

and without empirical dispersion correction (GD3BJ) (see SI, Table S3.2). Inspection of the optimized bond parameters (Table S3.2 in SI) reveals that the calculated structures are generally in good agreement with those experimentally observed. The dispersion corrected structures show slightly shorter Cu-Cu distances than those measured in the solid state, but this could be accounted for by the solid-state packing effects. In contrast, the optimizations conducted without a dispersion correction returned gas phase structures with slightly underestimated bond interactions.

Then, the hypothetical structures of cis-**2** and trans-**3** molecules were optimized and the energies of the two isomers were compared (Table 3.1). The results show that for both compounds **2** and **3** the cis isomer is more stable than the trans isomer. In the case of **2**, however, the Gibbs free energy difference is only 0.2 kJ·mol^{-1} in favor of the cis-isomer, for **3** the energy difference is more substantial, amounting to 15.8 kJ·mol^{-1}. The experimentally obtained isomer **2** is most likely stabilized by solid state effects, which cannot be reproduced by these gas phase calculations.

Table 3.1 Calculated energies (in a.u.) and the energy difference (in kJ·mol^{-1}) of the **2** and **3** cis- and trans-isomers.

	$\mathbf{2}_{cis}$	$\mathbf{2}_{trans}$	$\mathbf{3}_{cis}$	$\mathbf{3}_{trans}$
	PBE1PBE-D3	PBE1PBE-D3	PBE1PBE-D3	PBE1PBE-D3
E (a.u.)	-10383.77692	-10383.774290	-10854.820530	-10854.81715
H (a.u.)	-10383.77598	-10383.773346	-10854.819586	-10854.81621
G (a.u.)	-10384.00867	-10383.008598	-10855.092833	-10855.0868
$\Delta E_{cis\text{-}trans}$ (kJ·mol^{-1})	-6.9		-8.9	
$\Delta H_{cis\text{-}trans}$ (kJ·mol^{-1})	-6.9		-8.9	
$\Delta G_{cis\text{-}trans}$ (kJ·mol^{-1})	-0.2		-15.8	

The thermodynamic data for the dissociation reaction of **2**/**3** → 2 MesCu and 2 TerphSCu fragments were investigated. The data are summarized in Table 3.2. Without the dispersion effects, the Gibbs free binding energies are 336 and 320 kJ·mol^{-1} for **2** and **3**, respectively.

Table 3.2 Energies for the dissociation reaction **2**/**3** → 2 TerphSCu + 2 MesCu (kJ·mol^{-1}) with/without LD effects.

	2 PBE1PBE-D3	**2** PBE1PBE	**3** PBE1PBE-D3	**3** PBE1PBE
ΔE	740	508	759	502
ΔH	747	515	767	510
ΔG	549	336	562	320

However, when the dispersion correction is applied, the ΔG value is increased to 549 (for **2**) and 562 (for **3**) kJ·mol^{-1}. These data clearly suggest that dispersion effects play a significant role in the energy of the association of **2** and **3**. This is further corroborated by an energy decomposition analysis (EDA) which confirms that ca. 25 % (**2**) and 28 % (**3**) of the overall bonding energy can be attributed to dispersion (Figure 3.5).

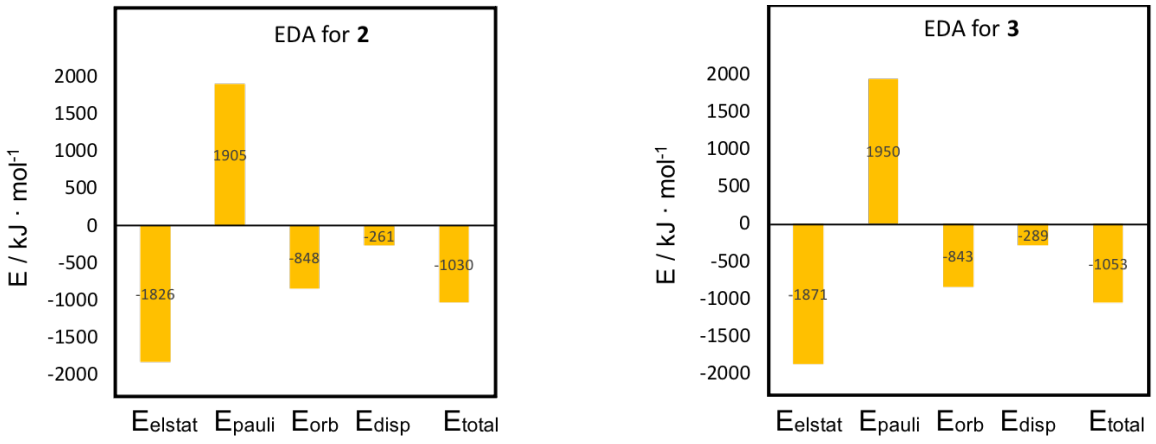

Figure 3.5 Summary of Energy Decomposition Analysis (EDA) results for **2** and **3** (kJ·mol^{-1}).

Conclusion

Four new mixed-ligand copper(I) thiolato compounds were synthesized by the treatment of large terphenyl thiols with mesitylecopper(I). These species have rare Cu_4 core arrays that are bridged by thiolato and organic groups and display a counterinitiative structural arrangement in the case of **3**. Dispersion forces are shown to be a significant factor in the molecular structures of the compounds, which is evidenced by structural and theoretical studies.

EXPERIMENTAL SECTION

General considerations.

All manipulations were carried out under anaerobic and anhydrous conditions by using Schlenk techniques or in a Vacuum Atmospheres OMNI-Lab drybox under an atmosphere of dry argon or nitrogen. Solvents were dried by the method of Grubbs[26] and co-workers, stored over potassium or sodium, and then degassed by the freeze-pump-thaw method. All physical measurements were made under strictly anaerobic and anhydrous conditions. The NMR spectra were recorded on a Varian Inova 600 MHz spectrometer, and the ^{1}H NMR spectra were referenced to the residual solvent signals in deuterated benzene, while the ^{13}C NMR spectra were referenced to the residual solvent signals in deuterated THF. IR spectra were recorded as Nujol mulls between CsI plates on a PerkinElmer 1430 spectrometer. UV−vis spectra were recorded as dilute hexane solutions in 3.5 mL quartz cuvettes using an Olis 17 modernized Cary 14 UV−vis−near-IR spectrophotometer or an HP 8452 diode-array spectrophotometer. The terphenyl thiols $HSAr^{Me6}$, $HSAr^{iPr4}$, $HSAr^{iPr6}$ [27] and mesitylcopper(I)[14] were prepared via literature methods. Unless otherwise stated, all materials were obtained from commercial sources and used as received.

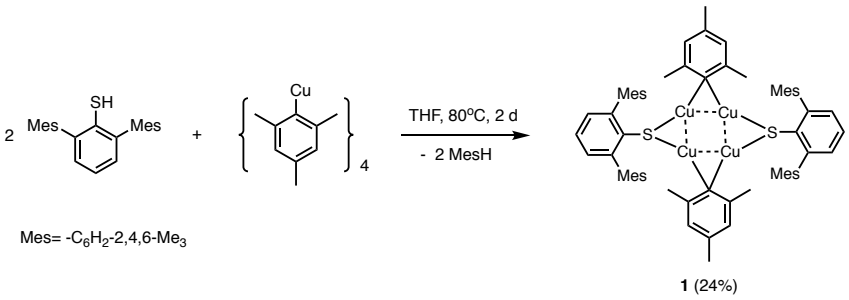

Figure 3.6 Synthesis of the complex **1**

{$Cu_2(SAr^{Me6})Mes\}_2$ (1) Solid terphenyl thiol $HSAr^{Me6}$ (0.346 g, 1 mmol) was combined with $\{CuMes\}_4$ (0.364 g, 0.5 mmol), and ca. 60 mL of THF was added. The solution was heated at 80°C for 2 days, yielding a pale yellow color. The solvent was then evaporated under reduced pressure to dryness, and the pale yellow residue was extracted with ca. 50 mL of hexane. The solution was filtered through Celite and concentrated to ca. 15 mL under reduced pressure until the formation of small colorless crystals was observed. The solution was stored in a ca. -18 °C freezer for 4 days to yield 0.287 g (24%) of **1** as colorless crystals which were suitable for X-ray crystallography. Mp: 198-201°C. ^{1}H NMR (600 MHz, benzene-d_6): δ= 7.11 (s, 1H), 6.82 (t, J = 7.2 Hz, 2H), 6.65 (d, J = 1.0 Hz, 2H), 6.64 (d, J = 1.0 Hz, 2H), 6.61 (s, 4H), 6.58 (s, 7H), 2.28 (s, 12H), 2.21 (s, 6H), 1.98 (s, 12H), 1.85 (s, 24H). ^{13}C NMR (150 MHz, benzene-d_6): δ= 155.96, 143.29, 139.72, 139.25, 137.12, 136.20, 134.71, 129.30, 128.84, 128.16, 125.49, 125.33, 29.02, 21.21, 21.03, 20.08. UV/vis: λ/nm (ε/M^{-1} cm^{-1}): 303 (1700). IR (Nujol; $\tilde{\nu}$/cm^{-1}): 1659w, 1590w, 1562w, 1455s, 1370s, 1258w, 1048w, 841m, 792m, 769w, 737m, 719w, 705w, 571w.

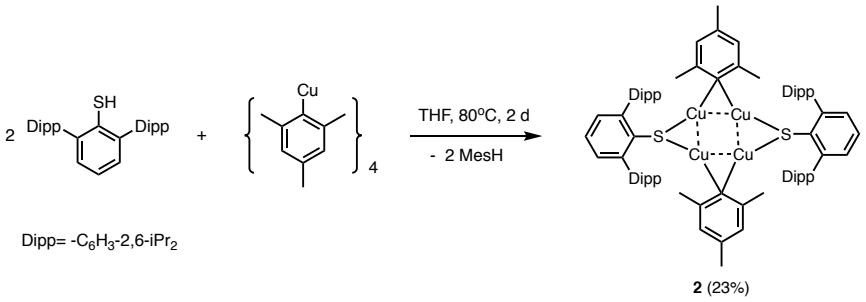

Figure 3.7 Synthesis of the complex **2**

{Cu$_2$(SAr^{iPr4})Mes}$_2$ (2). The synthesis of **2** was accomplished in a similar manner to that of **1** with the use of the terphenyl thiol HSAr^{iPr4} (0.43 g, 1 mmol) and {CuMes}$_4$ (0.364 g, 0.5 mmol) in ca. 60 mL of THF, yielding 0.31 g (23%) of colorless crystals which were suitable for X-ray crystallographic studies. Mp: decomposed at 190°C. ^{1}H NMR (600 MHz, benzene-d_6): δ 6.97-6.92 (m, 4H), 6.90 (d, J = 6.7 Hz, 8H), 6.88- 6.83 (m, 6H), 6.71 (s, 4H), 2.73 (m, J = 7.0 Hz, 8H), 2.33 (s, 6H), 2.29 (s, 12H), 1.20 (d, J = 6.9 Hz, 24H), 1.00 (d, J = 6.8 Hz, 24H). ^{13}C NMR (150 MHz, benzene-d_6) δ 156.17, 145.03, 142.55, 140.68, 139.96, 137.24, 132.73, 129.62, 129.60, 126.36, 126.34, 123.04, 30.74, 30.66, 30.11, 24.32, 23.76, 23.73. UV/vis: λ/nm (ε/M^{-1} cm^{-1}): 279 (3000). IR (Nujol; ṽ/cm^{-1}): 1930w, 1584w, 1569w, 1458s, 1371s, 1350m, 1319w, 1275w, 1255w, 1097w, 1050w, 1035m, 929w, 838s, 810m, 791s, 782s, 751s, 742s, 693w, 595w, 566w, 543w, 525w, 462w, 350w.

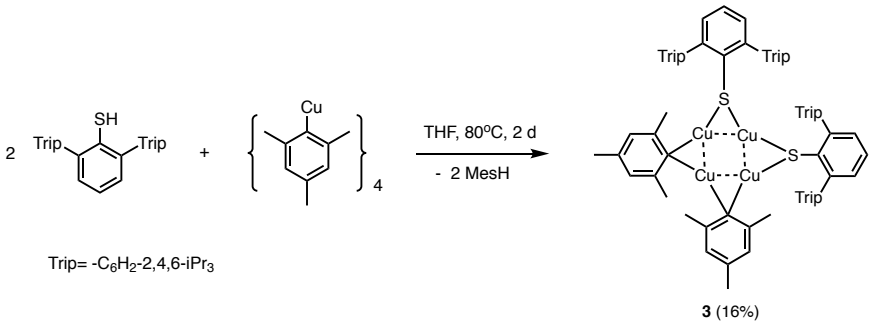

Figure 3.8 Synthesis of the complex **3**

{Cu_2(SAr^{iPr6})Mes}$_2$ (3). The terphenyl thiol $HSAr^{iPr6}$ (0.514 g, 1 mmol), {CuMes}$_4$ (0.364 g, 0.5 mmol) and ca. 60 mL of THF were combined in a Schlenk tube, and the solution was allowed to stir at 80°C for 2 days. The solvent was removed under reduced pressure, and the residue was extracted with ca. 50 mL of toluene, the resulting solution was filtered through Celite and the filtrate was concentrated to ca. 10 mL under reduced pressure and stored at room temperature for 4 days, yielded 0.24 g (16%) colorless crystals which were suitable for X-ray crystallography. Mp: 227-231°C. ^{1}H NMR (600 MHz, benzene-d_6): δ 7.26 (d, J = 13.0 Hz, 3H), 7.11 – 7.03 (m, 3H), 6.96 (dd, J = 14.8, 7.5 Hz, 3H), 6.76 – 6.64 (m, 4H), 6.54 (s, 2H), 6.36 (d, J = 18.9 Hz, 3H), 3.14 (q, J = 7.0 Hz, 2H), 2.95 (m, J = 19.8, 6.8 Hz, 5H), 2.89 – 2.64 (m, 3H), 2.61 – 2.53 (m, 2H), 2.52 – 2.32 (m, 8H), 2.26 (s, 5H), 2.08 (d, J = 13.4 Hz, 1H), 2.05 (s, 2H), 1.83 (s, 5H), 1.61 (d, J = 6.8 Hz, 5H), 1.47 – 1.24 (m, 24H), 1.23 (d, J = 6.9 Hz, 2H), 1.18 – 1.09 (m, 15H), 1.05 (d, J = 7.0 Hz, 6H), 1.01 (d, J = 6.9 Hz, 6H), 0.97 (d, J = 6.9 Hz, 6H), 0.72 (d, J = 6.8 Hz, 5H). ^{13}C NMR (150 MHz, benzene-d_6): δ 153.69, 153.02, 147.52, 147.42, 147.37, 145.57, 144.88, 142.78, 139.25, 138.04, 137.97, 137.65, 134.96, 130.66, 130.43, 128.92, 127.93, 124.09, 123.71, 121.52, 121.41, 120.98, 34.63, 32.56, 31.68, 31.01, 30.67, 30.64, 30.32, 28.82, 26.15, 25.74, 25.14, 24.98, 24.81, 24.79, 24.44, 24.08, 23.66, 23.25, 23.03, 22.19, 20.92. UV/vis: λ/nm (ε/M^{-1} cm^{-1}): 273 (2900). IR (Nujol; $\tilde{\nu}$/cm^{-1}): 1600m, 1589w, 1560w, 1455s, 1375s, 1355m, 1310w, 1255w, 1164w, 1096w, 936w, 872m, 843m, 796m, 761w, 741m, 723m, 688w, 645w, 518w, 459w.

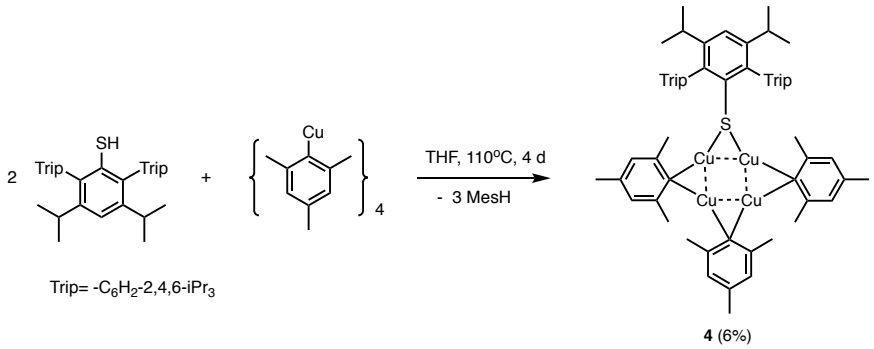

Figure 3.9 Synthesis of the complex **4**

{$Cu_4(SAr^{iPr8})Mes_3$} (4). Complex **4** was prepared in a manner analogous to that used for complex **3**. $HSAr^{iPr8}$ (0.4 g, 0.67 mmol) and $\{CuMes\}_4$ (0.243 g, 0.33 mmol) were combined as solids and ca. 50 mL of toluene was added, mixture was stirred at 110°C for 4 days. The solvent was then removed under reduced pressure to afford an off-white residue. The residue was dissolved in ca. 50 mL of toluene, and the solvent was concentrated under reduced pressure to ca. 4 mL. The solution was then stored at a 5°C refrigerator for 5 days to afford 0.11 g (6%) of product **4** as colorless blocks. Mp: 185-188°C. ^{1}H NMR (600 MHz, benzene-d_6): δ 7.29 (d, J = 1.8 Hz, 1H), 7.08 (d, J = 1.9 Hz, 4H), 6.59 (s, 4H), 6.40 (s, 2H), 2.99 (td, J = 6.8, 2.0 Hz, 4H), 2.63 (d, J = 1.9 Hz, 12H), 2.55 (s, 2H), 2.51 (s, 6H), 2.44 – 2.39 (m, 2H), 1.99 (d, J = 1.7 Hz, 6H), 1.83 – 1.76 (m, 12H), 1.76 (s, J = 1.7 Hz, 3H), 1.22 (dd, J = 7.0, 1.9 Hz, 12H), 1.07 (ddd, J = 13.4, 6.8, 1.9 Hz, 24H). ^{13}C NMR (150 MHz, benzene-d_6): δ 154.19, 153.28, 146.90, 145.68, 140.18, 136.69, 136.54, 135.58, 126.07, 125.91, 122.10, 32.32, 30.82, 30.32, 29.54, 28.53, 26.76, 24.67, 24.36, 23.03, 21.05, 20.92. UV/vis: λ/nm (ε/M^{-1} cm^{-1}): 294 (2300). IR (Nujol; $\tilde{\nu}$/cm^{-1}): 1589w, 1518w, 1456s, 1372s, 1308w, 871w, 842w, 798w, 765w, 720w.

X-ray Crystallographic Studies.

Crystals of complexes **1** and **2** suitable for X-ray crystallographic study were obtained from concentrated hexane solution at -18°C after 4 to 5 days, **3** and **4** were recrystallized from concentrated toluene. Single crystals were removed from Schlenk tubes and immediately covered with a layer of hydrocarbon oil. Suitable crystals were selected, mounted on a nylon cryo loop, and then placed in the cold nitrogen stream of the diffractometer. Data for **1**-**4** were collected at 90(2) K with Cu $K\alpha_1$ radiation (λ = 1.5418 Å) using a Bruker DUO diffractometer in conjunction with a CCD detector. The collected reflections were corrected for Lorentz and polarization effects and for absorption by using Blessing's method as incorporated into the program SADABS.[28,29] The structures were solved by direct methods and refined with the SHELXTL (2012, version 6.1) or SHELXTL (2013) software packages.[30] Refinement was by full-matrix least-squares procedures, with all carbon-bound hydrogen atoms included in calculated positions and treated as riding atoms. The thermal ellipsoid plots were drawn using OLEX2 software.[31] A summary of the crystallographic and data collection parameters is given in Table S1 in SI.

Computational details

The geometry optimizations of both isomers **2** and **3** were performed with the Gaussian16 (Revision C.01) program[32] using the PBE1PBE hybrid exchange functional[33] and Def2-TZVP basis sets.[34] In addition, Grimme's empirical dispersion correction with Becke-Johnson damping (GD3BJ)[35] was used as well as an ultrafine integration grid. Full analytical frequency calculations were performed for the optimized structures to ensure the nature of the stationary points found (minima, no imaginary frequencies). The energy decomposition analyses (EDA)[36] were performed using ADF2021.102 program package.[37] These calculations utilized the PBE1PBE functional and

TZ2P basis sets[38] for all atoms with empirical dispersion correction (GD3BJ) and good numerical quality.

Author Contributions

P. P. Power proposed and supervised the overall project. W. Zou carried out all experimental section, including synthesis, spectroscopy and data analysis. P. S. Vasko performed theoretical studies. J. C. Fettinger finalized X-ray data. W. Zou, P. S. Vasko and P. P. Power wrote and edited the paper.

ASSOCIATED CONTENT

Supporting Information.

The following files are available free of charge. ^{1}H and $^{13}C\{^{1}H\}$ spectra, crystallographic data, and details of computational studies (PDF)

Accession Codes

CCDC 2129403-2129404, 2129407-2129408 contain the supplementary crystallographic data for this paper. These data can be obtained free of charge via www.ccdc.cam.ac.uk/data_request/cif, or by emailing data_request@ccdc.cam.ac.uk, or by contacting The Cambridge Crystallographic Data Centre, 12 Union Road, Cambridge CB2 1EZ, UK; fax: +44 1223 336033.

AUTHOR INFORMATION

Corresponding Author

Philip P. Power − Department of Chemistry, University of California, Davis, Davis, California 95616, United States; orcid.org/0000-0002-6262-3209; Email: pppower@ucdavis.edu

Petra Vasko − Department of Chemistry, University of Helsinki, P.O. Box 55, FI-00014, Finland, orcid.org/0000-0003-4202-6869; Email: petra.vasko@helsinki.fi

Authors

Wenxing Zou − Department of Chemistry, University of California, Davis, Davis, California 95616, United States; orcid.org/0000-0002-5462-8982

James C. Fettinger − Department of Chemistry, University of California, Davis, Davis, California 95616, United States; orcid.org/0000-0002-6428-4909

Notes

The authors declare no competing financial interest.

ACKNOWLEDGMENTS

We thank the U.S. National Science Foundation for funding (Grant No. CHE-1565501) and for purchase of a dual source X-ray diffractometer (Grant No. CHE-0840444). PV would like to thank the Academy of Finland for funding (project numbers 314794, 338271 and 338271) and the CSC – IT Center for Science, Finland, for computational resources.

REFERENCES

[1] Bradley, D. C. Steric Control of Metal Coordination. *Chem*. *Br*. **1975**, *11*, 393-397.

[2] Power, P. P. Some Highlights from the Development and Use of Bulky Monodentate Ligands, *J. Organomet. Chem.*, **2004**, *689*, 3904-3919.

[3] Lappert, M. F. Use of the Bulky Alkyl Ligand $(Me_3Si)_2CH^-$ to Stabilize Unusual Low Valent Transition Metal Alkyls and Dialkylstannylene Derivatives, *Adv. Chem.*, **1976**, *150*, 256-265.

[4] Coles, M. P. the Role of the Bis-trimethylsilylamido Ligand, $[N\{SiMe_3\}_2]^-$, in Main Group Chemistry. Part 1: Structural Chemistry of the s-block Elements, *Coord. Chem. Rev.*, **2015**, *297-298*, 2-23.

[5] Seidu, I.; Seth, M. and Ziegler, T. Role Played by Isopropyl Substituents in Stabilizing the Putative Triple Bond in Ar′EEAr′ [E=Si, Ge, Sn; Ar′=C_6H_3-2,6(C_6H_3-2,6-Pri_2)$_2$] and Ar*PbPbAr* [Ar*=C_6H_3-2,6(C_6H_2-2,4,6-Pri_3)$_2$]. *Inorg. Chem.*, **2013**, *52*, 8378-8388.

[6] Wagner, J. P. and Schreiner, P. R. London Dispersion in Molecular Chemistry-Reconsidering Steric Effects, *Angew. Chem. Int. Ed.,* **2015**, *54*, 12274-12296.

[7] Pollard, V. A.; Kennedy, A. R.; McLellan, R.; Ross, D.; Tuttle, T. and Mulvey, R. E. Structurally Defined Ring-Opening and Insertion of Pinacolborane into Aluminium-Nitrogen Bonds of Sterically Demanding Dialkylaluminium Amides, *Eur. J. Inorg. Chem.*, **2021**, 2021, 50-53.

[8] Grimme, S. and Schreiner, P. R. Steric Crowding Can Stabilize a Labile Molecule: Solving the Hexaphenylethane Riddle, *Angew. Chem. Int. Ed.,* **2011**, *50*, 12639-12642.

[9] Rekken, B. D.; Brown, T. M.; Fettinger, J. C.; Lips, F; Tuononen, H. M.; Herber, R. H. and Power, P. P. Dispersion Forces and Counterintuitive Steric Effects in Main Group Molecules: Heavier Group 14 (Si-Pb) Dichalcogenolate Carbene Analogues with Sub-90° Interligand Bond Angles, *J. Am. Chem. Soc.,* **2013**, *135*, 10134-10148.

[10] Liptrot, D. J.; Guo, J.; Nagase, S.; Power, P. P. Dispersion Forces, Disproportionation, and Stable High-Valent Late Transition Metal Alkyls, *Angew. Chem. Int. Ed.*, **2016**, *55*, 14766-14769.

[11] Li, H.; Hu, Y.; Wan, D.; Zhang, Z.; Fan, Q.; King, R. B.; Schaefer, H. F. Dispersion Effects in Stabilizing Organometallic Compounds: Tetra-1-norbornyl Derivatives of the First-Row Transition Metals as Exceptional Examples, *J. Phys. Chem. A*, **2019**, *123*, 9514-9519.

[12] Wagner, C. L.; Tao, L.; Thompson, E. J.; Stich, T. A.; Guo, J.; Fettinger, J. C.; Berben, L. A.; Britt, R. D.; Nagase, S.; Power, P. P. Dispersion-Force-Assisted Disproportionation: A Stable Two-Coordinate Copper(II) Complex, *Angew. Chem. Int. Ed.*, **2016**, *55*, 10444-10447.

[13] Zou, W.; Zhu, Q.; Fettinger, J. C. and Power, P. P. Dimeric Copper and Lithium Thiolates: Comparison of Copper Thiolates with Their Lithium Congeners, *Inorg. Chem.*, **2021**, *60*, 17641-17648.

[14] Tsuda, T.; Yazawa, T.; Watanabe, K.; Fujii, T. and Saegusa, T. Preparation of Thermally Stable and Soluble Mesitylcopper(I) and its Application in Organic Synthesis, *J. Org. Chem.*, **1981**, *46*, 192-194.

[15] Ito, M.; Hashizume, D.; Fukunaga, T.; Matsuo, T. and Tamao, K. Isolated Monomeric and Dimeric Mixed Diorganocuprates Based on the Size-Controllable Bulky "Rind" Ligands. *J. Am. Chem. Soc.*, **2009**, *131*, 18024-18025.

[16] Li, B.; Zhang, C.; Yang, Y.; Zhu, H. and Roesky, H. W. Synthesis and Characterization of Heterobimetallic Al-O-Cu Complexes toward Models for Heterogeneous Catalysts on Metal Oxide Surfaces, *Inorg. Chem.*, **2015**, *54*, 6641-6646.

[17] Pyykkö, P. and Atsumi, M. Molecular Single-Bond Covalent Radii for Elements 1-118, *Chem. Eur. J.,* **2009**, *15*, 186-197.

[18] Tatewaki, H.; Hatano, Y.; Naka, T.; Noro, T. and Yamamoto. S. Atomic Radii for Depicting Atoms in a Molecule II: the Effective Atomic Radius and van der Waals Radius from ^{1}H to ^{54}Xe, *Bull. Chem. Soc. Jpn.*, **2010**, *83,* 1203-1210.

[19] Dance, I. G.; Bowmaker, G. A.; Clark, G. R. and Seadon, J. K. the Formation and Crystal and Molecular Structures of Hexa(μ-organothiolato) Tetracuprate(I) Cage Dianions: Bis(tetramethylammonium) Hexa(μ-methanethiolato)-Tetracuprate(I) and Two Polymorphs of Bis(tetramethylammonium) hexa(μ-benzenethiolato)-Tetracuprate(I), *Polyhedron,* **1983**, *2*, 1031-1043.

[20] Stollenz, M. and Meyer, F. Mesitylcopper-A Powerful Tool in Synthetic Chemistry, *Organometallics*, **2012**, *31*, 7708-7727.

[21] Rungthanaphatsophon, P.; Barnes, C. L. and Walensky, J. R. Copper(I) Clusters with Bulky Dithiocarboxylate, Thiolate, and Selenolate Ligands, *Dalton Trans*., **2016**, *45*, 14265–14276.

[22] Satyachand Harisomayajula, N. V.; Wu, B.-H.; Lu, D.-Y.; Kuo, T.-S.; Chen, I-C. and Tsai, Y.-C. Ligand-Unsupported Cuprophilicityin the Preparation of Dodecacopper(I) Complexes and Raman Studies, *Angew. Chem. Int. Ed*., **2018**, *57*, 9925-9929.

[23] Satyachand Harisomayajula, N. V.; Makovetskyi, S.; Tsai, Y.-C. Cuprophilic Interactions in and between Molecular Entities, *Chem. Eur. J*., **2019**, *25*, 8936-8954.

[24] Chiarella, G. M.; Melgarejo, D. Y.; Rozanski, A.; Hempte, P.; Perez, L. M.; Reberb, C. and Fackler, J. P. Jr. A Short, Unsupported Cu(I)--Cu(I) interaction, 2.65 Å, in A Dinuclear Guanidine Chloride Complex, *Chem. Commun*., **2010**, *46*, 136-138.

[25] Pratt, J.; Bryan, A. M.; Faust, M.; Boynton, J. N.; Vasko, P.; Rekken, B. D.; Mansikkamaki, A.; Fettinger, J. C.; Tuononen, H. M. and Power, P. P. Effects of Remote Ligand Substituents on the Structures, Spectroscopic, and Magnetic Properties of Two-Coordinate Transition-Metal Thiolate Complexes, *Inorg. Chem*., **2018**, *57*, 6491−6502.

[26] Pangborn, A. B.; Giardello, M. A.; Grubbs, R. H.; Rosen, R. K.; Timmers, F. J. Safe and Convenient Procedure for Solvent Purification, *Organometallics*, **1996**, *15*, 1518-1520.

[27] Barnett, B. R.; Mokhtarzadeh, C. C.; Lummis, P.; Wang, S.; Queen, J. D.; Gavenonis, J.; Schüwer, N.; Tilley, T. D.; Boynton, J. N.; Power, P. P.; Ditri, T. B.; Weidemann, N.; Agnew, D. W.; Figueroa, J. S.; Smith, P. W.; Carpenter, A. E.; Pratt, J. K.; Mendelson, N. D.; Figueroa, J. S. Terphenyl Ligands and Complexes, *Inorganic Synthesis*, **2018**, *37*, 85-122.

[28] Sheldrick, G. M. SADABS, Siemens Area Detector Absorption Correction; Göttingen Universitaï: Göttingen, Germany, **2008**, p33.

[29] Blessing, R. H. An Empirical Correction for Absorption Anisotropy. *Acta Cryst. Sect. A: Found. Cryst.,* **1995**, *51*, 33–38.

[30] Sheldrick, G. M. SHELXTL, version 6.1; Bruker AXS: Madison, WI, **2002**.

[31] Dolomanov, O. V.; Bourhis, L. J.; Gildea, R. J.; Howard, J. A. K.; Puschmann, H. OLEX2: A Complete Structure Solution, Refinement and Analysis Program. *J. Appl. Cryst.,* **2009**, *42*, 339–341.

[32] Gaussian 16, Revision C.01, Frisch, M. J.; Trucks, G. W.; Schlegel, H. B.; Scuseria, G. E.; Robb, M. A.; Cheeseman, J. R.; Scalmani, G.; Barone, V.; Petersson, G. A.; Nakatsuji, H.; Li, X.; Caricato, M.; Marenich, A. V.; Bloino, J.; Janesko, B. G.; Gomperts, R.; Mennucci, B.; Hratchian, H. P.; Ortiz, J. V.; Izmaylov, A. F.; Sonnenberg, J. L.; Williams-Young, D.; Ding, F.; Lipparini, F.; Egidi, F.; Goings, J.; Peng, B.; Petrone, A.; Henderson, T.; Ranasinghe, D.; Zakrzewski, V. G.; Gao, J.; Rega, N.; Zheng, G.; Liang, W.; Hada, M.; Ehara, M.; Toyota, K.; Fukuda, R.; Hasegawa, J.; Ishida, M.; Nakajima, T.; Honda, Y.; Kitao, O.; Nakai, H.; Vreven, T.; Throssell, K.; Montgomery, J. A.; Peralta, Jr., J. E.; Ogliaro, F.; Bearpark, M. J.; Heyd, J. J.; Brothers, E. N.; Kudin, K. N.; Staroverov, V. N.; Keith, T. A.; Kobayashi, R.; Normand, J.; Raghavachari, K.; Rendell, A. P.; Burant, J. C.; Iyengar, S. S.; Tomasi, J.; Cossi, M.; Millam, J. M.; Klene, M.;

Adamo, C.; Cammi, R.; Ochterski, J. W.; Martin, R. L.; Morokuma, K.; Farkas, O.; Foresman, J. B. and Fox, D. J. Gaussian, Inc., Wallingford CT, 2019.

[33] a) Perdew, J. P.; Burke, K. and Ernzerhof, M. Generalized Gradient Approximation Made Simple, *Phys. Rev. Lett.,* **1996**, *77*, 3865-3868. b) Perdew, J. P.; Burke, K. and Ernzerhof, M. Generalized Gradient Approximation Made Simple, *Phys. Rev. Lett.*, **1997**, *78*, 1396-1396. c) Adamo C. and Barone, V. Toward Reliable Density Functional Methods without Adjustable Parameters: the PBE0 Model. *J. Chem. Phys.*, **1999**, *110*, 6158-6169.

[34] a) Weigend, F. and Ahlrichs, R. Balanced Basis Sets of Split Valence, Triple Zeta Valence and Quadruple Zeta Valence Quality for H to Rn: Design and Assessment of Accuracy. *Phys. Chem. Chem. Phys.,* **2005**, *7*, 3297-3305. b) Weigend, F. Accurate Coulomb-Fitting Basis Sets for H to Rn. *Phys. Chem. Chem. Phys.*, **2006**, *8*, 1057-1065.

[35] Grimme, S.; Ehrlich S. and Goerigk, L. Effect of the Damping Function in Dispersion Corrected Density Functional Theory. *J. Comp. Chem.* **2011**, *32*, 1456-1465.

[36] a) Rodríguez, J. I.; Bader, R. F. W.; Ayers, P.W.; Michel, C.; Götz, A.W. and Bo, C. A High Performance Grid-Based Algorithm for Computing QTAIM Properties. *Chem. Phys. Lett.*, **2009**, *472*, 149-152, b) Rodríguez, J. I. An Efficient Method for Computing the QTAIM Topology of A Scalar Field: the Electron Density Case. *J. Comp. Chem.*, **2013**, *34*, 681-686.

[37] a) Te Velde, G.; Bickelhaupt, F. M.; Baerends, E. J.; Fonseca Guerra, C.; van Gisbergen, S. J. A.; Snijders, J. G. and Ziegler, T. Chemistry with ADF. *J. Comp. Chem.*, **2001**, *22*, 931-967, b) ADF 2021.1, SCM, Theoretical Chemistry, Vrije Universiteit, Amsterdam, The Netherlands, http://www.scm.com.

[38] van Lenthe, E. and Baerends, E. J. Optimized Slater-type Basis Sets for the Elements 1-118. *J. Comp. Chem.*, **2003**, *24*, 1142-1156.

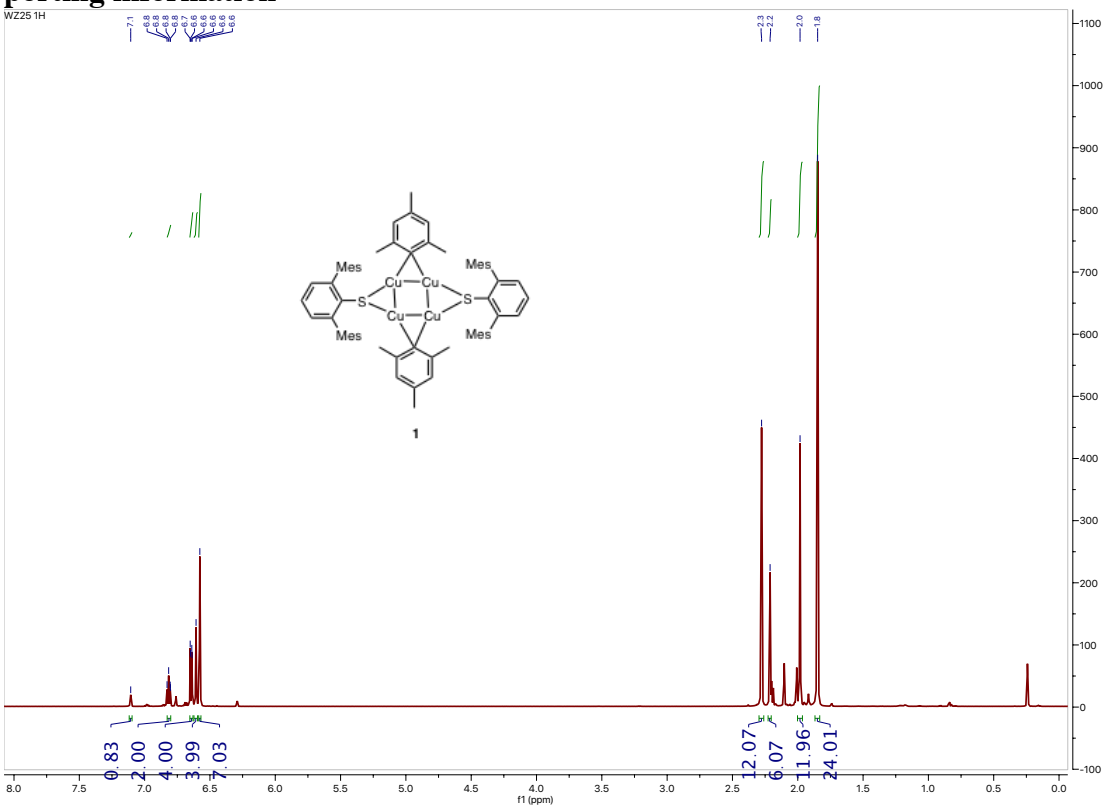

Figure S3.1 ^{1}H NMR spectrum of $\{Cu_2(SAr^{Me6})Mes\}_2$ (**1**) in C_6D_6 (600 MHz, 298 K)

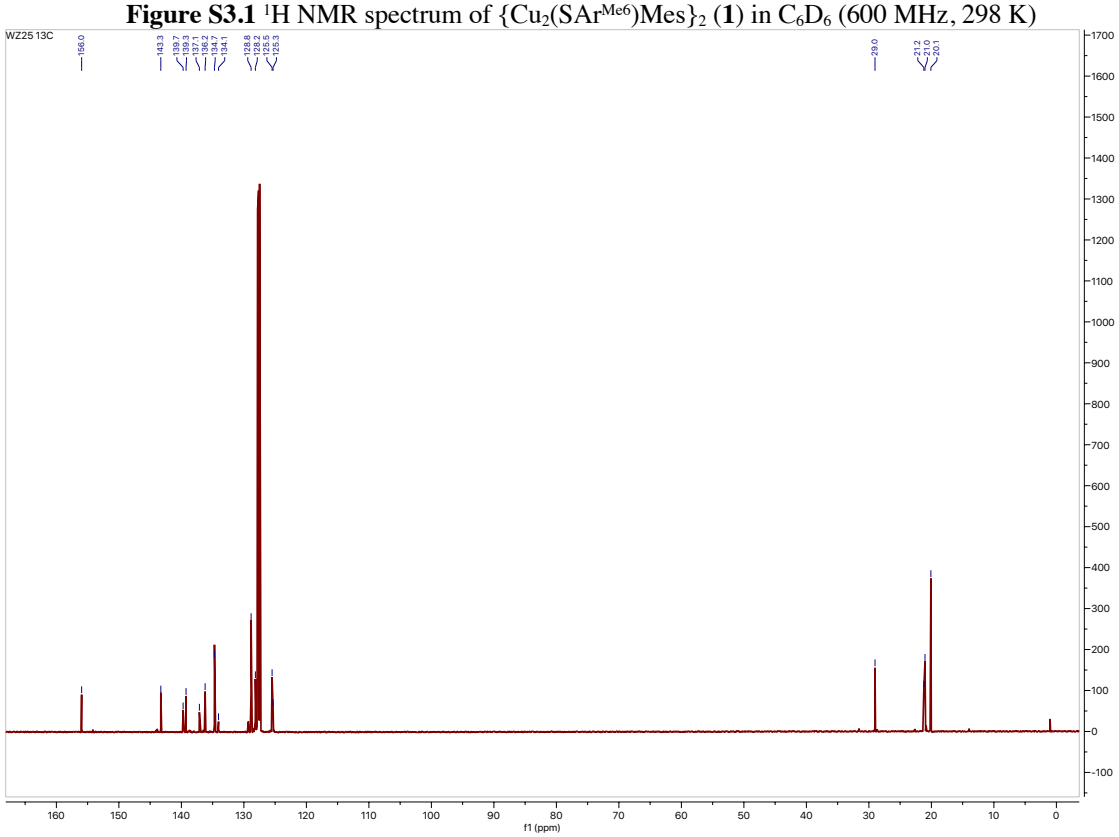

Figure S3.2 $^{13}C\{^{1}H\}$ NMR spectrum of $\{Cu_2(SAr^{Me6})Mes\}_2$ (**1**) in C_6D_6 (600 MHz, 298 K)

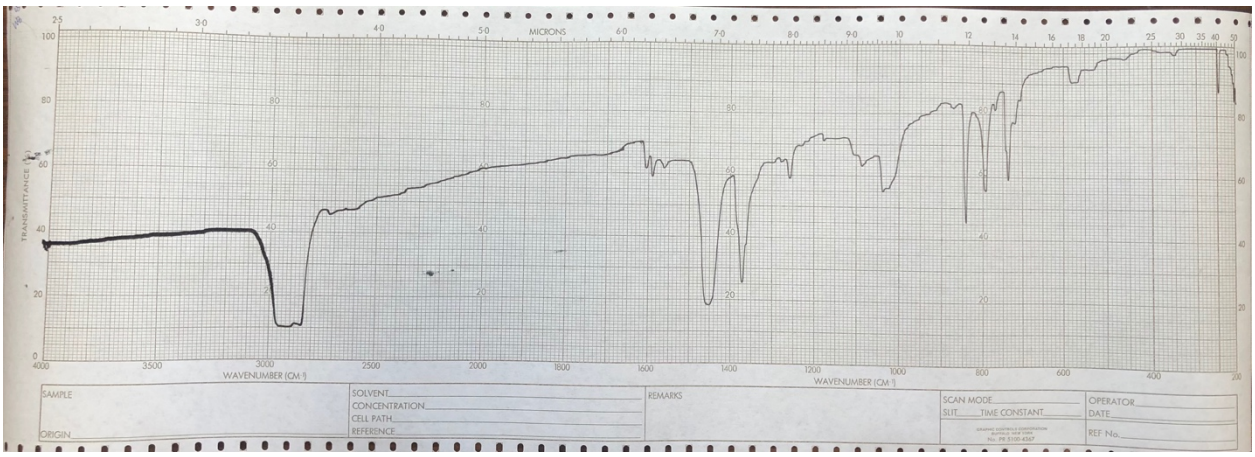

Figure S3.3 Infrared spectrum of a Nujol mull of $\{Cu_2(SAr^{Me6})Mes\}_2$ (**1**) at 25°C

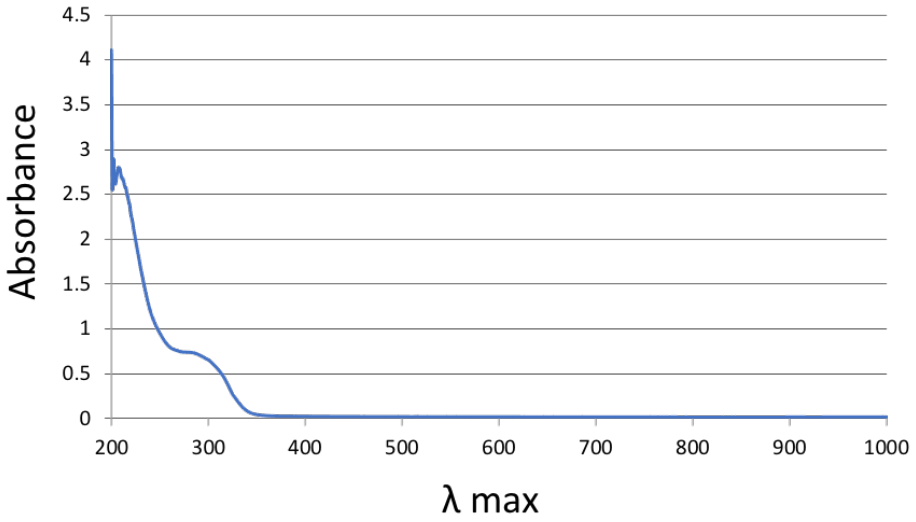

Figure S3.4 UV-Vis spectrum of $\{Cu_2(SAr^{Me6})Mes\}_2$ (**1**) at 25 °C (144 μM in hexanes)

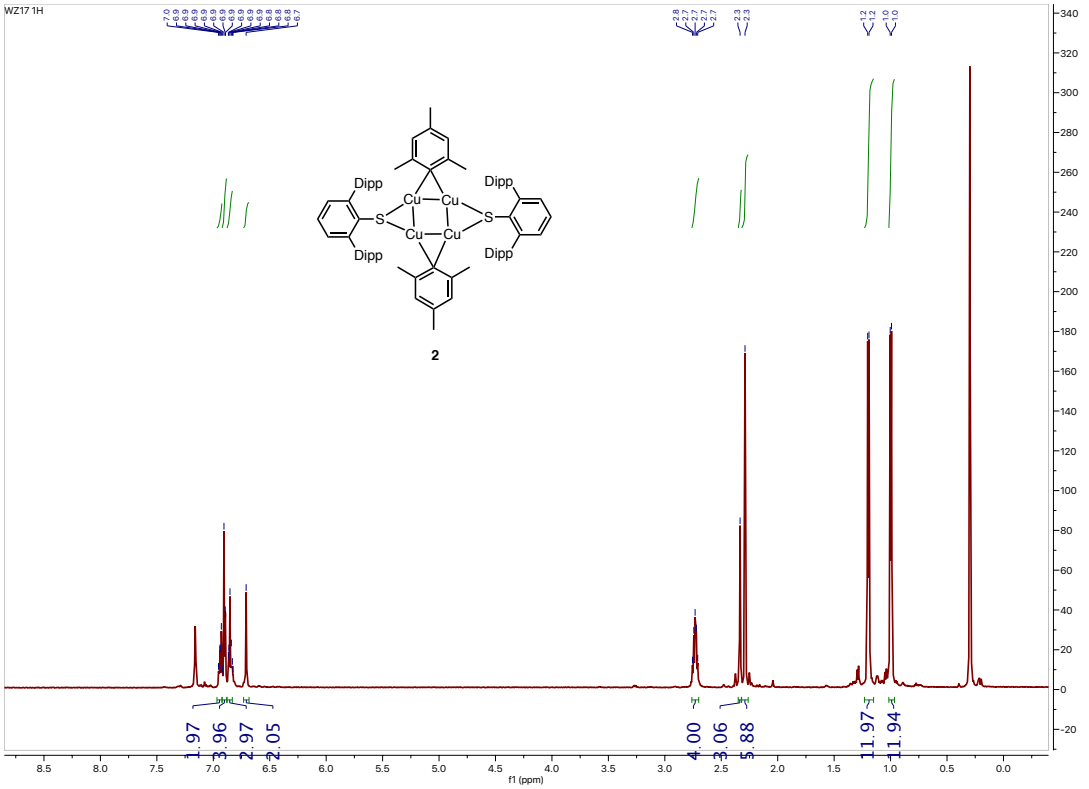

Figure S3.5 ^{1}H NMR spectrum of {$Cu_2(SAr^{iPr4})Mes$}$_2$ (**2**) in C_6D_6 (600 MHz, 298 K)

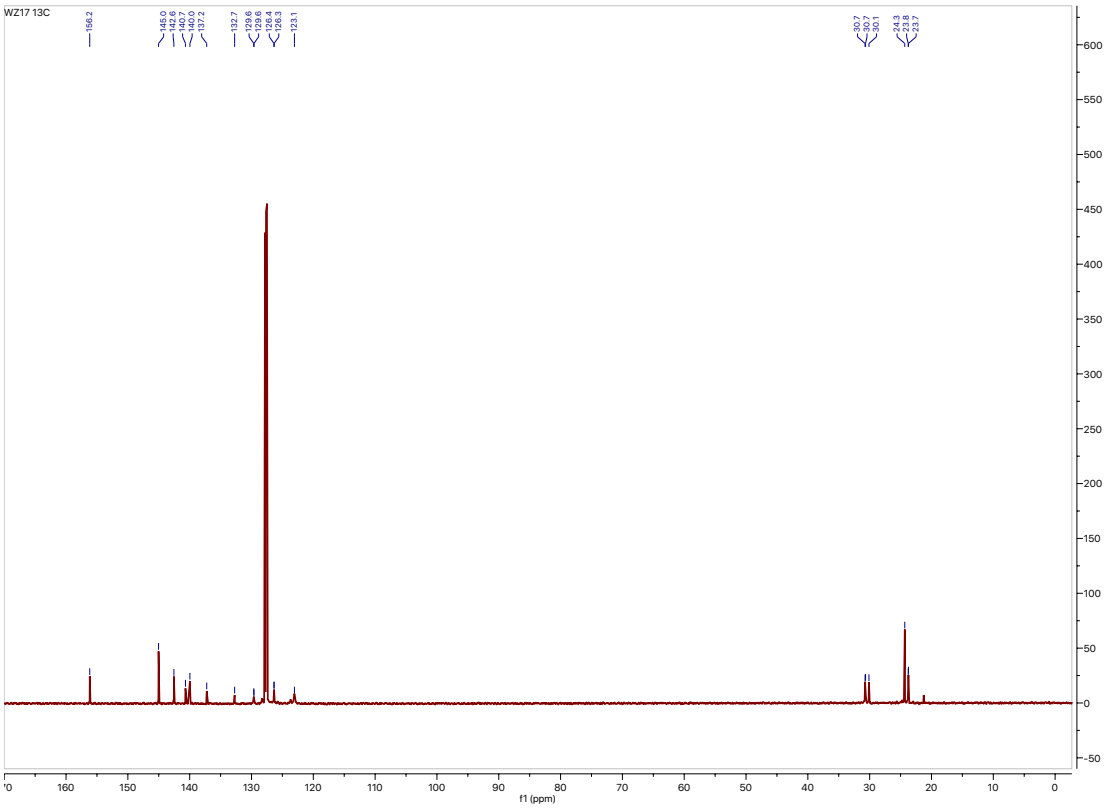

Figure S3.6 ^{13}C{^{1}H} NMR spectrum of {$Cu_2(SAr^{iPr4})Mes$}$_2$ (**2**) in C_6D_6 (150 MHz, 298 K)

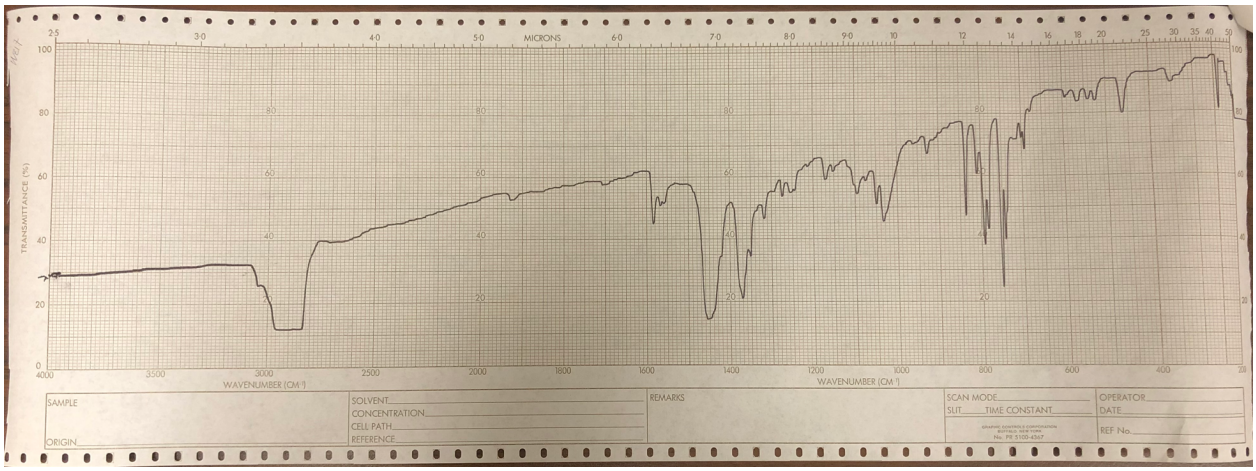

Figure S3.7 Infrared spectrum of a Nujol mull of $\{Cu_2(SAr^{iPr4})Mes\}_2$ (**2**) at 25°C

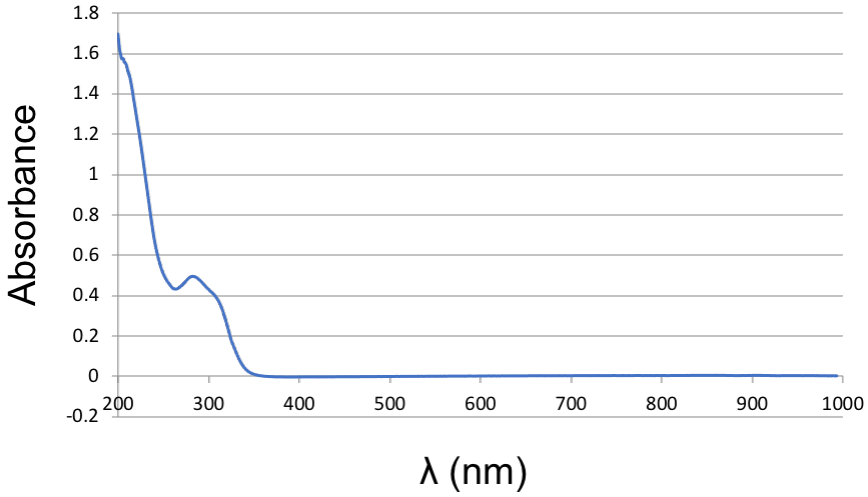

Figure S3.8 UV-Vis spectrum of $\{Cu_2(SAr^{iPr4})Mes\}_2$ (**2**) at 25 °C (163 μM in hexanes)

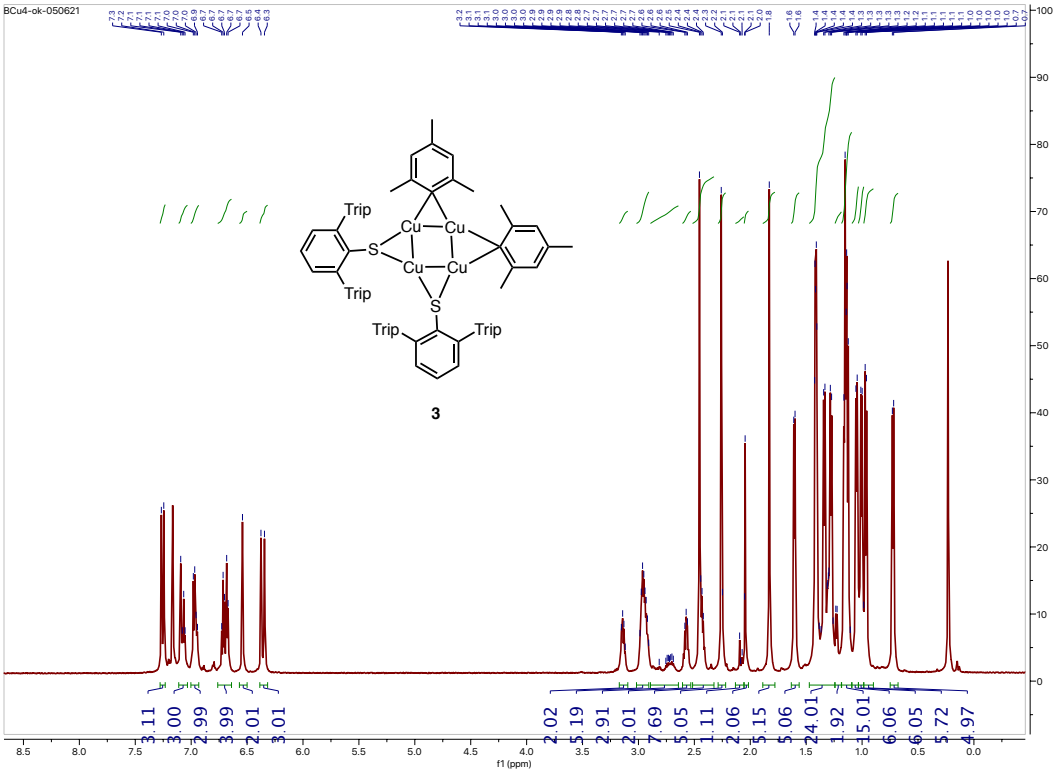

Figure S3.9 ^{1}H NMR spectrum of {$Cu_2(SAr^{iPr6})Mes$}$_2$ (**3**) in C_6D_6 (600 MHz, 298 K)

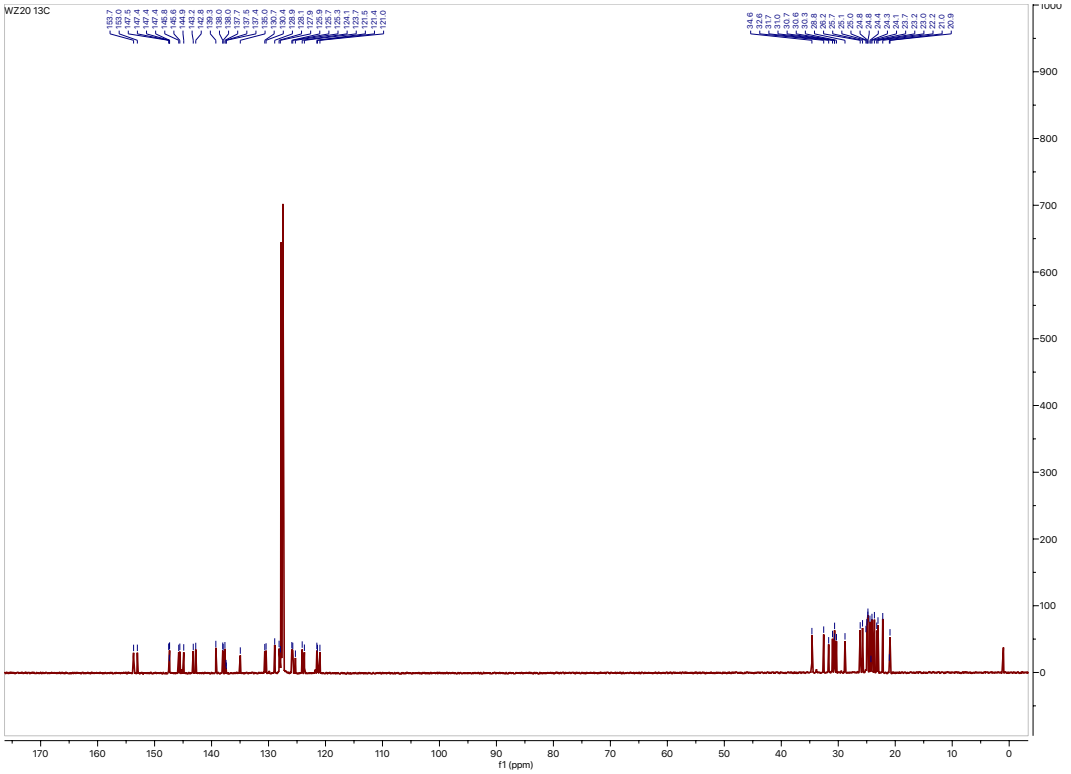

Figure S3.10 ^{13}C{^{1}H} NMR spectrum of {$Cu_2(SAr^{iPr6})Mes$}$_2$ (**3**) in C_6D_6 (150 MHz, 298 K)

Figure S3.11 Infrared spectrum of a Nujol mull of $\{Cu_2(SAr^{iPr6})Mes\}_2$ (**3**) at 25°C

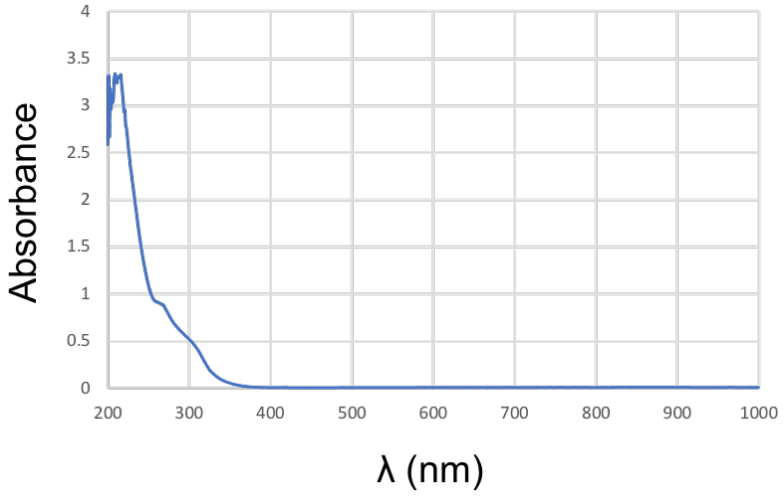

Figure S3.12 UV-Vis spectrum of $\{Cu_2(SAr^{iPr6})Mes\}_2$ (**3**) at 25 °C (279 μM in hexanes)

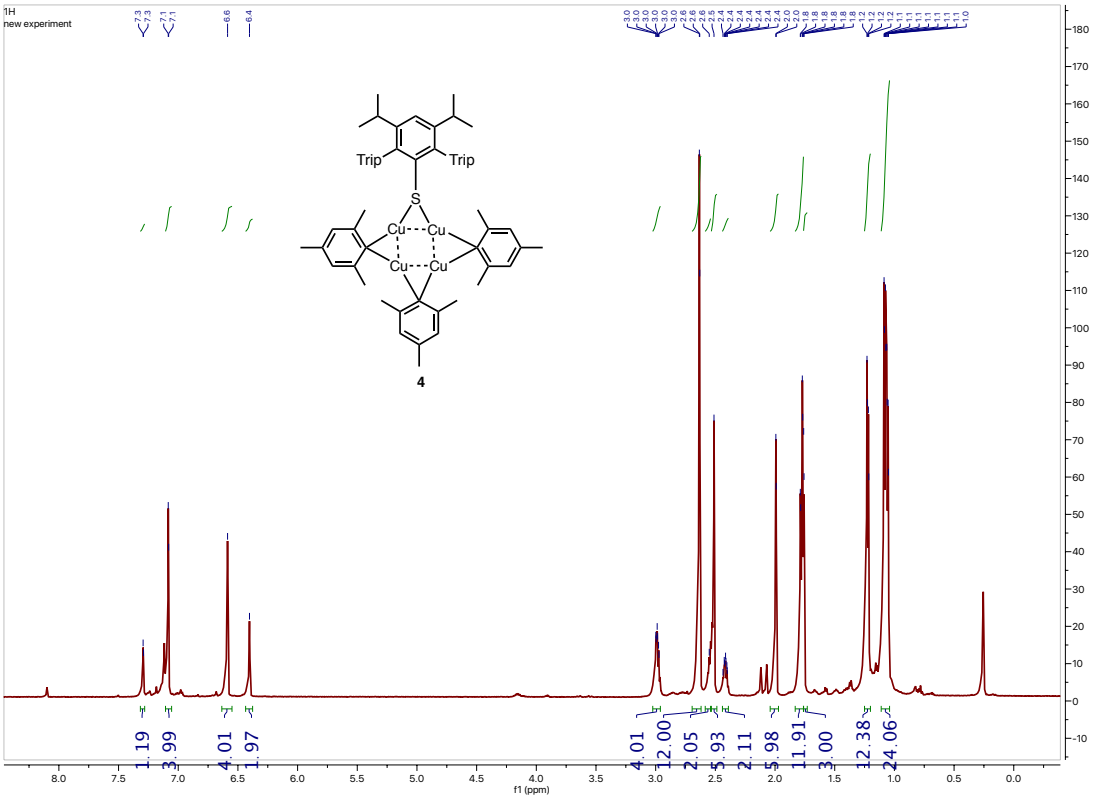

Figure S3.13 ^{1}H NMR spectrum of {$Cu_4(SAr^{iPr8})Mes_3$} (**4**) in C_6D_6 (600 MHz, 298 K)

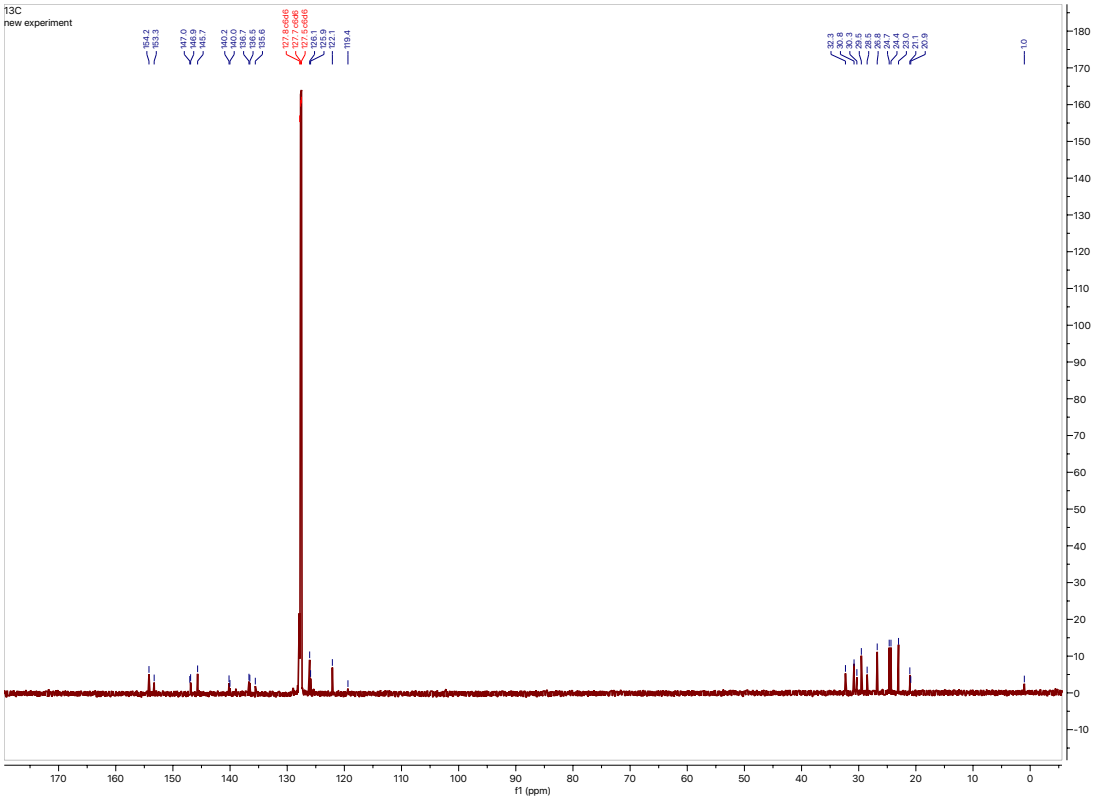

Figure S3.14 ^{13}C{^{1}H} NMR spectrum of {$Cu_4(SAr^{iPr8})Mes_3$} (**4**) in C_6D_6 (150 MHz, 298 K)

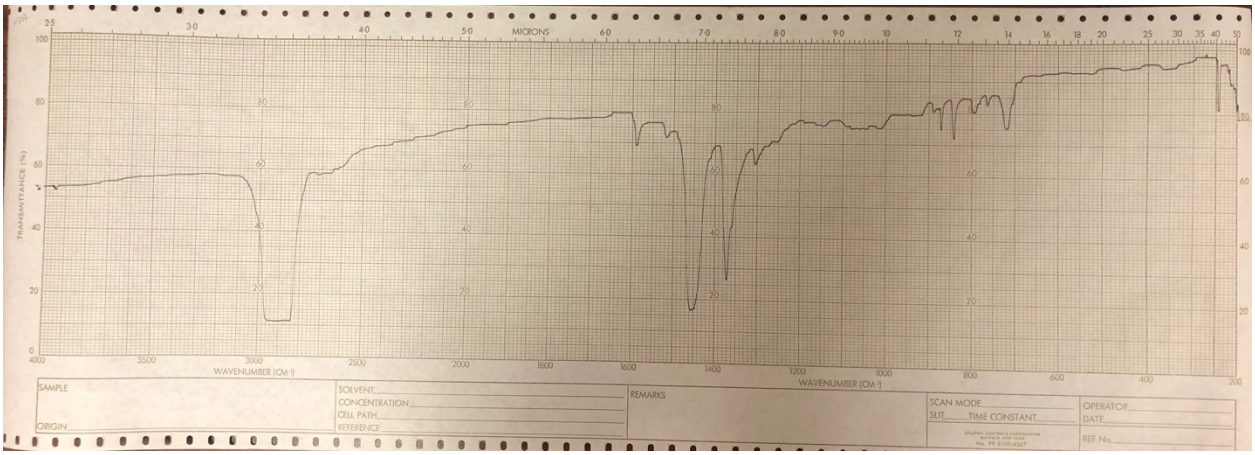

Figure S3.15 Infrared spectrum of a Nujol mull of {$Cu_4(SAr^{iPr8})Mes_3$} (**4**) at 25°C

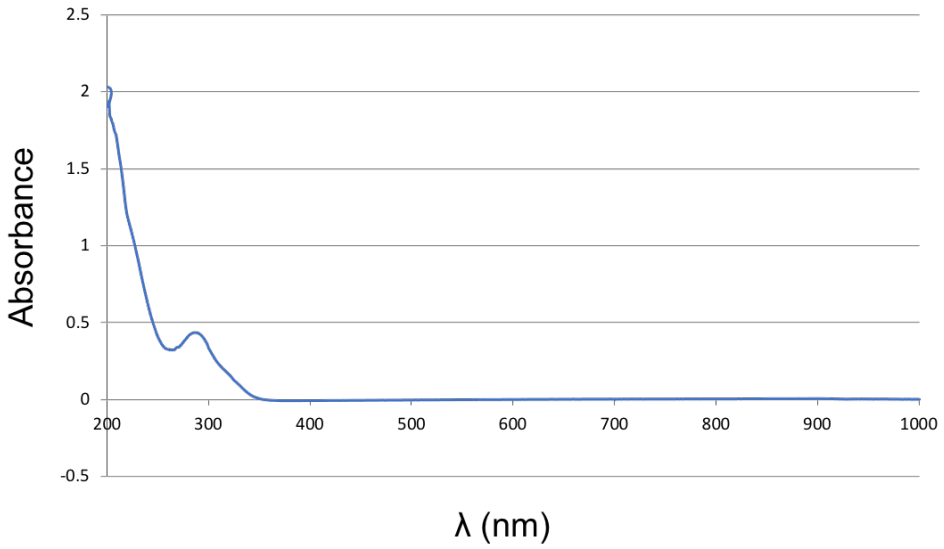

Figure S3.16 UV-Vis spectrum of {$Cu_4(SAr^{iPr8})Mes_3$} (**4**) at 25 °C (181 μM in hexanes)

Crystallography data

Table S3.1 Crystallographic parameters of **1**-**4**.

	1	**2**	**3**	**4**
formula	$C_{66}H_{72}Cu_4S_2$	$C_{78}H_{96}Cu_4S_2$	$C_{104}H_{136}Cu_4S_2$	$C_{69}H_{94}Cu_4S$
fw	1183.56	1351.82	1704.4	1209.70
color	colorless	colorless	colorless	colorless
cyst syst	monoclinic	monoclinic	triclinic	monoclinic
space group	C 2/c	P 2_1/n	P-1	P2_1/m
a, Å	25.0546(15)	12.6435(9)	15.6890(9)	12.1537(7)
b, Å	14.1816(9)	19.3995(17)	16.6057(10)	19.5933(12)
c, Å	32.2662(19)	14.6899(15)	18.1676(11)	14.0502(9)
α, deg	90	90	90.1316(10)	90
β, deg	96.6995(10)	108.793(9)	90.1437(10)	109.4542(9)
γ, deg	90	90	99.8453(10)	90
V, Å^3	11386.4(12)	3411.0(5)	4663.4(5)	3154.8(3)
Z	8	2	2	2
Density (calculated)	1.381 Mg/m^3	1.316 Mg/m^3	1.214 Mg/m^3	1.273 Mg/m^3
Absorption coefficient	1.587 mm^{-1}	2.281 mm^{-1}	0.989 mm^{-1}	1.401 mm^{-1}
F(000)	4928	1424	1816	1280
Crystal size	0.409 x 0.320 x 0.250 mm^3	0.476 x 0.371 x 0.267 mm^3	0.357 x 0.314 x 0.254 mm^3	0.368 x 0.237 x 0.232 mm^3
Crystal color and habit	Colorless Block	Colorless Block	Colorless Block	Colorless Block
Theta range for data collection	1.952 to 27.544°	3.911 to 69.613°	1.961 to 27.524°	2.079 to 27.547°
Index ranges	-32<=h<=32, -18<=k<=18, -41<=l<=41	-14<=h<=15, -23<=k<=22, -17<=l<=16	-20 <= h <= 20, -21 <= k <= 21, -23 <= l <= 23	-15<=h<=15, -25<=k<=25, -18<=l<=18

Reflections collected	50858	18204	42567	28803
Independent reflections	13126 [R(int) = 0.0493]	6264 [R(int) = 0.0208]	21444 [Rint = 0.0452]	7481 [R(int) = 0.0415]
Data / restraints / parameters	13126 / 0 / 667	6264 / 0 / 571	21444/0/1023	7481 / 0 / 366
Goodness-of-fit on F^2	1.031	1.053	1.021	1.030
Final R indices [I>2sigma(I)]	R_1 = 0.0332, wR_2 = 0.0732	R_1 = 0.0289, wR_2 = 0.0770	R_1 = 0.0410, wR_2 = 0.0829	R_1 = 0.0312, wR_2 = 0.0754
R indices (all data)	R_1 = 0.0493, wR_2 = 0.0792	R_1 = 0.0297, wR_2 = 0.0776	R_1 = 0.0663, wR_2 = 0.0917	R_1 = 0.0433, wR_2 = 0.0810
Largest diff. peak and hole	0.442 and -0.316 e.Å^{-3}	0.343 and -0.346 e.Å^{-3}	0.392 and -0.457 e.Å^{-3}	0.440 and -0.359 e.Å^{-3}

Computational details

Table S3.2 Optimized bond parameters of **2** and **3**.

	2 PBE1PBE-D3	**2** PBE1PBE	**3** PBE1PBE-D3	**3** PBE1PBE
Cu-Cu (Å)	2.465	2.509	2.433	2.463
	2.812	2.928	2.446	2.467
	2.466	2.509	2.701	2.800
	2.811	2.929	2.710	2.805
Cu-S (Å)	2.199	2.203	2.191	2.221
	2.202	2.208	2.232	2.215
Cu-C_{Mes} (Å)	2.003	2.005	2.022	2.013
	2.008	2.006	2.010	2.017
Cu-Cu-Cu (°)	77.15	83.43	71.97, 71.94	77.94, 77.92
	102.85	96.57	99.88, 116.17	93.00, 111.14
Cu-S-Cu (°)	79.40	83.21	75.28	78.29
Cu-C_{Mes}-Cu (°)	75.85	77.44	74.92	75.47
S-Cu-Cu-S/C (°)	66.52	50.56	16.03	5.90

Chapter 4. London Dispersion Effects in a Distannene/Tristannane Equilibrium: Energies of their Interconversion and the Suppression of the Monomeric Stannylene Intermediate

Wenxing Zou,[a] Markus Bursch*,[b] Kristian L. Mears,[a] Cary R. Stennett,[a] Ping Yu,[a†] James C. Fettinger,[a] Stefan Grimme*[c] and Philip P. Power*[a]

[a]Departmentof Chemistry (†NMR Facility), University of California, Davis1 Shields Ave, Davis, CA, 95616

[b]M. Bursch, Max-Planck-Institut für Kohlenforschung, D-45470 Mülheim an der Ruhr

[c]S. Grimme, Mulliken Center for Theoretical Chemistry, Universität Bonn, D-53115 Bonn

Reprinted with permission from *Angew. Chem. Int. Ed.* ASAP, doi: 10.1002/anie.202301919.

Abstract

Reaction of $\{LiC_6H_2\text{-}2,4,6\text{-}Cyp_3\cdot Et_2O\}_2$ (Cyp=cyclopentyl) (**1**) of the new dispersion energy donor (DED) ligand, 2,4,6-triscyclopentylphenylwith $SnCl_2$ afforded a mixture of the distannene $\{Sn(C_6H_2\text{-}2,4,6\text{-}Cyp_3)_2\}_2$ (**2**), and the cyclotristannane $\{Sn(C_6H_2\text{-}2,4,6\text{-}Cyp_3)_2\}_3$(**3**). **2** is favored in solution at higher temperature (345K or above) whereas **3** is preferred near 298K. Van't Hoff analysis revealed the **3** to **2** conversion has a ΔH = 33.36 kcal mol^{-1} and ΔS = 0.102 kcal mol^{-1} K^{-1}, which gives a $\Delta G_{300\,K}$= +2.86 kcal mol^{-1}, showing that the conversion of **3** to **2** is an endergonic process. Computational studies show that DED stabilization in **3** is-28.5 kcal mol^{-1} per $\{Sn(C_6H_2\text{-}2,4,6\text{-}Cyp_3)_2$ unit, which exceeds the DED energy in **2** of -16.3 kcal mol^{-1} per unit. The data clearly show that dispersion interactions are the main arbiter of the **3** to **2** equilibrium. Both **2** and **3** possess

large dispersion stabilization energies which suppress monomer dissociation (supported by EDA results).

In the mid-1980s Masamune and Sita synthesized the tristannanes $\{Sn(C_6H_3\text{-}2,6\text{-}Et_2)_2\}_3$ [1] and $\{Sn(C_6H_2\text{-}2,4,6\text{-}i\text{Pr}_2)_2\}_3$,[2] characterized them spectroscopically and determined the detailed structure for $\{Sn(C_6H_3\text{-}2,6\text{-}Et_2)_2\}_3$,[1] which revealed its triangular Sn_3 core arrangement. The structure of $\{Sn(C_6H_2\text{-}2,4,6\text{-}i\text{Pr}_2)_2\}_3$ was described subsequently,[3] along with simpler, higher yielding, salt metathesis synthetic routes.[3] The existence of an equilibrium between the dimeric and trimeric structures was also noted,[2] and this was verified later by Weidenbruch and co-workers.[4,5] In a key finding, it was shown also that $\{Sn(C_6H_2\text{-}2,4,6\text{-}iPr_2)_2\}_3$ converts to the corresponding distannene $\{Sn(C_6H_2\text{-}2,4,6\text{-}i\text{Pr}_2)_2\}_2$ with the generation of a monomeric stannylene $:Sn(C_6H_2\text{-}2,4,6\text{-}i\text{Pr}_2)_2$ either upon heating to 80 °C in d_8-toluene or photolysis of a solution of the trimer at -78 °C in methylcyclohexane (Scheme 4.1).[2] Both the distannane $\{Sn(C_6H_2\text{-}2,4,6\text{-}i\text{Pr}_2)_2\}_2$ and stannylene $:Sn(C_6H_2\text{-}2,4,6\text{-}i\text{Pr}_2)_2$ were trapped by reactions with phenylacetylene, a diene or a diketone.[4,5] We showed recently that a very rare non-dissociating solution-stable distannene $\{Sn(C_6H_2\text{-}2,4,6\text{-}Cy_3)_2\}_2$ (Cy = cyclohexyl), which is stabilized by using a hydrogen-rich, dispersion energy donor (DED)[6] ligand $\text{-}C_6H_2\text{-}2,4,6\text{-}Cy_3$ (Scheme 4.1).[7] The dimeric structure of this compound has a Sn=Sn double bond which remains intact even upon heating to 100 °C in d8- toluene, and no evidence for a trimeric species $\{Sn(C_6H_2\text{-}2,4,6\text{-}Cy_3)_2\}_3$ was detected.[7] Computational analysis revealed that the thermal robustness of the distannene $\{Sn(C_6H_2\text{-}2,4,6\text{-}Cy_3)_2\}_2$ is a result of increased dispersion stabilization energy caused by several close interligand contacts between ortho-cyclohexyl C–H moieties across the Sn=Sn bond.[7] Use of the less sterically demanding and relatively hydrogen-poor ligand $\text{-}C_6H_2\text{-}2,4,6\text{-}Ph_3$ (Ph = phenyl)

yielded only a monomeric stannylene :Sn(C_6H_2-2,4,6-Ph_3)$_2$.[7] Given the key role of dispersion interactions in various organometallic species with unusual structures or in counterintuitive spectroscopic and structural behavior,[8-20] we investigated the new DED ligand, -C_6H_2-2,4,6-Cyp_3 (Cyp = cyclopentyl),[21,22] which has one fewer CH_2 unit per alkyl substituent than -C_6H_2-2,4,6-Cy_3,[7] in order to throw further light on DED ligand effects on the behavior of these compounds. We found that both the dimeric {Sn(C_6H_2-2,4,6-Cyp_3)$_2$}$_2$ (**2**) and the related trimer {Sn(C_6H_2-2,4,6-Cyp_3)$_2$}$_3$ (**3**) are isolated by a simple salt metathesis reaction from $SnCl_2$ and the lithium salt of the -C_6H_2-2,4,6-Cyp_3 ligand (Scheme 4.2). The energy barrier for the dimer/trimer interconversion is established by van't Hoff analysis and DFT calculations but we have been unable to detect the presence of the monomer :Sn(C_6H_2-2,4,6-Cyp_3)$_2$ in solution (Scheme 4.3).

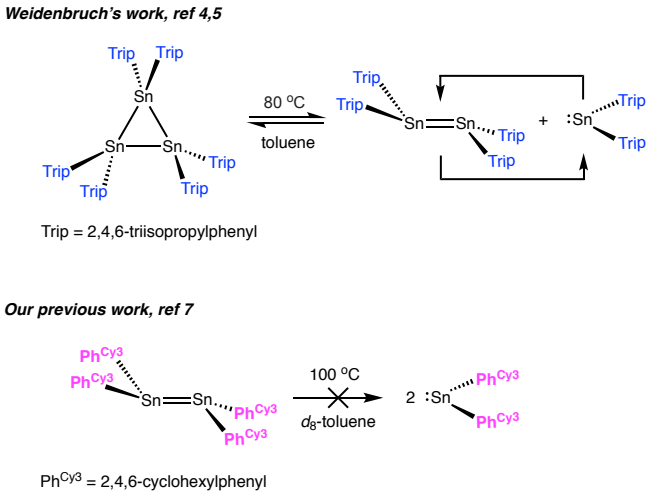

Scheme 4.1 Dissociating distannene (Weidenbruch)[4,5] and non-dissociating distannane (this group's previous work).[7]

Treatment of BrC_6H_2-2,4,6-Cyp_3,[21,22] with 2.1 equiv. of *tert*-BuLi in Et_2O afforded the dimeric lithium etherate salt {LiC_6H_2-2,4,6-Cyp_3·Et_2O}$_2$ (**1**) (Figure 4.1). The lithium reagent **1** features a planar Li_2O_2 core (as the sum of interior angles is 360.0(11)°). A key feature of the structure of **1**

is the eclipse of the ortho cyclopentyl rings from the two -C_6H_2-2,4,6-Cyp_3 ligands across the Li_2C_2 core (Figure 4.1) where six H…H approaches shorter than 2.4 Å are seen (shown as the red dashed lines in Figure 4.1). The lithium atoms are bonded to the C_{ipso} atoms of the phenyl groups with asymmetric Li–C distances of 2.245(2) and 2.147(3) Å. The coordination sphere of the lithium atoms is completed by a diethyl ether donor molecule. The internal C–Li–C angle is 114.26(11)° while that at the C_{ipso} atom is near 65.74(11)°. The central phenyl rings are not arranged orthogonally to the Li_2C_2 core but are tilted at an angle of 85.76(10)° with respect to the Li_2C_2 planes.

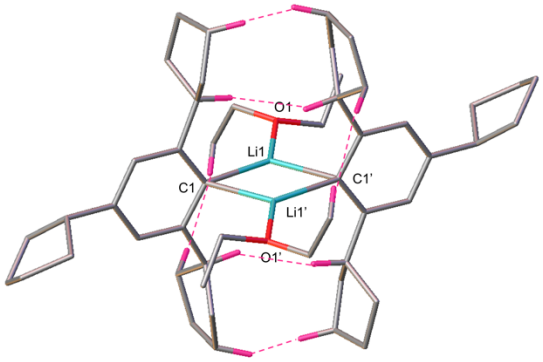

Figure 4.1 Molecular structure of **1**. Interligand H…H contacts less than the sum of the van der Waals radii (ca. 2.4 Å) of two hydrogen atoms are indicated with red dashed lines. Selected bond lengths (Å) and angles (°): Li1-C1 = 2.245(2), Li1-C1′= 2.147(3), Li1-O1 = 1.947(7), Li1--Li1′ = 2.399(5), Li1-C1- Li1′ = 65.74(11), C1-Li1-C1′= 114.26(11), C1-Li1-O1 = 115.8(4), C1′-Li1- O1 = 129.0(4).

Addition of 1 equiv. of the {LiC_6H_2-2,4,6-Cyp_3·Et_2O}$_2$ salt (**1**) to $SnCl_2$ in Et_2O at -78 °C (Scheme 4.2), yielded a bright red solution, suggesting the formation of a dimeric distannene species.[7] Overnight stirring afforded, upon workup, a mixture of large crop of yellow crystal plates co-crystallized with a smaller quantity of red crystals. Attempted recrystallization of the reaction

residue using a mixture of toluene and hexane (v/v = 1:1) yielded only yellow crystalline plates. Single crystal X-ray crystallography of the red crystals revealed a dimeric structure of formula for $\{Sn(C_6H_2\text{-}2,4,6\text{-}Cyp_3)_2\}_2$ (**2**) (Figure 4.2), whose core arrangement bears a resemblance to those of the previously reported distannenes.[7,23,24] The yellow crystals, however, displayed a trimeric structure of formula $\{Sn(C_6H_2\text{-}2,4,6\text{-}Cyp_3)_2\}_3$ (**3**) (Figure 4.3), which has similarities (cf. Sn–Sn = 2.92(10) Å) to those of the cyclotristannane species (see above) which feature triangular Sn_3 cores with Sn-Sn bond distances of 2.86 and 2.94(2) Å respectively, as reported by Masamune,[1] Cardin and coworkers.[3]

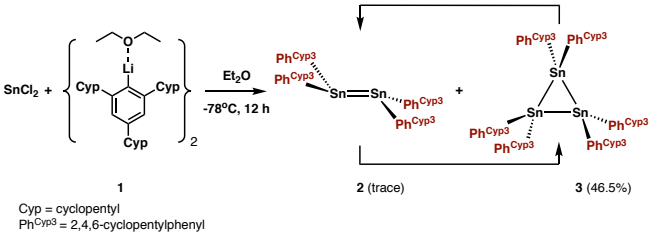

Scheme 4.2 Synthesis of distannene **2** and tristannane **3**.

Structures **2** and **3** represent the first instance of dimeric and trimeric tin $(SnR_2)_n$ (n = 2 or 3) derivatives of a ligand that is common to the two structures. As shown in Figure 4.2, complex **2** is a distannene that has a folded, trans-pyramidalized tin coordination geometries, in which the sum of interligand angles at tin is 343.35(4)°. The Sn–Sn distance is 2.717(6) Å, which is at the short end of the known range (2.70-3.00 Å)[25-30] of Sn–Sn distances for distannenes with hydrocarbyl ligands. It is marginally longer than the Sn–Sn bond length (2.701(7) Å) in $\{Sn(C_6H_2\text{-}2,4,6\text{-}Cy_3)_2\}_2$,[7] where dispersion energies are calculated to be higher. The relatively short Sn–Sn length in **2** indicates substantial strengthening of the interaction between the two $Sn(C_6H_2\text{-}2,4,6\text{-}Cy_3)_2$ units, due to the interligand LD dispersion attraction across the Sn=Sn bond. The C1–Sn1–C22 and C43–Sn2–C64 angles are 106.6(2)° and 112.9(2)°, respectively, these values resemble those

in the previously reported species.[31,32] All C–Sn bond lengths fall within the range 2.172(5)-2.210(5) Å, which is close to the sum (2.17 Å) of the single bond radii of carbon (0.77 Å) and tin (1.40 Å).[33] In the structure of **3** (Figure 4.3), the average Sn–Sn distance in the Sn_3 core is 2.92(10) Å, which lies between the two previously known values for cyclotristannanes,[1,3] and is somewhat longer than the sum of the radii of two Sn atoms (2.8 Å).[33] Each Sn atom is bonded to two -C_6H_2-2,4,6-Cyp_3 ligands, giving a distorted tetrahedral tin environment. There are several close interligand H…H contacts within the sum (ca. 2.4 Å) of the van der Waals radii of two hydrogen atoms (indicated with red dashed lines in Figure 4.3), suggesting significant interligand LD dispersive interactions between the ortho cyclopentyl substituents.

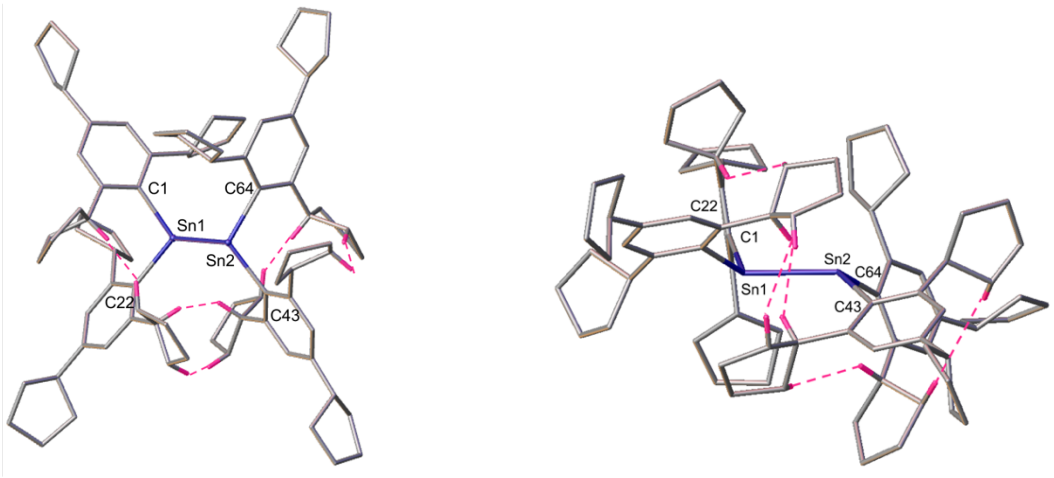

Figure 4.2 Two views of the molecular structure of the distannene **2** (left: top view, right: side view). Interligand H…H contacts across the Sn–Sn bond less than the sum of the van der Waals radii (ca. 2.4 Å) of two hydrogen atoms are indicated with red dashed lines. All other hydrogens are not shown. Selected bond lengths (Å) and angles (°): Sn1-Sn2 = 2.716(6), Sn1-C1 = 2.172(5), Sn1- C22 = 2.19(5), Sn2-C43 = 2.208(5), Sn2-C64 = 2.21(5), C1–Sn1–C22 = 106.6(2) (2), C43-Sn2-C64 = 112.9(2).

Although the dimer **2** co-crystallizes with the trimer **3** (Scheme 4.2), attempts to isolate a large amount of **2** for characterization proved difficult on account of its high solubility in hydrocarbon solution. Computational analysis revealed a dispersion stabilization energy for the cyclotristannane **3** of -28.5 kcal mol^{-1} per {Sn(C_6H_2-2,4,6-Cyp_3)$_2$ unit and -16.3 kcal mol^{-1} per Sn(C_6H_2-2,4,6-Cyp_3)$_2$ unit for the distannene **2**. The greater stabilization energy in **3** in the solid state thus suggests the dynamic equilibrium between **2** and **3** is greatly affected by attractive dispersion interactions. Energy decomposition analysis (EDA) for complex **2** yielded a London dispersion (LD) energy of E_{disp} = -32.45 kcal mol^{-1}. The magnitude is less than that of the corresponding cyclohexyl substituted {Sn(C_6H_2-2,4,6-Cy_3)$_2$}$_2$ (-46.38 kcal mol^{-1}).[7] This can be attributed to the smaller number of close H···H contacts between Sn(C_6H_2-2,4,6-Cyp_3)$_2$ units in comparison to those in the corresponding Sn(C_6H_2-2,4,6-Cy_3)$_2$ fragments.

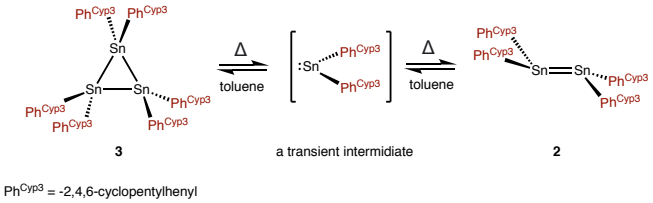

Scheme 4.3 Proposed suppression of the conversion of complex **2** or **3** into the monomeric stannylene by LD effects.

Moreover, unlike the structurally characterized cyclotristannanes, {Sn(C_6H_2-2,4,6-*i*Pr_3)$_2$}$_3$,[4,5] and {Sn(C_6H_3-2,6-Et_3)$_2$}$_3$,[1,33,34] which dissociate to give an equilibrium concentration of the corresponding stannlyene in solution under mild conditions, the {Sn(C_6H_2-2,4,6-Cyp_3)$_2$}$_3$ (**3**) is apparently converted directly to {Sn(C_6H_2-2,4,6-Cyp_3)$_2$}$_2$ (**2**) at elevated temperature and a monomeric stannylene is not detected in solution by ^{119}Sn NMR spectroscopy (Scheme 4.3). It

appears that any monomeric stannylene :Sn(C_6H_2-2,4,6-Cyp_3)$_2$ that is generated very rapidly associates to the distannene {Sn(C_6H_2-2,4,6-Cyp_3)$_2$}$_2$ (**2**) (Scheme 4.3). An examination of variable-temperature (VT) ^{119}Sn NMR spectrum of **3** over the temperature range of -90 to +100 °C showed the thermal conversion of the trimer **3** to the dimer **2** in d_8-toluene with increasing temperature (see Figure S4.13-S4.22 in ESI for further details). At near ambient temperature (285 to 315 K), only a single resonance at δ = -343.3 ppm is detected within a scan range of -500 to 3000 ppm, which corresponds to the cyclotristannane **3** (cf. δ = -378.9 ppm or the cyclotristannane {Sn(C_6H_2-2,4,6-iPr_3)$_2$}$_3$,[3] δ = -416.5 ppm for {Sn(C_6H_2-2,4,6-Et_3)$_2$}$_3$,[1] and $\delta_{calc.}$ = -340.1 ppm for **3**).[35,36] Upon heating the solution, the signal for **3** diminishes in intensity and a new signal appeared at δ = 417.5 ppm (computational study revealed a δ calc. of 505.9 ppm for the dimer **2**).[35,36] This new signal intensifies as the temperature is increased further. This behavior is consistent with the formation of the distannene **2** as the temperature increases (cf. δ = 361.3 ppm for the previously reported distannene {Sn(C_6H_2-2,4,6-Cy_3)$_2$}$_2$,[7] δ = 427 ppm for {Sn(C_6H_2-2,4,6-*i*Pr_3)$_2$}$_2$ which dissociates at ambient temperature,[2] and δ = 630.7 ppm for {Sn(SiMetBu_2)$_2$}$_2$).[24] No other signal was detected in the chemical shift range 1200 to 3000 ppm (cf. ^{119}Sn signal of Lappert's stannylene monomer :Sn{CH($SiMe_3$)$_2$}$_2$ appears at +2328 ppm).[37] This excludes the presence of a measurable amount of the monomeric :Sn(C_6H_2-2,4,6-Cyp_3)$_2$ given that the chemical shifts of the ^{119}Sn signals of monomeric diorganostannylenes fall within the range +723 to +2328 ppm,[38-45] This is also in agreement with the calculated monomer signal at $\delta_{calc.}$ = +2313 ppm. Cooling the solution to 300 K resulted in the disappearance of the signal of **2** at δ = 417.5 ppm and the reappearance of the signal of **3** at δ = -343. 3 ppm, underlining the reversibility of the process shown in Scheme **3**. Furthermore, in comparison to the variable temperature (VT) ^{1}H NMR data, DOSY NMR experiments on trimer **3** carried out at 373 K, indicated that **3** was fully

converted to **2** with a corresponding diffusion coefficient of 1.70×10^{-9} m^2 s^{-1} in d_8-toluene. A hydrodynamic radius of **2** from this value was calculated to be 5.01 Å, which is good agreement to the crystallographic radius of **2** (4.73 Å) derived from the cell volume, assuming a spherical shape. Apparently, any monomeric :Sn(C_6H_2-2,4,6-Cyp_3)$_2$ that is formed as a transient intermediate during the thermal conversion of **3** to **2** is below the limit of detection by ^{119}Sn NMR spectroscopy under the experimental conditions. The lack of significant amounts of monomeric :Sn(C_6H_2-2,4,6-Cyp_3)$_2$, which is a reflection of the relative thermal stabilities of {Sn(C_6H_2-2,4,6-Cyp_3)$_2$}$_3$ (**3**) and {Sn(C_6H_2-2,4,6-Cyp_3)$_2$}$_2$ (**2**), is likely the consequence of the enhanced dispersion interactions in **2** and **3** species. A suitable trapping agent, 2,3-dimethyl-1,3-butadiene was used for further detection of the presence of the stannylene. Upon heating **3** in the presence of 2,3-dimethyl-1,3-butadiene in toluene, the corresponding stannacyclopentenes **4** can be isolated as a colorless solid in low yield (7.8%), evidenced by the ^{119}Sn chemical shift of **4** at -84.7 ppm (cf. δ = -83.3 ppm of the stannacyclopentenes {Sn(C_6H_2-2,4,6-*i*Pr_3)$_2$}$_3$)[4] (see ESI for details). The monomeric stannylene is therefore considered to exist in solution at elevated temperatures but the extent of formation of the monomer is too small to be detected in ^{1}H NMR, ^{119}Sn NMR or ^{1}H DOSY spectra even. Van′t Hoff analysis of the VT ^{1}H NMR data yielded a $\Delta H_{conv.}$ value of 35.06 kcal mol^{-1} for the conversion of **3** into **2**. The $\Delta G_{conv.}$ 300 K = 2.66 kcal mol^{-1} which leads to a $\Delta S_{conv.}$ value of 0.102 kcal mol^{-1} K^{-1} (see ESI for further details). The structural data for **2** and **3** and their cyclohexyl substituted counterparts are strongly stabilized by dispersion effects to the extent that the dimeric structure can be isolated in each case in contrast to the instability of the {Sn(C_6H_2-2,4,6-*i*Pr_3)$_2$}$_2$ distannene.[4,5] In addition, the dispersion effects prevent dissociation of the distannenes so that the monomeric stannylenes :Sn(C_6H_2-2,4,6-Cyp_3)$_2$ and :Sn(C_6H_2-2,4,6-Cy_3)$_2$

are not detected, in contrast to {Sn(C_6H_2-2,4,6-*i*Pr_3)$_2$}$_2$ which was detected spectroscopically and easily trapped chemically.

Quantum chemical calculations for compounds {Sn(C_6H_2-2,4,6-Cyp$_3$)$_2$}$_3$ (**3**) and {Sn(C_6H_2-2,4,6-Cyp$_3$)$_2$}$_2$ (**2**) were performed at the hybrid B3LYP-D4/def2-TZVP or def2-QZVP[46-48] level on r^{2}SCAN-3c[CPCM][49-51] geometries. The calculated structural parameters match the experimental data values closely (for further details see the ESI). The orbital analysis of {Sn(C_6H_2-2,4,6-*i*Pr_3)$_2$}$_3$ (Figure 4.4) reveals three Sn–Sn single bonds with Wiberg bond indices of 0.83. The HOMO of **3** is represented by two degenerate molecular orbitals of the Sn–Sn bonds and the LUMO of the respective antibonding p-orbital combinations (for further details see the ESI). EDA of {Sn(C_6H_2-2,4,6-*i*Pr_3)$_2$}$_3$,[3] reveals a high LD interaction energy contribution of $E_{disp.}$ = -85.6 kcal mol^{-1} which partially compensates for the strong Pauli repulsive interaction of 447.68 kcal mol^{-1} (Figure 4.5). The large $E_{disp.}$ (-85.6 kcal mol^{-1}) / $E_{int.}$ (-91.8 kcal mol^{-1}) = 0.9 ratio indicates the importance of LD for the overall interaction energy and impressively demonstrates its significance for stabilizing cyclotristannane **3**.

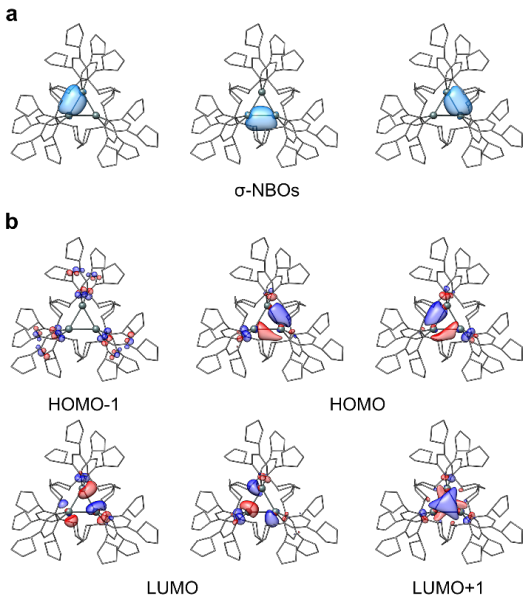

Figure 4.4 a) NBOs of the Sn-Sn single bonds in **3** (B3LYP-D4/def2-TZVP/def2-SVP@Ph), and b) molecular frontier orbitals (B3LYP-D4/def2-QZVP) of **2** at the (iso surface value = 0.05 a.u.).

EDA of $\{Sn(C_6H_2\text{-}2,4,6\text{-}^iPr_3)_2\}_3$ (**3**) reveals a high London dispersion interaction energy contribution of E_{disp}=-85.6 kcal mol^{-1} which partially compensates for the strong Pauli repulsive interaction of 447.68 kcal mol^{-1} (Figure 4.5). The large E_{disp} (-85.6 kcal mol^{-1}) / E_{int} (-91.8 kcal mol^{-1}) = 0.9 ratio indicates the importance of London dispersion for the overall interaction energy and impressively demonstrates its significance for stabilizing cyclotristannane **3**.

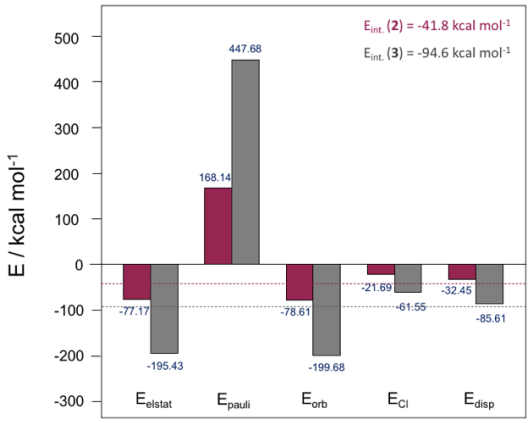

Figure 4.5 Energy decomposition analysis of **2** (red) and **3** (grey) at B3LYP-D4/def2-TZVP level. The dashed lines represent the overall interaction energies of the corresponding stannylene fragments SnR_2.

In conclusion, the specifically designed substituent -C_6H_2-2,4,6-Cyp_3 (Cyp = cyclopentyl) was synthesized as an enhanced dispersion energy donating (DED) ligand via the synthesis of its lithium salt $\{LiC_6H_2\text{-}2,4,6\text{-}Cyp_3\cdot Et_2O\}_2$ (**1**),[52] its distannene $\{Sn(C_6H_2\text{-}2,4,6\text{-}Cyp_3)_2\}_2$ (**2**) and the cyclotristannane $\{Sn(C_6H_2\text{-}2,4,6\text{-}Cyp_3)_2\}_3$ (**3**) derivatives. Computational results showed that this ligand produces a lower dispersion energy of stabilization than -C_6H_2-2,4,6-Cy_3 in the distannene

$\{Sn(C_6H_2\text{-}2,4,6\text{-}Cy_3)_2\}_2$ probably as a result of fewer close H···H contacts between the two $Sn(C_6H_2\text{-}2,4,6\text{-}Cyp_3)_2$ units. In addition, the trimer **3** is proved to be the predominant species in solution as a result of greater dispersion interaction between its three $:SnR_2$ units. For the first time, we have supplied the energy values of any Sn dimer-trimer equilibrium via VT multinuclear NMR spectroscopy which revealed that $\{Sn(C_6H_2\text{-}2,4,6\text{-}Cy_3)_2\}_3$ (**3**) converts to the $\{Sn(C_6H_2\text{-}2,4,6\text{-}Cy_3)_2\}_2$ (**2**) at high temperatures (thermodynamically favored at 70 °C) and is in equilibrium with **2**. However, a monomeric stannylene $:Sn(C_6H_2\text{-}2,4,6\text{-}Cyp_3)_2$ was not observed in solution over a wide temperature range. The detailed mechanism whereby **3** is transformed into **2** remains under investigation.

Author Contributions

P. P. Power proposed and supervised the overall project. W. Zou synthesized and characterized the distannene (**2**) and cyclotristannane (**3**). K. L. Mears performed NMR studies. C. R. Stennett prepared the lithium salt (**1**). J. C. Fettinger finalized X-ray data. W. Zou wrote the initial manuscript, K. L. Mears and P. P. Power edited the paper.

Acknowledgements

We thank the U.S. National Science Foundation for funding (Grant No. CHE-2152760) and for purchase of a dual source X-ray diffractometer (Grant No. CHE-1531193). We thank Dr. Derrick C. Kaseman for his assistance with VT NMR experiments. S. G. and M. B. gratefully acknowledge financial support by the Max Planck Society through the Max Planck fellow program.

Keywords: London dispersion • Organotin • Cyclotristannane • Equilibrium • Energy Decomposition Analysis

[1] S. Masamune, L. R. Sita, *J. Am. Chem. Soc.* **1983**, *105*, 630-631.

[2] S. Masamune, L. R. Sita, *J. Am. Chem. Soc.* **1985**, *107*, 6390-6391.

[3] F. J. Brady, C. J. Cardin, D. J. Cardin, M. A. Convery, M. M. Devereux, G. A. Lawless, *J. Organometallic Chem.* **1991**, *421*, 199-203.

[4] M. Weidenbruch, A. Schaefer, H. Kilian, S. Pohl, W. Saak, H. Marsmann, *Chem. Ber.* **1992**, *125*, 563-566.

[5] A. Schaefer and M. Weidenbruch, Phosphorus, *Sulfur and Silicon and the Related Elements*, **1992**, *65*, 13-16.

[6] S. Grimme, R. Huenerbein, S. Ehrlich, *ChemPhysChem,* **2011**, *12*, 1258-1261.

[7] C. R. Stennett, M. Bursch, J. C. Fettinger, P. P. Power, S. Grimme, *J. Am. Chem. Soc.* **2021**, *143*, 21478-21483.

[8] S. Grimme, P. R. Schreiner, *Angew. Chem. Int. Ed.* **2011**, *50*, 12639-12642.

[9] P. R. Schreiner, L. V. Chernish, P. A. Gunchenko, E. Y. Tikhonchuk, H. Hausmann, M. Serafin, S. Schlecht, J. E. P. Dahl, R. M. K. Carlson, A. A. Fokin, *Nature*, **2011**, *477*, 308-311.

[10] H. Arp, J. Baumgartner, C. Marschner, *J. Am. Chem. Soc.* **2012**, *134*, 6409–6415.

[11] B. D. Rekken, T. M. Brown, J. C. Fettinger, F. Lips, H. M. Tuononen, R. H. Herber, P. P. Power, *J. Am. Chem. Soc.* **2013**, *135*, 10134-10148.

[12] C. L. Wagner, L. Tao, E. J. Thompson, T. A. Stich, J. Guo, J. C. Fettinger, L. A. Berben, R. D. Britt, S. Nagase, P. P. Power, *Angew. Chem. Int. Ed.* **2016**, *55*, 10444-10447.

[13] S. Roesel, H. Quanz, C. Logemann, J. Becker, E. Mossou, L. Canadillas- Delgado, E. Caldeweyher, S. Grimme, P. R. Schreiner, *J. Am. Chem. Soc.* **2017**, *139*, 7428-7431.

[14] A. Casitas, J. A. Rees, R. Goddard, E. Bill, S. DeBeer, A. Fürstner, *Angew. Chem. Int. Ed.* **2017**, *56*, 10108-10113.

[15] S. Roesel, C. Balestrieri, P. R. Schreiner, *Chem. Sci.* **2017**, *8*, 405-410.

[16] H. Li, Y. Hu, D. Wan, Z. Zhang, Q. Fan, R. B. King, H. F. Schaefer, *J. Phys. Chem. A*, **2019**, *123*, 9514-9519.

[17] M. Bursch, E. Caldeweyher, A. Hansen, H. Neugebauer, S. Ehlert, S. Grimme, *Acc. Chem. Res.* **2019**, *52*, 258–266.

[18] H. F. König, H. Hausmann, P. R. Schreiner, *J. Org. Chem.* **2022**, *87*, 13168–13177.

[19] K. L. Mears, C. R. Stennett, J. C. Fettinger, P. Vasko, P. P. Power, *Angew. Chem. Int. Ed.* **2022**, *134*, e202201318.

[20] J.-D. Guo, D. J. Liptrot, S. Nagasa, P. P. Power, *Chem. Sci.* **2015**, *6*, 6235-6244.

[21] L. A. Mclean, A. J. B. Watson, *Eur. J. Org. Chem.* **2021**, *35*, 4943-4945.

[22] L. Salvi, N. R. Davis, S. Z. Ali, S. L. Buchwald, *Org. Lett.* **2012**, *14*, 170-173.

[23] V. Y. Lee, T. Fukawa, M. Nakamoto, A. Sekiguchi, B. L. Tumanskii, M. Karni, Y. Apeloig. *J. Am. Chem. Soc.* **2006**, *128*, 11643-11651.

[24] T. Fukawa, V. Y. Lee, M. Nakamoto, A. Sekiguchi, *J. Am. Chem. Soc.* **2004**, *126*, 11758-11759.

[25] H. Lei, J. C. Fettinger, P. P. Power, *Organometallics*, **2010**, *29*, 5585-5590.

[26] M. Stürmanna, W. Saaka, K. W. Klinkhammerb, M. Weidenbruch, *Z. A norg. Allg. Chem.* **1999**, *625*, 1955-1956.

[27] K. Klinkhammer, *Polyhedron*, **2002**, *21*, 587-598.

[28] J. Henning, L. Wesemann, *Angew. Chem. Int. Ed.* **2012**, *51*, 12869-12873.

[29] C. Jones, A. Sidiropoulos, N. Holzmann, G. Frenking, A. Stasch, *Chem. Commun.* **2012**, *48*, 9855-9857.

[30] D. E. Goldberg, D. H. Harris, M. F. Lappert, K. M. Thomas, *J. C. S. Chem. Comm.* **1976**, *7*, 261-262.

[31] C. Stanciu, A. F. Richards, P. P. Power, *J. Am. Chem. Soc.* **2004**, *126*, 4106-4107.

[32] T. Y. Lai, J. C. Fettinger, P. P. Power, *J. Am. Chem. Soc.* **2018**, *140*, 5674–5677.

[33] P. Pyykkö, M. Atsumi, *Chem. Eur. J.* **2009**, *15*, 186-197.

[34] L. R. Sita, I. Kinoshita, *J. Am. Chem. Soc.* **1991**, *113*, 1856-1857.

[35] SO-ZORA-revPBE/TZP level

[36] Stückrath, J. B.; Gasevic, T.; Bursch, M.; Grimme, S. *Inorg. Chem.* **2022**, *61*, 3903–3917.

[37] K. W. Zilm, G. A. Lawless, R. M. Merrill, J. M. Millar and G. G. Webb, *J. Am. Chem. Soc.*, **1987**, *109*, 7236-7238.

[38] A. D. Phillips, S. Hino, P. P. Power, *J. Am. Chem. Soc.* **2003**, *125*, 7520-7521.

[39] C. Eaborn, M. S. Hill, P. B. Hitchcock, D. Patel, J. D. Smith, S. Zhang, *Organometallics*, **2000**, *19*, 49-53.

[40] Grützmacher, H. Pritzkow, F. T. Edelmann, *Organometallics*, **1991**, *10*, 23-25.

[41] T. Tajima, N. Takeda, T. Sasamori, N. Tokitoh, *Organometallics,* **2006**, *25*, 3552-3553.

[42] G. H. Spikes, Y. Peng, J. C. Fettinger, P. P. Power, *Z. Anorg. Allg. Chem.* **2006**, *632*, 1005-1010.

[43] M. Kira, R. Yauchibara, R. Hirano, C. Kabuto and H. Sakurai, *J. Am. Chem. Soc.* **1991**, *113*, 7785-7787.

[44] N. Tokitoh, M. Saito and R. Okazaki, *J. Am. Chem. Soc.*, **1993**, *115*, 2065-2066.

[45] M. L. McCrea-Hendrick, M. Bursch, K. L. Gullett, L. R. Maurer, J. C. Fettinger, S. Grimme and P. P. Power, *Organometallics*, **2018**, *37*, 2075-2085.

[46] M. Bursch, J.-M. Mewes, A. Hansen, S. Grimme, *Organometallics*, **2018**, *37*, 2075-2085.

[47] A. Klamt, *J. Phys. Chem.* **1995**, *99*, 2224-2235.

[48] A. D. Becke, *J. Chem. Phys.* **1993**, *98*, 5648-5656.

[49] E. Caldeweyher, S. Ehlert, A. Hansen, H. Neugebauer, S. Spicher, C. Bannwarth, S. Grimme, *J. Chem. Phys.* **2019**, *150*, 154122.

[50] S. Grimme, A. Hansen, S. Ehlert, J.-M. Mewes, *J. Chem. Phys.* **2021**, *154*, 064103.

Supplementary Information

S1. Experimental Procedures

General information.

All manipulations were carried out under anaerobic and anhydrous conditions by using Schlenk techniques or in a Vacuum Atmospheres OMNI-Lab drybox under an atmosphere of dry argon or nitrogen. Solvents were dried by the method of Grubbs[S1] and co-workers, stored over potassium or sodium, and then degassed by the freeze-pump-thaw method. All physical measurements were made under strictly anaerobic and anhydrous conditions. The NMR spectra were recorded on a 500 MHz Bruker Advanced DRX spectrometer, the ^{1}H NMR and ^{13}C NMR spectra were referenced to the residual solvent signals in deuterated toluene. IR spectra were recorded as Nujol mulls between CsI plates on a PerkinElmer 1430 spectrometer. UV−vis spectra were recorded as dilute hexane solutions in 3.5 mL quartz cuvettes using an Olis 17 modernized Cary 14 UV−vis−near-IR spectrophotometer or an HP 8452 diode-array spectrophotometer. The precursor

BrC_6H_2-2,4,6-Cyp_3 was prepared via literature methods.[S2,S3] Unless otherwise stated, all materials were obtained from commercial sources and used as received.

Synthesis of $\{LiC_6H_2$-2,4,6-$Cyp_3 \cdot Et_2O\}_2$ (1): 1,3,5-tricyclopentyl-bromobenzene BrC_6H_2-2,4,6-Cyp_3 (6.0 g, 16.67 mmol) was dissolved in ca. 60 mL of Et_2O and cooled to ca. 0°C. 20 mL of a 1.7 M (34 mmol) of *tert*-BuLi in pentane was then added dropwise to the stirred solution over ca. 10 minutes. The mixture was allowed to warm to ambient temperature and stirred for eight hours. The solvent was then removed completely under reduced pressure to afford white powder residue, and ca. 70 mL of hexane was added to the residue. The solution was then heated to ca. 65°C the filtered through Celite at this temperature, the solution was then concentrated to ca. 50 mL under reduced pressure until the formation of small colorless crystals was observed. The solution was stored in a ca. -38 °C freezer for 2 days to yield 3.62 g (60.0%) of **1** as colorless crystals which were suitable for X-ray crystallography. ^{1}H NMR (500 MHz, toluene-d_8): δ 7.10 (s, 2H), 3.23 (q, J = 8.5 Hz, 2H), 3.03 (t, J = 8.4 Hz, 1H), 2.88 (q, J = 7.0 Hz, 4H), 2.21 (d, J = 10.6 Hz, 4H), 2.10 – 1.98 (m, 6H), 1.90 (d, J = 12.9 Hz, 8H), 1.79 (dt, J = 23.9, 7.5 Hz, 4H), 1.71 – 1.60 (m, 2H), 0.62 (t, J = 7.0 Hz, 6H). ^{13}C NMR (125 MHz, toluene-d_8): δ= 158.48, 143.88, 137.08, 118.89, 65.50, 53.10, 46.97, 37.23, 35.06, 26.78, 25.63, 13.87. Mp: 132-135°C. UV/vis: λ/nm (ε/M^{-1} cm^{-1}): 272 (2200). IR (Nujol; $\tilde{\nu}$/cm^{-1}): 1581m, 1529m, 1453s, 1404w, 1421w, 1374s, 1301w, 1258w, 1206w, 1182w, 1150w, 1139m, 1056m, 867m, 793w, 720m, 398m.

Synthesis of $\{Sn(C_6H_2$-2,4,6-$Cyp_3)_2\}_3$ (3): A solution of 2,4,6-tricyclopentylphenyllithium etherate (**1**) (1.81 g, 5 mmol) in ca. 50 mL of diethyl ether was added dropwise to a slurry of $SnCl_2$ (0.47 g, 2.5 mmol) in ca. 10 mL of diethyl ether at -78°C. The solution turned orange-yellow immediately then became bright red. The reaction was then allowed to warm slowly to room

temperature and stirred for ten hours. Removal of solvent under reduced pressure afforded a red residue, and ca. 80 mL of toluene was added. The solution was heated to ca. 50°C then filtered thorough celite at this temperature. The solution was concentrated under reduced pressure to ca. 50 mL and stored in a ca. -38°C freezer for 3 days. 0.785 g of **3** (46%) was afforded as yellow plates that were suitable for X-ray determination. ^{1}H NMR (500 MHz, toluene-d_8) δ 7.12 (s, 2H), 3.67 (s, 2H), 3.29 (t, J = 8.2 Hz, 2H), 2.82 (p, J = 9.1 Hz, 3H), 2.51 – 2.36 (m, 4H), 1.97 (d, J = 12.1 Hz, 9H), 1.72 (dd, J = 10.7, 5.6 Hz, 9H), 1.64 – 1.54 (m, 20H), 1.37 (t, J = 6.9 Hz, 3H), 1.16 (d, J = 8.5 Hz, 4H). ^{13}C NMR (500 MHz, toluene-d_8) δ 137.11, 122.90, 46.38, 36.35, 34.67, 26.42, 25.52, 25.44. Mp: 176-180°C. UV/vis: λ/nm (ε/M^{-1} cm^{-1}): 310 (15000). IR (Nujol; $\tilde{\nu}$/cm^{1}): 2720w, 1566w, 1543w, 1450s, 1421w, 1368s, 1298w, 1077m, 1013m, 866w, 797m, 725m, 378w.

Synthesis of 3,4-Dimethyl-1,1-bis(2,4,6-tricyclopentylphenyl)-1-stanna-3-cyclopentene (4): $\{Sn(C_6H_2\text{-}2,4,6\text{-}Cyp_3)_2\}_3$ (**3**) (0.511 g, 0.25 mmol) was combined with 2,3-dimethyl-1,3-butadiene (0.093 g, 1.125 mmol) in ca. 50 mL of toluene. The solution was heated to 85°C and stirred for 12 h. The solvent was removed under reduced pressure to afford a white residue, and ca. 50 mL of THF was added. The solution was then filtered thorough celite and was concentrated under reduced pressure to ca. 5 mL. Storage in a ca. -78°C freezer for 7 days afforded 0.050 g of 4 (7.8%) as colorless block. ^{1}H NMR (500 MHz, toluene-d_8) δ 7.14 (s, 4H), 3.56 (s, 2H), 3.36 – 3.22 (m, 4H), 2.97 – 2.86 (m, 2H), 2.23 (s, 10H), 2.05 – 1.88 (m, 20H), 1.86 – 1.53 (m, 38H). ^{13}C NMR (500 MHz, toluene-d_8) δ 152.34, 146.87, 142.74, 131.65, 122.39, 67.36, 50.25, 46.30, 36.45, 34.68, 28.53, 25.81, 25.48, 21.40. ^{119}Sn NMR (187 MHz, Toluene-d_8) δ -84.70 ppm.

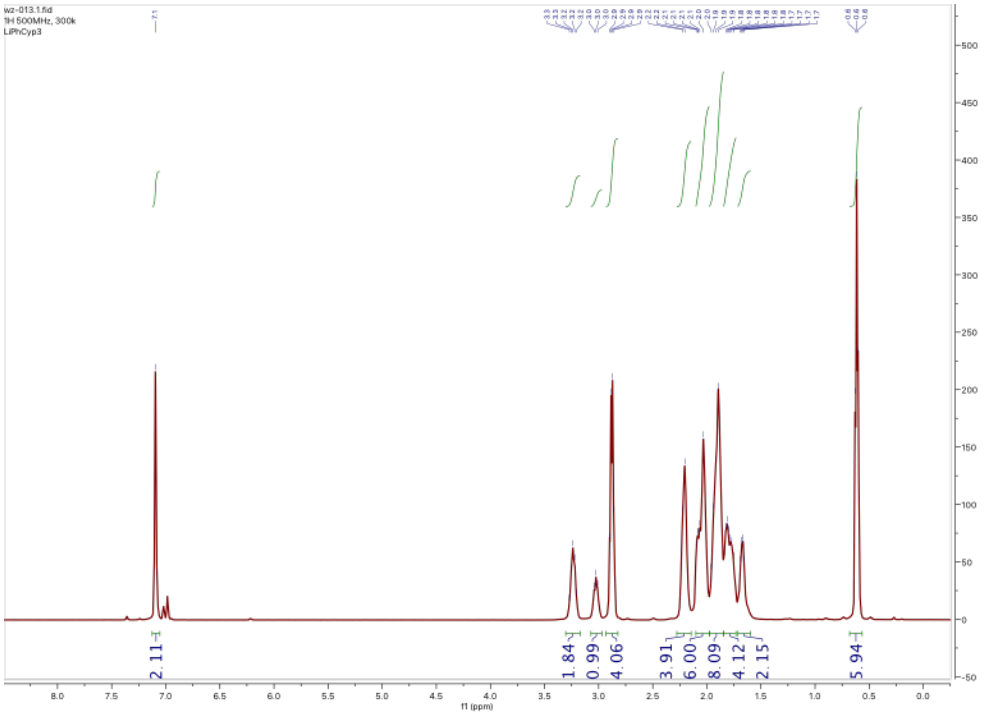

Figure S4.1 ^{1}H NMR spectrum of $\{LiC_6H_2$-2,4,6-$Cyp_3 \cdot Et_2O\}_2$ (**1**) in C_7D_8 at 298 K.

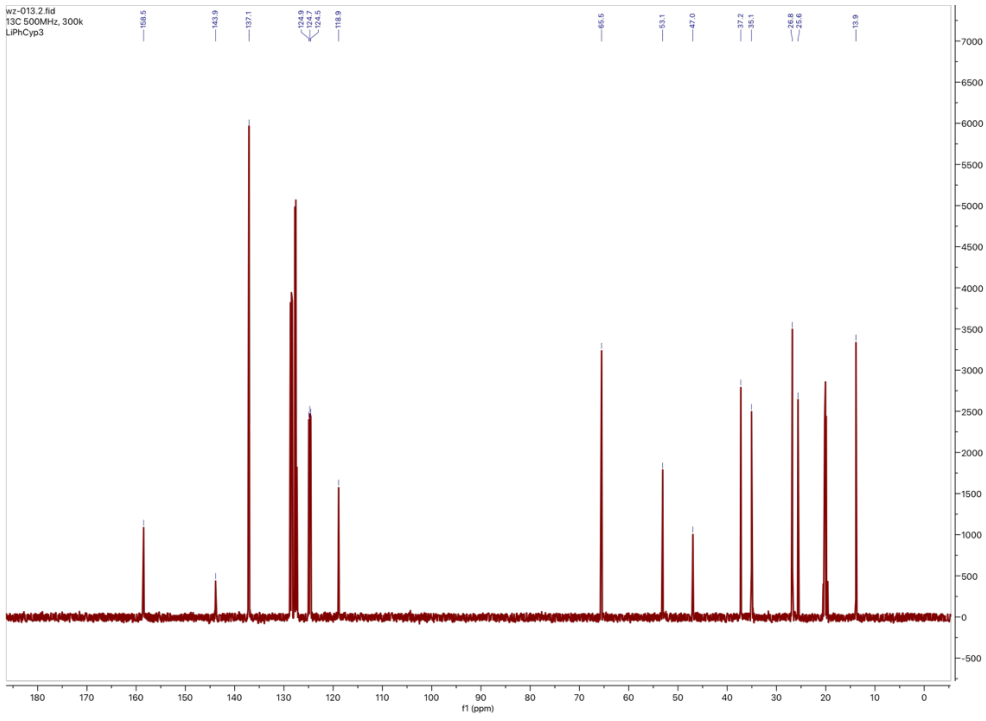

Figure S4.2 ^{13}C NMR spectrum of $\{LiC_6H_2$-2,4,6-$Cyp_3 \cdot Et_2O\}_2$ (**1**) in C_7D_8 at 298 K.

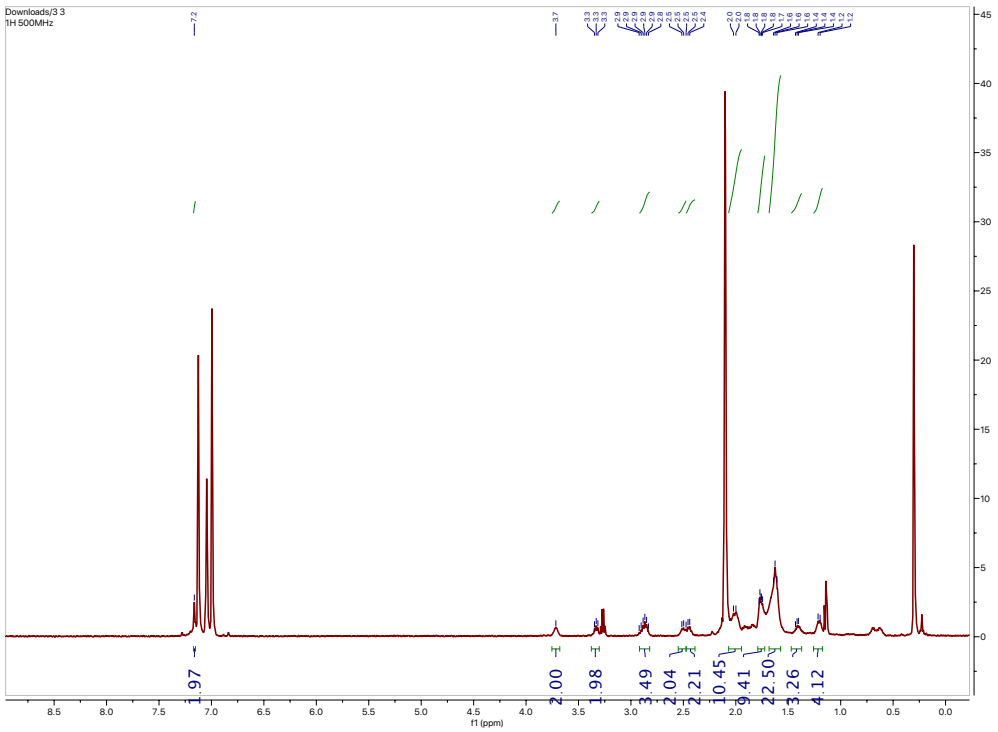

Figure S4.3 ^{1}H NMR spectrum of $\{Sn(C_6H_2\text{-}2,4,6\text{-}Cyp_3)_2\}_3$ (**3**) in C_7D_8 at 283 K.

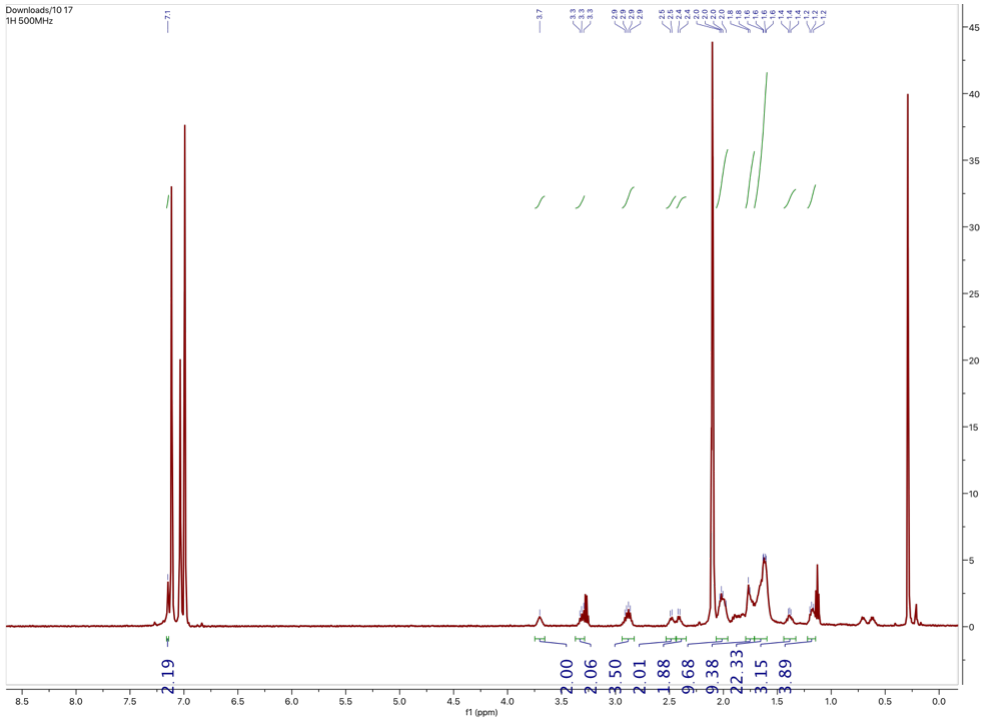

Figure S4.4 ^{1}H NMR spectrum of $\{Sn(C_6H_2\text{-}2,4,6\text{-}Cyp_3)_2\}_3$ (**3**) in C_7D_8 at 300 K.

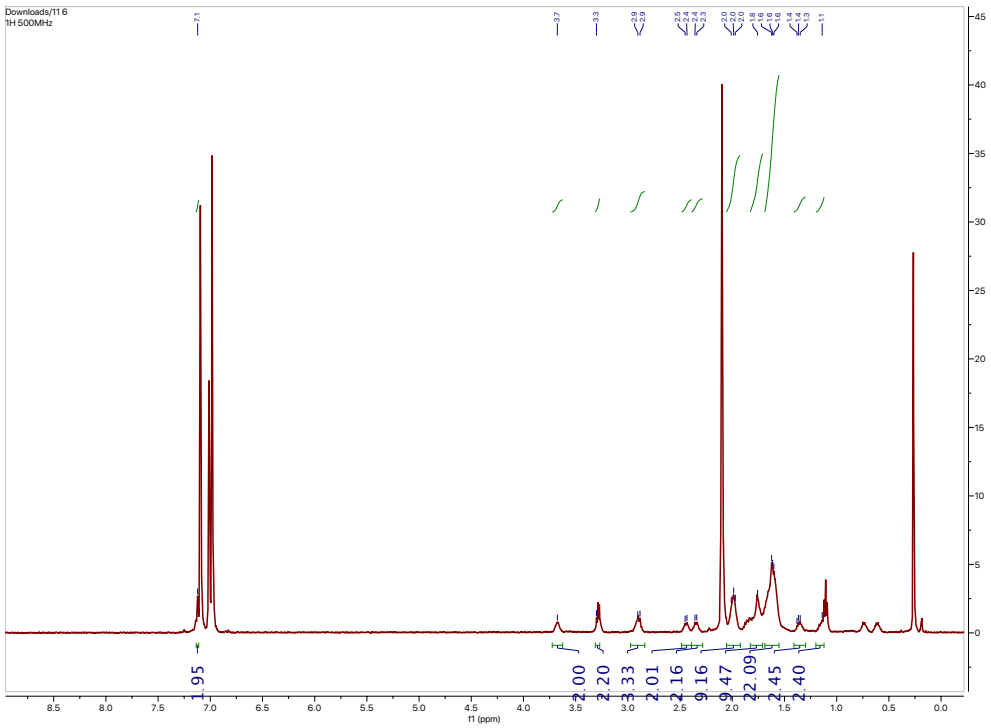

Figure S4.5 ^{1}H NMR spectrum of $\{Sn(C_6H_2\text{-}2,4,6\text{-}Cyp_3)_2\}_3$ (**3**) in C_7D_8 at 315 K.

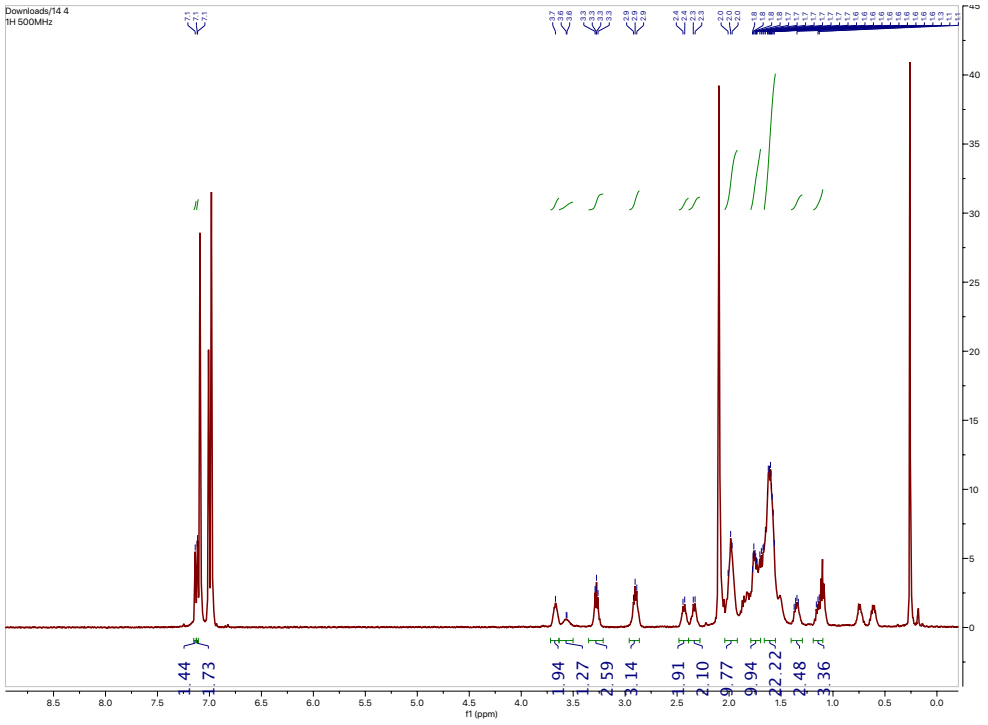

Figure S4.6 ^{1}H NMR spectrum of $\{Sn(C_6H_2\text{-}2,4,6\text{-}Cyp_3)_2\}_3$ (**3**) in C_7D_8 at 330 K.

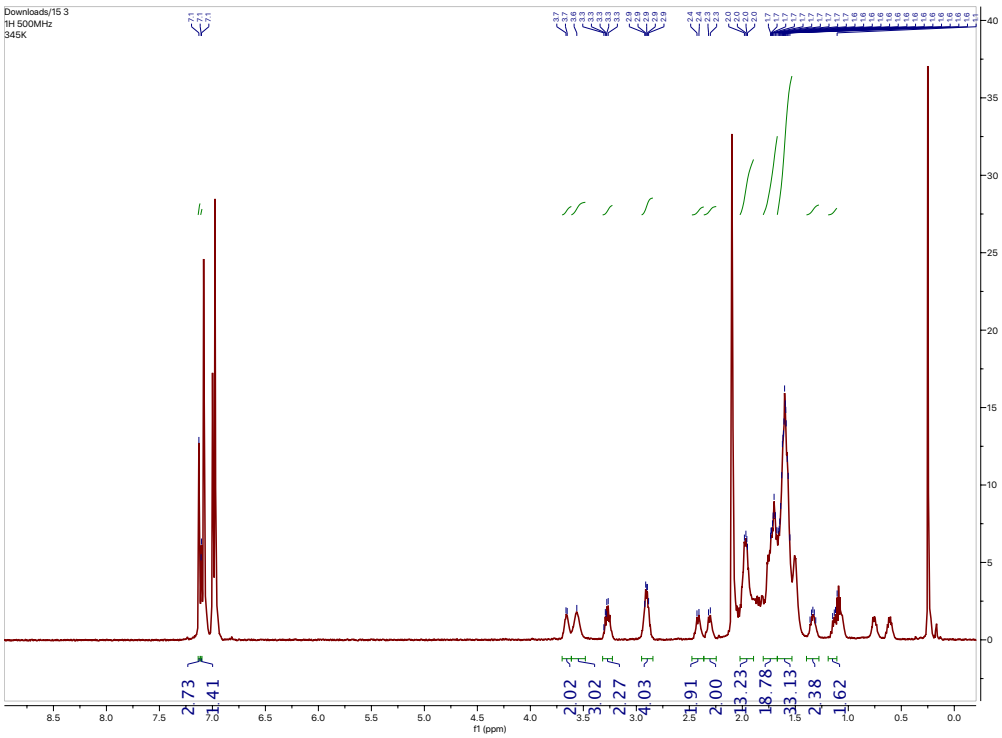

Figure S4.7 ^{1}H NMR spectrum of $\{Sn(C_6H_2\text{-}2,4,6\text{-}Cyp_3)_2\}_3$ (**3**) in C_7D_8 at 345 K.

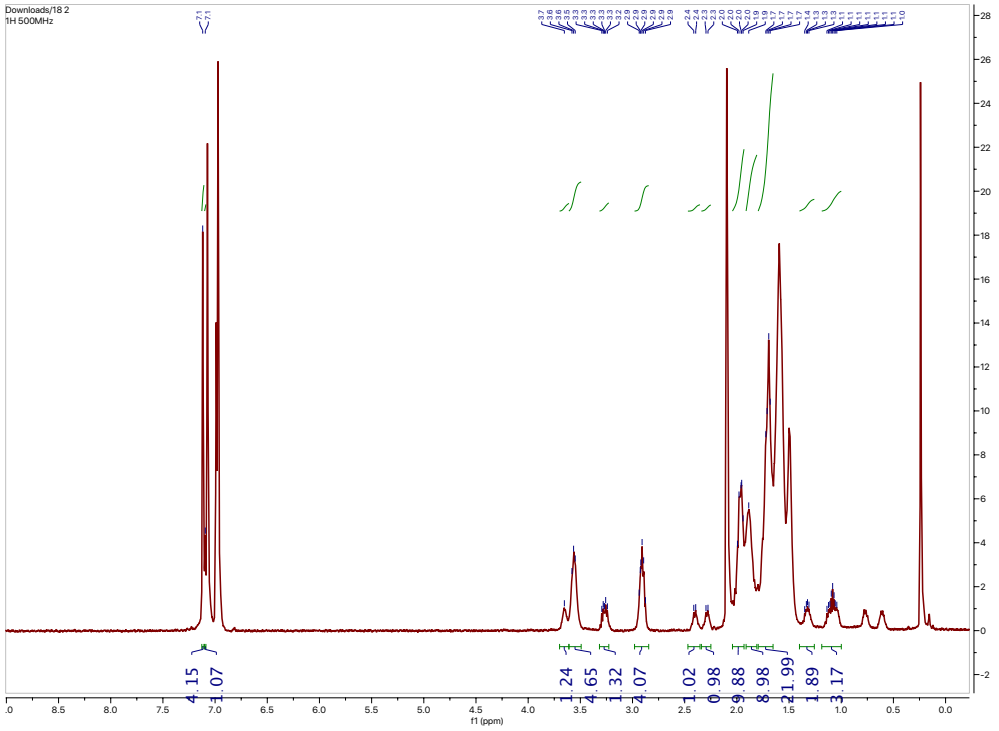

Figure S4.8 ^{1}H NMR spectrum of $\{Sn(C_6H_2\text{-}2,4,6\text{-}Cyp_3)_2\}_3$ (**3**) in C_7D_8 at 360 K.

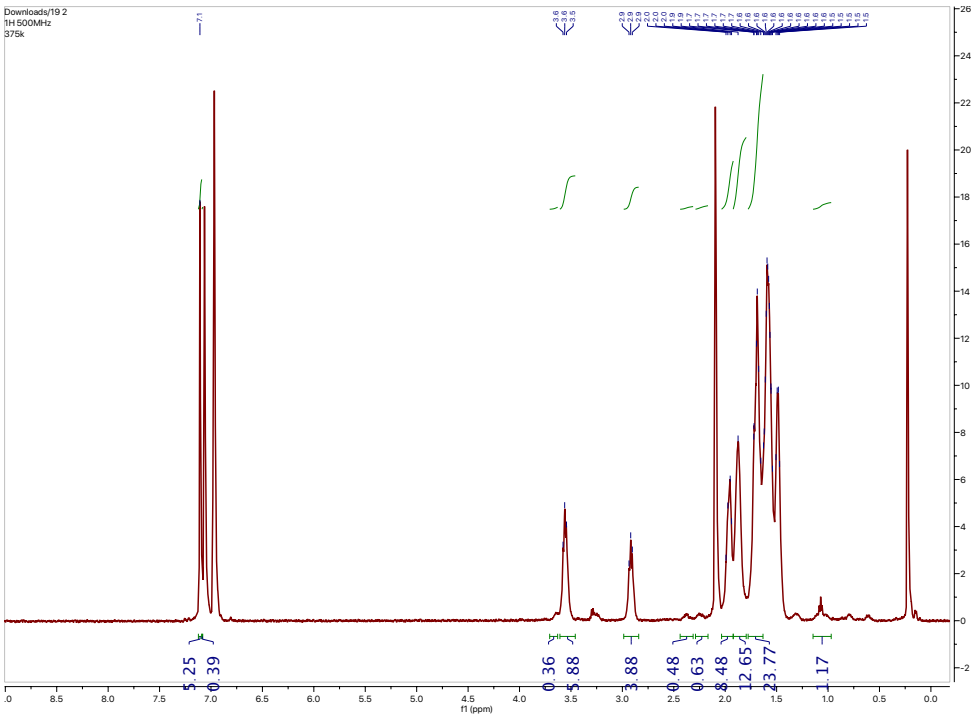

Figure S4.9 ^{1}H NMR spectrum of $\{Sn(C_6H_2\text{-}2,4,6\text{-}Cyp_3)_2\}_3$ (**3**) in C_7D_8 at 375 K.

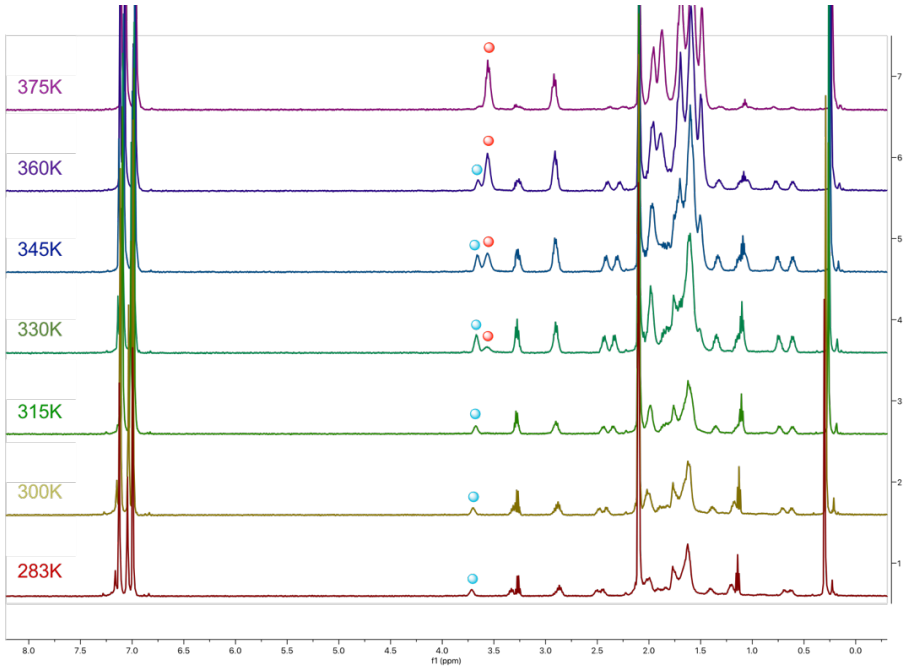

Figure S4.10 Variable temperature ^{1}H NMR spectra (scan range of 8.25 to -0.25 ppm) of the interconversion of complexes **2** and **3** in C_7D_8. The trimer **3** indicated by blue sphere and the dimer **2** indicated by red sphere.

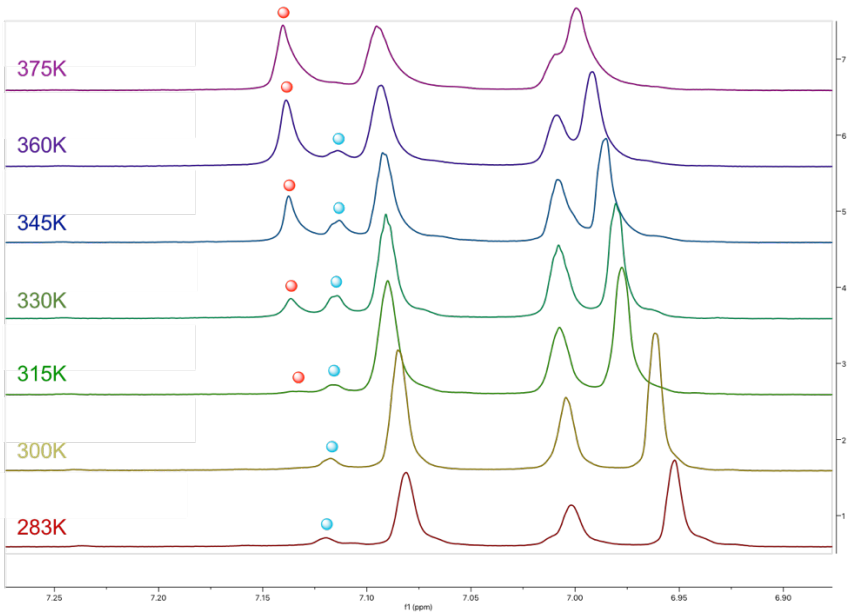

Figure S4.11 Details of variable temperature ^{1}H NMR spectra (scan range of 7.25 to 6.9 ppm) of the interconversion of complexes **2** and **3** in C_7D_8. The trimer **3** indicated by blue sphere and the dimer **2** indicated by red sphere.

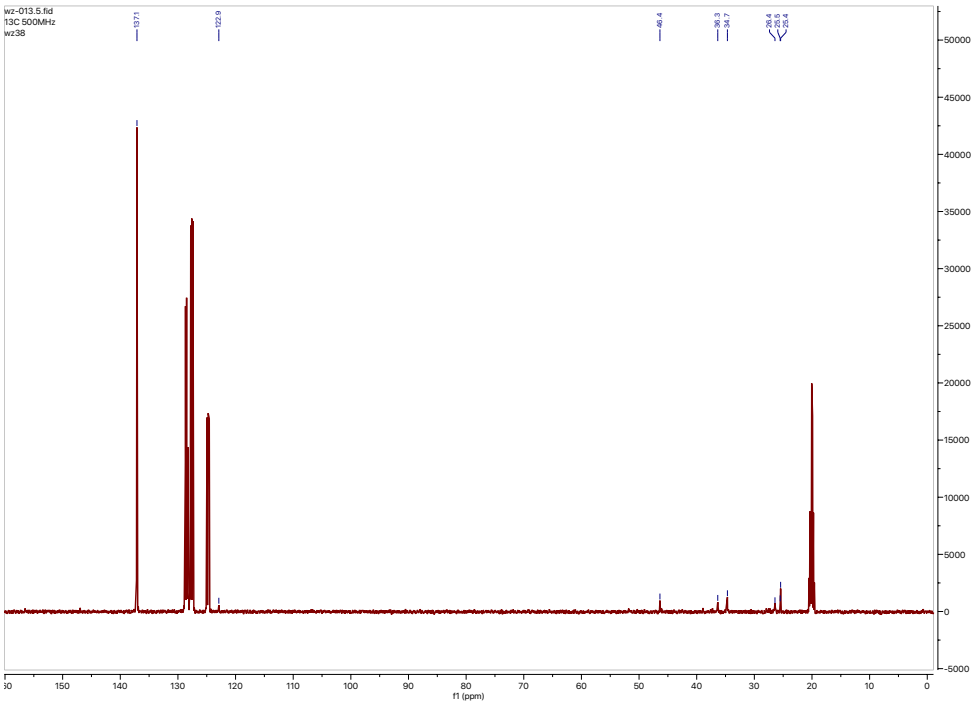

Figure S4.12 ^{13}C NMR spectrum of $\{Sn(C_6H_2\text{-}2,4,6\text{-}Cyp_3)_2\}_3$ (**3**) in C_7D_8 at 375 K.

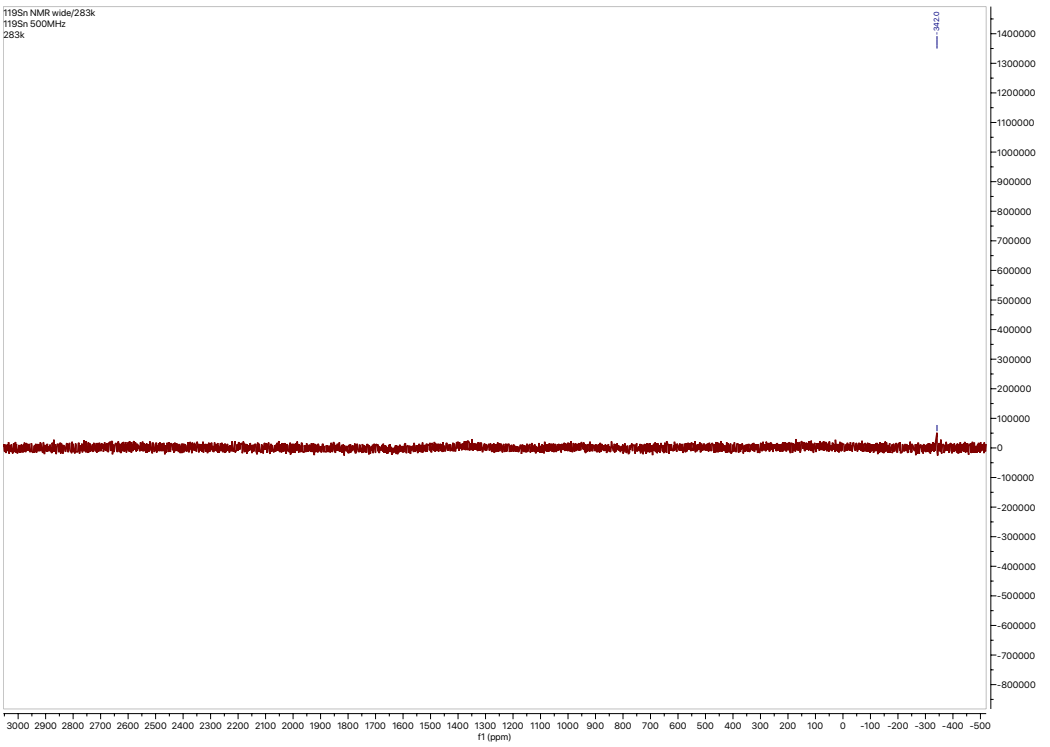

Figure S4.13 $^{119}Sn\{^{1}H\}$ NMR spectrum of $\{Sn(C_6H_2\text{-}2,4,6\text{-}Cyp_3)_2\}_3$ (**3**) in C_7D_8 at 283 K.

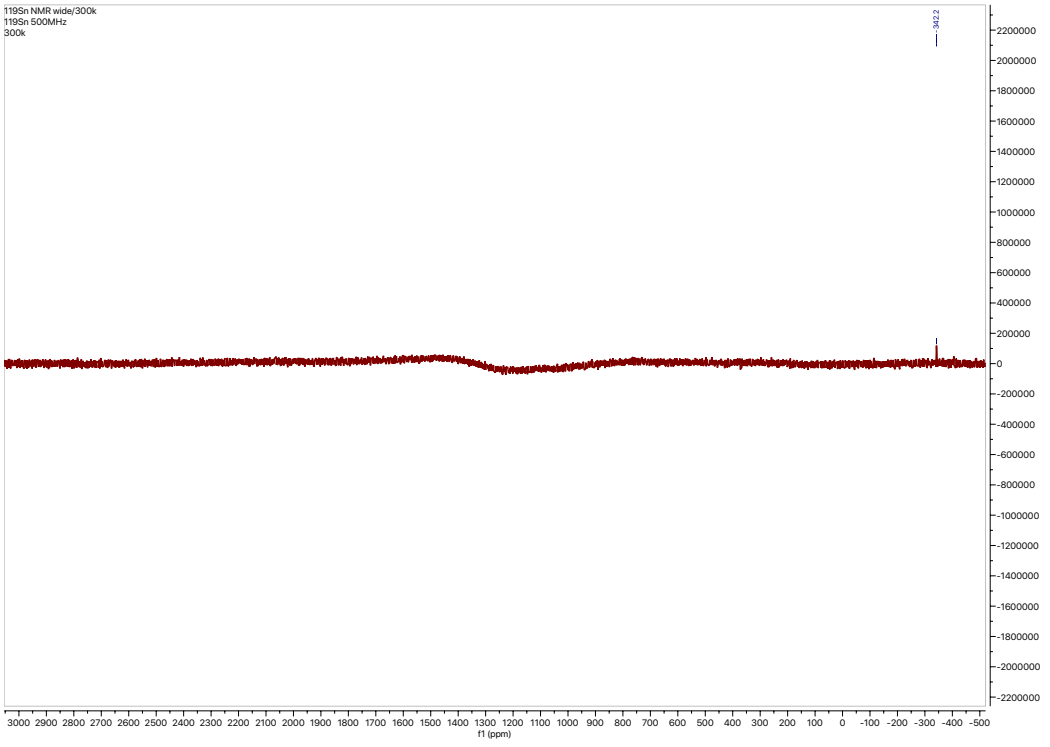

Figure S4.14 $^{119}Sn\{^{1}H\}$ NMR spectrum of $\{Sn(C_6H_2\text{-}2,4,6\text{-}Cyp_3)_2\}_3$ (**3**) in C_7D_8 at 300 K.

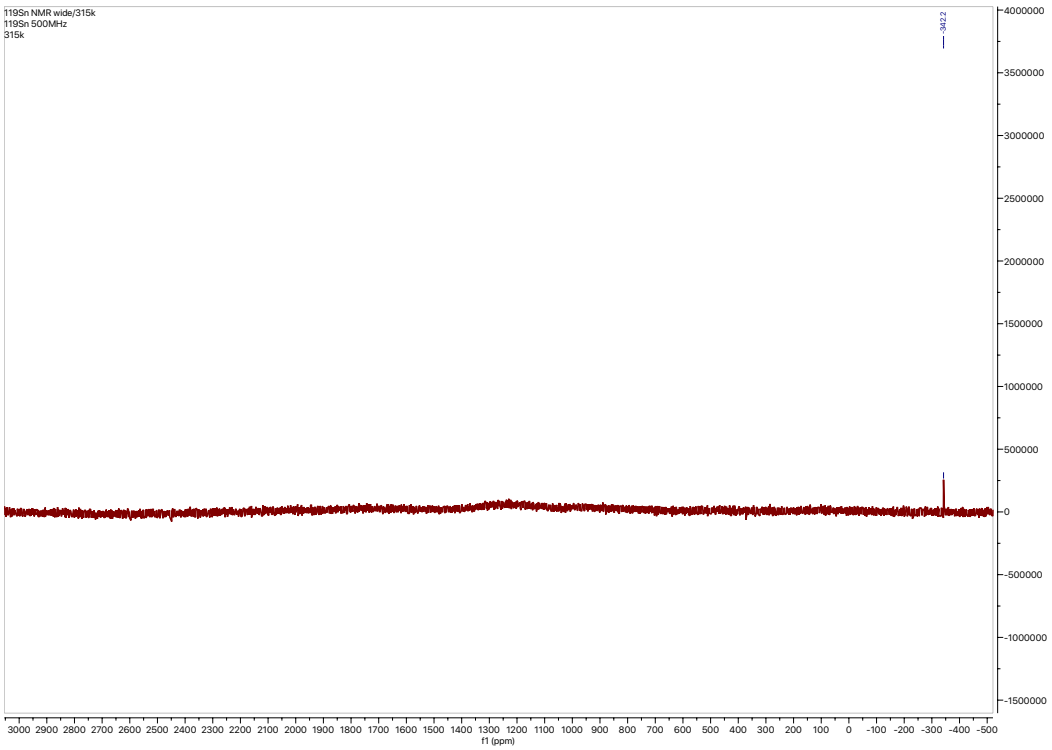

Figure S4.15 $^{119}Sn\{^{1}H\}$ NMR spectrum of $\{Sn(C_6H_2\text{-}2,4,6\text{-}Cyp_3)_2\}_3$ (**3**) in C_7D_8 at 315 K.

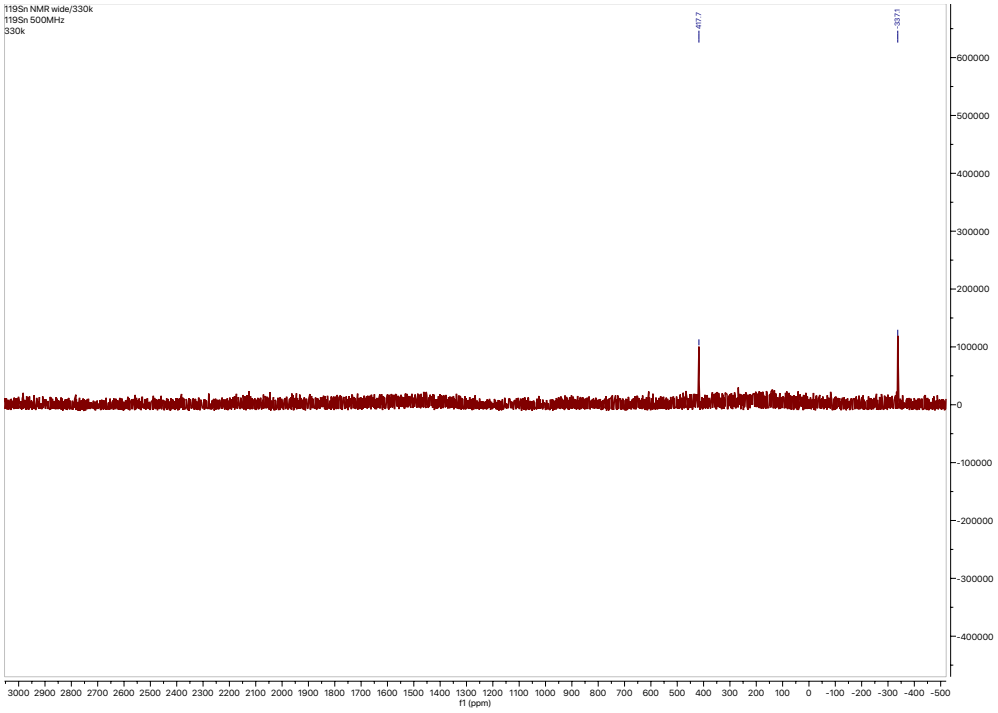

Figure S4.16 $^{119}Sn\{^{1}H\}$ NMR spectrum of $\{Sn(C_6H_2\text{-}2,4,6\text{-}Cyp_3)_2\}_3$ (**3**) and $\{Sn(C_6H_2\text{-}2,4,6\text{-}Cyp_3)_2\}_2$ (**2**) C_7D_8 at 330 K.

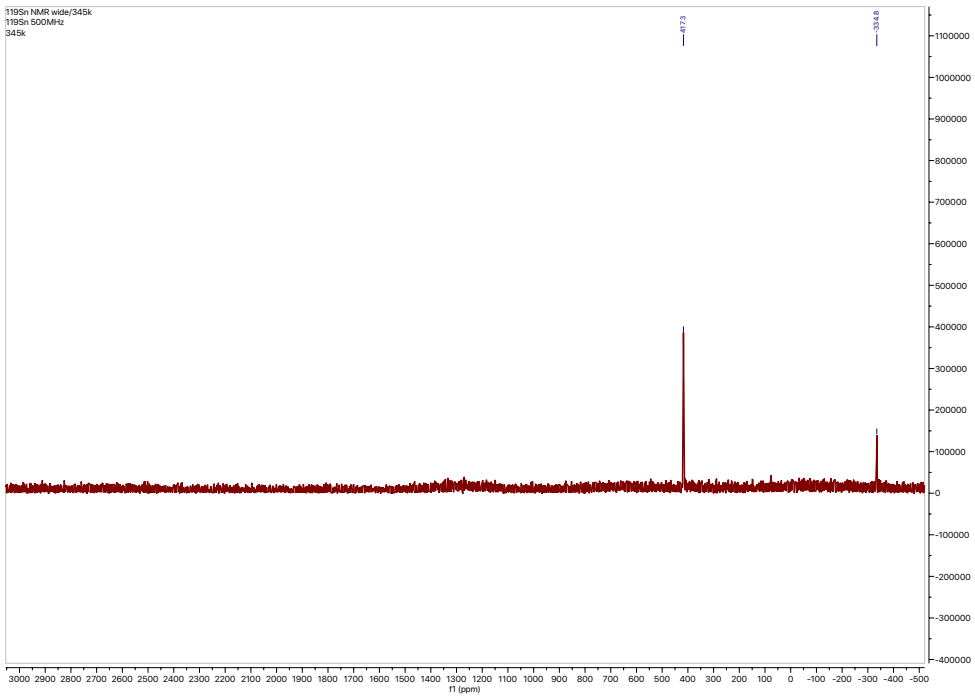

Figure S4.17 $^{119}Sn\{^{1}H\}$ NMR spectrum of $\{Sn(C_6H_2\text{-}2,4,6\text{-}Cyp_3)_2\}_3$ (**3**) and $\{Sn(C_6H_2\text{-}2,4,6\text{-}Cyp_3)_2\}_2$ (**2**) in C_7D_8 at 345 K.

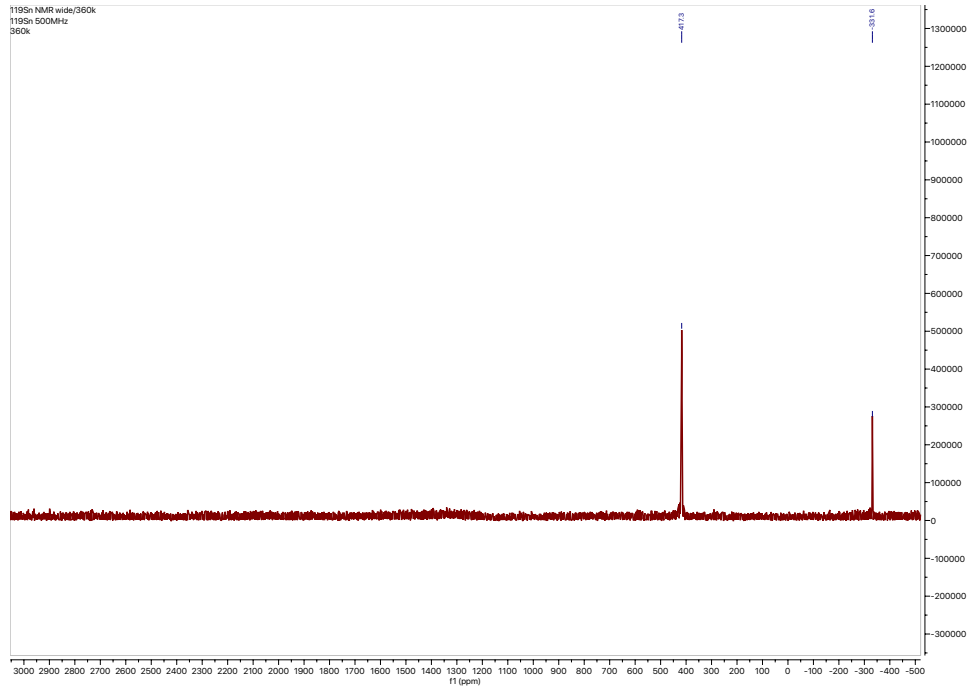

Figure S4.18 $^{119}Sn\{^{1}H\}$ NMR spectrum of $\{Sn(C_6H_2\text{-}2,4,6\text{-}Cyp_3)_2\}_3$ (**3**) and $\{Sn(C_6H_2\text{-}2,4,6\text{-}Cyp_3)_2\}_2$ (**2**) in C_7D_8 at 360 K.

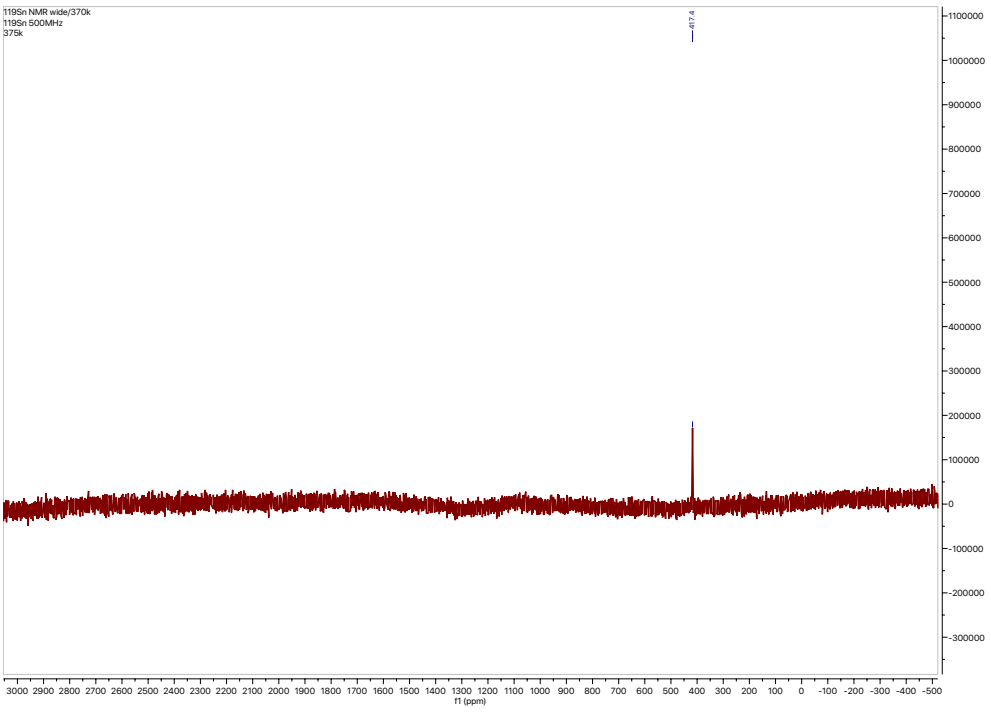

Figure S4.19 $^{119}Sn\{^{1}H\}$ NMR spectrum of $\{Sn(C_6H_2\text{-}2,4,6\text{-}Cyp_3)_2\}_2$ (**2**) in C_7D_8 at 375 K.

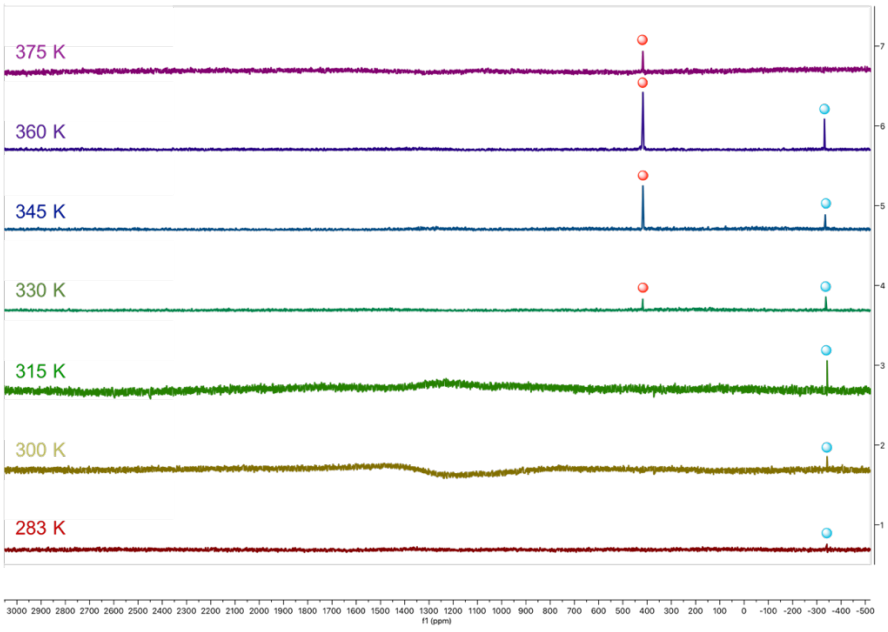

Figure S4.20 Variable temperature ^{1}H NMR spectra (temperature range of 283 to 375 K) of the interconversion of complexes **2** and **3** in C_7D_8. The trimer **3** indicated by blue sphere and the dimer **2** indicated by red sphere.

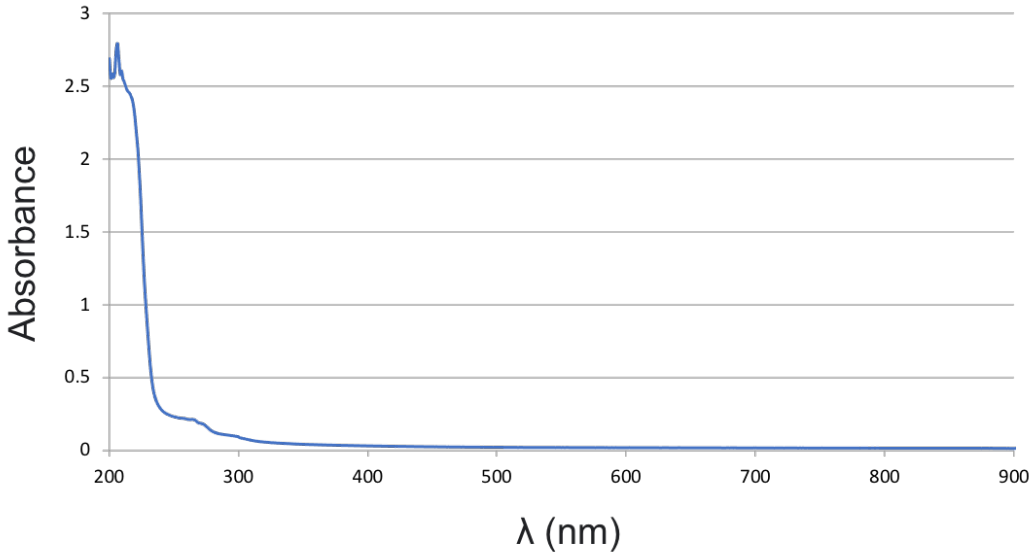

Figure S4.21 UV-Vis spectrum of {Li(C_6H_2-2,4,6-Cyp_3)·OEt_2}$_2$ (**1**) at 25 °C (82 μM in hexanes).

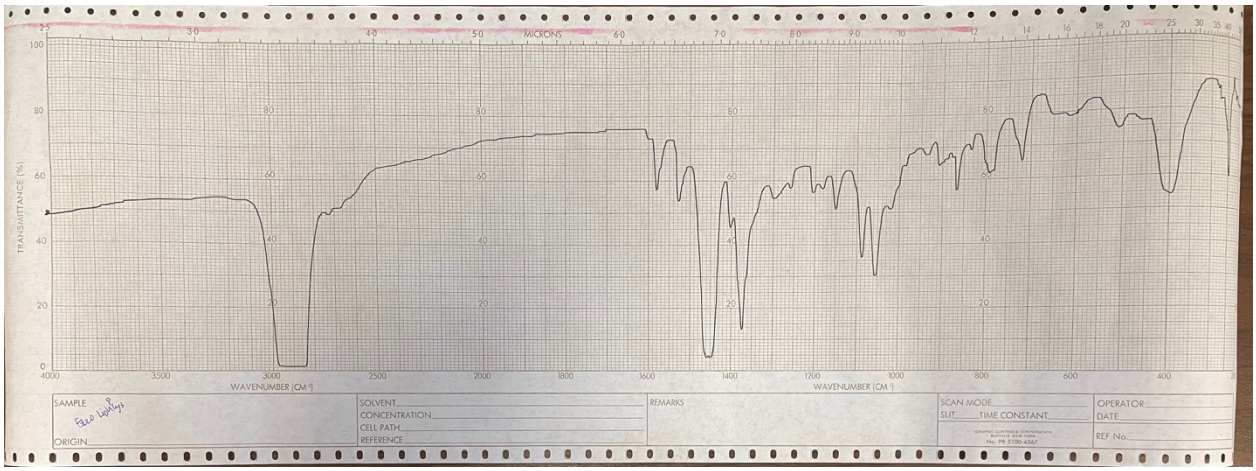

Figure S4.22 Infrared spectrum of a Nujol mull of {Li(C_6H_2-2,4,6-Cyp_3)·OEt_2}$_2$ (**1**) at 25°C.

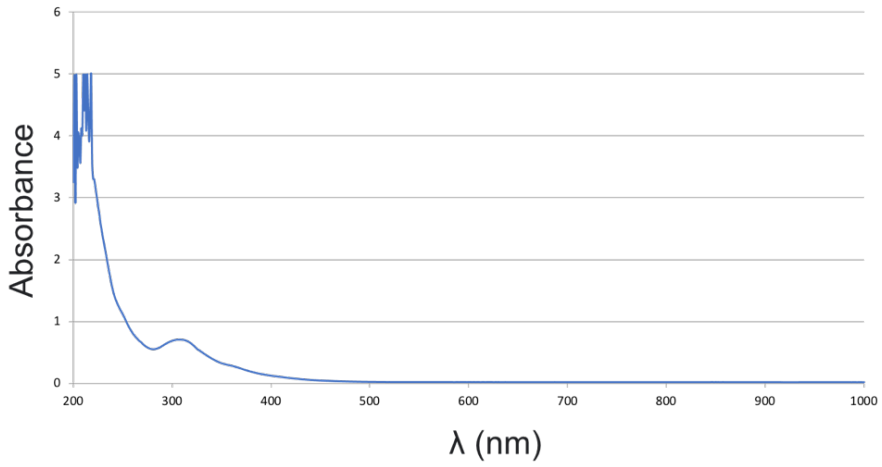

Figure S4.23 UV-Vis spectrum of $\{Sn(C_6H_2\text{-}2,4,6\text{-}Cy^p{}_3)_2\}_3$ (**3**) at 25 °C (48 μM in hexanes).

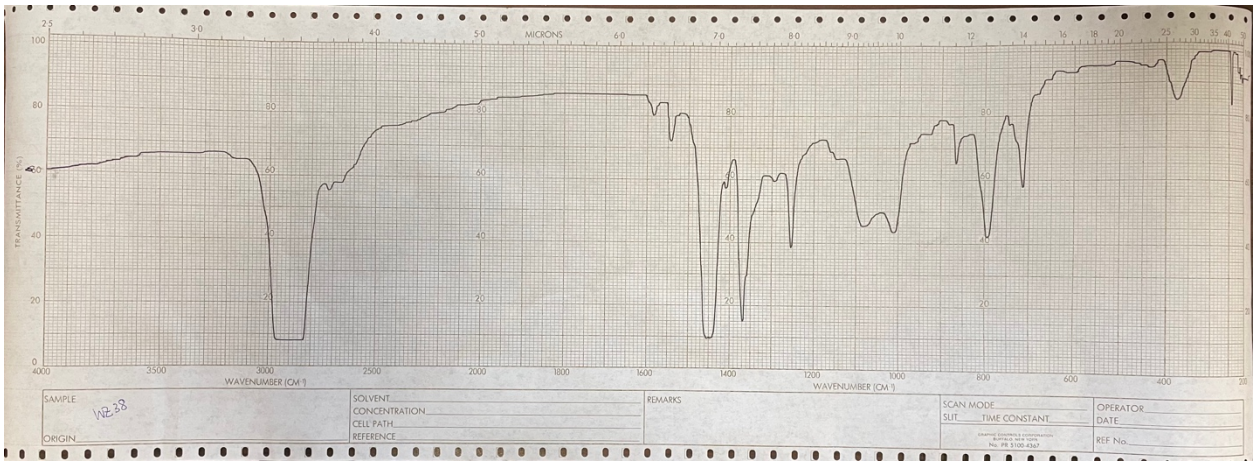

Figure S4.24 Infrared spectrum of a Nujol mull of $\{Sn(C_6H_2\text{-}2,4,6\text{-}Cyp_3)_2\}_3$ (**3**) at 25°C.

Van't Hoff analysis

The cyclotristannane **3** was dissolved in d_8-toluene and transferred to a sealed J. Young NMR tube. The tube was inserted into a temperature-controlled NMR probe and ^{1}H NMR spectra were collected at 15 K intervals from 180 to 375 K. Concentrations of the distannene **2** and cyclotristannane **3** were determined by integration of the meta hydrogens of the central rings of the ligands. The equilibrium constant of the reaction was calculated according to the expression:

a). Complex **3** to **2**:

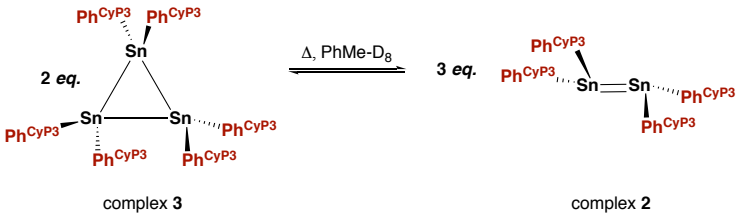

complex **3** complex **2**

The equilibrium constant (K_{eq}) was calculated as:

$$K_{eq} = \frac{[\mathbf{Dimer}]^3}{[\mathbf{Trimer}]^2}$$

The concentrations of the species were determined according to their relative integrations. A Van't Hoff plot of Ln(K_{eq}) against 1/T was constructed for the above reaction. ΔS and ΔH were calculated using the gradient and intercept of the plot:

$$Ln(K_{eq}) = \frac{-\Delta H}{R} \cdot \frac{1}{T} + \frac{\Delta S}{R}$$

$$y = m \cdot x + c$$

The free energy ΔG was then calculated $\Delta G = \Delta H - T\Delta S$ using equation below:

Table S4.1 Determined concentrations, equilibrium constants and natural logs used for van't Hoff analysis for complex **3**.

Temperature (K)	$C_{[Trimer]}$	$C_{[Dimer]}$	K_{eq}	$Ln(K_{eq})$	1/T
283.0	2.01	0.10	0.0002426	-8.323	0.00353
300.0	1.83	0.34	0.0117364	-4.445	0.00333
315.0	1.74	0.74	0.1338433	-2.011	0.00317
330.0	1.72	1.44	1.0093245	0.00928	0.00303
345.0	1.42	2.73	10.090467	2.31159	0.00290
360.0	1.07	4.15	62.427612	4.13416	0.00278
375.0	0.39	5.25	951.36384	6.85792	0.00267

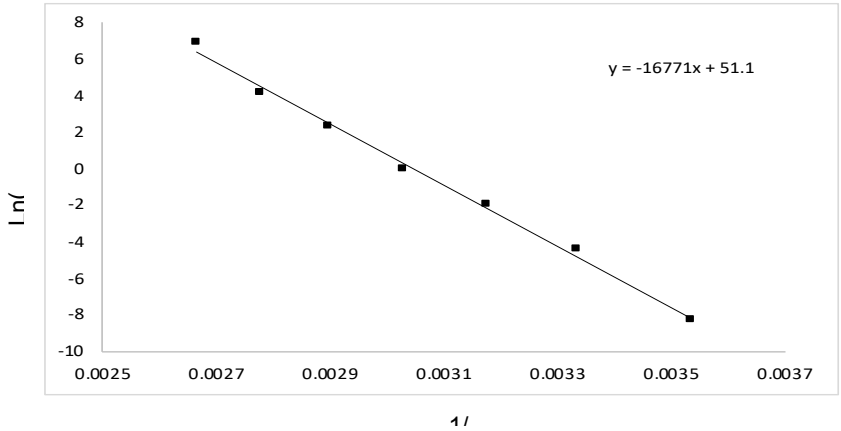

Figure S4.25 Van't Hoff plot of $Ln(K_{eq})$ against 1/T for the equilibrium between **2** and **3**.

Table S4.2 Calculated thermodynamic parameters of the dissociation reaction of complex **3**.

Gradient = -16771	ΔS (kJ mol^{-1} K^{-1})	ΔS (kcal mol^{-1} K^{-1})	ΔH (kJ mol^{-1})	ΔH (kcal mol^{-1})
Intercept = 51.1	+0.04248	+0.101637	+139.43	+33.357

Table S4.3 Temperature dependence on free energy (ΔG) for the dissociation of complex **3**.

Temperature (K)	ΔG
283.0	4.59398225
300.0	2.86614211
315.0	1.34157727
330.0	-0.1829876
345.0	-1.7075524
360.0	-3.2321172
375.0	-4.7566821

b). Complex $\{Sn(C_6H_2\text{-}2,4,6\text{-}^iPr_2)_2\}_3$ to $\{Sn(C_6H_2\text{-}2,4,6\text{-}^iPr_2)_2\}_2$:

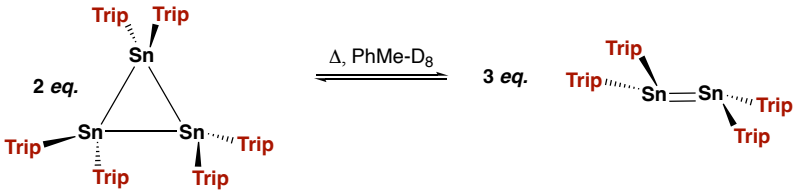

Table S4.4 Determined concentrations, equilibrium constants and natural logs used for van't Hoff analysis for complex $\{Sn(C_6H_2\text{-}2,4,6\text{-}^iPr_2)_2\}_3$.

Temperature (K)	$C_{[Trimer]}$	$C_{[Dimer]}$	K_{eq}	$Ln(K_{eq})$	1/T
298.8	2.00	0.15	0.00084375	-7.0776543	0.00334672
312.0	1.93	0.31	0.007997799	-4.828589	0.00320513
325.9	1.69	0.40	0.022408179	-3.7983293	0.00306843
337.6	1.69	0.69	0.115020132	-2.1626481	0.00296209
343.5	1.69	1.22	0.635778859	-0.4529045	0.00291121
354.9	1.80	2.09	2.817694136	1.03591887	0.0028177
363.8	2.09	4.33	23.46593161	3.15554965	0.00274876
369.0	1.93	5.80	52.38046659	3.95853375	0.00271003

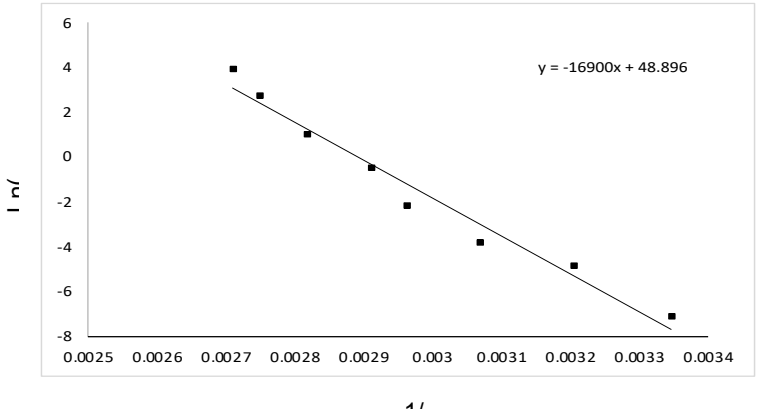

Figure S4.26 Van't Hoff plot of Ln(K_{eq}) against 1/T for the equilibrium between {Sn(C_6H_2-2,4,6-^{i}Pr$_2$)$_2$}$_3$ and {Sn(C_6H_2-2,4,6-^{i}Pr$_2$)$_2$}$_2$.

Table S4.5 Calculated thermodynamic parameters of the dissociation reaction of complex {Sn(C_6H_2-2,4,6-^{i}Pr$_2$)$_2$}$_3$.

Gradient = -16900	ΔS (kJ mol^{-1} K^{-1})	ΔS (kcal mol^{-1} K^{-1})	ΔH (kJ mol^{-1})	ΔH (kcal mol^{-1})
Intercept = 48.896	+0.407	+0.0972	+140.51	+33.61

Table S4.6 Temperature dependence on free energy (ΔG) for dissociation of complex $\{Sn(C_6H_2\text{-}2,4,6\text{-}^iPr_2)_2\}_3$.

Temperature (K)	ΔG
298.8	4.55455082
312.0	3.2707992
325.9	1.91896985
337.6	0.78109911
343.5	0.20730104
354.9	-0.9013935
363.8	-1.7669533
369.0	-2.2726737

Estimate of Error: The uncertainty in the integration was estimated to be 10% due to broadening. The VT apparatus indicated an uncertainty in the temperature of 1%.

DOSY NMR Analysis

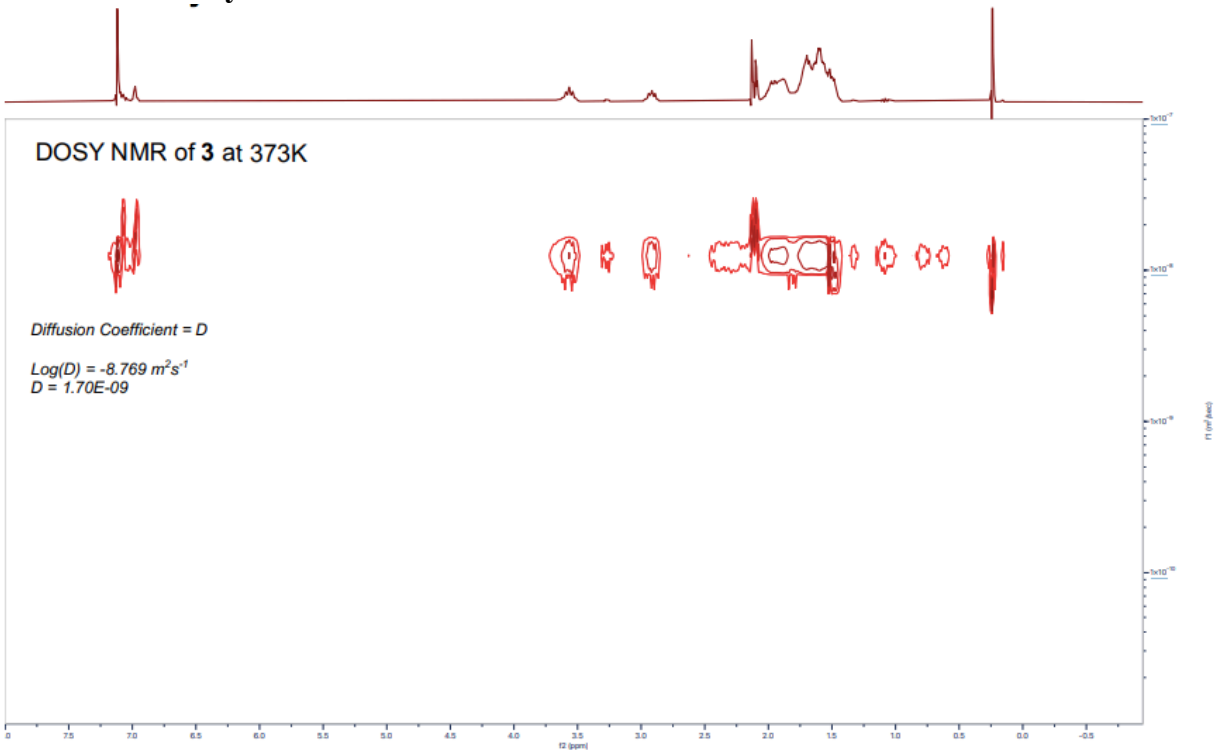

Figure S4.27 DOSY NMR of 3 at 373 K showing its conversion to 2 and the corresponding diffusion coefficient.

At 373 K, the entirety of 3 is converted to 2. The DOSY NMR was obtained at this temperature and the hydrodynamic radius of 2 in toluene was calculated using the following equation:

$$r = \frac{kT}{6\pi\eta D}$$

Where k is the Boltzmann constant, T is the temperature, η is the viscosity of toluene at 373 K and D is the diffusion coefficient. Following the calculation, r = 5.01 Å. Comparing this with the approximated spherical radius using the volume (r_v) from the crystal structure of **2**, we find that r_v = 4.73 Å. These values are in good agreement, suggesting that the species observed at 373 K is indeed the distannene **2**, generated from the cyclotristannane **3**.

Crystallographic Data

	1	**2**	**3**
formula	$C_{50}H_{78}Li_2O_2$	$C_{84}H_{116}Sn_2$	$C_{126}H_{174}Sn_3$
fw	725.0	1363.14	2044.71
color	colorless	red	yellow
cyst syst	Triclinic	Triclinic	Triclinic
space group	P-1	P-1	R-3c
a, Å	9.424(5)	12.508(11)	24.303(2)
b, Å	10.748(6)	14.438(13)	24.303(2)
c, Å	11.561(6)	20.6912(19)	75.010(10)
α, deg	78.395(2)	93.931(16)	90.0
β, deg	88.0(2)	103.427(15)	90.0
γ, deg	81.439(2)	100.302(15)	120.0
V, Å^3	1134.3(11)	3552.0(6)	38369(9)
Z	1	2	12
Density (calculated), Mg/m^3	1.061	1.275	1.062
Absorption coefficient, mm^{-1}	0.455	0.747	0.622
F(000)	400.0	1440	12960
Crystal size, mm^3	0.407 x 0.341 x 0.258	0.324 x 0.266 x 0.168	0.431 x 0.234 x 0.217
Crystal color and habit	colorless block	red plate	yellow plate
Theta range for data collection, deg	7.806 to 136.822	1.443 to 25.460	2.010 to 25.469
Index ranges	-9<=h<=1, -12<=k<=12, -13<=l<=13	-15<=h<=15, -17<=k<=17, -24<=l<=24	-25<=h<=24, -29<=k<=29, -90<=l<=90
Reflections collected	19522	19530	7906
Independent reflections	4134, [$R_{(int)}$ = 0.041]	12634 [$R_{(int)}$ = 0.045]	7906, [$R_{(int)}$ = ?]
Data / restraints / parameters	4134/0/302	12634 / 35 / 802	7906 / 93 / 413

Goodness-of-fit on F^2	1.101	1.042	1.094
Final R indices [I>2sigma(I)]	$R_1 = 0.0797$, $wR_2 = 0.1911$	$R_1 = 0.0592$, $wR_2 = 0.1011$	$R_1 = 0.0549$, $wR_2 = 0.1161$
R indices (all data)	$R_1 = 0.0805$, $wR_2 = 0.1922$	$R_1 = 0.1002$, $wR_2 = 0.1135$	$R_1 = 0.0636$, $wR_2 = 0.1221$
Largest diff. peak and hole, e.Å^{-3}	0.32/-0.48	0.850/-0.917	1.832/-1.542

Computational Details

General remarks, geometry optimizations and single point energies

Computed structures and orbitals were visualized with UCSF Chimera[4] 1.10.2. Quantum mechanical calculations were performed with the TURBOMOLE 7.5.1[5] and ORCA 5.0.3[6] program packages. Geometries were pre-optimized with the GFN2-xTB[7] extended tight binding method applying the generalized born solvation with solvent accessible surface (GBSA)[8] model for toluene. Final geometries were optimized applying r^{2}SCAN-3c[9] with the COSMO[10] implicit continuum solvation model for toluene as implemented in TURBOMOLE. All calculations were accelerated by applying the resolution-of-identity (RI) approximation for Coulomb integrals[11] with matching default auxiliary basis sets.[12]

Gas phase single point energies were calculated at the B3LYP-D4/def2-QZVP[13-16] level applying *DEFGRID3* and *TightSCF* options as implemented in ORCA. Energy decomposition analysis (EDA)[17] was performed at the BLYP-D4/def2-TZVP level (For the tristannane, def2-TZVP was used for the tin atoms and the attached phenyl units, the remaining parts of the ligand were treated with the def2-SVP basis set). The D4 correction to repulsive density functionals such as B3LYP

was found to reproduce the London dispersion contribution obtained from sophisticated, DLPNO-CCSD(T) based local energy decomposition schemes well.[18,19] Default def2 effective core potentials as implemented in TURBOMOLE were applied for Sn.

NMR parameter calculations

NMR chemical shifts δ for ^{119}Sn nuclei were calculated relative to tetramethylstannane:

$$\delta(X) = \sigma(X_{ref}) - \sigma(X)$$

Isotropic chemical shielding (σ) and coupling constants were calculated applying the Amsterdam Modeling Suite AMS2022.101[20-22] program package. The revPBE[23] functional was applied with the all-electron ZORA/TZP[24] basis set and the zeroth-order regular approximation (ZORA)[25,26] including spin-orbit corrections (SO-ZORA).[27] The COSMO[28] implicit solvation model was applied for toluene (*surf Esurf, solv Eps=2.38 Rad=3.48*; *div ndiv=5* settings). Otherwise, default settings including gauge-including atomic orbital (GIAO) were applied as implemented in AMS. The chemical Shift was averaged for all symmetry equivalent tin atoms.

Table S4.7 Calculated ^{119}Sn NMR chemical shifts at the SO-ZORA-revPBE(COSMO)/TZP level.

#	$\delta_{calc}(^{119}Sn)$
2	505.9
3	-340.1
Stannylene$_r$	2313.1

Cartesian Coordinates (XYZ format)

Stannylene

101

r^2SCAN-3c

Sn	-0.0553150	-2.5995402	-0.4453146
C	-2.8717078	0.8851979	0.1629562
H	-3.1255429	1.8096752	-0.3536015
C	-3.4737821	0.6256176	1.3924152
C	2.9404833	0.7334417	0.1279038
H	3.2405293	1.4108479	0.9260202
C	-6.4065745	2.2021182	3.2588023
H	-7.1419544	1.8253274	3.9767298
H	-6.9247522	2.9243836	2.6177246
C	3.1408794	0.0119511	-2.1456130
H	3.5927095	0.1108757	-3.1308980
C	3.5245411	0.8876148	-1.1279517
C	-1.6005826	-1.1761051	0.2753207
C	1.3564996	-0.3255337	1.7536047
H	0.6417394	-1.1656246	1.7723009
C	1.5691720	-1.1016685	-0.6638026
C	2.3436161	-0.5315938	2.9203171
H	2.7095156	-1.5627810	2.9717549

H	3.2171434	0.1131651	2.7697201
C	-1.9432472	0.0052559	-0.4054440
C	-4.4236984	1.6190851	2.0068760
H	-4.5722914	2.4406635	1.2898561
C	-3.1492126	-0.5644047	2.0466170
H	-3.6169884	-0.7903321	3.0030631
C	-1.3088726	0.3763025	-1.7254387
H	-0.6320205	-0.4385201	-2.0313149
C	1.9710344	-0.2452279	0.3757948
C	-2.6622285	-4.7823365	3.3044849
H	-1.9474175	-5.4570017	2.8163138
H	-3.4790894	-5.3971126	3.6962279
C	2.1813246	-0.9771811	-1.9279856
C	-2.2292785	-1.4623136	1.5050410
C	-3.9363196	2.2269069	3.3371523
H	-3.5700255	1.4169436	3.9806542
H	-3.1069336	2.9278768	3.1943269
C	-3.1310787	-3.7311311	2.2977684
H	-3.3767497	-4.1397369	1.3111843
H	-4.0184426	-3.2036822	2.6743110
C	-1.9462318	-2.7516330	2.2462863
H	-1.1320170	-3.2901161	1.7239577
C	-5.8101426	1.0788501	2.3961818

H	-6.4254532	0.8287669	1.5251825
H	-5.6890313	0.1641248	2.9910474
C	4.5154387	1.9921831	-1.3825964
H	4.7121332	2.5031865	-0.4280165
C	4.0403924	3.0472545	-2.4021525
H	3.6164259	2.5293997	-3.2717087
H	3.2546424	3.6924974	-1.9949771
C	1.8319380	-1.9166966	-3.0624639
H	1.0130065	-2.5852832	-2.7326102
C	0.5805855	0.9294264	2.1888205
H	1.2097265	1.8135721	2.0195235
H	-0.3460456	1.0587266	1.6204156
C	2.9781541	-2.8410319	-3.5062232
H	3.8666916	-2.2317009	-3.7215287
H	3.2502752	-3.5692387	-2.7342173
C	6.5081609	2.8978947	-2.3999477
H	7.2308064	2.7701242	-3.2121733
H	7.0503705	3.3332518	-1.5526995
C	-5.1914637	2.8820073	3.9527076
H	-5.1987360	3.9608168	3.7648758
H	-5.2148192	2.7484053	5.0389352
C	5.8696898	1.5673114	-1.9742769
H	6.4817191	1.0009324	-1.2640370

H	5.6998253	0.9282974	-2.8506166
C	5.3191957	3.8173977	-2.7996721
H	5.3797506	4.7741072	-2.2704586
H	5.3247526	4.0456045	-3.8702895
C	-2.2839334	0.6336907	-2.8932687
H	-2.6726661	-0.3001898	-3.3135342
H	-3.1450356	1.2029124	-2.5252814
C	-0.4680189	1.6644139	-1.6959368
H	-1.0580174	2.4662298	-1.2316188
H	0.4529253	1.5416098	-1.1170146
C	2.4337796	-3.4755323	-4.7879397
H	3.2195440	-3.9000834	-5.4210037
H	1.7496086	-4.2916074	-4.5243941
C	-1.5189276	-2.6324105	3.7279119
H	-2.0253027	-1.7810965	4.1942930
H	-0.4434420	-2.4474146	3.8156499
C	-1.9533724	-3.9608072	4.4042840
H	-2.6447598	-3.7537777	5.2280765
H	-1.1038664	-4.5044991	4.8291620
C	1.3739768	-1.2747765	-4.3898568
H	0.3217982	-0.9749290	-4.3504394
H	1.9569350	-0.3666178	-4.5775879
C	0.3435534	0.7115942	3.6878109

H	0.2131521	1.6542983	4.2293919
H	-0.5758050	0.1319061	3.8243438
C	1.5710194	-0.0970999	4.1889682
H	1.2495397	-0.9656213	4.7738892
H	2.2087104	0.5044866	4.8448628
C	-1.4855450	1.4755450	-3.9196423
H	-1.2168871	0.8830658	-4.8008202
H	-2.0874891	2.3167817	-4.2787670
C	1.6554614	-2.3343927	-5.4875609
H	0.7315213	-2.7054003	-5.9419334
H	2.2525969	-1.8949908	-6.2933072
C	-0.2146066	1.9664671	-3.1765489
H	0.6635144	1.4024598	-3.5099421
H	-0.0047834	3.0259246	-3.3573917

Distannene (**2**)

202

r^2SCAN-3c

Sn	-0.9189443	1.2166748	-0.3256484
C	-2.9618335	4.9975289	0.7446936
H	-3.0538646	5.9714179	0.2668141
C	-3.4682385	4.8343470	2.0305086
C	2.7168026	3.8010487	0.2787525

H	3.1338023	4.4118206	1.0780159
C	-5.7388324	6.9538398	4.2524824
H	-6.4470803	6.7023630	5.0482789
H	-6.1577675	7.8082300	3.7091529
C	2.8607898	2.9406544	-1.9410888
H	3.3758892	2.8709981	-2.8975627
C	3.3824260	3.7598926	-0.9430372
C	-2.1862906	2.7032447	0.6957108
C	0.9346462	3.1458781	1.8895130
H	0.0085337	2.5599667	1.8916852
C	1.0128349	2.2684019	-0.5161292
C	1.8306483	2.5970549	3.0218073
H	1.8093683	1.5006157	3.0500881
H	2.8708068	2.8900013	2.8391702
C	-2.3185919	3.9539705	0.0680738
C	-4.0851438	5.9923087	2.7683279
H	-4.0963290	6.8626799	2.0948701
C	-3.3720296	3.5721949	2.6199597
H	-3.7768832	3.4213469	3.6181197
C	-1.7816883	4.2205262	-1.3186577
H	-1.3385662	3.2899898	-1.7183272
C	1.5464508	3.0710544	0.5123245
C	-3.5317035	-0.6027838	4.0658564

H	-3.5589841	-1.4528753	3.3726635
H	-4.1704239	-0.8568896	4.9175184
C	1.7007724	2.1879144	-1.7455772
C	-2.7631746	2.5001802	1.9678993
C	-3.3406907	6.3939223	4.0565237
H	-3.1373161	5.4886061	4.6427509
H	-2.3761120	6.8698305	3.8495831
C	-3.9968904	0.6691313	3.3421305
H	-4.8161387	0.4994924	2.6363589
H	-4.3392071	1.4123239	4.0732228
C	-2.7114022	1.1597055	2.6590911
H	-2.4528026	0.4036517	1.9042395
C	-5.5175718	5.7776177	3.2865115
H	-6.2562793	5.7364762	2.4788191
H	-5.5664630	4.8243284	3.8285279
C	4.6530345	4.5384554	-1.1548299
H	4.8355237	5.1502462	-0.2581404
C	4.6720474	5.4727892	-2.3761811
H	4.3346733	4.9167937	-3.2604999
H	4.0083634	6.3359090	-2.2564335
C	1.2401766	1.3102838	-2.8877897
H	0.3857306	0.7100736	-2.5388351
C	0.5639455	4.5510322	2.3922209

H	1.4171529	5.2312002	2.2658210
H	-0.2901642	4.9691184	1.8491338
C	2.3107485	0.3131447	-3.4232943
H	3.3163144	0.6078992	-3.1082405
H	2.1355413	-0.6803038	-3.0018225
C	6.9558945	4.6512856	-1.9541013
H	7.5783045	4.1781785	-2.7203701
H	7.6296369	4.9817301	-1.1563951
C	-4.3284438	7.3120357	4.8046203
H	-4.0993469	8.3647892	4.6079535
H	-4.2631128	7.1690695	5.8879166
C	5.9013825	3.6695313	-1.4027269
H	6.2281849	3.1432584	-0.4993128
H	5.6554204	2.9069091	-2.1526836
C	6.1535270	5.8592602	-2.5192460
H	6.3620818	6.7580908	-1.9280497
H	6.4199341	6.0891236	-3.5558079
C	-2.8191110	4.6877627	-2.3551264
H	-3.5213935	3.8932724	-2.6308080
H	-3.4051417	5.5119221	-1.9299272
C	-0.7013262	5.3101141	-1.4214973
H	-1.0445634	6.2011682	-0.8797721
H	0.2479626	4.9925656	-0.9789410

C	2.1743943	0.3160867	-4.9644327
H	2.9936551	0.8905487	-5.4151188
H	2.2132666	-0.6927490	-5.3897456
C	-1.6868468	1.0188984	3.8003685
H	-1.8121276	1.8624296	4.4915784
H	-0.6528355	1.0314373	3.4411728
C	-2.0613634	-0.3140602	4.4829791
H	-1.9474840	-0.2510977	5.5698904
H	-1.4027541	-1.1190331	4.1350060
C	0.7661101	2.0762210	-4.1398678
H	-0.2337086	2.5062336	-4.0069082
H	1.4574916	2.9023214	-4.3551604
C	0.2759463	4.3210908	3.8788554
H	0.3402000	5.2395257	4.4722269
H	-0.7453399	3.9366976	3.9837885
C	1.3016298	3.2491496	4.3252868
H	0.8368278	2.5116478	4.9881126
H	2.1256358	3.7047633	4.8848668
C	-1.9691342	5.1872747	-3.5385784
H	-1.8338307	4.3848007	-4.2725908
H	-2.4556046	6.0164492	-4.0620509
C	0.8419322	1.0271132	-5.2501004
H	0.0069221	0.3213362	-5.1484580

H	0.7925590	1.4580229	-6.2562320
C	-0.5967087	5.5973383	-2.9303795
H	0.2083130	4.9960611	-3.3666216
H	-0.3549395	6.6468728	-3.1259854
H	2.0198256	-5.5728394	4.6076626
H	2.1586509	-6.7355686	2.5059524
C	1.8398987	-4.9620587	3.7165795
H	2.3761097	-4.0140140	3.8509788
H	5.5788623	-1.2697131	3.3886603
H	3.3584665	-5.4796214	2.2100398
C	2.2969583	-5.6518474	2.4164846
H	-0.2248698	-5.6038066	3.5615893
H	-0.0742380	-3.9426424	4.1606896
C	0.3576032	-4.6773691	3.4717016
H	5.8854744	-1.5788503	1.6733995
C	5.1729761	-1.1323558	2.3804188
H	3.2141601	-1.6789058	3.1389833
H	3.8346861	-2.8346104	1.9570234
C	3.7844781	-1.7693680	2.2060526
H	4.4089726	0.8442357	2.8234892
C	1.3803104	-5.0887572	1.2986874
H	-5.1194560	-6.7889881	2.3028866
H	5.8648235	0.8874001	1.8137270

C	4.9386782	0.3345547	2.0071375
H	0.8726972	-5.8975867	0.7624198
C	0.3371851	-4.1888743	2.0105882
H	-1.3213061	-6.2639530	1.6364012
H	-5.6227904	-8.8799524	1.2257452
H	1.9323467	-4.5109298	0.5506632
H	0.7512819	-3.1640501	2.0333023
C	-5.1662994	-6.7517515	1.2092716
H	2.1518401	-0.5186443	1.4989889
C	3.0743402	-0.9465946	1.0804124
C	-1.7654249	-5.3335638	1.2852130
H	-3.1520840	-7.4734759	0.9912110
C	-5.8013001	-8.0090390	0.5856662
H	-6.8861992	-7.9053918	0.4838468
C	-1.0356003	-4.1424299	1.3789182
C	4.0364984	0.2325331	0.7740749
H	-5.7414180	-5.8583687	0.9347388
H	5.9283376	-4.0786756	-1.0658819
C	-3.7728436	-6.6727184	0.5614024
H	4.6444969	-0.0017249	-0.1083629
H	4.7708583	-2.1782156	-0.5332927
C	-3.0402674	-5.3683323	0.7283808
C	2.7033355	-1.7740945	-0.1306840

H	3.4894034	1.1528352	0.5504280
H	-4.5751815	-9.1633308	-0.8158142
H	5.1901423	-5.5640442	-1.6757794
H	7.7770483	-4.8581515	-2.3685876
C	3.7466081	-2.3526384	-0.8571260
C	5.6311939	-4.6086973	-1.9797824
C	-5.0960361	-8.1999804	-0.7888991
C	-1.6023144	-2.9484662	0.9033000
Sn	-0.2448253	-1.2220457	0.7627490
C	1.3676918	-2.0068844	-0.5188346
H	-0.8279989	-5.0053284	-1.4220564
C	-4.0840645	-7.0450945	-0.9005435
C	6.8378022	-4.7683192	-2.9235283
H	-5.8054334	-8.1974300	-1.6225335
C	-3.6114621	-4.1623860	0.3151085
C	3.5115082	-3.1419351	-1.9799261
H	6.7316051	-5.6805729	-3.5207772
H	-3.1838671	-7.3081322	-1.4666166
C	-2.9259214	-2.9519033	0.4136423
H	5.8748793	-1.9588140	-2.6437508
C	4.6471538	-3.7309071	-2.7726656
C	1.1165278	-2.7882316	-1.6643822
H	0.1005482	-5.0398607	-2.9364125

C	-0.6795212	-4.5004430	-2.3825799
H	-4.5403346	-6.1788291	-1.3970069
H	-4.6154090	-4.1676030	-0.1031597
C	2.1906500	-3.3385416	-2.3716749
H	7.7410549	-2.9339449	-3.7779264
C	5.5917700	-2.6939019	-3.4082021
C	6.8169605	-3.5164419	-3.8489542
H	-0.9954547	-2.5916430	-1.5008182
C	-0.2730306	-3.0284986	-2.1995424
H	4.2211388	-4.3434138	-3.5819140
H	1.9952303	-3.9289232	-3.2654354
H	-3.0314759	-0.8341574	0.3598243
H	-2.7977862	-4.1724228	-2.5510466
H	-2.2032282	-5.3409689	-3.7323438
C	-3.6105723	-1.6826912	-0.0321316
C	-1.9592969	-4.4055008	-3.2173848
H	-5.1540124	-1.3819637	1.5161320
H	6.7121344	-3.8220154	-4.8957021
H	5.1179561	-2.1448175	-4.2293194
C	-5.0609891	-1.4719032	0.4292732
H	-5.6791325	-2.3220642	0.1144878
C	-0.5442859	-2.4091172	-3.5894586
H	-2.7779059	-1.2863909	-2.0368501

C -3.7419786 -1.4687161 -1.5514828

H 0.3541531 -2.4891019 -4.2124413

H -4.1773958 -2.3719046 -1.9979618

C -1.7092505 -3.2333723 -4.1974492

H -0.7765405 -1.3411897 -3.5034328

H -5.1737491 0.6836392 0.2286739

H -2.6120507 -2.6274541 -4.3286439

H -1.4312701 -3.6088070 -5.1882457

C -5.4814250 -0.2068229 -0.3334516

C -4.7064279 -0.2710501 -1.6807947

H -4.1419224 0.6558334 -1.8388083

H -6.5652231 -0.1445076 -0.4724663

H -5.3781537 -0.3898424 -2.5368932

Cyclotristannane (3)

303

r^2SCAN-3c

Sn -1.6781523 0.1644453 -0.0264646

C -5.1023020 1.5581468 -2.5311957

H -5.9068017 2.2750886 -2.3849295

C -4.3678722 -1.8680304 0.2259062

H -3.5260495 -1.6936388 -0.4482494

C -4.1710669 -1.0224357 1.4653883

C	-3.0717452	-0.1591950	1.6611185
C	-3.0715790	0.5077409	-1.7192026
C	-4.1097850	1.4521662	-1.5532540
C	-5.1576786	-1.1148618	2.4505787
H	-6.0054371	-1.7750895	2.2768770
C	-3.0210865	-0.2528540	-2.9047547
C	-4.4400747	-3.3961489	0.5094374
H	-3.4633578	-3.8761674	0.3949550
H	-4.7663662	-3.5698698	1.5418300
C	-5.4545132	2.2046438	0.5204171
H	-6.3074660	1.9333992	-0.1128023
H	-5.3077389	1.3884738	1.2323732
C	-5.0861454	-0.3917733	3.6362337
C	-5.6847533	-1.5448342	-0.5527772
H	-6.2021103	-0.6793508	-0.1290807
H	-5.4349309	-1.2879848	-1.5886796
C	-1.9623778	-1.3094797	-3.1509244
H	-1.0603590	-1.0244329	-2.5921599
C	-2.9568726	0.5380094	2.8807513
C	-4.0277257	-0.0971040	-3.8642731
H	-3.9990869	-0.6964035	-4.7714343
C	-4.2096275	2.4033531	-0.3769034
H	-3.3156412	2.2872339	0.2518812

C	-3.9715449	0.4182511	3.8361173
H	-3.9013645	0.9786161	4.7653231
C	-5.0845149	0.7907344	-3.6908783
C	-4.3066645	3.8977435	-0.7538967
H	-3.3694889	4.2979444	-1.1521282
H	-5.0718208	4.0350581	-1.5280530
C	-1.8111434	1.4904449	3.1587339
H	-0.9278807	1.1277038	2.6151998
C	-5.4879463	-3.9449170	-0.4647070
H	-5.0453901	-4.0837427	-1.4601976
H	-5.8971704	-4.9100999	-0.1460865
C	-2.4324441	-2.7117586	-2.6544669
H	-2.0179790	-2.9410112	-1.6670054
H	-3.5255653	-2.7084139	-2.5661950
C	-2.0065739	-3.7130679	-3.7335985
H	-2.6101839	-4.6278509	-3.7185710
H	-0.9580710	-3.9992436	-3.5922417
C	-6.1554941	0.9307876	-4.7388513
H	-5.9516712	0.2028981	-5.5390463
C	-2.1450763	2.9296580	2.6622987
H	-1.6868809	3.1311792	1.6892622
H	-3.2315940	3.0158552	2.5493988
C	-6.5317390	-2.8261226	-0.5121402

H	-7.1391629	-2.8559900	0.4030268
H	-7.2173196	-2.9066471	-1.3630728
C	-7.5955449	0.7033392	-4.2479898
H	-7.7659760	1.3025419	-3.3440530
H	-7.7923475	-0.3432988	-3.9911541
C	-1.5700908	-1.5443102	-4.6389640
H	-1.8952833	-0.7373535	-5.3011406
H	-0.4788715	-1.5971375	-4.7012391
C	-2.1505574	-2.9097646	-5.0264257
H	-3.2119981	-2.8190735	-5.2955087
H	-1.6286121	-3.3621803	-5.8771369
C	-1.6620171	3.8847495	3.7580912
H	-0.5897481	4.0811182	3.6416596
H	-2.1870669	4.8468451	3.7362640
C	-6.1578869	-0.5033443	4.6863879
H	-5.9030754	0.1771839	5.5131610
C	-1.4310025	1.6806625	4.6550452
H	-0.3405791	1.6414144	4.7394014
H	-1.8362043	0.8991975	5.3033611
C	-7.5829321	-0.1656257	4.2152642
H	-7.7907937	-0.7091650	3.2844880
H	-7.7147609	0.9019617	4.0081989
C	-8.4644576	1.2192992	-5.4067902

H	-9.4357271	1.5862300	-5.0600305
H	-8.6630621	0.4056769	-6.1134881
C	-6.2562858	2.3287501	-5.3783022
H	-6.2396857	3.0832519	-4.5815168
H	-5.4150113	2.5428562	-6.0463109
C	-1.9026314	3.0879490	5.0413674
H	-2.9742254	3.0852467	5.2846721
H	-1.3645099	3.4886096	5.9079129
C	-5.7104729	3.5656034	1.2147868
H	-6.7530327	3.8738472	1.0812306
H	-5.5355797	3.5046098	2.2945852
C	-7.6216358	2.3311202	-6.0966284
H	-7.4974550	2.1085171	-7.1617278
H	-8.1043084	3.3114032	-6.0308605
C	-6.3451764	-1.9158695	5.2712136
H	-6.3962865	-2.6367100	4.4450154
H	-5.5105712	-2.2162741	5.9140236
C	-8.4831062	-0.6816446	5.3515528
H	-8.6590776	0.1159539	6.0818310
H	-9.4636021	-0.9989787	4.9826051
C	-4.7477812	4.5761313	0.5460533
H	-5.2135812	5.5517375	0.3707675
H	-3.8745269	4.7474000	1.1866121

C	-7.6940612	-1.8486299	6.0141452
H	-8.2338812	-2.7988286	5.9516358
H	-7.5344643	-1.6422644	7.0779319
Sn	0.6966624	-1.5355452	-0.0264646
C	1.2017563	-5.1977965	-2.5311957
H	0.9831164	-6.2529847	-2.3849295
C	3.8016979	-2.8486731	0.2259062
H	3.2297590	-2.2068291	-0.4482494
C	2.9709887	-3.1010321	1.4653883
C	1.6737396	-2.5806119	1.6611185
C	1.0960730	-2.9139359	-1.7192026
C	0.7972797	-4.2852614	-1.5532540
C	3.5443379	-3.9092498	2.4505787
H	4.5399911	-4.3133163	2.2768770
C	1.7295212	-2.4899107	-2.9047547
C	5.1611886	-2.1471430	0.5094374
H	5.0885383	-1.0612721	0.3949550
H	5.4747811	-2.3428593	1.5418300
C	0.8179791	-5.8260689	0.5204171
H	1.4793602	-6.4291254	-0.1128023
H	1.4514159	-5.2908737	1.2323732
C	2.8823583	-4.2088445	3.6362337
C	4.1802423	-4.1507236	-0.5527772

H	3.6893902	-5.0315097	-0.1290807
H	3.8328930	-4.0627958	-1.5886796
C	2.1152316	-1.0447292	-3.1509244
H	1.4173644	-0.4060814	-2.5921599
C	1.0125064	-2.8297315	2.8807513
C	2.0979574	-3.4395608	-3.8642731
H	2.6026466	-3.1151091	-4.7714343
C	0.0234489	-4.8473209	-0.3769034
H	-0.3229820	-4.0150465	0.2518812
C	1.6235564	-3.6485843	3.8361173
H	1.1031759	-3.8679888	4.7653231
C	1.8574614	-4.7986863	-3.6908783
C	-1.2222126	-5.6785526	-0.7538967
H	-2.0373846	-5.0670351	-1.1521282
H	-0.9585524	-6.4098547	-1.5280530
C	-0.3851914	-2.3137187	3.1587339
H	-0.5126798	-1.3674202	2.6151998
C	6.1603714	-2.7802424	-0.4647070
H	6.0593200	-2.3275647	-1.4601976
H	7.2008564	-2.6520494	-0.1460865
C	3.5646738	-0.7506791	-2.6544669
H	3.5559799	-0.2771155	-1.6670054
H	4.1083379	-1.6990222	-2.5661950

C	4.2188981	0.1187900	-3.7335985
H	5.3129284	0.0534399	-3.7185710
H	3.9424820	1.1699080	-3.5922417
C	2.2716613	-5.7962080	-4.7388513
H	2.8001207	-5.2557475	-5.5390463
C	-1.4646200	-3.3225196	2.6622987
H	-1.8682403	-3.0264713	1.6892622
H	-0.9960102	-4.3065701	2.5493988
C	5.7133635	-4.2435906	-0.5121402
H	6.0429414	-4.7547014	0.4030268
H	6.1258901	-4.7970586	-1.3630728
C	3.1886628	-6.9296044	-4.2479898
H	2.7549536	-7.3768035	-3.3440530
H	4.1934792	-6.5767215	-3.9911541
C	2.1224573	-0.5875834	-4.6389640
H	1.5862085	-1.2726867	-5.3011406
H	1.6225974	0.3838539	-4.7012391
C	3.5952088	-0.4075551	-5.0264257
H	4.0473883	-1.3721352	-5.2955087
H	3.7260396	0.2706707	-5.8771369
C	-2.5332832	-3.3817237	3.7580912
H	-3.2394780	-2.5512959	3.6416596
H	-3.1039576	-4.3174780	3.7362640

C	3.5148524	-5.0812144	4.6863879
H	2.7980919	-5.2008052	5.5131610
C	-0.7399952	-2.0796158	4.6550452
H	-1.2512171	-1.1156574	4.7394014
H	0.1393743	-2.0397983	5.3033611
C	3.9349022	-6.4841990	4.2152642
H	4.5095517	-6.3924427	3.2844880
H	3.0762587	-7.1321598	4.0081989
C	3.1762847	-7.9400849	-5.4067902
H	3.3441481	-8.9646944	-5.0600305
H	3.9802046	-7.7052703	-6.1134881
C	1.1113861	-6.5824775	-5.3783022
H	0.4496684	-6.9453523	-4.5815168
H	0.5053276	-5.9609654	-6.0463109
C	-1.7229266	-3.1917017	5.0413674
H	-1.1847893	-4.1183781	5.2846721
H	-2.3389696	-2.9260050	5.9079129
C	-0.2326667	-6.7282163	1.2147868
H	0.0216662	-7.7852215	1.0812306
H	-0.2672913	-6.5462575	2.2945852
C	1.7920086	-7.7660903	-6.0966284
H	1.9226981	-7.5472450	-7.1617278
H	1.1843949	-8.6742386	-6.0308605

C	4.8317798	-4.5371492	5.2712136
H	5.4816011	-4.2209916	4.4450154
H	4.6746353	-3.6641576	5.9140236
C	4.8318747	-7.0057631	5.3515528
H	4.2291198	-7.5569582	6.0818310
H	5.5969420	-7.6962305	4.9826051
C	-1.5891553	-6.3997648	0.5460533
H	-2.2011551	-7.2909625	0.3707675
H	-2.1741055	-5.7291387	1.1866121
C	5.4479910	-5.7389375	6.0141452
H	6.5407972	-5.7313361	5.9516358
H	5.1894748	-5.7039053	7.0779319
Sn	0.9814899	1.3710999	-0.0264646
C	3.9005457	3.6396497	-2.5311957
H	4.9236854	3.9778961	-2.3849295
C	0.5661743	4.7167035	0.2259062
H	0.2962905	3.9004679	-0.4482494
C	1.2000782	4.1234677	1.4653883
C	1.3980057	2.7398069	1.6611185
C	1.9755060	2.4061950	-1.7192026
C	3.3125054	2.8330951	-1.5532540
C	1.6133407	5.0241115	2.4505787
H	1.4654459	6.0884058	2.2768770

C	1.2915653	2.7427647	-2.9047547
C	-0.7211139	5.5432919	0.5094374
H	-1.6251806	4.9374395	0.3949550
H	-0.7084149	5.9127292	1.5418300
C	4.6365341	3.6214251	0.5204171
H	4.8281058	4.4957262	-0.1128023
H	3.8563231	3.9023998	1.2323732
C	2.2037871	4.6006178	3.6362337
C	1.5045110	5.6955578	-0.5527772
H	2.5127201	5.7108605	-0.1290807
H	1.6020379	5.3507807	-1.5886796
C	-0.1528538	2.3542088	-3.1509244
H	-0.3570054	1.4305143	-2.5921599
C	1.9443661	2.2917220	2.8807513
C	1.9297684	3.5366648	-3.8642731
H	1.3964403	3.8115126	-4.7714343
C	4.1861786	2.4439678	-0.3769034
H	3.6386232	1.7278126	0.2518812
C	2.3479885	3.2303332	3.8361173
H	2.7981887	2.8893727	4.7653231
C	3.2270535	4.0079519	-3.6908783
C	5.5288771	1.7808092	-0.7538967
H	5.4068735	0.7690908	-1.1521282

H	6.0303732	2.3747966	-1.5280530
C	2.1963349	0.8232738	3.1587339
H	1.4405605	0.2397164	2.6151998
C	-0.6724252	6.7251594	-0.4647070
H	-1.0139298	6.4113074	-1.4601976
H	-1.3036860	7.5621493	-0.1460865
C	-1.1322297	3.4624377	-2.6544669
H	-1.5380009	3.2181266	-1.6670054
H	-0.5827726	4.4074361	-2.5661950
C	-2.2123242	3.5942779	-3.7335985
H	-2.7027445	4.5744111	-3.7185710
H	-2.9844110	2.8293356	-3.5922417
C	3.8838327	4.8654204	-4.7388513
H	3.1515505	5.0528494	-5.5390463
C	3.6096964	0.3928616	2.6622987
H	3.5551212	-0.1047079	1.6892622
H	4.2276042	1.2907149	2.5493988
C	0.8183755	7.0697132	-0.5121402
H	1.0962216	7.6106915	0.4030268
H	1.0914296	7.7037057	-1.3630728
C	4.4068821	6.2262652	-4.2479898
H	5.0110224	6.0742616	-3.3440530
H	3.5988683	6.9200203	-3.9911541

C	-0.5523665	2.1318936	-4.6389640
H	0.3090748	2.0100402	-5.3011406
H	-1.1437259	1.2132836	-4.7012391
C	-1.4446513	3.3173197	-5.0264257
H	-0.8353902	4.1912087	-5.2955087
H	-2.0974275	3.0915096	-5.8771369
C	4.1953003	-0.5030257	3.7580912
H	3.8292261	-1.5298223	3.6416596
H	5.2910244	-0.5293671	3.7362640
C	2.6430346	5.5845586	4.6863879
H	3.1049835	5.0236213	5.5131610
C	2.1709977	0.3989533	4.6550452
H	1.5917961	-0.5257571	4.7394014
H	1.6968300	1.1406008	5.3033611
C	3.6480300	6.6498247	4.2152642
H	3.2812419	7.1016077	3.2844880
H	4.6385022	6.2301980	4.0081989
C	5.2881729	6.7207857	-5.4067902
H	6.0915790	7.3784644	-5.0600305
H	4.6828576	7.2995934	-6.1134881
C	5.1448997	4.2537274	-5.3783022
H	5.7900174	3.8621004	-4.5815168
H	4.9096837	3.4181092	-6.0463109

C	3.6255580	0.1037527	5.0413674
H	4.1590147	1.0331314	5.2846721
H	3.7034795	-0.5626046	5.9079129
C	5.9431396	3.1626129	1.2147868
H	6.7313665	3.9113743	1.0812306
H	5.8028709	3.0416477	2.2945852
C	5.8296272	5.4349701	-6.0966284
H	5.5747569	5.4387279	-7.1617278
H	6.9199135	5.3628353	-6.0308605
C	1.5133966	6.4530187	5.2712136
H	0.9146854	6.8577016	4.4450154
H	0.8359359	5.8804317	5.9140236
C	3.6512315	7.6874078	5.3515528
H	4.4299579	7.4410042	6.0818310
H	3.8666601	8.6952092	4.9826051
C	6.3369365	1.8236335	0.5460533
H	7.4147363	1.7392250	0.3707675
H	6.0486324	0.9817387	1.1866121
C	2.2460702	7.5875674	6.0141452
H	1.6930840	8.5301646	5.9516358
H	2.3449895	7.3461697	7.0779319

S7. References

[S4.1] A. B. Pangborn, M. A. Giardello, R. H. Grubbs, R. K. Rosen, F. J. Timmers, *Organometallics*, **1996**, *15*, 1518-1520.

[S4.2] L. A. Mclean, A. J. B. Watson, Eur. *J. Org. Chem.* **2021**, *35*, 4943-4945.

[S4.3] L. Salvi, N. R. Davis, S. Z. Ali, S. L. Buchwald, *Org. Lett.* **2012**, *14*, 170-173.

[S4.4] E. F. Pettersen, T. D. Goddard, C. C. Huang, G. S. Couch, D. M. Greenblatt, E. C. Meng, T. E. Ferrin, *J. Comput. Chem.* **2004**, *25*, 1605-1612.

[S4.5] F. Furche, R. Ahlrichs, C. Hättig, W. Klopper, M. Sierka, F. Weigend, Turbomole. *WIREs Comput Mol Sci* **2014**, *4*, 91-100.

[S4.6] F. Neese, *WIREs Comput. Mol. Sci.* **2022**, e1606.

[S4.7] C. Bannwarth, S. Ehlert, S. Grimme, *J. Chem. Theory Comput.* **2019**, *15*, 1652-1671.

[S4.8] S. Ehlert, M. Stahn, S. Spicher, S. Grimme, *J. Chem. Theory Comput.* **2021**, *17*, 4250-4261.

[S4.9] S. Grimme, A. Hansen, S. Ehlert, J. M. Mewes, *J. Chem. Phys.* **2021**, *154*, 064103.

[S4.10] A. Klamt, G. Schüürmann, *J. Chem. Soc., Perkin Trans. 2* **1993**, *0*, 799-805.

[S4.11] K. Eichkorn, O. Treutler, H. Öhm, M. Häser, R. Ahlrichs, *Chem. Phys. Lett.* **1995**, *240*, 283-289.

[S4.12] F. Weigend, *Phys. Chem. Chem. Phys.* **2006**, *8*, 1057.

[S4.13] A. D. Becke, *J. Chem. Phys.* **1993**, *98*, 5648-5652.

[S4.14] E. Caldeweyher, S. Ehlert, A. Hansen, H. Neugebauer, S. Spicher, C. Bannwarth, S. Grimme, *J. Chem. Phys.* **2019**, *150*, 154122.

[S4.15] M. Bursch, E. Caldeweyher, A. Hansen, H. Neugebauer, S. Ehlert, S. Grimme, *Acc. Chem. Res.* **2019**, *52*, 258-266.

[S4.16] F. Weigend, R. Ahlrichs, *Phys. Chem. Chem. Phys.* **2005**, *7*, 3297-3305.

[S4.17]M. von Hopffgarten, G. Frenking, *Wiley Interdiscip. Rev. Comput. Mol. Sci.* **2012**, *2*, 43-62.

[S4.18]M. Bursch, L. Kunze, A. M. Vibhute, A. Hansen, K. M. Sureshan, P. G. Jones, S. Grimme, D. B. Werz, *Chem. - A Eur. J.* **2021**, *27*, 4627-4639.

[S4.19]M. Bursch, E. Caldeweyher, A. Hansen, H. Neugebauer, S. Ehlert, S. Grimme, *Acc. Chem. Res.* **2019**, *52*, 258-266.

[S4.20]ADF 2019.3, SCM, Theoretical Chemistry, Vrije Universiteit, Amsterdam, The Netherlands, Http://Www.Scm.Com.

[S4.21]G. Schreckenbach, T. Ziegler, *J. Phys. Chem.* **1995**, *99*, 606-611.

[S4.22]M. Krykunov, T. Ziegler, E. Van Lenthe, *Int. J. Quantum Chem.* **2009**, *109*, 1676-1683.

[S4.23]Y. Zhang, W. Yang, *Phys. Rev. Lett.* **1998**, *80*, 890.

[S4.24]E. van Lenthe, E. J. Baerends, *J. Comput. Chem.* **2003**, *24*, 1142-1156.

[S4.25]E. van Lenthe, E. J. Baerends, J. G. Snijders, *J. Chem. Phys.* **1993**, *99*, 4597-4610.

[S4.26]E. van Lenthe, E. J. Baerends, J. G. Snijders, *J. Chem. Phys* **1994**, *101*, 9783-9792.

[S4.27]E. van Lenthe, J. G. Snijders, E. J. Baerends, *J. Chem. Phys.* **1996**, *105*, 6505-6516.

[S4.28]C. C. Pye, T. Ziegler, *Theor. Chem. Acc.* **1999**, *101*, 396-408.

Chapter 5. Reactivity of Diarylstannylene $Sn(Ar^{iPr4})_2$ (Ar^{iPr4} = C_6H_3-2,6-(C_6H_3-2,6-$^iPr_2$)$_2$) with alkynes

Wenxing Zou, James. C. Fettinger, Philip Power

Abstract

Treatment of diarylstannylene $Sn(Ar^{iPr4})_2$ (Ar^{iPr4} = C_6H_3-2,6-(C_6H_3-2,6-iPr_2)$_2$) with alkynes (phenylacetylene and diphenylacetylene) at elevated temperature (60^{o}C for phenylacetylene and 120^{o}C for diphenylacetylene) afforded rare aryl vinyl stannylene complexes $Ar^{iPr4}Sn\{C(C_6H_5)=C(H)(Ar^{iPr4})\}$ (**1**) and $Ar^{iPr4}Sn\{C(C_6H_5)=C(H)(C_6H_5)\}$ (**2**). This finding represents a new type of reactions of stannylenes and alkynes in which C≡C moieties insert into Sn-C bond in an irreversible manner. The structure of complex **1** was confirmed by single X-ray crystallography and complex **2** was fully characterized by X-ray crystallography and spectroscopy (NMR, UV-vis and Infrared). Proposed mechanisms of the generation of complex **1** was described.

The study of group 14 tetrylenes (:ER_2, E = Si, Ge, Sn, Pb, R = bulky organic group), the heavier carbene analogues, has undergone very rapid growth in the recent decades due to their unique structures and chemical properties.[1-8] Of particular interest is the synthesis, characterization and reactivity study of stannylenes[9-11] which have the general formula of SnR_2 (R = bulky organic ligands). Beginning with the landmark synthesis of dialkyl tin derivative $Sn\{CH(SiMe_3)_2\}_2$ [12] by Lappert and $Sn\{N(SiMe_3)_2\}_2$ by Lappert[13] and Zuckerman[14] in the 1970s, many stannylene complexes have been isolated with the use of various sterically encumbered ligands. Subsequent examples include tin dichalcogenolates,[15-18] diaryl stannylene stabilized by bulky terphenyl ligand,[19-20] diborylstannylene,[21] and benzannulated N-Heterocyclic stannylenes.[22]

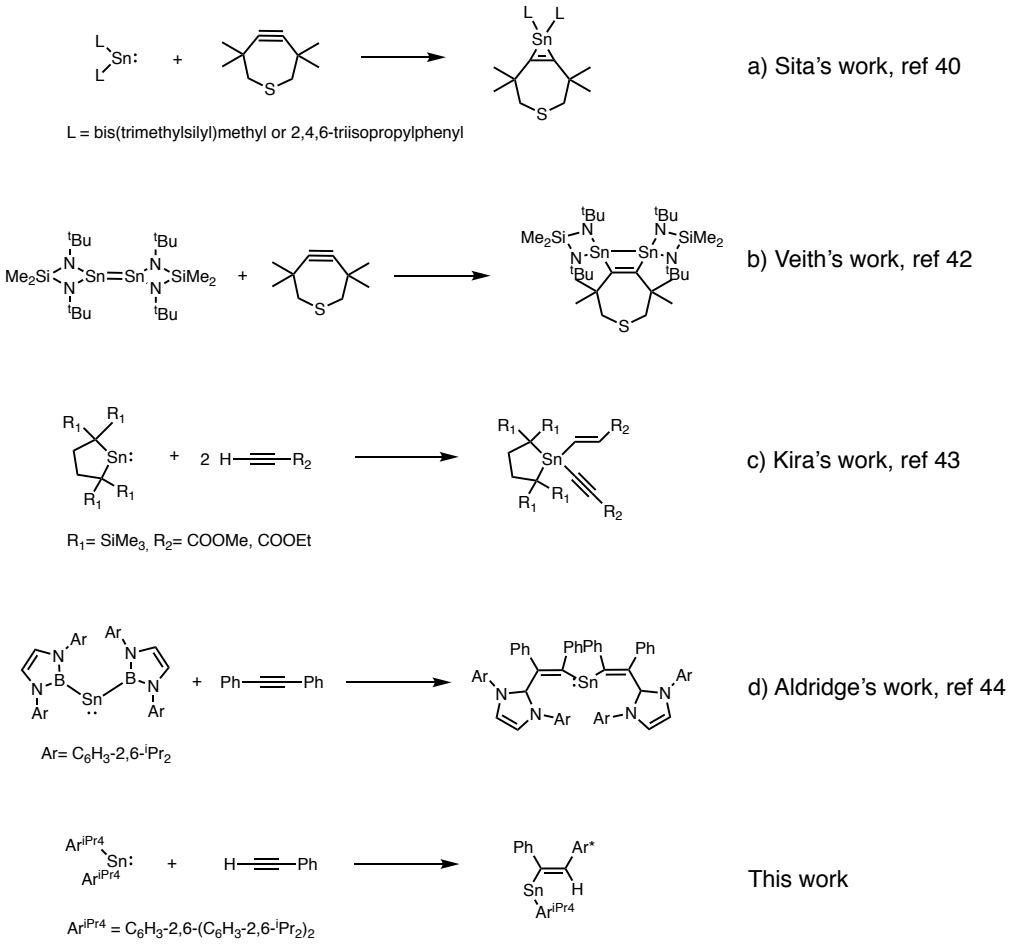

Scheme 5.1 Reactions of stannylenes with alkynes.

Structural and theoretical studies showed that stannylenes feature a vacant p orbital as well as a non-bonded pair of electrons,[5,11,23,24] and display electron acceptor and donor characteristics. Like other heavier group 14 carbene analogues,[25] stannylenes typically display high reactivity towards small molecules due to their relatively modest HOMO-LUMO gap[26-29] and well-defined Sn^{I} radical character.[30-32] The reactivities of stannylenes with small molecules thus have been well studied and early reports have shown that they react with H_2,[33-35] CO_2,[36-38] RNH_2 (R = Me or H),[32] ROH,[39] and other unsaturated organic molecules[26] under mild conditions.

Reports of stannylene activation of alkynes remain scarce, however. In late 1980s, Sita and coworkers reported a reversible complexation of a parent stannylene with a strained cycloheptyne ring which afforded a 1:1 complex adduct (Scheme 5.1, a).[40] It is noteworthy that the resulting addition product dissociated back to the corresponding stannylene and free alkyne at elevated temperature, indicating this coordination can also be understood in terms of a weak π-complex binding.[41] Veith's group reported the synthesis of the first distannacyclobutene, which was prepared from a formal [2+2] cycloaddition reaction of diamidostannylene (equilibrated with the corresponding distannene) with a strained cyclic alkyne under ambient conditions (Scheme 5.1, b).[42] In contrast to those simple coordination/cycloaddition mentioned above, Kira et al. reported a more complicated reaction of diaryl stannylene and methyl/ethyl propynoates, afforded a 1:2 adduct complex (Scheme 5.1, c).[43] However, treatment of the same starting reagents with non-terminal alkynes afforded no reaction. A double insertion reaction of bis(boryl)stannylenes and alkynes was reported by Aldridge and co-workers, showing the treatment of bis(boryl)stannylene with diphenylacetylene yielded a borane-appended (vinyl) Sn(II) species (Scheme 5.1, d).[44]

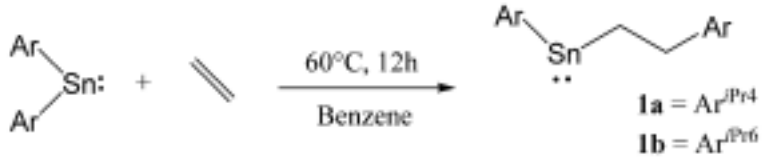

Scheme 5.2 The reaction of $SnAr_2$ species with ethylene.[26]

More recently, the Power group showed that the diarylstannylenes $Sn(Ar^{iPr4})_2$ underwent a facile migratory insertion reaction with ethylene, two aryl(alkyl) stannylene species were thus synthesized (Scheme 5.2).[26] . This finding provides more insight into the insertion reactions of stannylenes and unsaturated organic molecules. Inspired by these previously reported stannylation

reactions, we became interested in exploring the possibility of stannylenes reacting with alkynes in an irreversible manner.

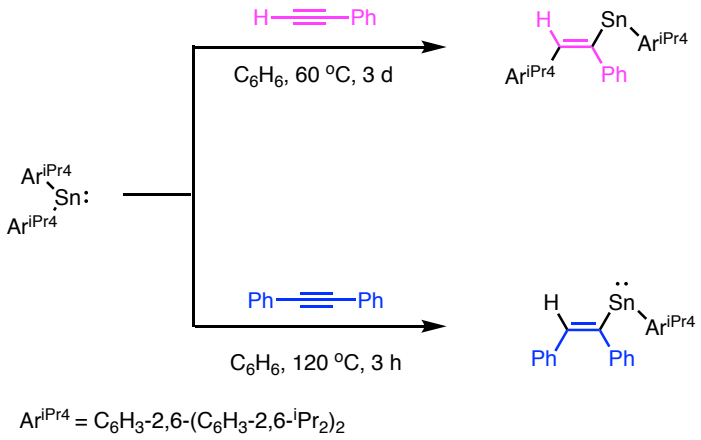

Scheme 5.3 Insertion reactions of diarylstannylene with alkynes.

Herein we describe the insertion reactions of the diarylstannylene $Sn(Ar^{iPr4})_2$ (Ar^{iPr4} = C_6H_3-2,6-(C_6H_3-2,6-iPr_2)$_2$) with phenylacetylene and diphenylacetylene (Scheme 5.3). The reaction of $Sn(Ar^{iPr4})_2$ and 1.5 equiv. of phenylacetylene in benzene at 60°C for 3 days (or with 1.2 equiv. of diphenylacetylene in benzene at 120°C for 4 h) resulted in a color change from dark blue to dark red. Benzene was then removed under reduced pressure to afford a dark red residue. Recrystallization of the reaction residue with Et_2O yielded red crystal blocks which were suitable for single X-ray crystallography.

X-ray crystallographic examination of **1** showed that the phenylacetylene molecule inserted into one of the Sn-C_{ipso} bonds of $Sn(Ar^{iPr4})_2$, which gives rise to a monomeric aryl vinyl divalent tin complex. Complex **1** features an expected mononuclear two-coordinate tin center, with an angle defined by the two substituents at the tin metal (105.6(4)°) which is somewhat narrower than those of the previously reported diaryl stannylene complexes (cf. $Sn(Ar^{iPr4})_2$: 117.56(8)°;[45] $Sn(Ar^{iPr6})_2$

(Ar^{iPr6} = C_6H_3-2,6-(C_6H_2-2,4,6-iPr_3)$_2$):107.61(9)°;[20] Sn(Ar^{iPr4}-4-Cl)$_2$: 115.12(8);[46] Sn(Ar^{iPr4}-3,5-*i*Pr$_2$)$_2$: 123.4(2)°;[46] Sn(Ar^{iPr4}-4-$SiMe_3$)$_2$: 115.37(9)° [46]) but considerably wider than those related aryl alkyl substituted stannylenes (cf. $Ar^{iPr4}SnCH_2CH_2Ar^{iPr4}$: 94.7(5)°;[26] $Ar^{iPr6}SnCH_2CH_2Ar^{iPr6}$: 99.22(1)° [26]). The Sn-C1 and Sn-C39 bond lengths in **1** are 2.23(9) and 2.28(4) Å, which slightly exceed the sum of the single bond radii of carbon (0.77 Å) and tin (1.4 Å)[47] and can be compared to the Sn-C_{ipso} distances observed in other aryl (alkyl) stannylenes (cf. Sn{C(Ph)=C(Ph)B(NDippCH)$_2$}$_2$: 2.22(2) Å;[44] Sn{C(Ph)=C(H)B(NDippCH)$_2$} {NDipp($SiMe_3$)}: 2.25(1) Å;[44] $Ar^{iPr4}SnCH_2CH_2Ar^{iPr4}$: 2.15(4) Å;[26] $Ar^{iPr6}SnCH_2CH_2Ar^{iPr6}$: 2.20(12) Å [26]). C1 and C2 have essentially planar coordination (a sum of interior angles of 359.6(10)° for C1 and 361.0(17)° for C2) which are consistent with their sp^2 hybridization.

The use of diphenylacetylene, a more sterically demanding alkyne, also yielded a monomeric organotin species with only one terphenyl ligand Ar^{iPr4} bonded directly to tin. The tin atom of **2** has a bent two-coordinate configuration with C1-Sn-C15 angle of 98.57(13)°, which is much narrower than that of **1** but is comparable to that of those aryl alkyls substituted stannylenes (cf. $Ar^{iPr4}SnCH_2CH_2Ar^{iPr4}$: 94.7(5)°;[26] $Ar^{iPr6}SnCH_2CH_2Ar^{iPr6}$: 99.22(1)° [26]). H1, C2, C9 atoms lie essentially coplanar to the C1-Sn1-C3 plane with a twist angle of 7.01(14)°, while the two phenyl rings on the vinyl substituent is nearly orthogonal to each other (a twist angle of 86.3(2)°).

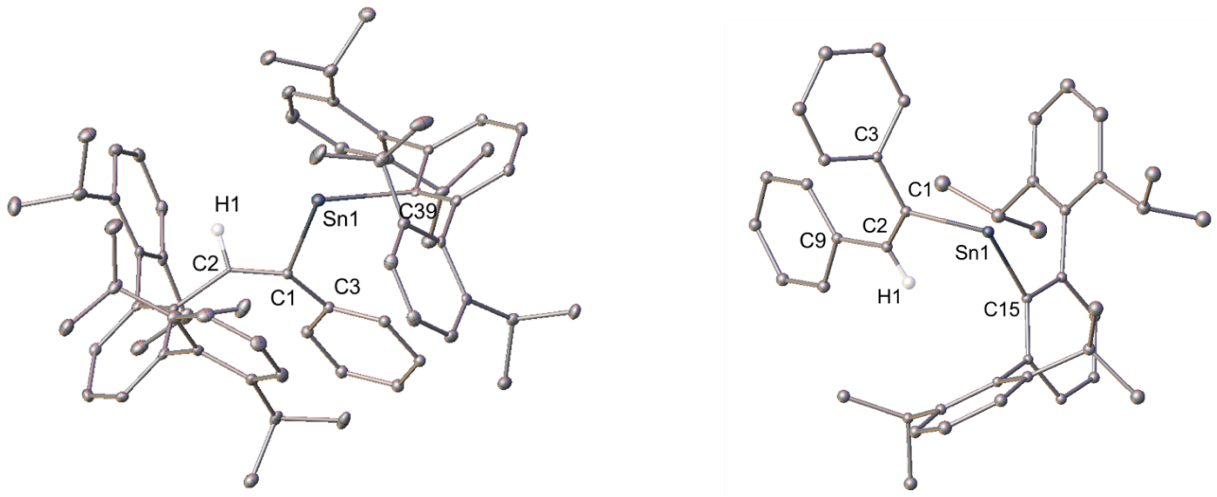

1 **2**

Figure 5.1 Crystal structures of **1** and **2**. Selected bond lengths (Å) and angles (°) of **1**: C1-C2 1.33 (4); C1-C3 1.52(6); C1-Sn1 2.23(9); Sn1-C39 2.28(4); C2-C1-C3: 126.6(15); C3-C1-Sn1: 128.7(10); C2-C1-Sn1: 108.1(11); C1-Sn1-C39: 105.6(4). Selected bond lengths (Å) and angles (°) of **2**: C1-C2 1.35(5); C1-Sn1 2.21(4); Sn1-C15 2.21(4); C1-C3 1.47(5); C3-C1-Sn1 111.5(2); C2-C1-Sn1 121.8(3); C2-C1-C3 126.7(3); C1-Sn1-C15 98.57(13).

Compound **2** was characterized by NMR (^{1}H, ^{13}C and ^{119}Sn), UV-vis and Infrared spectroscopy. Inspection of the ^{119}Sn NMR spectroscopy of compound **2** revealed a single resonance at 1601 ppm, which falls within the range observed for other related monomeric divalent organotin species (cf. $Ar^{iPr4}SnCH_2CH_2Ar^{iPr4}$: 1809 ppm;[26] $Ar^{iPr6}SnCH_2CH_2Ar^{iPr6}$:1946 ppm;[26] Sn{C(Ph)=C(H) B(NDippCH)$_2$}$_2$: 1730 ppm;[44] Sn{C(Ph)=C(Ph)B(NDippCH)$_2$}$_2$: 1670 [44]), indicating the monomeric structure of **2** in solution. The UV-vis spectrum of **2** shows a broad absorption band at 518 nm, tailed into visible region. The absorption is attributed to n→p transition[12,46,48,49] which is directly correlated to the HOMO-LUMO energy gap. This value is comparable to those of other monomeric alkyl/aryl stannylene species (cf. $Ar^{iPr4}SnCH_2C_6H_5$: 486 nm;[50] $Ar^{iPr4}SnCH_2C_6H_4$-3-Me:

490 nm;[50] $Ar^{iPr4}SnCH_2CH_2tBu$: 486 nm;[51] $Ar^{iPr6}SnCH_2CH_2tBu$: 484 nm;[51] $Ar^{iPr4}SnR$ (R = norbornyl, 494 nm; norbornenyl, 502 nm)[52]).

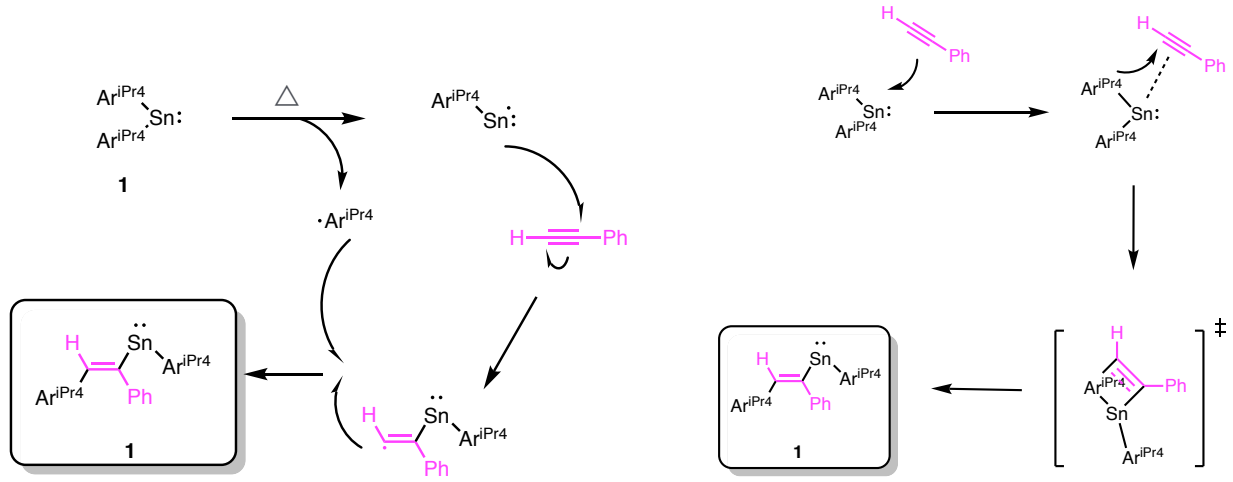

Figure 5.2 Two proposed mechnisms for the formation of **1**.

Two mechanisms of the formation of compounds **1** have been proposed (Figure 5.2) based on known literature.[26] Homolytic cleavage of a Sn-C bond is initiated upon heating, followed by the formation of a $:\dot{S}nAr^{iPr4}$ radical and a terphenyl carbon radical $\cdot Ar^{iPr4}$. The reaction of the $:\dot{S}nAr^{iPr4}/\cdot Ar^{iPr4}$ radical pair with phenylacetylene yields the product as shown in Figure 5.2. A non-radical formation mechanism for **1** is also possible with the formation of a four-membered ring intermediate involved (Figure 5.2, right).

In summary, the reactions of $Sn(Ar^{iPr4})_2$ with phenylacetylene or diphenylacetylene at elevated temperature via an irreversible insertion route to afford products **1** and **2**. The structures of **1** and **2** were confirmed by X-ray crystallography and spectroscopy. Further investigation of the reaction mechanisms is ongoing.

Author Contributions

P. P. Power proposed and supervised the overall project. W. Zou carried out all experiments, including synthesis, spectroscopy and data analysis. J. C. Fettinger finalized X-ray data. W. Zou and P. P. Power wrote and edited the manuscript.

References

[1] Neumann, W. P. Germylenes and Stannylenes, *Chem. Rev.* **1991**, *91*, 311-334.

[2] Kühl, O.; N-heterocyclic Germylenes and Related Compounds, *Coord. Chem. Rev.* **2004**, *248*, 411-427.

[3] Hill, N. J.; West, R. Recent Developments in the Chemistry of Stable Silylenes, *J. Organomet. Chem.* **2004**, *689*, 4165-4183.

[4] Ottosson H.; Steel, P. G. Silylenes, Silenes, and Disilenes: Novel Silicon-Based Reagents for Organic Synthesis? *Chem. Eur. J.* **2006**, *12*, 1576-1585.

[5] Mizuhata, Y.; Sasamori T.; Tokitoh, N. Stable Heavier Carbene Analogues, *Chem. Rev.* **2009**, *109*, 3479-3511.

[6] Asay, M.; Jones C.; Driess, M. N-Heterocyclic Carbene Analogues with Low-Valent Group 13 and Group 14 Elements: Syntheses, Structures, and Reactivities of a New Generation of Multitalented Ligands, *Chem. Rev.* **2011**, *111*, 354-396.

[7] Sen, S. S.; Khan, S.; Nagendran, S.; Roesky, H. W. Interconnected Bis-Silylenes: A New Dimension in Organosilicon Chemistry, Acc. Chem. Res. 2012, 45, 578-587.

[8] Prabusankar, G.; Sathyanarayana, A.; Suresh, P.; Babu, C. N.; Srinivas, K. and Metla, B. P. R. N-heterocyclic Carbene Supported Heavier Group 14 Elements: Recent Progress and Challenges, *Coord. Chem. Rev.* **2014**, *269*, 96-133.

[9] Benet, S.; Cardin, C. J.; Cardin, D. J.; Constantine, S. P.; Heath, P.; Rashid, H.; Teixeira, S.; Thorpe, J. H.; Todd, A. K. Syntheses and Crystal Structures of Heteroleptic Stannylenes and Germylenes, *Organometallics*, **1999**, *18*, 389-398.

[10] Setaka, W.; Sakamoto, K.; Kira, M.; Power, P. P. Synthesis and Structure of Stable Tri-tert-butylgermyl-Substituted Stannylene and Germylene, *Organometallics*, **2001**, *20*, 4460-4462.

[11] Arp, H.; Baumgartner, J.; Marschner, C.; Müller, T. A Cyclic Disilylated Stannylene: Synthesis, Dimerization, and Adduct Formation, *J. Am. Chem. Soc.* **2011**, *133*, 5632-5635.

[12] Davidson, P. J.; Lappert, M. F. Stabilization of Metals in a Low Coordinative Environment Using the Bis(trimethylsilyl)methyl Ligand. Colored Tin(II) and Lead(II) Alkyls, *J. Chem. Soc., Dalton Trans.* **1976**, *21*, 2268-2274.

[13] Harris, D. H.; Lappert, M. F. Monomeric, Volatile Bivalent Amides of Group IVB Elements, $M(NR^1_2)_2$ and $M(NR^1R^2)_2$ (M=Ge, Sn, or Pb; $R^1 = Me_3Si$, $R^2 = Me_3C$), *J. C. S. Chem. Commun.* **1974**, *21*, 895-896.

[14] Schaeffer Jr. C. D.; Zuckerman, J. J. Tin(II) Organosilylamines, *J. Am. Chem. Soc.* **1974**, *96*, 7160-7162.

[15] Cetinkaya, B.; Gumrukcu, I.; Lappert, M. F.; Atwood, J. L.; Rogers, R. D.; Zaworotko, M. J. Bivalent Germanium, Tin, and Lead 2,6-di-tert-Butylphenoxides and the Crystal and Molecular Structures of $M(OC_6H_2Me\text{-}4\text{-}But_2\text{-}2,6)_2$ (M = Ge or Sn), J. Am. Chem. Soc. 1980, 102, 2088-2089.

[16] Hitchcock, P. B.; Lappert, M. F.; Samways, B. J.; Weinberg, E. L. Metal (Li, Ge^{II}, Ge^{III}, Sn^{II}, and Pb^{II}) 2,6-Dialkylbenzenethiolates; X-Ray Crystal Structures of Sn(SAr), (Ar = C_6H_2But,-2,4,6)

and $[M(SAr')_2]_3$ (M = Sn or Pb, Ar' = $C_6H_3Pri_2$-2,6), J. Chem. Soc. Chem. Commun. 1983, 24, 1492-1494.

[17] Seligson, A. L.; Arnold, J. Synthesis, Structure, and Reactivity of Homoleptic Tin(II) and Lead(II) Chalcogenolates and Their Conversion to Metal Chalcogenides. X-ray Crystal Structures of $\{Sn[TeSi(SiMe_3)_3]\}_2$ and $(PMe_3)Sn[TeSi(SiMe_3)_3]_2$, J. Am. Chem. Soc. 1993, 115, 8214-8220.

[18] Rekken, B. D.; Brown, T. M.; Fettinger, J. C.; Lips, F.; Tuononen, H. M.; Herber, R. H.; Power, P. P. Dispersion Forces and Counterintuitive Steric Effects in Main Group Molecules: Heavier Group 14 (Si-Pb) Dichalcogenolate Carbene Analogues with Sub-90° Interligand Bond Angles, J. Am. Chem. Soc. 2013, 135, 10134-10148.

[19] Eichler, B. E.; Power, P. P. Characterization of the Sterically Encumbered Terphenyl-Substituted Species 2,6-$Trip_2H_3C_6Sn$-$Sn(Me)_2C_6H_3$-2,6-$Trip_2$, an Unsymmetric, Group 14 Element, Methylmethylene, Valence Isomer of an Alkene, Its Related Lithium Derivative 2,6-$Trip_2H_3C_6(Me)_2S$ -Sn(Li)(Me)C_6H_3-2,6-$Trip_2$, and the Monomer Sn(t-Bu)C_6H_3-2,6-$Trip_2$ (Trip = C_6H_2-2,4,6-i-Pr_3), Inorg. Chem. 2000, 39, 5444-5449.

[20] McCrea-Hendrick, M. L.; Bursch, M.; Gullett, K. L.; Maurer, L. R.; Fettinger, J. C.; Grimme, S.; Power, P. P. Counterintuitive Interligand Angles in the Diaryls $E\{C_6H_3$-2,6-$(C_6H_2$-2,4,6-$iPr_3)_2\}_2$ (E = Ge, Sn, or Pb) and Related Species: The Role of London Dispersion Forces, *Organometallics*, **2018**, *37*, 2075-2085.

[21] Protchenko, A. V.; Birjkumar, K. H.; Dange, D.; Schwarz, A. D.; Vidovic, D.; Jones, C.; Kaltsoyannis, N.; Mountford P.; Aldridge, S. A Stable Two-Coordinate Acyclic Silylene, *J. Am. Chem. Soc.* **2012**, *134*, 6500-6503.

[22] Zabula, A. V.; Hahn, F. E. Mono- and Bidentate Benzannulated N-Heterocyclic Germylenes, Stannylenesand Plumbylenes, *Eur. J. Inorg. Chem.* **2008**, *33*, 5165-5179.

[23] Mohapatra, C.; Scharf, L. T.; Scherpf, T.; Mallick, B.; Feichtner, K.-S.; Schwarz, C.; Gessner, V. H. Isolation of a Diylide-Stabilized Stannylene and Germylene: Enhanced Donor Strength through Coplanar Lone Pair Alignment, *Angew. Chem. Int. Ed.* **2019**, *58*, 7459-7463.

[24] Zamanzadeha, A. H.; Mohebia, N.; Kassaeea, M. Z.; Cummings, P. T.; Dong, K. Novel N-heterocyclic Stannylenes (NHSns) Using DFT, *Phys. Chem. Res.* **2019**, *7*, 511-521.

[25] Lee, V. Y.; Sekiguchi, A. *Organometallic Compounds of Low-Coordinate Si, Ge, Sn and Pb: From Phantom Species to Stable Compounds, Chapter 4: Heavy Analogs of Carbenes: Silylenes, Germylenes, Stannylenes and Plumbylenes*, New Jersey, Wiley, 2010, 139-197, doi: 10.1002/9780470669266.

[26] Lai, T. Y.; Guo, J.-D.; Fettinger, J. C.; Nagase, S.; Power, P. P. Facile Insertion of Ethylene into a Group 14 Element-Carbon Bond: Effects of the HOMO-LUMO Energy Gap on Reactivity, *Chem. Commun.* **2019**, *55*, 405-407.

[27] Moraru, I.-T.; Nemes, G. A DFT Investigation of a Polycyclic Stannylene Model; Structural Characterization and Stability Assessment, *Stud. Univ. Babes-Bolyai Chem.* **2019**, *64*, 435-446.

[28] Abedini, N.; Kassaee, M. Z. Novel Azaborastannylenes by DFT, *Comput. Theor. Chem.* **2020**, *1190*, 112998-113004.

[29] Banerjee, S.; Vanka, K. Computational Insights into Hydroboration with Acyclic α-Borylamido-Germylene and Stannylene Catalysts: Cooperative Dual Catalysis the Key to System Efficiency, *Polyhedron*, **2022**, *222*, 115907-115925.

[30] Lee, V. Y.; Sekiguchi, A. Si-, Ge-, and Sn-Centered Free Radicals: from Phantom Species to Grams-Order-Scale Materials, *Eur. J. Inorg. Chem.* **2005**, *7*, 1209-1222.

[31] Becker, J. Y.; Lee, V. Y.; Nakamoto, M.; Sekiguchi, A.; Chrostowska, A.; Dargelos, A. Electrochemical Properties and Computations of Stable Radicals of the Heavy Group 14 Elements (Si, Ge, and Sn), *Chem. Eur. J.* **2009**, *15*, 8480-8484.

[32] Lim, L. F.; Judd, M.; Vasko, P.; Gardiner, M. G.; Pantazis, D. A.; Cox, N.; Hicks, J. Crystalline Germanium(I) and Tin(I) Centered Radical Anions, *Angew. Chem. Int. Ed.* **2022**, *61*, e2022012.

[33] Peng, Y.; Ellis, B. D.; Wang, X.; Power, P. P. Diarylstannylene Activation of Hydrogen or Ammonia with Arene Elimination, *J. Am. Chem. Soc.* **2008**, *130*, 12268-12269.

[34] Peng, Y.; Guo, J.-D.; Ellis, B. D.; Zhu, Z.; Fettinger, J. C.; Nagase, S.; Power, P. P. Reaction of Hydrogen or Ammonia with Unsaturated Germanium or Tin Molecules under Ambient Conditions: Oxidative Addition versus Arene Elimination. *J. Am. Chem. Soc.* **2009**, *131*, 16272-16282.

[35] Turnell-Ritson, R. C.; Sapsford, J. S.; Cooper, R. T.; Lee, S. S.; Földes, T.; Hunt, P. A.; Pápai, I.; Ashley, A. E. Base-induced Reversible H_2 Addition to a Single Sn(II) Centre, *Chem. Sci.* **2018**, *9*, 8716-8722.

[36] Harris, L. A.-M.; Coles, M. P.; Fulton, J. R. Synthesis and Reactivity of Tin Amide Complexes, *Inorganica Chim. Acta,* **2011**, *369*, 97-102.

[37] Ferro, L.; Hitchcock, P. B.; Coles, M. P.; Cox, H.; Fulton, J. R. Activation of Carbon Dioxide by Divalent Tin Alkoxides Complexes, *Inorg. Chem.* **2011**, *50*, 1879-1888.

[38] Protchenko, A. V.; Fuentes, M. Á.; Hicks, J.; McManus, C.; Tirfoin, R.; Aldridge, S. Reactions of a Diborylstannylene with CO_2 and N_2O: Diboration of Carbon Dioxide by a Main Group Bis(boryl) Complex, *Dalton Trans.* **2021**, *50*, 9059-9067.

[39] Erickson, J. D.; Vasko, P.; Riparetti, R. D.; Fettinger, J. C.; Tuononen, H. M.; Power, P. P. Reactions of m-Terphenyl-Stabilized Germylene and Stannylene with Water and Methanol: Oxidative Addition versus Arene Elimination and Different Reaction Pathways for Alkyl- and Aryl-Substituted Species, *Organometallics*, **2015**, *34*, 5785-5791.

[40] Sita, L. R.; Bickerstaff, R. D. Synthesis and Crystal Structure of the First Stannacyclopropene Derivative, *J. Am. Chem. Soc.* **1988**, *110*, 5208-5209.

[41] Boatz, J. A.; Gordon, M. S. Theoretical Studies of the Metallacyclopropenes c-[$MX_2C_2H_2$] (M = C, Si, Ge, Sn; X = H, F), *J. Phys. Chem.* **1990**, *94*, 5488-5493.

[42] Krebs, A.; Jacobsen-Bauer, A.; Haupt, E.; Veith, M.; Huch, V. Synthesis and Structure of Digerma- and Distannacyclobutenes, *Angew. Chem. Int. Ed.* **1989**, *28*, 603-604.

[43] Xu, J.; Xiao, X.-Q.; Yan, C.; Li, Z.; Lu, Q.; Yang, Q.; Lai, G.; Kira, M. Reactions of an Isolable Dialkylstannylene with Propynoates and Benzyne, *Organometallics*, **2018**, *37*, 2399-2405.

[44] Protchenko, A. V.; Blake, M. P.; Schwarz, A. D.; Jones, C.; Mountford, P.; Aldridge, S. Reactivity of Boryl- and Silyl-Substituted Carbenoids toward Alkynes: Insertion and Cycloaddition Chemistry, *Organometallics,* **2015**, *34*, 2126-2129.

[45] Spikes, G. H.; Peng, Y.; Fettinger, J. C.; Power, P. P. Synthesis and Characterization of the Monomeric Sterically Encumbered Diaryls E{C_6H_3-2,6-(C_6H_3-2,6-Pr*i*$_2$)$_2$}$_2$ (E = Ge, Sn, or Pb), *Z. Anorg. Allg. Chem.* **2006**, *632*, 1005-1010.

[46] Wilfling, P.; Schittelkopf, K.; Flock, M.; Herber, R. H.; Power, P. P.; Fischer, R. C. Influence of Ligand Modifications on Structural and Spectroscopic Properties in Terphenyl Based Heavier Group 14 Carbene Homologues, *Organometallics*, **2015**, *34*, 2222-2232.

[47] Pyykkö, P.; Atsumi, M. Molecular Single-Bond Covalent Radii for Elements 1-118, *Chem. Eur. J.* **2009**, *15*, 186-197.

[48] Kira, M.; Yauchibara, R.; Hirano, R.; Kabuto, C.; Sakurai, H. Chemistry of Organosilicon Compounds. 287. Synthesis and X-ray Structure of the First Dicoordinate Dialkylstannylene that is Monomeric in the Solid State, *J. Am. Chem. Soc.* **1991**, *113*, 7785-7787.

[49] Henning, J.; Eichele, K.; Fink, R. F.; Wesemann, L. Structural and Spectroscopic Characterization of Tin–Tin Double Bonds in Cyclic Distannenes, *Organometallics*, **2014**, *33*, 3904-3918.

[50] Lai, T. Y.; Fettinger, J. C.; Power, P. P. Facile C-H Bond Metathesis Mediated by a Stannylene, *J. Am. Chem. Soc.* **2018**, *140*, 5674–5677.

[51] Wang, S.; McCrea-Hendrick, M.; Weinstein, C. M.; Caputo, C. A.; Hoppe, E.; Fettinger, J. C.; Olmstead, M. M.; Power, P. P. Tin(II) Hydrides as Intermediates in Rearrangements of Tin(II) Alkyl Derivatives, *J. Am. Chem. Soc.* **2017**, *139*, 6596-6604.

[52] Wang, S.; McCrea-Hendrick, M. L.; Weinstein, C. M.; Caputo, C. A.; Hoppe, E.; Fettinger, J. C.; Olmstead, M. M.; Power, P. P. Dynamic Behavior and Isomerization Equilibria of Distannenes Synthesized by Tin Hydride/Olefin Insertions: Characterization of the Elusive Monohydrido Bridged Isomer, *J. Am. Chem. Soc.* **2017**, *139*, 6586-6595.

Supporting Information

All manipulations were carried out under anaerobic and anhydrous conditions by using Schlenk techniques or in a Vacuum Atmospheres OMNI-Lab drybox under an atmosphere of dry argon or

nitrogen. Solvents were dried by the method of Grubbs[1] and co-workers, stored over potassium or sodium, and then degassed by the freeze-pump-thaw method. All physical measurements were made under strictly anaerobic and anhydrous conditions. The NMR spectra were recorded on a Varian Inova 600 MHz spectrometer, and the ^{1}H NMR and ^{13}C NMR spectra were referenced to the residual solvent signals in deuterated benzene. IR spectra were recorded as Nujol mulls between CsI plates on a PerkinElmer 1430 spectrometer. UV−vis spectra were recorded as dilute hexane solutions in 3.5 mL quartz cuvettes using an Olis 17 modernized Cary 14 UV−vis−near-IR spectrophotometer or an HP 8452 diode-array spectrophotometer. The $Sn(Ar^{iPr4})_2$ was prepared via literature method.[2] Unless otherwise stated, all materials were obtained from commercial sources and used as received.

Synthesis of complex **1**:

$Sn(Ar^{iPr4})_2$ (0.914 g, 1 mmol) and phenylacetylene (0.216 g, 2 mmol) were dissolved in ca. 30 mL of benzene. The reaction solution was then heated to 60°C and stirred for 3 days. The color of solution turned from blue to dark red which indicated the reaction's completed. Solvent was removed under reduced pressure; ca. 50 mL ether was then added into the reaction residue and the resulting red solution was filtered through celite. The filtrate was concentrated under reduced pressure until the formation of small red crystals was observed. The solution was storage in -30 °C freezer for 4 days to afford red crystals which were suitable for X-ray crystallography.

Synthesis of complex **2**:

$Sn(Ar^{iPr4})_2$ (Ar^{iPr4} = C_6H_3-2,6-(C_6H_3-2,6-$^{i}Pr_2$)$_2$) (0.914 g, 1 mmol) was mixed with diphenylacetylene (0.213 g, 1.2 mmol), followed by addition of ca. 60 mL of benzene, the reaction mixture was stirred for 4 hours at 120 °C, the color of solution became dark red after 2 hours.

Solvent was removed under reduced pressure; ca. 50 mL hexane was added to the reaction residue then the resulting red solution was filtered through celite. The filtrate was concentrated under reduced pressure until the formation of small red crystals was observed. Storage of the reaction in -30 °C freezer for 3 days resulted in the product in a red crystal form with 55% yield. ^{1}H NMR (599 MHz, Benzene-d_6) δ: 7.58 (s, 1H), 7.42 (d, J = 7.5 Hz, 2H), 7.37 (d, J = 7.5 Hz, 1H), 7.14 (d, J = 6.8 Hz, 4H), 7.10 (d, J = 7.8 Hz, 3H), 7.05 (t, J = 7.9 Hz, 3H), 6.85 (td, J = 17.7, 7.9 Hz, 4H), 6.73 (d, J = 7.6 Hz, 2H), 3.33 (p, J = 6.9 Hz, 4H), 1.24 (d, J = 6.9 Hz, 12H), 1.11 (d, J = 6.7 Hz, 12H). ^{13}C NMR (101 MHz, Benzene-d_6) δ: 193.50, 181.44, 146.94, 146.79, 145.00, 138.84, 136.68, 136.43, 130.30, 128.96, 128.73, 127.32, 126.84, 125.71, 124.98, 123.59, 31.02, 26.62, 22.88. ^{119}Sn NMR (149 MHz, Benzene-d_6) δ: 1607. 19. UV/vis: λ/nm (ε/ M^{-1} cm^{-1}): 518 (3300).

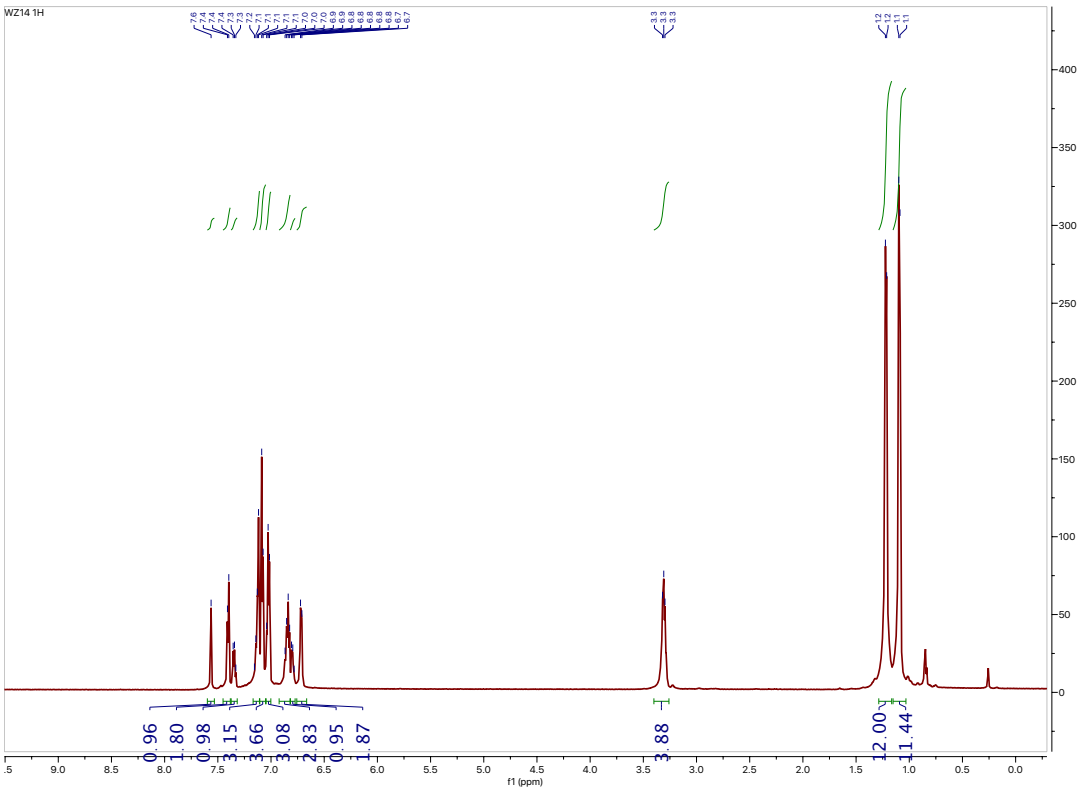

Figure. S5.1 ^{1}H NMR spectrum of (**2**) in C_6D_6 (600 MHz, 298 K)

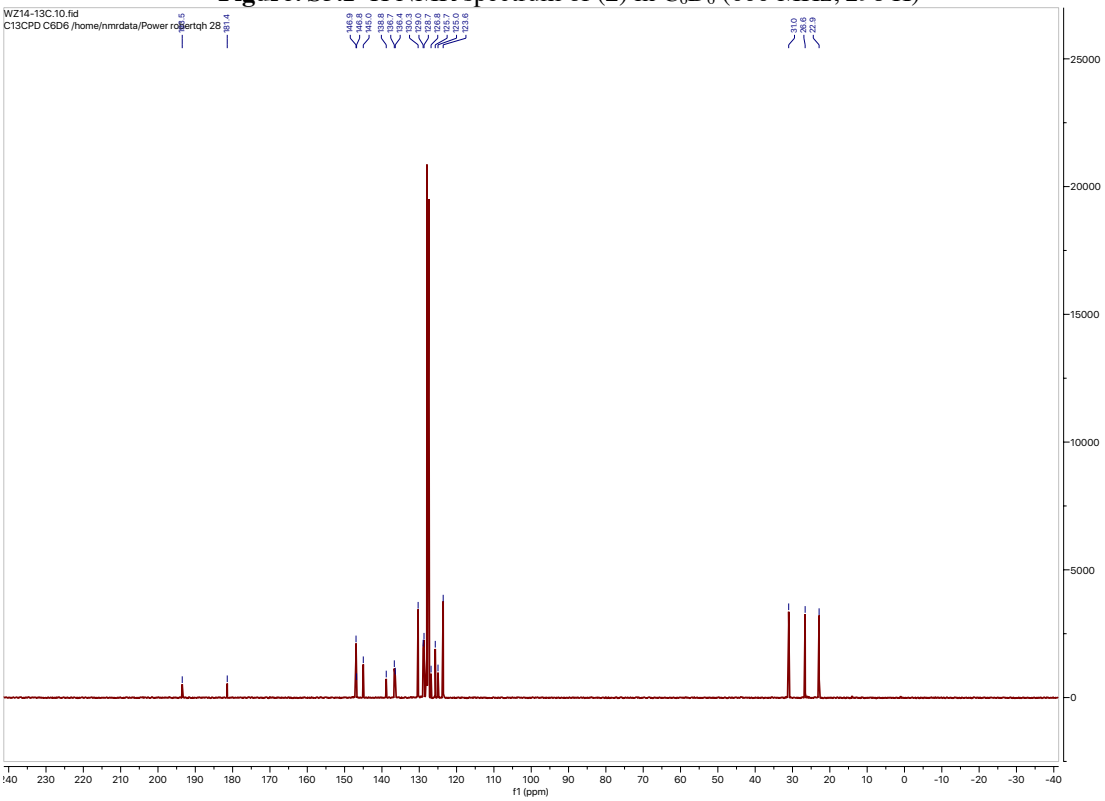

Figure. S5.2 $^{13}C\{^{1}H\}$ NMR spectrum of (**2**) in C_6D_6 (600 MHz, 298 K)

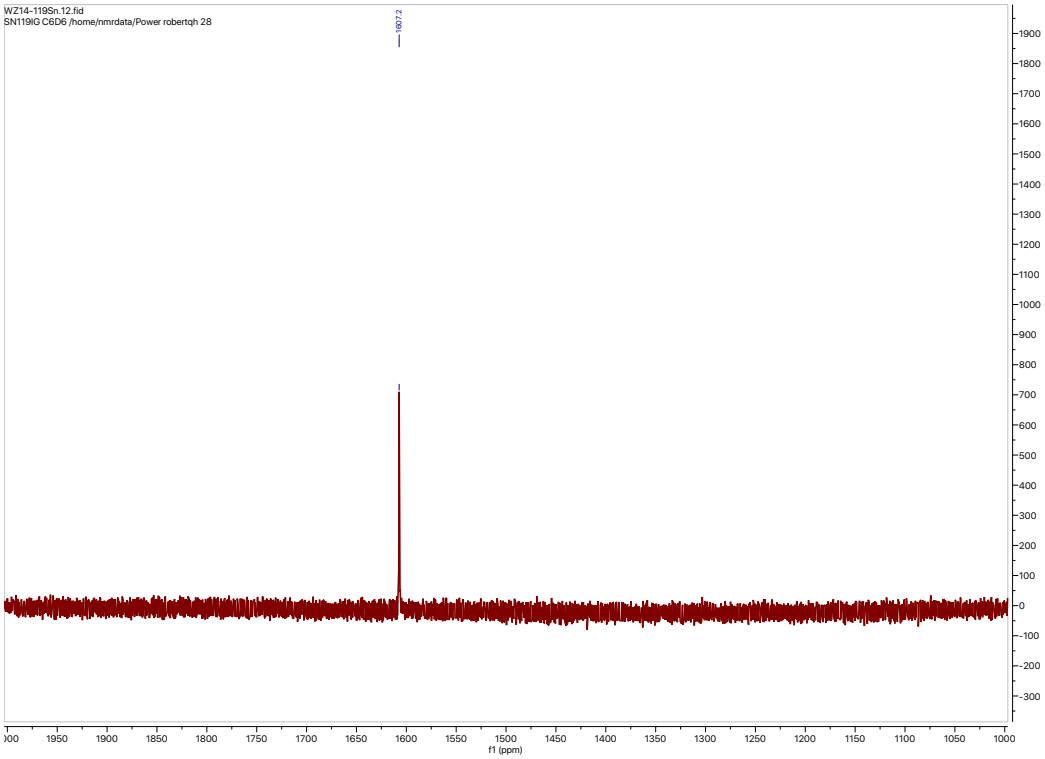

Figure. S5.2 $^{119}Sn\{^{1}H\}$ NMR spectrum of (**2**) in C_7D_8 (500 MHz, 298 K).

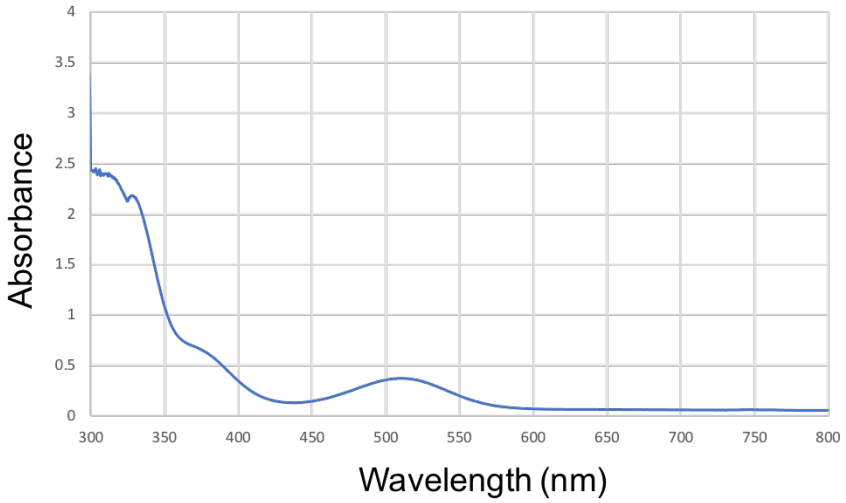

Figure. S5.3 UV-Vis spectrum of (**2**) at 25 °C (42 μM in hexanes).

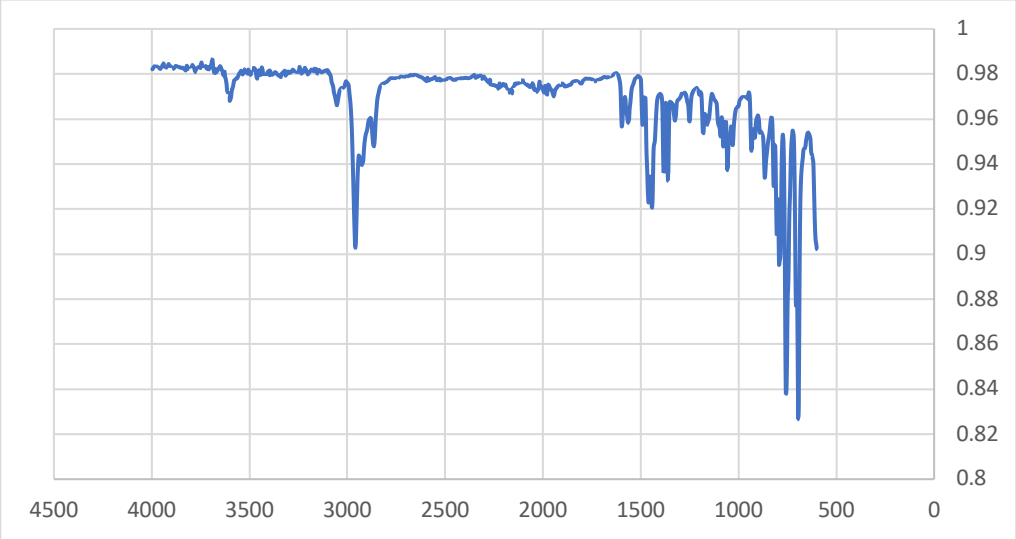

Figure S5.4 FTIR spectrum of (**2**).

Crystallographic Data

	1	**2**
formula	$C_{72}H_{90}OSn$	$C_{44}H_{49}Sn$
fw	1090.12	696.59
color	red	red
cyst syst	Triclinic	Triclinic
space group	P-1	P-1
a, Å	17.8418(9)	9.6848(11)
b, Å	17.8598(9)	11.7885(13)
c, Å	19.2380(10)	18.193(2)
α, deg	88.9389(8)	90.359(2)
β, deg	81.5494(8)	100.783(2)
γ, deg	89.9199(8)	107.774(2)
V, $Å^3$	6062.6(5)	1938.6(4)
Z	4	2
Density (calculated), Mg/m^3	1.194	1.193
Absorption coefficient, mm^{-1}	0.464	0.686
F(000)	2320	725
Crystal size, mm^3	0.288 x 0.218 x 0.188	0.381 x 0.33 x 0.266
Crystal color and habit	red block	red block
Theta range for data collection, deg	1.837 to 25.250	4.16 to 61.4
Index ranges	-21<=h<=21,	-13<=h<=13,

	-21<=k<=21, -23<=l<=23	-16<=k<=16, -26<=l<=26
Reflections collected	43731	31833
Independent reflections	21950 [R(int) = 0.0589]	11908 [R(int) = 0.0211]
Data / restraints / parameters	21950 / 149 / 1434	11908 / 0 / 193
Goodness-of-fit on F^2	1.135	1.014
Final R indices [I>2sigma(I)]	R1 = 0.0619, wR2 = 0.1091	R1 = 0.0992, wR2 = 0.2606
R indices (all data)	R1 = 0.0931, wR2 = 0.1183	R1 = 0.1042, wR2 = 0.2673
Largest diff. peak and hole, e.$Å^{-3}$	0.678/-0.842	12.56/-5.26

References:

[1] Pangborn, A. B.; Giardello, M. A.; Grubbs, R. H.; Rosen, R. K.; Timmers, F. J. Safe and Convenient Procedure for Solvent Purification, *Organometallics*, **1996**, *15*, 1518-1520.

[2] McCrea-Hendrick, M. L.; Bursch, M.; Gullett, K. L.; Maurer, L. R.; Fettinger, J. C.; Grimme, S.; Power, P. P. Counterintuitive Interligand Angles in the Diaryls E{C_6H_3-2,6-(C_6H_2-2,4,6-iPr_3)$_2$}$_2$ (E = Ge, Sn, or Pb) and Related Species: The Role of London Dispersion Forces, *Organometallics*, **2018**, *37*, 2075-2085.